The Development and Function of Cerebellar Nucleo-Olivary Neurons

Prekop, Hong-Ting

Awarding institution:
King's College London

The Development and Function of Cerebellar Nucleo-Olivary Neurons

Hong-Ting Prekop

Centre for Developmental Neurobiology

King's College London

Thesis submitted for the degree of Doctor of Philosophy (PhD)

September 2017

ABSTRACT

The neuronal circuitry between the cerebellum and inferior olive is of crucial importance in motor function. While the climbing fibres that send olivary signals to the cerebellum have been shown to play a significant role in modulating cerebellar output, little is known of the origins or function of the nucleo-olivary neurons of the cerebellar nuclei that send reciprocal feedback to the inferior olive.

In this thesis, the *Sox14* gene is identified as a novel genetic developmental marker for nucleo-olivary neurons of the lateral and interposed, but not medial, cerebellar nuclei. Using *Sox14-GFP* and *Sox14-Cre* knock-in and *Sox14* knock-out mouse lines, in combination with birth dating, marker analysis and tract tracing techniques, I characterised the projections and development of nucleo-olivary neurons. These experiments established that *Sox14* is expressed in early born GABAergic nuclear projection neurons that exclusively target the inferior olive. A separate population of $Sox14^{+}$ cells in Nucleus Y target the oculomotor nucleus. Sox14 expression is observed from E12.5 directly ventral to the nuclear transitory zone, where glutamatergic nuclear cells are known to reside during development.

Injection of Cre-dependent AAV-mCherry-flex-dtA was used to drive expression of diphtheria toxin A subunit in *Sox14* expressing cells. Ablation of $Sox14^{+}$ nucleo-olivary neurons leads to some deficits in motor performance and motor learning. However, no deficits in associative motor learning were observed, suggesting that models of associative learning that invoke a key role for the nucleo-olivary feedback may be incorrect or incomplete.

This work establishes that nucleo-olivary neurons of the lateral and interposed cerebellar nuclei comprise a homogeneous and genetically distinct population and sheds light on the function of this projection in cerebellar function. Furthermore, this thesis establishes Sox14 transgenic mice as a unique tool in cerebellar research that will provide an important window on the function of the cerebellum in future studies.

ACKNOWLEDGMENTS / FUNDING

With gratitude, this thesis represents independent research funded by the National Institute for Health Research (NIHR) Biomedical Research Centre at South London and Maudsley NHS Foundation Trust and King's College London. The views expressed are my own and not necessarily those of the NHS, the NIHR, or the Department of Health.

I would like to thank Prof. Thomas Jessell and Dr. Laskaro Zagoraiou for the generation of the Sox14-Gfp and Sox14-Cre mouse lines. The mice are central to the research, so thank you for the generosity in making the mice available. Thank you to Stephanie and Reinko at Noldus, who arranged the trial period for use of the Erasmus ladder. They were so kind in arranging to come to help me set up and provided technical assistance in the analysis of the data.

I owe much of this work to the dedicated supervision from Alessio Delogu and Richard Wingate. Alessio, I can't think of a more competent and knowledgeable mentor that I could have had. The range of skills that you have acquired throughout your career and was able to impart onto me (as best as you could!) is inspiring. I have learnt a lot of technical skills and even though not all of them worked out, you encouraged me to troubleshoot and supported new ideas. Richard, our discussions helped me enormously to think through the data and put them into context. Your enthusiasm for the subject and positivity in general is infectious and was crucial in keeping me on track, particularly over the writing up period.

I also have many to thank and acknowledge in both the labs that I was a part of. Thanks to Polona and Olivier for the collaborative efforts in the production of AAVs and for general lab assistance. Without you both, my weekends would have been filled with long journeys for short tasks in the lab! Thanks to Marcela, Tristan, Micha, Margarita, Flo and Leigh for all the help provided for my work at the CDN, the pub trips, coffee breaks, constant snacks and for increased happiness in general!

I would like to acknowledge assistance with some of the data presented in this thesis. I had the opportunity to supervise Niyoti for her master's research project and Daniel for his Erasmus project, who both helped with the production of the Cre-expressing

HEK293 cell line presented in Chapter 3. I am very grateful to Anna, an Erasmus student, who I only knew for a short while before I left the lab. She helped with the *Gad1* ISH for the ablation analysis presented in Chapter 5 and repeating some of the BrdU data presented in Chapter 4.

Special thanks to the other labs at the Wohl and IoP, especially to Cathy Fernandes for lending me equipment for mouse behavioural tests and helping me to perform the pilot testing in Appendix D. Thank you to all those in Deepak Srivastava's lab for help in primary cell culture work and the antibodies "borrowed". Thank you to all in the Wohl for the lunch times and the socials. You all made it such a pleasant and friendly work environment to be part of. During the relentless hours spent in the animal facility, I would like to thank Ted, John and Louis for their dedication and assistance in caring for the mice and for me in times of panic.

This research project has been a steadfast pursuit during four years in which my life has radically changed. I must thank all those outside my "science world" for their support and affection throughout. To my various housemates, especially Esme and Hannah, thank you for bearing with my crazy use of the fridge. Christchurch Kensington is the sole reason I chose to complete a PhD in London. Thank you to all in this adopted family for your love, prayers and friendship over the years. Thank you to my real family for loving me regardless of what path I choose in life. Mum and dad, you are my role models, with your hard work ethic and inexhaustible love for others. You have shown me what it looks like to prioritise people and give time generously.

Chris, thank you for dating, proposing to and marrying a PhD student! Your support has been unconditional and constant. Thank you for the emotional support, the endless cups of tea and the proof-reading. You have made all the transitions over the past years effortless with your loving compromises.

Lastly, I would like to thank God for his work in my life. Soli Deo gloria.

The highest reward for a person's toil is not what they get for it,

but what they become by it.

-John Ruskin

TABLE OF CONTENTS

TABLE OF FIGURES

TABLE OF TABLES

1 INTRODUCTION

1.1 WHAT ARE CEREBELLAR NUCLEI?

The cerebellar nuclei are the final output units for cerebellar processing. For the most part, the nuclear output is a high frequency tonic excitation, which is directed towards the midbrain and thalamus. However, a distinct, long-range inhibitory axon tract allows the cerebellum to influence the activity of the inferior olive, which in turn drives Purkinje cell activity via climbing fibres. Cerebellar nuclear output is modulated by the patterned firing of inhibitory Purkinje cells. They thus form the final common pathway for the integrated activity of a series of nested re-entrant loops via the inferior olive but also via the thalamus, cortex and pons (**Figure 1–1**).

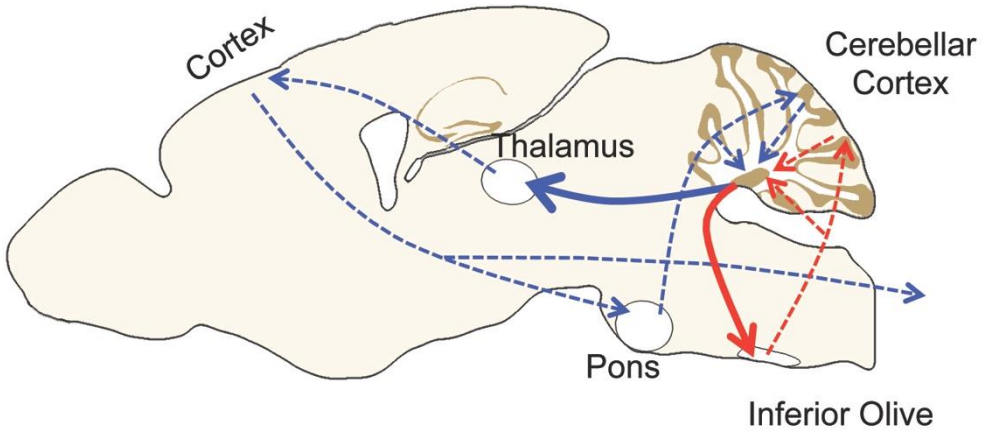

Figure 1–1 The cerebellar nuclei are central to cerebellar circuitry.
They lie at the centre of two cerebellar loops: the cerebello-thalamo-cerebro-cortical circuit (blue) which link the cerebellum back to the cerebral cortex and the olivo-cortico-nucleo-olivary loop (red). (Prekop et al., 2017)

Despite the central position of the cerebellar nuclei within these major long range networks, relatively little is known about their component cell types, the synaptic arrangement of their component interneurons or their processing role. In recent years, significant progress has been made in understanding the development of the

cerebellar nuclear glutamatergic projection neurons, but in reality, the picture is partial and less is known of other, equally significant, nuclear neuronal types and key questions about their specification and lineage remain unanswered. In addition, nothing is known of the factors that regulate nucleogenesis. Major questions remain as to how nuclei achieve their spatial arrangement, integrate cell types of different origins and make connections. For a population of such significance for a wide variety of brain functions this is a major omission.

Models of cerebellar function have traditionally overlooked the cerebellar nuclei, focusing on the cerebellar cortex as the site of cerebellar processing. However, models are increasingly being reconsidered to recognise how plasticity and modulation within the cerebellar nuclei by mossy fibre and climbing fibre collaterals place these cells at the heart of cerebellar networks (Person and Raman, 2012b; Pugh and Raman, 2008). Similarly, while some nuclear disorders in humans have been described, the lack of anatomical and molecular description has hampered a systematic analysis of clinical disorders.

Though cerebellar cortical architecture has been well studied, the circuitry and contribution of the cerebellar nuclei are less well understood. The focus of the current thesis was to better define nuclear cell types, in particular the GABAergic neurons and their connectivity both within the cerebellar nuclei and beyond the cerebellum. By identifying the various cell types and understanding how they are produced in the developing brain, the cerebellar nuclei can be examined functionally as processors to understand how the cerebellum works and how cerebellar defects can result in behavioural deficits. The following sections further describe the

backdrop to the explorations in this thesis, which aims to build on current knowledge of the cerebellar nuclei and its functions.

1.2 STRUCTURE OF THE CEREBELLUM

The cerebellum is a laminar hindbrain derived structure that has been highly conserved throughout evolution. The highly stereotyped cellular organisation of the cerebellar cortex was first characterised in detail by Ramon y Cajal (1911) by studying histological stains to postulate connectivity and cell type. The cerebellum is organised into a simple three layered cortex comprising molecular, Purkinje and internal granule cell layers. Internal to this, cerebellar nuclei are embedded within the white matter.

The majority of cerebellum is comprised of GABAergic and glutamatergic neurons with some glycinergic neurons present. Purkinje cells are the prominent GABAergic neurons of the cerebellar cortex, with their soma making up the Purkinje cell layer, while Golgi cells exist in the granule cell layer and GABAergic interneurons (stellate and basket cells) are found in the molecular layer. Within the granule cell layer are the glutamatergic interneurons: granule neurons and unipolar brush cells (UBCs).

Despite the dense packing of neurons, the circuitry of the cerebellar cortex has long been understood from historical histological observations. Inputs to the cerebellum are of two different kinds: Mossy fibres target the internal layer of excitatory granule neurons. These project parallel fibres into the molecular layer where they synapse with the vast dendritic trees of the inhibitory Purkinje cells. Purkinje cells

also receive inputs from excitatory climbing fibres from the inferior olive, and project to the cerebellar nuclei situated in the white matter (**Figure 1–2**). As well as granule and Purkinje cells, locally interacting inhibitory interneurons and glutamatergic unipolar brush cells participate in local networks within the cerebellar cortex.

From the cerebellar nuclei, two long-range projections connect the cerebellum to the rest of the central nervous system. Separate populations of glutamatergic projection neurons project to the contralateral midbrain, the contralateral hindbrain and the thalamus, the latter comprising a vital link in the assorted cerebello-thalamo-cerebro-cortical circuits which link the cerebellum back to different parts of the cerebral cortex (D'Angelo and Casali, 2013). The nucleo-olivary neuronal projections form part of the olivo-cortico-nucleo-olivary circuit, a closed feedback loop between the inferior olive, cerebellar cortex and cerebellar nuclei, made up at a fine scale of individual closed loops, or cerebellar modules, of local connections via the nuclei (**Table 1-1**) (Fredette and Mugnaini, 1991; Ruigrok, 2011). While this closed nucleo-olivary loop model is challenged by the existence of bilaterally projections from the neurons (Teune et al., 2000; Uusisaari and De Schutter, 2011), it remains a compelling architecture to describe the functional properties of the cerebellar circuit. Other forms of efferent connections have also been found linking the nuclei to the vestibular nuclei and the cerebellar cortex (Bagnall et al., 2009; Houck and Person, 2014).

Table 1-1 Inputs and outputs of the cerebellar modules

Inputs	Corticopontine connectivity	Spinal and trigeminal	Spinal, trigeminal, auditory, visual and vestibular	Vestibular and corticopontine connectivity
Cerebellar cortex	Lateral hemisphere	Intermediate hemisphere	Vermis	Flocculus
Output nuclei	Lateral cerebellar nucleus	Interposed cerebellar nucleus	Medial cerebellar nucleus	Vestibular nuclei
Olivary targets	IOPr IODM	IOM IOD	IOB IOC	IOK IOVL
Glutamatergic projection targets	Motor and premotor cortices (cerebellothalamic and cerebellorubral pathways)	Lateral descending systems (rubrospinal and corticospinal pathways)	Medial descending systems (vestibulospinal, tectospinal and reticulospinal pathways)	Vestibuloocular, vestibulospinal amd vestibulocerebellar pathways
Function	Motor planning and cognition	Conscious motor control of skeletal muscles Regulation of limb muscle tone and movement	Subconscious regulation of balance, posture, reflex activity Eye, head and neck muscle response to visual and auditory stimuli	Subconscious regulation of balance, posture, reflex activity

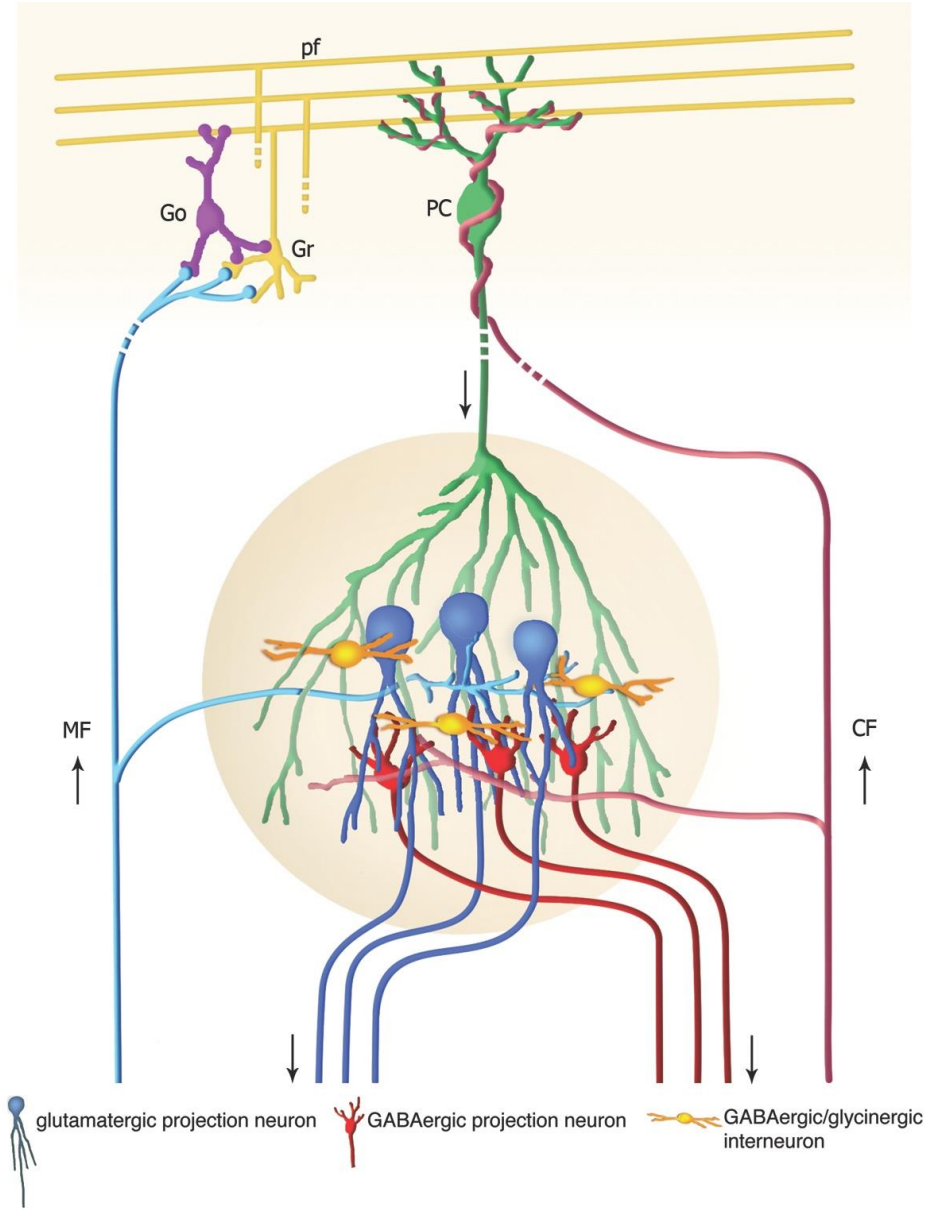

Figure 1–2 The cellular composition of the cerebellar nuclei.

Nuclei receive inputs from the Purkinje cells in the cerebellar cortex (green), as well as collaterals from the mossy fibres (light blue) and climbing fibres (pink) as they travel to the cortex. Within the nuclei, there are two types of projection neuron: large glutamatergic cells (blue), which are efferent cells in the cerebello-thalamo-cerebro-cortical circuits, and the nucleo-olivary neurons (red), which project to the inferior olive, forming the olivo-cerebellar loop. Interneurons (orange) participate in as yet uncharacterised local circuits. (Prekop et al., 2017)

1.3 NUCLEAR CELLS AS COMPONENTS OF MODELS OF CEREBELLAR FUNCTION

1.3.1 CIRCUITRY IS LINKED TO FUNCTION

As the cerebellar nuclei are the sole final output of the cerebellum, the nuclear projection neurons should play key roles in cerebellar function. The inputs to the cerebellar nuclei comprise a complex matrix, modulating cerebellar output by influencing the spontaneous baseline firing rate of nuclear neurons (Heck et al., 2013; Person and Raman, 2011). The most significant of these inputs are Purkinje cells from cerebellar cortical layers directly above the corresponding part of the cerebellar nuclei: the medial receiving input from the vermis, the interposed from the paravermis, and the lateral receiving the bulk of its input from the hemispheric Purkinje cells (Voogd and Glickstein, 1998). Sugihara *et al.* mapped Purkinje cell projections to the various nuclei and found correspondence between adolase C expression in subsets of Purkinje cells and the terminations in specific nuclear subdivisions, demonstrating some conservation of topographic organisation (Sugihara and Quy, 2007).

In addition to afferents from the Purkinje cells, the cerebellar nuclei also receive collaterals from mossy fibres and climbing fibres. These send signals directly to the cerebellar nuclei, bypassing cerebellar cortical processing (Voogd and Glickstein, 1998). In the overlying cerebellar cortex, mossy fibres and climbing fibres are topographically mapped onto granule cells and Purkinje cells and their collateral projections to cerebellar nuclei follow approximately the same topography. Mossy fibres from the pontine nuclei, nucleus reticularis tegmenti pontis and lateral reticular nucleus send their cortical terminations such that they divide the cerebellar

cortex into zones to process information from particular parts of the body or sensory modes (Apps and Hawkes, 2009; Shinoda et al., 1999; Uusisaari and De Schutter, 2011). In contrast, the collaterals of these mossy fibres target the cerebellar nuclei bilaterally and show a looser zonal organisation (Voogd and Glickstein, 1998; Wu et al., 1999). Likewise, anterograde tracing from the inferior olive has revealed a strict topographic alignment of climbing fibres to the zebrin II positive Purkinje cell parasagittal zones in the contralateral cerebellar cortex (Sugihara et al., 2009). The collaterals of these same climbing fibres target the contralateral cerebellar nuclei and terminate in specific areas of the nuclei (Blenkinsop and Lang, 2011; Sugihara and Shinoda, 2007; Sugihara et al., 1999).

The neuronal architecture of the cerebellar nuclei lends itself to functionally integrate and modulate inputs from the cerebral cortex before descending down the brain stem to the spinal cord and peripheral nervous system. The nuclear cells are predicted to take Purkinje cell output and integrate this with inputs from the other afferents to the cerebellar nuclei. Evidence of synaptic plasticity at the cerebellar nuclei shows that the nuclear cells are involved in signal generation, not merely relaying information from the Purkinje cells, but modulating cerebellar cortical output (Morishita and Sastry, 1996; Ohyama et al., 2006; Zheng and Raman, 2010). When Purkinje cell and nuclear neurons are monitored simultaneously, they do not give the expected reciprocal firing rates that would result from Purkinje cell inhibition (Armstrong and Edgley, 1984a, b; McDevitt et al., 1987a, b). Instead nuclear neurons are extremely sensitive to the synchronicity of activity from Purkinje cell inputs (Person and Raman, 2012a), suggesting that the development of

a mapping of Purkinje cell populations into the nuclei is a critical factor in cerebellum function.

1.3.2 CONVERGENT NETWORKS WITHIN THE CEREBELLAR NUCLEI

Relatively little is known of how inputs to the cerebellar nuclei are organised at a cellular level and the intrinsic networks that are built up by interneurons and local collaterals. A natural entry point to these questions is trying to understand the degree of convergence of a relatively orderly Purkinje cell layer on to the three dimensional assembly of nuclear neurons. If a Purkinje cell neuron predominantly innervates one nuclear neuron within its field more than the rest, then heavy fluctuations in the inhibitory postsynaptic potentials (IPSPs) of the recipient nuclear neuron would be expected, since the Purkinje cell would exert a greater dominance over the outcome of that neuron. On the other hand, if many Purkinje cells have equal contribution on the one nuclear neuron, the signal from any one Purkinje cell will be dampened by the noise of the many inputs; this would lead to low levels of fluctuations.

The latter has been shown to occur in electrophysiological recordings of nuclear neurons (Uusisaari and De Schutter, 2011). It should be noted that most of the electrophysiology research on the cerebellar nuclei has been done on the large glutamatergic projection neurons, as these are the most easily identified. In terms of numbers, there are around 20 Purkinje cell to every nuclear neuron (Person and Raman, 2012b; Sultan et al., 2002) with inputs targeting both glutamatergic (Aizenman et al., 2003; Matsuno et al., 2016) and GABAergic projection neurons (Teune et al., 1998). However, since the Purkinje cell axonal target field is wide and

conical (Chan-Palay, 1973a), it is estimated that each Purkinje cell can encompass tens of nuclear neurons complicating a simple explanation of convergence. Similarly the proximity of axons terminations to the soma is likely to be of considerable significance in determining synaptic strength (De Zeeuw and Berrebi, 1995). Chan-Palay noted that around 14% of larger neurons in the lateral nucleus were not innervated directly on their soma by Purkinje cells, setting apart a subset of projections neurons (Chan-Palay, 1973d), which may comprise the glycinergic, nucleo-cortical neurons (Uusisaari and Knöpfel, 2010).

It is known that the cell types in the cerebellar nuclei are mostly highly spontaneously active with unusually high resting membrane potentials (Uusisaari and De Schutter, 2011). The inhibitory input into the cerebellar nuclei from the Purkinje cells thus works to modulate this intrinsic firing. The current theory is that many Purkinje cells synapse onto each nuclear neuron, providing tonic inhibition by the simple spiking of Purkinje cells (Blenkinsop and Lang, 2011; Uusisaari and De Schutter, 2011). Each individual simple spike contributes little to the outcome of the nuclear neuron, but when many simple spikes are synchronised, the overall effect from many specialised Purkinje cells will result in a stronger depression of the nuclear neuron. In addition, climbing fibre signalling onto Purkinje cells evoke complex spikes. These complex spikes also depress nuclear neurons strongly, even when they are unsynchronised, unlike the simple spikes (Blenkinsop and Lang, 2011).

The electrophysiological properties of nuclear cells are for the most part, very similar (Czubayko et al., 2001). The cells are known to have a physiological

property called rebound spiking wherein the intrinsic firing rate increases following release of suppression (Shin and De Schutter, 2006). Therefore, a synchronous pause of Purkinje cell firing would lift the inhibition and generate rebound firing in the nuclear neurons. This rebound firing has been shown to correlate well with graded activation of Purkinje cells and can regulate the timing and extent of muscle contractions (Witter et al., 2013). However, the nucleo-olivary neurons may not exhibit rebound firing properties (Najac and Raman, 2015).

Whilst considerable speculation has been directed to the role of Purkinje cells, the influence of collateral afferents on the activity the cerebellar nuclei is largely unknown. Lu *et al.* (2016) found that activation of the inferior olive caused inhibition of nuclear neurons, showing that indirect climbing fibre influence via the inhibitory Purkinje cells exceeds the direct activation given to nuclear cells by excitatory climbing fibre collaterals. More work remains to be done to understand if there is convergence of different afferents onto a single nuclear neuron, and whether specific cell types are targeted more than other. There is currently no reliable way to differentiate between the cell types apart from size and neurotransmitter release, and yet it has been shown that the somatic sizes of the various types of cells overlap extensively, raising queries regarding the studies that have relied on soma size to differentiate neuronal subtypes (Uusisaari et al., 2007).

Taking the characteristics of these cellular components into account, the circuitry of the cerebellum has been modelled to make sense of the functional phenotypes seen in patients with cerebellar defects and experiments where cerebellar circuitry has been disrupted. The cerebellum is well known for its role in motor learning, fine-

tuning of movement, movement coordination and other sensory-motor processing (Buckner, 2013). These functions centre on the cerebellar circuitry loops mentioned above. acting as feed-back and feed-forward systems. Three main functions of the cerebellum are reviewed below: its role in motor learning, motor timing, and non-motor cognition.

1.3.3 CEREBELLAR ROLE IN MOTOR LEARNING

Cerebellar motor learning has mainly been examined using associative learning exercises where a conditioned Pavlovian response is acquired through the repeated pairing of an unconditioned stimulus with a conditioned stimulus. This learning requires feedback control and it has long been theorised that climbing fibres relay the signal for unconditioned stimuli, while mossy fibres relay the signal for conditioned stimuli. Both these fibre pathways then converge in the cerebellar cortex, where long term potentiation or depression occur based on the timing of these two signals (Albus, 1971; Hesslow and Ivarsson, 1996; Ito, 2001; Marr and Thach, 1991; Rasmussen and Hesslow, 2014). While the Purkinje cells make synapses with tens, if not hundreds of thousands passing parallel fibres, each Purkinje cell only receives input from a single climbing fibre with a low firing rate, all-or-nothing response. The mossy fibre input provides a graded input and modulates the constant single-spike Purkinje cell firing rate, while an action potential from a climbing fibre can override single-spike firing and produce a complex spike (Harvey and Napper, 1991). It is thought that the climbing fibre signal “teaches” while the Purkinje cells compare the two inputs and learn through synaptic plasticity at the parallel fibre-Purkinje cell synapse.

Interestingly, it has since been shown that plasticity at this junction is not necessary for motor learning (Schonewille et al., 2011), and furthermore, that plasticity also exists between interneurons of the cerebellar cortex and parallel-fibres (Jörntell et al., 2010). Thus motor learning is complex, beyond the one site of Purkinje cell plasticity. Given the complementary roles the mossy fibres and climbing fibres are thought to have in motor learning models, these direct afferents into the cerebellar nuclei appear to provide a direct short-cut to modulate the final cerebellar output. Therefore the role of cerebellar nuclei in motor learning needs to be explored (De Zeeuw and Ten Brinke, 2015). The fact that nucleo-olivary neurons provide GABAergic feedback to inferior olive, the source of climbing fibres, has led to theories about their role in motor learning (Andersson et al., 1988; Medina et al., 2002; Rasmussen and Hesslow, 2014).

The conditioned eyeblink response, also known as the nictitating membrane reflex, is a commonly used behavioural paradigm to look at associative motor learning. Acquisition, extinction and reacquisition of conditioned responses were studied following lesions or chemical inactivation in the cerebellar cortex, cerebellar nuclei and inferior olive (Mccormick et al., 1981; McCormick et al., 1985; Yeo et al., 1985). These studies are the basis of the current understanding about the role of the olivo-cerebellar modules in motor learning. Specifically in the cerebellar nucleus, McCormick *et al.* (Mccormick et al., 1981; McCormick and Thompson, 1984) found that lesions of the interposed and lateral nuclei abolished learned conditioned responses and prevented acquisition of learning in naïve animals. Over the last few decades, the region involved in the paradigm has been localised to an area in the dorsolateral portion of the contralateral anterior interposed nucleus. While only

small areas of the cerebellar cortex and nucleus are dedicated to the conditioned eyeblink response, it is assumed that the specific connectivities of each cerebellar module are responsible for various modes of motor function using similar processes.

1.3.4 CEREBELLAR ROLE IN MOTOR TIMING

It is known from human patient data that the cerebellum plays a part in timing of motor tasks since those with cerebellar atrophy or lesions show a larger variability in motor timing compared to controls (Torriero et al., 2007), but that not all temporal aspects of motion are abolished (Buhusi and Meck, 2005; Schaal et al., 2004; Spencer et al., 2003). So the cerebellum acts to some extent as an internal clock (Ivry and Spencer, 2004). It has been proposed that the role of the cerebellum during timing may involve feed-forward control, using past experiences to predict future output to result in a faster, more automated movement (Ohyama et al., 2003).

Much of the motor timing theory focuses on the synchronising properties of olivary cells. The olivary cells that send climbing fibres up to the cerebellum have gap junctions so the cells can be electrically coupled (Llinas et al., 1974; Sotelo et al., 1974). Each cell also displays the spontaneous generation of subthreshold oscillations that oscillate at a frequency of around 10 Hz (Blenkinsop and Lang, 2006; Lampl and Yarom, 1997; Llinás, 2011). These fluctuations in resting membrane potential enable rhythmic action potentials that are more likely to spike near the AP threshold; coupled cells then exhibit synchronous firing. This synchronicity is displayed in the cerebellar cortex as Purkinje cells also show synchronous complex spiking. Thus the cerebellum and infer olive are inextricably linked.

The Purkinje cells are able to exhibit synchronous firing of complex spikes, controlled by strong synaptic input from the climbing fibres (De Schutter and Steuber, 2009; Lang et al., 2006; Lang et al., 1999; Welsh et al., 1995). Due to this fact, the climbing fibres can also be considered as a timing signal and, together, the cerebellar-olivary connectivity may be involved in timing of motion, time-related error correction, and the onset of movements. The cerebellar nuclei play an important feedback role in the olivo-cerebellar loop, which sends feedback from the Purkinje cells to the olivary cells to adjust the climbing fibre signals (Kazantsev et al., 2004; Lefler et al., 2013). Studies that have shown that the nucleo-olivary feedback onto the olivary cells can decrease firing rates and reduce coupling and thus spike synchrony (Lefler et al., 2014).

1.3.5 NON-MOTOR FUNCTIONS OF THE CEREBELLUM

In the last two decades, neuronal tracing techniques (Middleton and Strick, 1994) and brain imaging analysis (Stoodley et al., 2012) showing cerebellar connections with non-motor cortical areas have implicated a role in cognition as well as motor control; in error-prediction, working memory, language and attention (Ito, 2008). In both humans (Kipping et al., 2013) and non-human primates (Kelly and Strick, 2003; Strick et al., 2009), cerebellar loops to the pre-frontal cortex have been shown to exist (Dum et al., 2002; Middleton and Strick, 2001). While the cerebello-cortico projections are from the glutamatergic projection neurons, the cerebello-olivary modules will no doubt play important roles in modulating the final output of these excitatory projections as they form recurrent loops that influence all cerebellar processing.

Behaviourally, higher cognitive dysfunctions are seen alongside motor deficits in patients subjected to cerebellar damage (Schmahmann, 2010; Schmahmann and Sherman, 1998). In animal models, this has been shown to be true using CHD7 mice, a model of the human CHARGE syndrome. The mutation causes vermal hypoplasia via changes in expression of transcription factor *Otx2* at the midbrain-rhombomere 1 boundary (Yu et al., 2013), leading to cognitive deficit. In particular, there is growing evidence that developmental changes in the cerebellum are linked to the cognitive defects displayed in autism spectrum disorder (ASD). Damage to specific cerebellum regions are associated with ASD-like symptoms and these regions are distinct from other regions that cause ADHD or developmental dyslexia (Stoodley, 2014).

1.4 NUCLEUS ANATOMY AND CELLULAR DIVERSITY

The earliest descriptions of cerebellar nuclear neurons distinguished cells with long axons from those with short axons (Saccozzi, 1887) and identified large and small soma size (Lugaro, 1895). The most detailed morphological studies of the rat and primate dentate (lateral) cerebellar nucleus were carried out by Victoria Chan-Palay in the 1970s. Using Golgi, Nissl and Weigert preparations combined with electron microscopy, she mapped out the complex, non-uniform cellular organisation of the nucleus (Chan-Palay, 1973b, c; Chan-Palay, 1977) and demonstrated the presence of two types of projection neurons with at least three different types of cells with short axons and small soma. These latter neurons were designated as local interneurons on the basis of dendrite and axon morphology and could be distinguished by their multipolarity or bipolarity and fusiform soma.

Based on neurotransmitter content and neuronal connectivity, at least six distinct populations have been identified: large glutamatergic projection neurons, GABAergic projection neurons, glycinergic projection neurons and various types of interneurons (**Figure 1–2**) (Batini et al., 1992; Chen and Hillman, 1993; Fredette et al., 1992; Fredette and Mugnaini, 1991). More information on each cell type is described below, though it is still unknown how the cell types work together to integrate the diverse nuclear inputs from Purkinje cells and mossy and climbing fibre collaterals. There is thought to exist a complex intrinsic network connected by the local neurons as well as collaterals from the cerebellar nuclei projection neurons.

1.4.1 GLUTAMATERGIC PROJECTION NEURONS

The excitatory glutamatergic projection neurons innervate the red nucleus, thalamus, or brainstem, and are the largest neurons in the cerebellar nuclei. Due to their size, it is thought that much of the electrophysiological work done on the cerebellar nuclear cells indiscriminately target these cells over other cell types (Uusisaari et al., 2007). They are known to fire spontaneously at high frequencies, modulated by inhibitory signals received directly from the Purkinje cells. Their dendritic trees are extensive and target various extracerebellar targets. The glutamatergic projection neurons also synapse with climbing fibre and mossy fibre collaterals, and may communicate with local interneurons. The large sizes of these cells make them easily distinguishable. Uusisaari *et al.* simply refer to these cells as the GAD^- large cells. They have also been shown to express VGlut2, but not VGlut1 (Bagnall et al., 2009). The glutamatergic projection neurons fit the description of the “large columnar cells” mentioned in Chan-Palay's seminal work (Chan-Palay, 1973b, c), which lie in the

central region of the lateral nucleus and have a distinctive elongated cell soma that have radial orientation so that the axes gather towards one point.

1.4.2 NUCLEO-OLIVARY PROJECTION NEURONS

The GABAergic nucleo-olivary projection neurons are small cells which target the inferior olive (De Zeeuw et al., 1997; Fredette and Mugnaini, 1991; Mugnaini and Oertel, 1985; Ruigrok, 1997; Teune et al., 1998). The olivo-cerebellar circuitry is important for cerebellar function models but still, not much is known about these nucleo-olivary cells in terms of their properties. Like the glutamatergic projection neurons, they fire spontaneously but at a lower frequency. It's not known how their firing is modulated by nuclear afferents but they also receive signals directly from the Purkinje cells (Teune et al., 1998). The nucleo-olivary cells have been identified using GAD67-EGFP mice (Uusisaari et al., 2007). The GAD67 positive cells were studied for their morphological and electrophysiological properties. Uusisaari *et al.* came to the conclusion from the shallow frequency to current relationship, and their frequency adaptation that these cells are relaying information about phase shift rather than firing rate information.

1.4.3 GLYCINERGIC PROJECTION NEURONS

Glycinergic cells are long been noted in the cerebellar nuclei (Bäurle and Grüsser - Cornehls, 1997; Chen and Hillman, 1993; Chung et al., 2009) though only recently have they been further characterised. Using a GlyT2-EGFP transgenic mouse line, two types of glycinergic projection neurons have identified (Bagnall et al., 2009; Uusisaari and Knöpfel, 2010). The first type exists exclusively in the medial nuclei and is large, spontaneously active glycinergic neurons that project to the ipsilateral

vestibular nuclei and reticular neurons of the medulla. These cells have many parallels with the glutamatergic neurons in terms of their size and firing properties, only the glutamatergic projection neurons of the medial cerebellar nuclei project to the contralateral vestibular nuclei.

The second glycinergic neuronal type is found in the lateral cerebellar nuclei and projects to the cerebellar cortex. They most likely target Golgi interneurons, which express glycine receptors, unlike most cells of the granule cell layer (Uusisaari and Knöpfel, 2011). Unlike the other cerebellar nuclei cell types, these nucleo-cortical cells do not fire spontaneously and so are intrinsically silent (Uusisaari and Knöpfel, 2010). It is not known what function these nucleo-cortical connections perform, but their existence points to yet another feedback loop that should be considered in cerebellar function models.

1.4.4 INTERNEURONS

Relatively little is known about the local interneurons. Chan-Palay (1973c) noted small GABAergic neurons with fusiform or multipolar somas, limited dendritic trees and short axons, but it is possible that some of the cells observed could be the small nucleo-olivary neurons. Studies working with the GlyT2-EGFP mice or GlyT2 immunochemistry have also found smaller glycinergic cells in the lateral and interposed cerebellar nuclei. Because glycinergic terminals are found mainly on adjacent, presumptive glutamatergic projection neurons, it has been suggested that these are interneurons (Bagnall et al., 2009; De Zeeuw and Berrebi, 1995), which colocalise with GABA (Chen and Hillman, 1993). GABAergic terminals that did not

derive from Purkinje cells are also indicative of GABAergic interneurons or possibly local collaterals from the nucleo-olivary neurons.

Though it is not possible to differentiate nucleo-olivary neurons from other nuclear GABAergic cell types based on size, there are some electrophysiological differences that aid identification (Uusisaari and Knöpfel, 2012). From electrophysiological work done with GAD67-EGFP transgenic mice, at least two groups of local interneurons are thought to exist, which are characterised by their different electrophysiological properties. The first group provide local inhibition but it is still unclear whether these cells are GABAergic or glycinergic, or both since electrophysiology using Gad67-EGFP and GlyT2-EGFP mice gave very similar results (Uusisaari and Knöpfel, 2010). Studies have concluded that small GABAergic and glycinergic neurons of the cerebellar nuclei are partially overlapping neuronal populations, so that there may be $GABA^{+}/Glycine^{-}$ cells, $GABA^{+}/Glycine^{+}$ cells and $GABA^{-}/Glycine^{+}$ cells (Chan-Palay, 1977; Chen and Hillman, 1993; Husson, 2015; Sultan et al., 2002; Uusisaari and Knöpfel, 2010).

A second group of non-GABAergic interneurons have been discovered, with firing properties that differ from the GABAergic/glycinergic interneurons mentioned above, with faster intrinsic firing rates (Uusisaari and Knöpfel, 2008). These were first noted by Uusisaari and colleagues as small Gad67 negative cells that are distinct from large Gad67 negative cells, which are the glutamatergic projection neurons. So far, their electrophysiological profile has not matched with any other type of local interneuron, and it has been suggested that these could be glutamatergic local neurons (Uusisaari and Knöpfel, 2010). Husson *et al.* (2014) also found that

these small glycinergic neurons are distinct from nucleo-olivary neurons. However, not much is known about their role in cerebellar nuclei circuitry, besides that they receive signals from the cerebellar cortex directly.

1.5 DEVELOPMENT OF THE CEREBELLUM

The origins of the cerebellum, which sits at the boundary of the midbrain and hindbrain, were an intensely investigated problem at the end of the last century. The advent of molecular techniques revised the concept that the cerebellum received contributions from both midbrain and hindbrain and identified the cerebellar anlage within the dorsal part of rhombomere (r)1 of the anterior hindbrain (Millet et al., 1996; Wingate and Hatten, 1999; Zervas et al., 2004). This region is set up by secreted molecules, such as Fgf8, BMP and Wnts from the isthmic organiser and adjacent roof plate, and by transcription factors *Otx2*, *Gbx2*, *Pax* genes, and *Lmx1b* (Chizhikov et al., 2006; Chizhikov et al., 2010; Sotelo, 2004).

Within the r1, all the cell types of the cerebellum arise from two germinal regions: the ventricular zone (VZ) and the rhombic lip (RL) (**Figure 1–3**). The ventricular zone is a neuroepithelial zone that lines the dorsolateral part of the fourth ventricle (Hoshino et al., 2005; Pascual et al., 2007). The cerebellar (rostral) rhombic lip is the interface region between the roof plate of the fourth ventricle and the adjacent neuroepithelium (His, 1890; Wingate, 2001). These two distinct progenitor zones are defined by the mutually exclusive expression of basic helix-loop-helix (bHLH) transcription factors *Ptf1a* and *Atoh1* (Wingate, 2005). Ptf1a is expressed in the ventricular zone and characterises progenitors of GABAergic cells (Hoshino et al., 2005). The rhombic lip conversely expresses *Atoh1* (Ben-Arie et al., 1997). This

highly proliferative zone of Atoh1 induction gives rise to glutamatergic cerebellar neurons (Machold and Fishell, 2005; Wang et al., 2005).

The production of different cellular subtypes is temporally controlled (**Figure 1–3**), with the first neurons to be produced in the embryonic cerebellum being the glutamatergic nuclear projections neurons (E10.5-E12.5 in mice) (Leto et al., 2006) from the rhombic lip. The rhombic lip progenitor cells subsequently produce granule cell precursors that populate the external granule layer (EGL) (Machold and Fishell, 2005; Wang et al., 2005). These produce the unipolar brush cells in late embryonic stages and, postnatally, the numerous granule cells through transit amplification (Ben-Arie et al., 1997; Englund et al., 2006). The rhombic lip progeny migrates across the dorsal surface of rhombomere 1 via the subpial rhombic lip migratory stream (RLS). The cerebellar nuclear cells congregate at the nuclear transitory zone (NTZ) while for the later born cells, the subpial rhombic lip migratory stream is replaced with the external granular layer (EGL). It is not known what signals the temporal switch in mammals between the rhombic lip production of nuclear neurons, and granule cells and unipolar brush cells. One difference is that Atoh1 expression is switched off in nuclear neurons as they leave the rhombic lip, while granule cell progenitors produced afterwards retain Atoh1 expression even after they have left the rhombic lip. This seems to play a role in facilitating the proliferation during transit amplification of the EGL (Butts et al., 2011).

Similarly, GABAergic nuclear projections neurons are presumed to be born from the ventricular zone at around E10.5-E12.5 in mice (Leto et al., 2006), followed shortly by GABAergic Purkinje cell projection neurons (E11.5-E13.5) (Fink et al., 2006;

Machold and Fishell, 2005; Wang et al., 2005). *Olig2* expression marks out early ventricular zone derivatives that become cerebellar GABAergic nuclear neurons and Purkinje cells. The distribution of *Olig2* changes over time to be taken over by *Gsx1* expression marking interneuron progenitors that are late born (Seto et al., 2014). From E13.5-P15, GABAergic interneurons arise from *Pax2*+ precursors in the ventricular zone that subsequently spreads and divides through the cerebellar white matter (Maricich and Herrup, 1999; Weisheit et al., 2006).

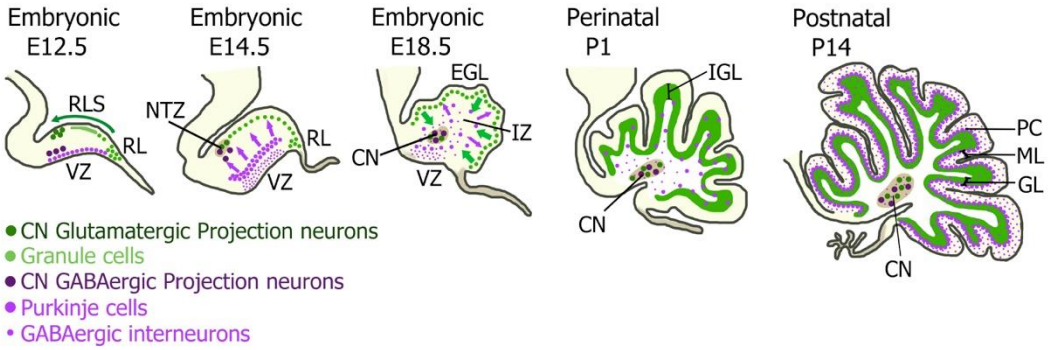

Figure 1–3 The developmental timeline of the cerebellum.

The cerebellar primordium depicted in sagittal view over the developmental timeline. GABAergic neurons are derived from the ventricular zone (VZ) while glutamatergic neurons arise at the rhombic lip (RL). The cerebellar nucleus projection neurons are the first born from both progenitor zones, preceding first Purkinje cells (VZ-derived) and then granule cells (RL-derived). Cerebellar nucleus interneurons are believed to be born alongside other cerebellar cortical interneurons, which are generated from E13 from the VZ and later a stem cell population within the future white matter. (Prekop et al., 2017)

1.6 DEVELOPMENT OF CEREBELLAR NUCLEI

Birth-dating has shown that some neurons within the cerebellar nuclei are among the first born cell types of the cerebellum (Altman and Bayer, 1978). Experiments using either BrdU or a replication defective adenovirus (Hashimoto and Mikoshiba, 2003) have shown that Purkinje cells are born around the same time as the early-born nuclear neurons. The time window for the production of glutamatergic and the GABAergic projection neurons in mice lies between E10.75-E12.5 (Elsen et al.,

2013) and appears to be regulated by a common temporal signal (Yamada et al., 2014). However, the allocation of GABAergic versus glutamatergic fate is strictly a property of progenitor position within either a *Ptf1a*- and *Atoh1*-positive pool (Hoshino et al., 2005; Machold and Fishell, 2005; Pascual et al., 2007; Wang et al., 2005; Yamada et al., 2014).

Though the birthdates of some cerebellar nuclear cells are known, there are more gaps in the knowledge of cerebellar nuclei development compared to their cortical counterparts. This has been in part, due to the less characterised cell types of the nuclei and especially the failure to distinguish the various nuclear cell types in developmental investigations. The glutamatergic nuclear projection neurons are the most well-researched cell type in terms of development, owing to the discovery of specific genetic markers Tbr1 and Lhx2/9 (Bulfone et al., 1999; Bulfone et al., 1995; Engelkamp et al., 1999; Fink et al., 2006).

1.6.1 ORIGIN OF GLUTAMATERGIC NEURONS

One key motif of cerebellar nuclei development is the assembly of neurons within an embryonic nuclear transitory zone (NTZ), which appears as almost a "staging post" in the formation of distinct cerebellar nuclei (**Figure 1–3**). The NTZ is thought to be a transient differentiation zone (Altman and Bayer, 1985), where nuclear neurons are defined by specific, temporally restricted, developmental transcription factor profiles (Fink et al., 2006). The derivation of glutamatergic projection neurons initially appeared to be via a radial migration from the ventricular zone (Altman and Bayer, 1985), but it is now known that the glutamatergic neurons are all derived from the rhombic lip (Wang et al., 2005). An initial detailed analysis of postmitotic

precursors of nuclear neurons identified the expression of the transcription factors *Lhx2/9*, *Meis1*, *Meis2,* and *Irx3,* as well as genes that are not frequently used as markers in development: *Gja9, Mbd2*, *Htr3a,* and *Girk4* (Morales and Hatten, 2006). Subsequent analyses showed that *Meis2* co-expresses with *Lhx2/9* in glutamatergic projection neurons of the lateral nuclear derived from the rhombic lip (Wang et al., 2005), while *Irx3* may instead represent a separate population of neurons, likely the GABAergic nucleo-olivary neurons (Yeung et al., 2016).

Glutamatergic projection neurons represent the first cohort in a sequence of neurogenesis from the rhombic lip that ends with the generation of granule cells (Machold and Fishell, 2005; Wang et al., 2005; Wingate and Hatten, 1999). A separate domain of *Atoh1* expression at the midbrain-hindbrain boundary gives rise to earlier born extracerebellar neurons (Green et al., 2014). At the rhombic lip, the different cerebellar nuclei are born sequentially in discrete temporal waves, with the most lateral being born first then becoming more medial. Glutamatergic projection neurons actively migrate from the rhombic lip into the RLS guided by diffusible netrin and slit proteins (Alcantara et al., 2000; Gilthorpe et al., 2002). The cells sequentially express *Pax6*, *Tbr2*, *Tbr1* and *Lmx1a* (Fink et al., 2006; Yeung et al., 2016) as they are born and the expression of these genes can be used to identify cellular commitment to a specific cell type. As the post-mitotic nuclear neurons enter the NTZ, *Tbr1* is upregulated and *Pax6* is downregulated (Fink et al., 2006). In *sey/sey* mutant mice that are *Pax6* null, rhombic lip derived nuclear neurons are absent from the cerebellum (Yeung et al., 2016).

The differential retention of some transcription factors, as well as the heterochronic shifts of others define particular nuclei and their efferent connectivity (Fink et al., 2006). The LIM-homeodomain gene *Lhx9* is expressed in the earliest born cells that become lateral glutamatergic projection neurons in the mouse and cells of the extra-cerebellar nuclei in chick, which do not develop lateral nuclei (Green and Wingate, 2014). Since thalamic connections appear to be restricted to these cells, *Lhx9* may play a part in specifying thalamic axon trajectory (Green and Wingate, 2014; Rose et al., 2009). The *Lhx9* expression declines when *Tbr1* expression begins to define a separate nucleus. *Tbr1* expression is retained until E14.5 for lateral and interposed nuclei, and into adulthood for the medial nucleus. In contrast, the lateral and interposed glutamatergic projection neurons express *Brn2* at early postnatal stages (Sugitani et al., 2002).

1.6.2 ORIGIN OF GABAERGIC PROJECTION NEURONS

The developmental origins of the GABAergic nucleo-olivary neurons are more enigmatic. It is assumed that they are born from the *Ptf1a*-expressing ventricular zone like other GABAergic cell types of the cerebellum, although direct evidence for this is lacking. Like the glutamatergic projection neurons, GABAergic neurons are likely to arise as part of a discrete temporal window of cell production. It is thought that the nucleo-olivary neurons are first in a ventricular zone temporal lineage (Kim et al., 2011) that subsequently gives rise to Purkinje cells (E10.5-E12.5 in mouse) followed by other GABAergic interneurons (Sudarov et al., 2011). In contrast to these later born cell types, both Purkinje cells and GABAergic nucleo-olivary neurons express *Neurog2* (Florio et al., 2012). Post-mitotic cells expressing *Neurog1* may also be candidate nucleo-olivary projection neurons (Zordan et al.,

2008). Irx3 immunopositive cells are evident in the ventricular zone from E10.25 to E12.5, the NTZ at E13.5 and by E15.5 the cells have migrated into an intermediate zone outside the NTZ (Morales and Hatten, 2006; Yeung et al., 2016). Irx3 expression persists in the sey/sey ("small eye" pax6 null) cerebellum confirming that the specification of GABAergic and glutamatergic neurons is independent of each other.

1.6.3 ORIGIN OF OTHER NUCLEAR NEURONS

Ventricular zone progenitors require the expression of *Ptf1a* for GABAergic specification, rather than defaulting to a granule cell or extra-cerebellar fate (Hoshino et al., 2005; Pascual et al., 2007). Within the ventricular zone, combinatorial genes expression demarcates discrete germ zones that are thought to give rise to the different types of cerebellar interneurons including nuclear interneurons (Chizhikov et al., 2006; Leto et al., 2012; Lundell et al., 2009; Mizuhara et al., 2010; Morales and Hatten, 2006; Sillitoe and Joyner, 2007; Sudarov et al., 2011; Zordan et al., 2008). Thus, for example, *Neurog1* and *Neurog2* expression defines subsets of the *Ptf1a*$^{+}$ ventricular zone population.

However, this topographic explanation of diversity is complicated by evidence that proliferation continues within a single population of *Pax2*$^{+}$ precursors from the ventricular zone (Maricich and Herrup, 1999) that persists in the prospective white matter well into post-natal development in mice. Heterotopic and heterochronic grafting experiments have found that *Pax2*$^{+}$ progenitors generate all the remaining inhibitory interneurons (Leto et al., 2006; Maricich and Herrup, 1999), including *Neurog1* (*Ngn1*)-positive interneurons of the cerebellar nuclei, which are born at E17.5 in mice (Obana et al., 2015). Mutation of Purkinje cell progenitor

transcription factors *Olig2* and *Gsx1* disrupt the production of *Pax2* lineages suggesting that the latter is derived from the former in development (Seto et al., 2014).

The origin and development of the various types of glycinergic projection neurons and interneurons in the nuclei have yet to be characterised. A subset of $Tbr1^+$ neurons in late gestation (E17.5) also express calretinin and these cells were shown to be medial nucleus projection neurons that project to the contralateral medial nucleus (Fink et al., 2006). On performing retrograde tracing, it was found that not all contralateral connections are from $Tbr1^+$ cells. In addition, the $Tbr1^+$ cells project to the ipsilateral vestibular nuclear and spinal cord but not to the contralateral red nucleus. This partially fits the description for the glycinergic projection neurons in the adult medial nucleus. Also, *Zac1* is expressed in the ventricular zone and the cortical transitory zone by E12, and then continues to be expressed in postmitotic neurons that end up in the medial cerebellar nuclei. These cells are GABAergic and small in size, though it is unclear whether they are interneurons or projection neurons.

1.6.4 NUCLEOGENESIS AND CELL MIGRATION

The varying developmental origins of different nuclear cell types require cells to recognise each other and assemble nuclei distant from their origins. How nucleogenesis - the migration, organisation and synaptogenesis of nuclear neurons – is achieved is unknown. Clearly, either intrinsic programming or cues in the surrounding environment or a combination of both will be key factors in this developmental process.

For rhombic lip derivatives, unipolar neuroblasts move within a sub-pial stream towards the NTZ guided by both diffusible netrin and slit (Alcantara et al., 2000; Gilthorpe et al., 2002). However, the cues that determine the position of the NTZ itself are unclear. One possible determinant is the underlying axon scaffold of the fasciculus uncinatus, to which first-born nuclear cells then contribute (Gilthorpe et al., 2002; Green et al., 2014). Changing the fate of nuclear neuroblasts blurs the boundaries between distinct populations in the NTZ but it does not compress or expand the map of presumptive nuclei. Thus, when either *Lhx9*, which specifies the lateral nucleus in mice, is overexpressed in chicks (Green and Wingate, 2014) or *Tbr1* is knocked down in mice (Fink et al., 2006), the total number of neurons remains similar but boundaries between populations become less discrete. From the NTZ, cells are then incorporated into the white matter through what might constitute an active radial migration or a passive translocation as a consequence of the overall pattern of cerebellar morphogenesis (Altman and Bayer, 1985; Elsen et al., 2013).

Evidence in favour of active radial migration being a component of nucleogenesis comes from the analysis of the *reeler* mutant mouse, which has cerebellar malformations dues to a deficiency in reelin, a protein that is involved in the migration of other cerebellar cell types (Rice and Curran, 2001). Neuroblasts that migrate from the rhombic lip are $Pax6^{+}$/$Reelin^{+}$ but the NTZ develops normally in the *reeler* mice, showing reelin is not essential in the RLS migration (Fink et al., 2006; Miyata et al., 1996). In contrast, the shape of the medial cerebellar nucleus is distorted at birth in the *reeler* mice. Therefore, reelin may be involved in the nucleogenesis of cerebellar nuclei after the cells gather at the NTZ.

In terms of circuit development, much of the research on the formation of the olivo-cerebellar circuitry has focused on the matching of climbing fibre to Purkinje cells. How the Purkinje cell axons are developmentally matched to cerebellar nuclear targets and the mechanisms that regulate mapping are unknown. Similarly, how the topography of collateral projections from different afferent populations is coordinated within the nucleus is an important question that remains to be addressed. It has been suggested that climbing fibre and mossy fibre collaterals form a template for topographic refinement of outputs of Purkinje cells to the cerebellar nuclei (Najac and Raman, 2017; Reeber et al., 2013).

1.6.5 Evolution and the diversification of cerebellar nuclei

While some aspects of the cerebellar circuit are among the most evolutionarily conserved across vertebrates, cerebellar nuclei are relatively variable in composition (Butts et al., 2011). There is some debate over whether an organism is considered to have cerebelloid structures if they lack cerebellar nuclei, since it is these cells that form the dominant output (Marzban et al., 2015). For example, teleost fish have no white matter or cerebellar nuclei. Instead, their Purkinje cells project to eurydendroid cells, which then project to other parts of the brain. However, eurydendroid cells also receive inputs from granule cells via parallel fibres and are found within the granule cell layer and so are not homologous to nuclear projection neurons in terms of inputs (Hashimoto and Hibi, 2012; Murakami and Morita, 1987).

The replacement of cerebellar nuclei by eurydendroid cells appears to be an ray-finned fish adaptation as there is evidence for a single cerebellar nucleus in the shark (Ebbesson and Campbell, 1973). Cerebellar nuclei are absent in lampreys, where the cerebellum is reduced or absent. Across fish species, the medial and dorsal octavolateral nuclei receive inputs from lateral line systems and are involved in spatial calculations that are analogous to those carried out in the cerebellum. It seems conceivable, though yet to be proved, that these may be considered as ontological homologues of cerebellar nuclei (Butler and Hodos, 2005).

Like sharks, amphibians have a single cerebellar nucleus, however the number and diversity of cerebellar nuclei increases in amniotes. There are two cerebellar nuclei in birds (Arends and Zeigler, 1991) and three sets of cerebellar nuclei in rodents: the medial, interposed and lateral (Goodman et al., 1963; Korneliussen, 1968). In cats, rabbits and primates, there are four major cerebellar nuclei: the medial, or fastigial, nucleus; the anterior and posterior interposed; and the lateral, or dentate, nucleus. Each of these nuclei can be functionally further subdivided such that complexity of cerebellar nuclear organisation is a marked feature of mammalian brains (De Zeeuw and Berrebi, 1995). This systematic variation in organisation suggests that comparative studies may offer an important insight into the significant genetic factors in the development of cerebellar nuclear diversity.

1.7 CEREBELLAR NUCLEI AND DISEASE

The relatively recent discoveries of the developmental lineages of cerebellar neurons highlight previously unexplored relationships in cerebellar disorders and disease. Glutamatergic neurons are formed from *Atoh1*$^{+}$ progenitors that not only generate

granule cells but also neurons in the pons, vestibular and auditory systems of the hindbrain (Wang et al., 2005; Wingate, 2001). Meanwhile, GABAergic neurons share a *Ptf1a*$^{+}$ progenitor transcriptional profile with auditory nuclei and, perhaps most prominently, the inferior olive (Hoshino et al., 2005).

This is particularly significant since developmental disorders where the cerebellar nuclei are exclusively malformed are rarely reported. Congenital dysplasia of the dentate and olivary nuclei (DOD), though seldom recorded (Golden and Harding, 2004), can sometimes be detected as a minor pathology of more extensive developmental defects (**Table 1-2**). Though pathogenesis may differ across different forms of DOD, it is interesting to note that many of the below conditions have pathologies of the inferior olive too. While the correlation in pathologies could be linked by lineage, the possibility of retrograde degeneration of the cerebellar nucleus as a result of inferior olive dysplasia cannot be discounted. Similarly, the possibility that the modularity of the cerebellar-inferior olive closed loop extends to a single cell level (Lu et al., 2016) means that heavily interconnected microzones might suffer a conductive degeneration when any element of the system is disrupted.

While DOD might represent a failure of *Ptf1a* lineage development, pontocerebellar dysplasia might conversely reflect a dysgenesis of *Atoh1* lineage neurons, affecting both precerebellar and granule cell populations in addition to portions of the dentate (lateral) nucleus. In both cases, the spectrum of associated phenotypes raises the possibility of a developmental origin within the specification or maturation of specific populations of derivatives.

Strokes in adults located at the thalamus or brainstem can also result in rare movement related disorders such as cerebellar outflow tremor, Holmes' tremor, palatal tremor and asterixis (Choi, 2016). These result from lesions to subcortical loops that have cerebellar involvement from the dentate (lateral) nucleus. Interestingly, there is often a delayed onset of tremor symptoms in these cases, linked to hypertrophy in the inferior olive. This is thought to be from a blockade of inhibitory nucleo-olivary signalling (Sanverdi et al., 2012).

Table 1-2 Cerebellar disorders exhibiting nuclear pathology

Disorder	***Aetiology***	***Pathology***	***Clinical Features***
Zellweger (Cerebro-hepato-renal) syndrome *(Müller et al., 2011; Powers et al., 1985; Volpe and Adams, 1972)*	Autosomal recessive disease caused by mutations in PEX genes. Migration failure from 14weeks of gestation in humans	Dysplasia of the dentate and olivary nuclei (DOD), as well as cerebellar hypoplasia and migrational defects in Purkinje cells	Developmental delay, seizures, EEG abnormalities, generalised hypotonia, renal cysts, and joint calcifications
Dentato-olivary dysplasia with intractable seizures in Infancy *(Harding and Boyd, 1991; Martland et al., 1997)*	Unknown, though suggested to be autosomal recessively inherited	DOD - The dentate nuclei are seen as a solid ovoid or tear-shaped structure rather than the characteristic thin, convoluted band.	Hypotonia with frequent seizures from birth and gross developmental delays. Survival is no longer than 3 years.
Joubert syndrome *(Joubert et al., 1968; Millen and Gleeson, 2008; Yachnis and Rorke, 1999)*	Autosomal recessive disease. ~ 50% cases genetically linked to mutations in genes that encode parts of primary cilia. May be important for sensing morphogens like Wnt and Shh during development	Fragmentation of the dentate (lateral) nucleus as one of many hindbrain symptoms, along with hypoplasia of vermis (molar tooth sign), dysplasia of the inferior olive and non-decussation of the superior cerebellar peduncle	Congenital ataxia, hypotonia, episodic breathing dysregulation, and mental retardation
Rhombencephalosynapis *(Elsen et al., 2013; Pasquier et al., 2009; Utsunomiya et al., 1998; Yachnis, 2002)*	Defective dorsal patterning and proliferation in the rhombic lips during early foetal development	Absence or severe dysgenesis of the cerebellar vermis. Fusing of the cerebellar hemispheres, peduncles and in the cerebellar nuclei.	Cerebellar dysfunction, hypotonia, nystagmus, ataxia, mild to severe mental and motor developmental delays

Disorder	*Aetiology*	*Pathology*	*Clinical Features*
Thanatophoric dysplasia *(Coulter et al., 1991; Hevner, 2005; Miller et al., 2009)*	Due to gain of function mutations of FGF receptor 3 (FGFR3), involved in various parts of brain development so pathological features are widespread across many brain regions as well as bones.	Primarily a skeletal dysplasia with macrocephaly. Abnormalities of the cerebellar cortex and cerebellar nuclei are enlarged and hyperconvoluted and dysplastic. Dysplasia of the inferior olive.	Generally a lethal condition - foetuses are usually stillborn or die as neonates due to respiratory failure. For the very few survivors, clinical symptoms include seizures, dependence on ventilator, and mental and motor impairments.
Pontocerebellar hypoplasias *(Namavar et al., 2011; Rudnik - Schöneborn et al., 2014)*	A group of neurodegenerative autosomal recessive disorders. Some variants are caused by tRNA splicing endonuclease mutations	Cerebellar hypoplasia and cerebellar and pons atrophy. Scattered loss of Purkinje cells and segmental loss of dentate nuclear neurons while specific regions of nucleus are preserved.	Severe mental and motor impairments as well as swallowing problems and seizures.
Autism spectrum disorder *(Jeong et al., 2012; Olivito et al., 2016; Yip et al., 2009)*	Heterogeneous: it may be caused by genetic, epigenetic or environmental factors during neurodevelopment.	Cerebellar vermal hypoplasia, reduction of superior cerebellar peduncle, decreased connectivity of dentatorubrothalamic tract. Lower levels of GABA synthesis found in cerebellar nuclear cells and Purkinje cells	Heterogeneous spectrum or clinical features affecting social interaction, communication, and behaviour

1.8 *SOX14* AND THE CEREBELLAR NUCLEI

The initial discovery that *Sox14* gene expression exists in the cerebellar nuclei has directed the experiments in my thesis. The gene is involved in the development of GABAergic interneurons in subcortical nuclei of the midbrain (Delogu et al., 2012; Jager et al., 2016). Having use of two mouse lines: the *Sox14-GFP* and *Sox14-Cre*, it seemed fitting to investigate the cells marked by this gene expression since so little is known about GABAergic cell types within the cerebellar nuclei. The possibility that this gene expression could specifically demarcate one GABAergic nuclear cell type is worth investigating, especially in light of the previously discussed gaps in knowledge concerning nuclear contributions to cerebellar function and disease.

In **Chapter 2**, I systematically examine the *Sox14* expressing nuclear neurons by identifying molecular and genetic markers that characterise the cells. In **Chapter 3**, adenoassociated viruses (AAVs) and retrograde tracers are used to map the projections of the cells. **Chapter 4** looks at the developmental expression of *Sox14* to investigate the function of the gene, as well as to further understanding of GABAergic nuclear cell development. In **Chapter 5**, AAVs are used to ablate *Sox14* expressing nuclear neurons in order to investigate the functional role of these cells in motor coordination and motor learning.

2 CHARACTERISATION

2.1 INTRODUCTION

This chapter details the characterisation of a previously undescribed *Sox14* expression in the cerebellum and the use of the *Sox14*$^{Gfp/+}$ knock-in mouse line to investigate *Sox14* as a potential cell marker for a cerebellar nuclear cell type. *Sox14*$^{Gfp/+}$ and *Sox14*$^{Cre/+}$ mutant mice were generated by the Jessell lab at Columbia University. In these transgenic lines, the *Sox14* allele coding sequence was replaced with a 5' splice substrate and an *EGFP* or *Cre* sequence, a bovine growth hormone polyadenylation sequence and neo cassette.

From previous studies characterising *Sox14* expressing neurons, I reasoned that *Sox14* expression would mark inhibitory neuronal subtypes similar to the observed subtype specific expression in the diencephalon. The aims of the experiments described in this chapter are, therefore, to determine 1) the identity of *Sox14* cells with respect to established markers for excitatory and inhibitory cerebellar neurons and 2) whether *Sox14* defines a homogeneous population of neurons. To accomplish this, I carried out a comprehensive investigation of the cerebellum, and in particular the cerebellar nuclei, first using the *Sox14*$^{Gfp/+}$ mouse line to visualise expression patterns and perform colocalisation analysis with known cell markers.

2.1.1 THE *SOX14* GENE

Sox14 is a member of the SRY-related *Sox* gene family, each of which shares a highly conserved HMG domain with more than 80% sequence identity. The *SoxB1 (Sox1*, *Sox2* and *Sox3*) and *SoxB2 (Sox14* and *Sox21)* sub-families of genes are

crucial for neuronal development (Schepers et al.). *SoxB1* genes help to establish and regulate pluripotency in embryonic stem cells, and later then help to maintain neural precursor cell properties. *SoxB1* genes are downregulated in order for neurogenesis to progress. This is thought to be controlled by *SoxB2* genes, which, by contrast, promote neural fate downstream of proneural genes (Hargrave et al., 2000b; Hargrave et al., 2000c; Hashimoto-Torii et al., 2003; Uchikawa et al., 1999; Wegner, 2011)*).* It is worth noting that the current understanding of *SoxB2* gene function is based on *Sox21*, not *Sox14* (Uchikawa et al., 1999).

The mammalian *SoxB2* family is related to the Drosophila *Dichaete* gene and is required for both the establishment of neural stem cells and for the expression of the proneural genes *achaete scute* and *asense* in neuroblasts (Phochanukul and Russell, 2010). The mammalian *Sox14* gene is also understood to share a homology with insect *SoxC* genes (Chintapalli et al., 2008; Crémazy et al., 2001; Wilson and Dearden, 2008). Beyond expression patterns, little is known about the *SoxC* group, especially in terms of its function (Phochanukul and Russell, 2010). Kirilly *et al.* (2009) identified *Sox14* in Drosophila to be necessary and sufficient to control dendritic pruning during transition from larva to pupa.

In mammals, *Sox14* is also expressed in cells of the urinary system, limbs and reproductive system (GUDMAP Consortium, http://www.gudmap.org. 2004). *Sox14* is expressed during development of the CNS mainly, but not exclusively, in a range of inhibitory neuron subtypes in the diencephalon, midbrain, hindbrain and spinal cord (Delogu et al., 2012; Hargrave et al., 2000a; McClellan et al., 2006).

Embryonic expression of *Sox14* has been found in various neurons of the subcortical visual shell (SVS), an interconnected series of GABAergic nuclei (Delogu et al., 2012). In particular, *Sox14*$^{+}$ cells in the intergeniculate leaflet (IGL) and ventral lateral geniculate nucleus have been studied in terms of their developmental origins. These cells are *Gad1* positive with characteristic interneuron-like morphology and the electrophysiological characterization is consistent with the GABAergic nature of these cells; whole-cell recordings and simultaneous paired recordings confirmed membrane properties that are compatible with GABAergic interneurons, while some of the *Sox14*$^{+}$ cells were able to generate inhibitory postsynaptic currents in the neighbouring target neurons (Jager et al., 2016). Thus far, it would appear that *Sox14* is mostly expressed in inhibitory cell types, with the exception of a non-GABAergic population in the ventromedial hypothalamus (VMH) (Delogu et al., 2012).

The initiation of *Sox14* developmental expression coincides with the cell-cycle exit in cells that have already initiated transcription of the pan-GABAergic *Gad1* gene, and maintained the first 3 weeks after birth (Delogu et al., 2012; Sellers et al., 2014). It has been shown that *Sox14* is required for cell migration in the diencephalon (Delogu et al., 2012; Jager et al., 2016).

2.1.2 IDENTIFYING THE CELLS OF THE CEREBELLAR NUCLEI

Various cell types have previously been identified in the cerebellar nuclei (See **Chapter 1.4**), mainly by looking at neurotransmitter type, soma size, and long-range connectivity. As yet, no specific gene has been identified as a marker of a particular nuclear cell type beyond development. Patterns of *Sox14* expression can be

visualised by observing endogenous GFP fluorescence in the *Sox14*$^{Gfp/+}$ heterozygous mouse at various neonatal and post-natal time-points. Two simple approaches were taken in this chapter to confirm whether *Sox14*$^{+}$ neurons in the cerebellar nuclei are GABAergic. I assessed 1) colocalisation of GFP with GABA/GAD and calcium binding proteins; 2) soma size (mean diameter and cross-sectional area) of *Sox14*$^{+}$ cells in relation to described cell types of the cerebellar nuclei, summarised in **Table 2-1**.

Table 2-1 Summary of cerebellar nuclear cell types listed by neurotransmitter type and soma size (mean diameter and cross-sectional area)

Cell type	***Target***	***Known Markers***	***Mean Soma diameter***	***Somatic cross-sectional area***
Glutamatergic Projection Neurons	Brainstem nuclei, cerebral cortex, spinal cord	VGlut2	23.57 ± 1.27 µm (1) 16-20µm (2) 26 ± 1.5 µm (3) 25 - 35 µm (4)	>180µm^2 (2) 322 ± 20 µm^2 (3)
GABAergic Projection Neurons	Inferior Olive	GABA, GAD65 GAD67	6-20µm (2) 17 ± 1.1 µm (3) 15 - 20µm (4) long axis, 13.4 ± 0.1 µm; short axis, 9.3 ± 0.1 µm (5)	<180µm^2 (2) 150 ± 15 µm^2 (3) 108 ± 4 µm2 (5)
Glycinergic Projection Neurons	Ipsilateral vestibular nuclei	GlyT2	20 to 35 µm (6)	
Glycinergic Projection Neurons	Cerebellar Cortex	GlyT2	23.3 ± 1.4µm (7)	256 ± 22 µm^2 (7)
GABAergic/ glycinergic interneurons	Local circuit	GlyT2, GABA	16 ± 1.3 µm (7) 6-8µm (2)	130 ± 15 µm^2 (7) <180µm^2 (2)
Non-GABAergic interneurons	Local circuit	?	<25µm (3)	<300µm^2 (3)

References: (1) Aizenman et al. (2003); (2) Chan-Palay (1973c); (3) Uusisaari et al. (2007); (4) Legendre and Courville (1987); (5) Najac and Raman (2015); (6) Bagnall et al. (2009); (7) Uusisaari and Knöpfel (2010)

2.1.2.1 GABA AND GAD

GABA (gamma-aminobutyric acid) is the most widespread inhibitory neurotransmitter in the central nervous system, (Awapara et al., 1950; Roberts and Frankel, 1950). GABA is stored in synaptic vesicles and is released from nerve endings in a $Ca2^{+}$-dependent fashion upon depolarization of the presynaptic membrane. During development, GABA release at synapses causes depolarization of the postsynaptic neuron rather than hyperpolarization and, postnatally, the GABAergic signals switch from being excitatory to inhibitory (Ganguly et al., 2001). After GABA is released into the synaptic cleft, its actions are terminated by reuptake into presynaptic terminals and the surrounding glia.

GABA-mediated inhibition works in two ways as there are two types of GABA receptors. $GABA_A$ receptors are ionotropic gated Cl^- ion channels, while $GABA_B$ receptors are metabotropic receptors which act via G protein-coupled mechanisms to indirectly alter membrane ion permeability and neuronal excitability. Activation of $GABA_A$ receptors causes an increase in Cl^- ion conductance since it increases the mean open time of the Cl^- ion channel itself (Macdonald and Twyman, 1991). This hyperpolarises the neuronal membrane and increases in the threshold for action potential generation. GABA inhibition via $GABA_B$ receptors varies more; in many brain regions, activation of $GABA_B$ receptors results in an increase in K^+ channel conductance, either directly or indirectly, again causing hyperpolarisation of the neuronal membrane (Bormann, 1988; Bowery, 1993). Some $GABA_B$ receptors may also act by changing Ca^{2+} conductance.

Antibodies against the GABA protein were used to compare the patterns of GABA expression with endogenous GFP. Clear identification of positive somas by IHC with GABA antibodies is hampered by the enrichment of GABA in the axoplasm and at synapses; therefore, I also used RNA *in situ* hybridisation histochemistry to label glutamate decarboxylase (GAD) mRNAs, which are instead enriched in the perinuclear cytoplasm (Martin and Rimvall, 1993). To accomplish this, I generated RNA probes against *Gad1* and *Gad2* mRNA. GAD is the rate-limiting enzyme for GABA synthesis (Erlander and Tobin, 1991). Its two isoforms, GAD67 and GAD65, are encoded by *Gad1* and *Gad2* genes, respectively, and the two genes are localised on different chromosomes (Karlsen et al., 1991; Kaufman et al., 1991; Martin and Rimvall, 1993). Both isoforms have been shown to exist in the cerebellar nuclei, with a predominance of Gad2 labelling in the lateral cerebellar nuclei (Esclapez et al., 1994; Greif et al., 1991).

2.1.2.2 CALCIUM BINDING PROTEINS

Neurons can be characterised by the combinatory expression of calcium-binding proteins. For example, in the cerebellar cortex, most Purkinje cells express both Parvalbumin (*PValb*) and Calbindin (*Calb1*) whereas basket, stellate and Golgi cells express *PValb* only (Bastianelli, 2003; Leto et al., 2006). By contrast, glutamatergic granule and unipolar brush cells are positive for Calretinin (*Calb2*), while lacking *Calb1* and *PValb* (Mugnaini et al., 2011). These protein combinations regulate intracellular calcium concentrations and change the sensitivity of calcium channels to modulate signalling and synapse stability (Bastianelli, 2003). Thus, throughout the brain, subpopulations of GABAergic neurons that express PValb are more electrically and metabolically active than other subpopulations (Bastianelli, 2003).

The Allen Brain Atlas (mouse.brain-map.org) ISH gene expression database was used to narrow the list of potential calcium-binding proteins to investigate. Database searches have shown calcium binding genes *PValb* and *Calb1* to be present in the cerebellar nuclei at P28, as the neurons mature and form synapses, while *Calb2* is present in the granule cell layer, but not the cerebellar nuclei. However, since *Calb2* has been identified as a potential downstream target of the transcription factor *Sox14* in *Sox14*$^{+}$ cells in the chick thalamus (Sellers et al., 2014), I also assessed whether there is *Calb2* expression in the cerebellar nuclei throughout development.

2.1.3 AIMS OF THE CHAPTER

I sought to characterise GFP^{+} cells of the *Sox14*$^{Gfp/+}$ mice in the cerebellum by immunohistochemistry in serial brain sections and primary cell culture, and by *in situ* hybridization for markers of inhibitory neurons. I also measured soma size in order to match the cells to known nuclear cell types.

2.2 RESULTS

I used the *Sox14*$^{Gfp/+}$ mice to show that *Sox14* expression is present in the cerebellar nuclei. The subsequent experiments investigate whether *Sox14*$^{+}$ cells represent one or more of the known populations of nuclear cells. Since *Sox14* expression, and therefore GFP expression in the *Sox14*$^{Gfp/+}$ cerebellum, declines and cannot be observed reliably beyond the first month post-birth, P14 and P21 stage brains were chosen as time points for investigation. By these stages, the different cerebellar nuclei can be distinguished as landmarks noted in adult brain atlases can be identified.

Sox14$^{Gfp/+}$ brains were collected at either P14 (n=4) or P21 (n=3) and cryosectioned into coronal slices. Thicker, 80-100µm floating sections were used for immunohistological experiments, while thinner 20µm sections from long fixation brains were collected onto glass slides for *in situ* hybridisation experiments. The following experiments targeted proteins linked to inhibitory neurons as previous *Sox14* studies have shown the gene to be expressed in various inhibitory interneuron populations.

2.2.1 *SOX14*$^{+}$ CELLS ARE NON-UNIFORMLY DISTRIBUTED ACROSS THE CEREBELLAR NUCLEI

Figure 2-1 shows the morphology of the cerebellar nuclei, as viewed from sagittal, mid-sagittal and coronal perspectives (Allen Brain Atlas, http://www.brain-map.org.), which are divided into the three main sub-regions: the lateral nuclei in green, interposed nuclei in yellow and medial nuclei in blue. All three nuclei display an irregular three-dimensional morphology. These outlines were used to derive the

boundaries of the sub-regions in tandem with the sectional maps (Paxinos and Franklin, 2004).

Figure 2-1 The morphology of the cerebellar nuclei.

*Sagittal (**A**), mid-sagittal (**B**) and coronal (**C**) views of the CN, which are divided into the three main sub-regions: lateral (Lat) CN in green, interposed (Int) CN in yellow and medial (Med) CN in blue. Note the irregular morphology in all directions. The Sagittal view is used in the images below to indicate the slice angle of the following figures, cut along the rostrocaudal axis. **D-G**) Coronal sections in reference of the whole brain seen from mid-sagittal view to show how the different nuclei intersect with rostral (**D**), central (**E**) and caudal (**F&G**) sections. (**D-E**) are viewed from the front with the lateral nuclei highlighted in green, while (**G**) is viewed from the rear with the medial nuclei highlighted. The outlines of the nuclear sub-regions throughout the thesis are drawn referencing this map along with "The Mouse in Stereotaxic Coordinates" Atlas (Paxinos and Franklin, 2004) as guidance for further subdivisions. Prominent morphological features were sought to identify the boundaries and the position of each slice along the rostrocaudal axis can be easily identified based on the total shape of the cerebellar nuclei. (Adapted using Allen Brain Atlas Brain Explorer 2 software for 3D navigation of interactive reference atlas viewer)*

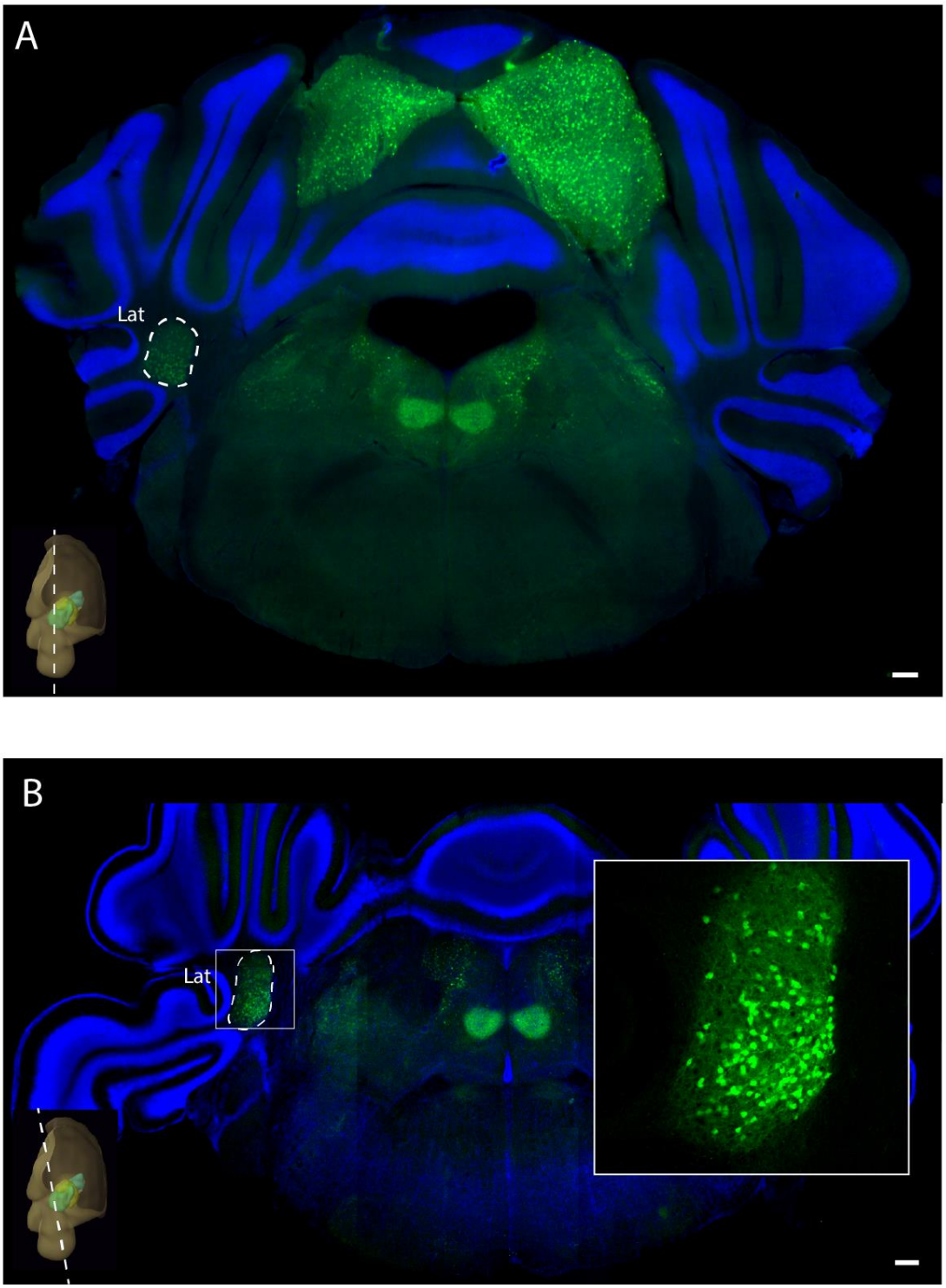

Figure 2-2 P21 Sox14$^{Gfp/+}$ coronal sections showing the rostral cerebellum

*Only the lateral (Lat) cerebellar nucleus is seen in rostral sections. Sox14^{+} cells are found in the cerebellar nucleus and these cells are distributed unevenly, seen clearly in the magnified image (**B**, **Inset**). Sox14^{+} populations in the inferior colliculus (**A**) and brainstem nuclei can also be seen (**A**&**B**).*

Lat = lateral nucleus. Scale: 200 µm

Figure 2-2-4 shows the *Sox14*$^{Gfp/+}$ mouse cerebellar nuclear sub-regions from a coronal perspective, moving from rostral to caudal. Using brightfield and background staining under fluorescent illumination, the boundaries of cerebellar nuclei are clearly visible as cell dense areas surrounded by the relatively cell-free white matter. The location of each slice along the rostrocaudal plane can be identified from the shape of the nuclei, the size of the 4th ventricle and the lobules of the cerebellar cortex. There is a systematic variation of the nuclear structures along the rostrocaudal axis. In this and subsequent chapters, I have used the anatomical nomenclature outlined in "The Mouse in Stereotaxic Coordinates" Atlas (Paxinos and Franklin, 2004).

At the most rostral tip of the cerebellar nuclear mass, only the lateral nucleus can be seen **(Figure 2-2)**. *Sox14*$^{+}$ cells are distributed irregularly, with more *Sox14* expressing cells in the ventral part of the lateral nucleus. In more caudal areas of the lateral nucleus (**Figure 2-2B**), the cells are yet more unevenly distributed, with a far higher density of cells in the ventromedial portion of the lateral nucleus, seen clearly in the magnified image inset.

Midway through the cerebellum, all sub-regions of the cerebellar nuclei can be seen in a single plane (**Figure 2-3**). The lateral nucleus merges with the interposed nuclei, while the superior vestibular nucleus and vestibulocerebellar nucleus are directly below the posterior interposed nucleus, and merge with the medial nucleus to form a ventral strip. *Sox14*$^{+}$ cells are sparsest in the dorsal regions of the nuclei, particularly in the dorsolateral and anterior interposed nuclei (**Figure 2-3A, Inset**). In contrast,

the parvicellular domain on the ventral border of the lateral nucleus is saturated with *Sox14*$^{+}$ cells. *Sox14*$^{+}$ cells are also found in superior vestibular and vestibulocerebellar nuclei. The boundary between these vestibular nuclei and the medial cerebellar nucleus are difficult to define. It appears that the medial nucleus does not contain *Sox14*$^{+}$ cells, given the *Sox14*$^{+}$ cells are tightly arranged to expose an unlabelled area where the medial nucleus sits.

In more caudal sections, the cerebellum is entirely separated from the medulla (**Figure 2-4).** The dorsolateral interposed nucleus forms a lateral protuberance, while the lateral nucleus diminishes and the posterior interposed nucleus becomes the main nucleus that spans the space from the ventral border to the dorsal parts of the nuclear mass. The caudal medial nucleus is seen clearly in **Figure 2-5A**, as an almond shape nucleus, which lies above the posterior interposed nucleus. A few, exceptional *Sox14*$^{+}$ cells are found in the ventral-most parts of the rostral medial nucleus (**Figure 2-4B**, **white arrowheads**), but no other *Sox14*$^{+}$ cells are seen in the core of the medial nucleus.

Figure 2-3 P21 Sox14$^{Gfp/+}$ coronal sections showing the central cerebellum

*All sub-regions of the cerebellar nuclei can be seen in a single plane (**A**). A magnified image of the lateral (Lat) and interposed (Int) nuclei in this plane is seen inset. The lateral nucleus merges with the interposed nuclei and the vestibular nuclei: superior vestibular nuclei (SuVe) and vestibulocerebellar nuclei (VeCb). More caudally (**B**), the lateral nucleus declines as the posterior interposed (IntP) nucleus takes over. There are Sox14^{+} cells throughout, except in the dorsal parts of the medial nucleus.*

Lat = lateral nucleus, LatPC = parvicellular lateral nucleus, IntDL = dorsolateral interposed nucleus, IntA= anterior interposed nucleus, IntP= posterior interposed nucleus, Med= Medial nucleus, VN= vestibular nucleus, RN= reticular nucleus. Scale: 200 µm

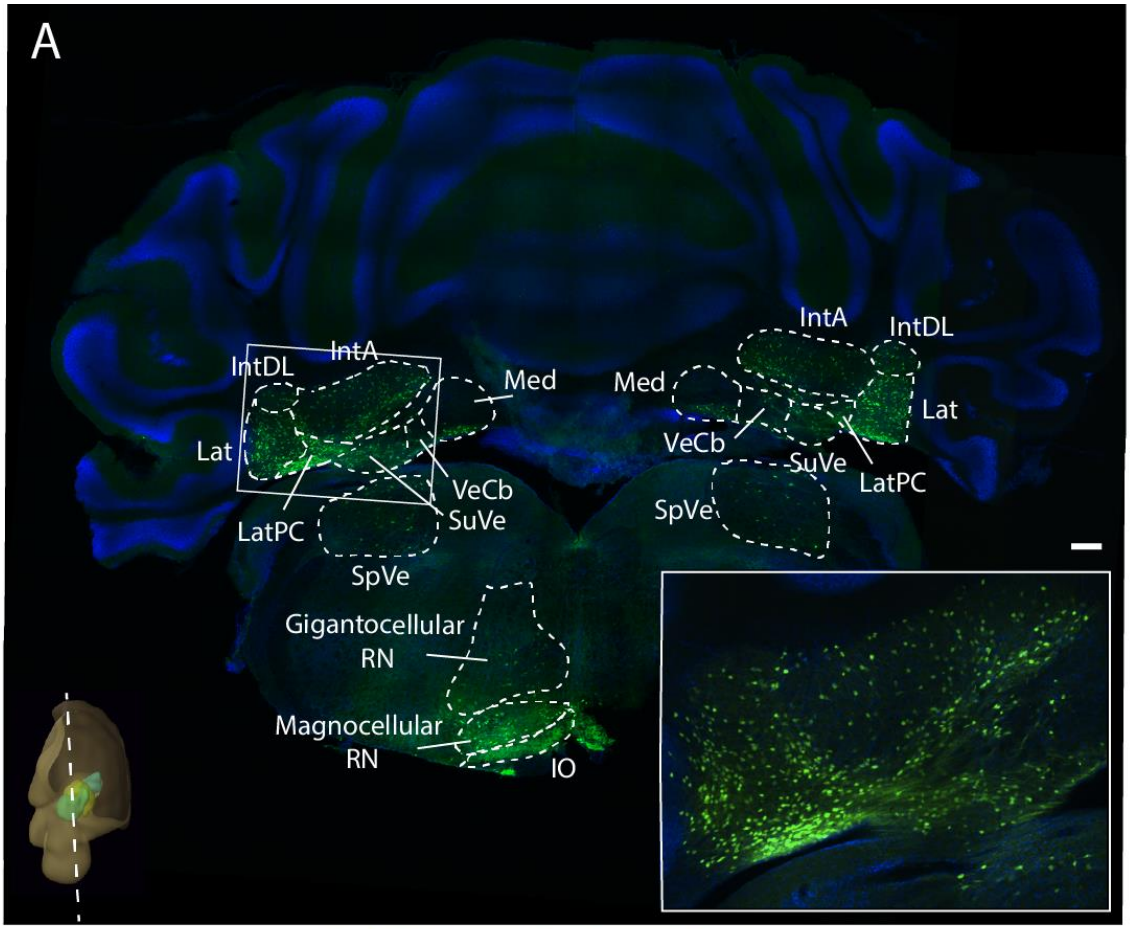
A
IntA
IntDL
Med
Lat
VeCb
SuVe
LatPC
SpVe
Gigantocellular
RN
Magnocellular
RN
IO

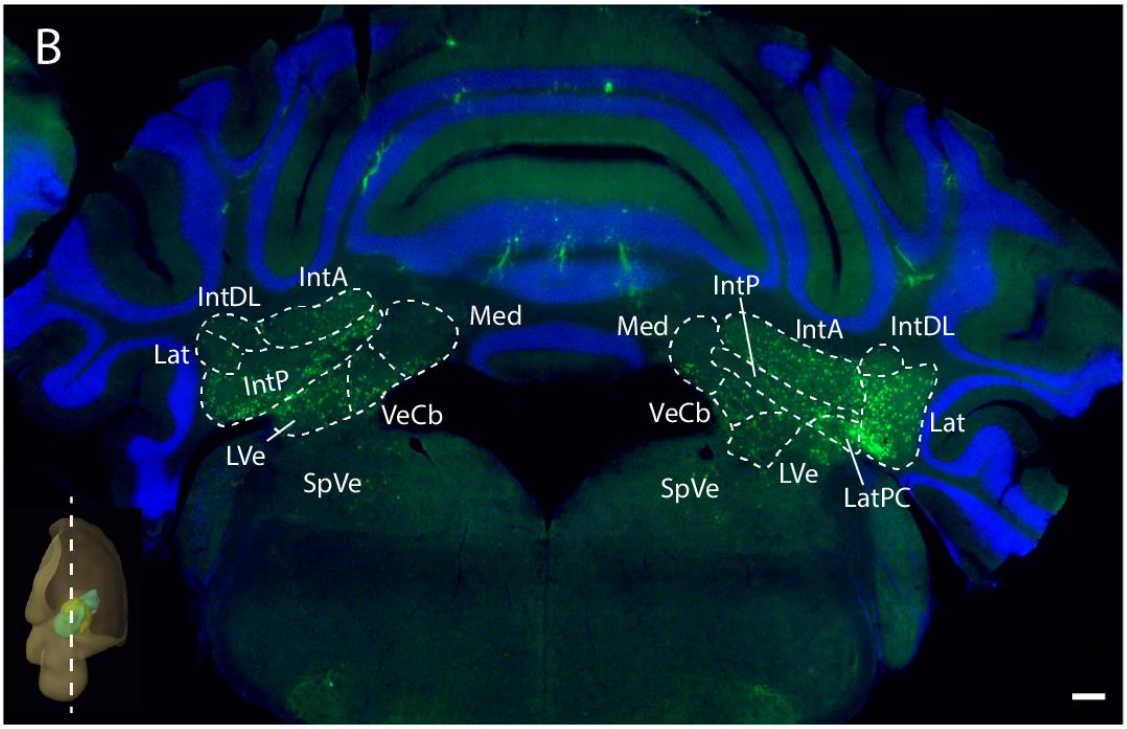
B
IntDL
IntA
Med
Lat
IntP
VeCb
LVe
SpVe
LatPC

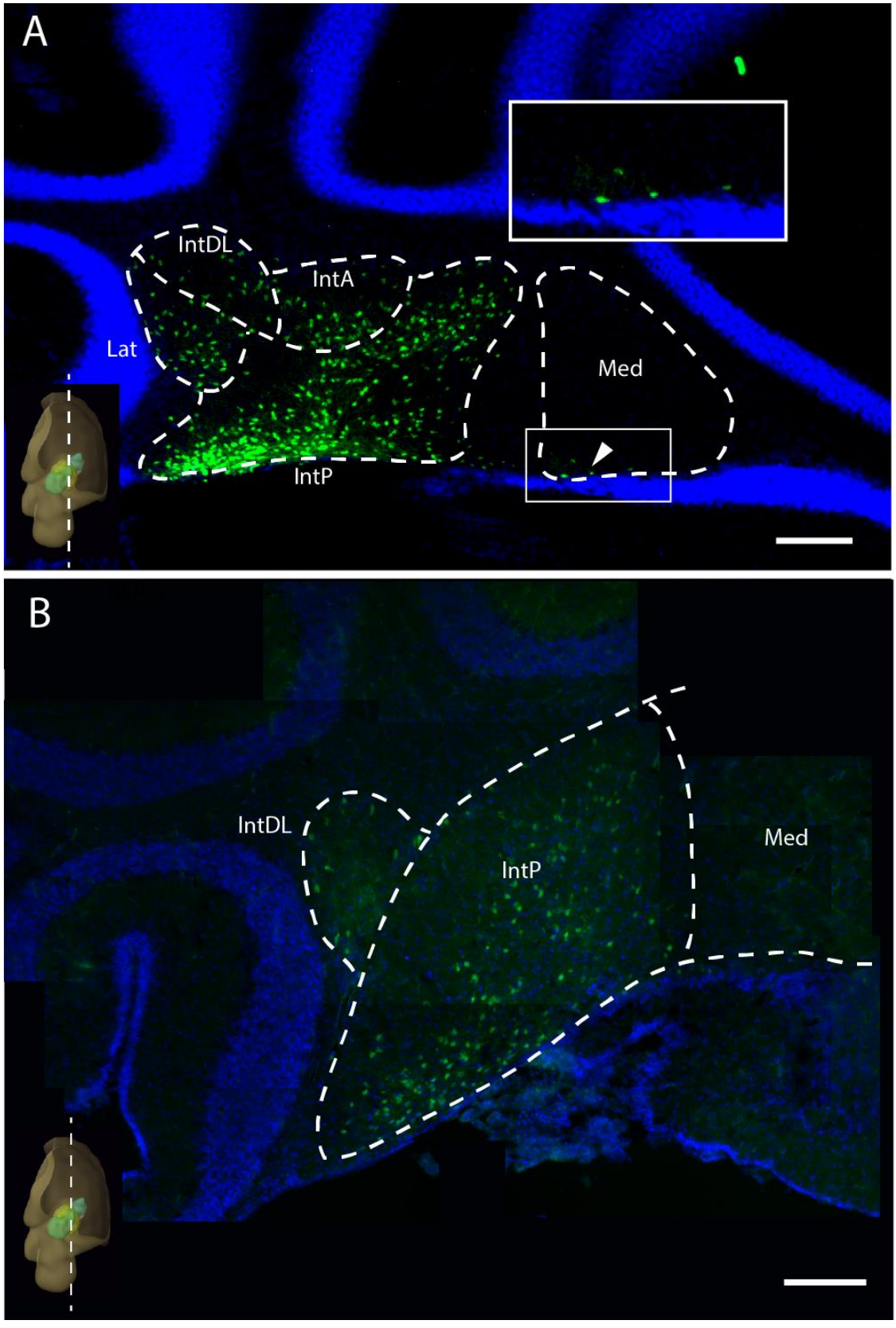
A
IntDL
IntA
Lat
Med
IntP
B
IntDL
IntP
Med

Figure 2-4 P21 Sox14$^{Gfp/+}$ coronal sections showing the caudal cerebellum

The cerebellar tissue completely separates from the brainstem and no vestibular nuclei are seen. ***A****) The lateral nucleus continues to recede so that it only occupies a small dorsolateral domain. Similarly the anterior interposed nucleus declines. Small numbers of Sox14^{+} cells are seen in the ventral edge of the medial nucleus (white arrowheads).* ***B****) More caudally, the dorsolateral interposed nucleus protrudes out, and the posterior interposed nucleus distinct from the medial nucleus, which is devoid of Sox14^{+} cells.*
Lat = lateral nucleus, LatPC = parvicellular lateral nucleus, IntDL = dorsolateral interposed nucleus, IntA= anterior interposed nucleus, IntP= posterior interposed nucleus, Med= Medial nucleus, Scale: 200 µm

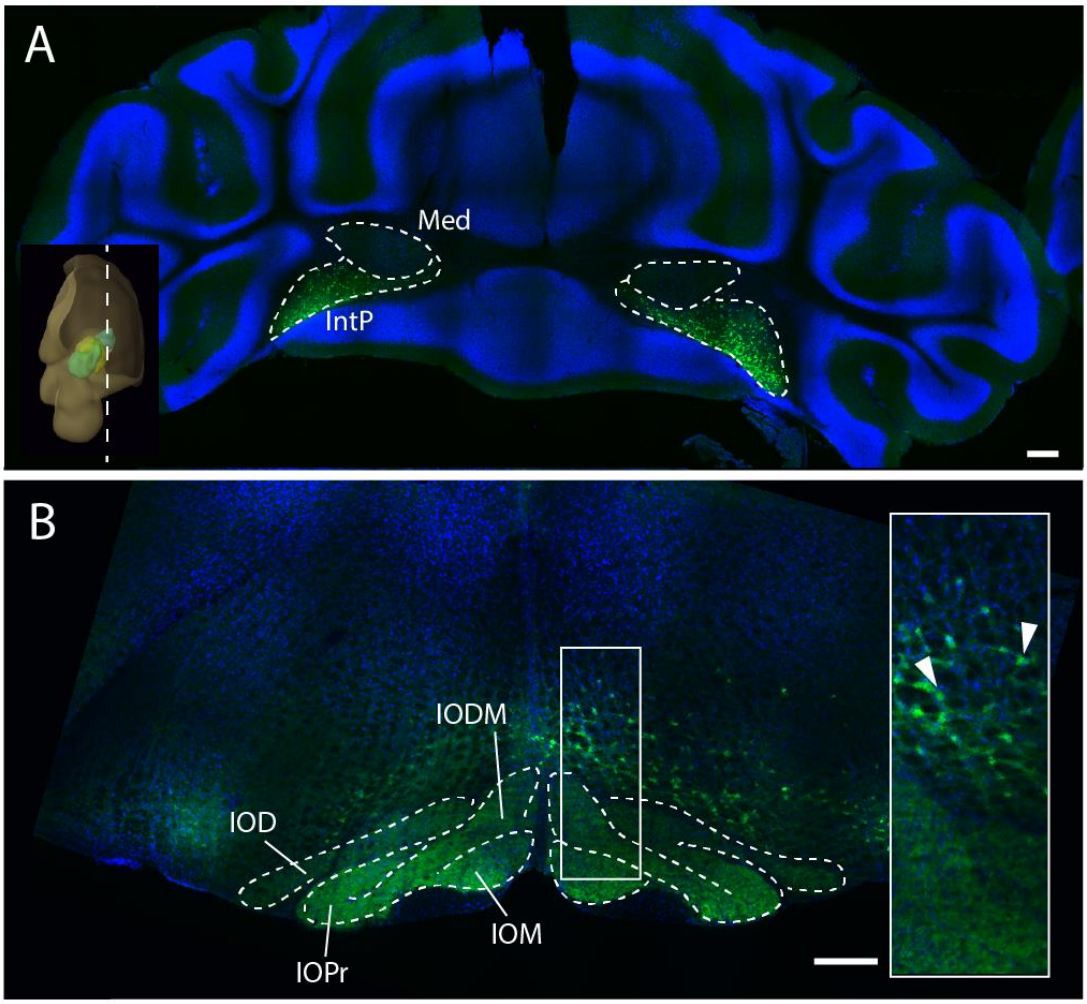

Figure 2-5 P21 Sox14$^{Gfp/+}$ coronal sections showing the caudal cerebellum and inferior olive

A*) Most caudally, the medial (Med) nucleus is seen clearly as an almond shape above the posterior interposed (IntP) nucleus. Though the shape of the nucleus is well defined by the background staining, again, no GFP^{+} cells are seen in this region.* ***B****) While somatic GFP is not seen within the inferior olive, axonal expression shows that GFP^{+} cells project to the region. Additionally, there are GFP^{+} cells dorsal to the structure (White arrowheads, inset). IOD= inferior olive dorsal nucleus; IODM= inferior olive dorsomedial cell group; IOM= inferior olive medial nucleus; IOPr= inferior olive principal nucleus. Scale: 200 µm*

2.2.2 IDENTIFICATION OF *SOX14*$^+$ CELLS BY IMMUNOHISTOCHEMISTRY

I next used immunohistochemical approaches both in hindbrain coronal sections and primary cell culture preparations to further identify *Sox14*$^+$ cells. **Figure 2-6** and **Figure 2-7** show staining in the lateral nucleus against proteins associated with inhibitory cell identity.

2.2.2.1 SOX14 IN SERIALLY SECTIONED BRAIN MATERIAL

Sox14$^{Gfp/+}$ P14 and P21 serial sections were stained with GABA antibodies (**Figure 2-6A**). GFP$^+$ cells appear to colocalise with GABA (**Figure 2-6A, white arrowheads**), though high background made it difficult to confirm that *Sox14*$^+$ cells are GABAergic**.**

In order to further define different types of GABAergic neurons, the *Sox14*$^{Gfp/+}$ sections were stained against different Ca^{2+} binding proteins, which are known to be expressed by various types of inhibitory neurons. I stained against PValb, Calb1 and Calb2 and looked for double expression alongside the endogenous GFP, which was stained against GFP for better visualization.

Figure 2-6B shows a high level of immunoreactivity to PValb throughout the nucleus. Purkinje cell axon terminals within the nuclei are also immunopositive to PValb and the consequent mesh of immunoreactive axonal tracts made double staining of GFP$^+$ cells difficult to interpret. Nevertheless, GFP$^+$ cells are located in the "holes" of non-immunoreactivity for PValb (**white arrowheads**), suggesting that the *Sox14*$^+$ cells do not express *PValb* at this stage.

Equally for Calb1, GFP^+ cells lie in the "holes" of non-immunoreactivity for (**Figure 2-6C white arrowheads**), while Purkinje cells express Calb1 and this also forms a mesh of immunoreactivity. $Calb2^+$ cells (**Figure 2-6D**) are found mainly in the granular layer (**orange arrowheads**) as well as cells in the cochlear and vestibular nuclei below the cerebellum, seen in the lower magnification image. However, no $GFP^+/Calb2^+$ cells were observed in the cerebellar nuclei at this level.

Thinner brain sections allowed a higher magnification analysis of double labelling, with fewer overlapping cell profiles across the depth of each section. In **Figure 2-7A**, some GFP^+ cells overlap with GABA immunoreactivity (**white arrowheads**) while others seemed to sit in the voids of non-immunoreactivity (**orange arrowheads**). For PValb (**Figure 2-7B**), some ambiguity in double labelling persists at high magnification (**orange arrowheads**). For Calb1 (**Figure 2-7C**) the location of the GFP^+ cells occur in the "holes" of non-immunoreactivity, suggesting that the *Sox14*$^+$ cells do not express *Calb1* in adulthood. Most nuclear cells appear to be negative for Calb2, but a single $GFP^-/Calb2^+$ cell is clearly visible (**Figure 2-7D, asterisk**). None of the GFP^+ cells colocalise with $Calb2^+$ cells (**white arrowheads**).

Overall, the immunohistochemistry data suggests that the *Sox14*$^+$ cells are GABAergic, but also that they do not express the Ca^{2+} binding proteins PValb, Calb1 or Calb2. To confirm this observation, I used both primary cell culture and RNA *in situ* hybridization to map protein and RNA distribution against Sox14-GFP expression.

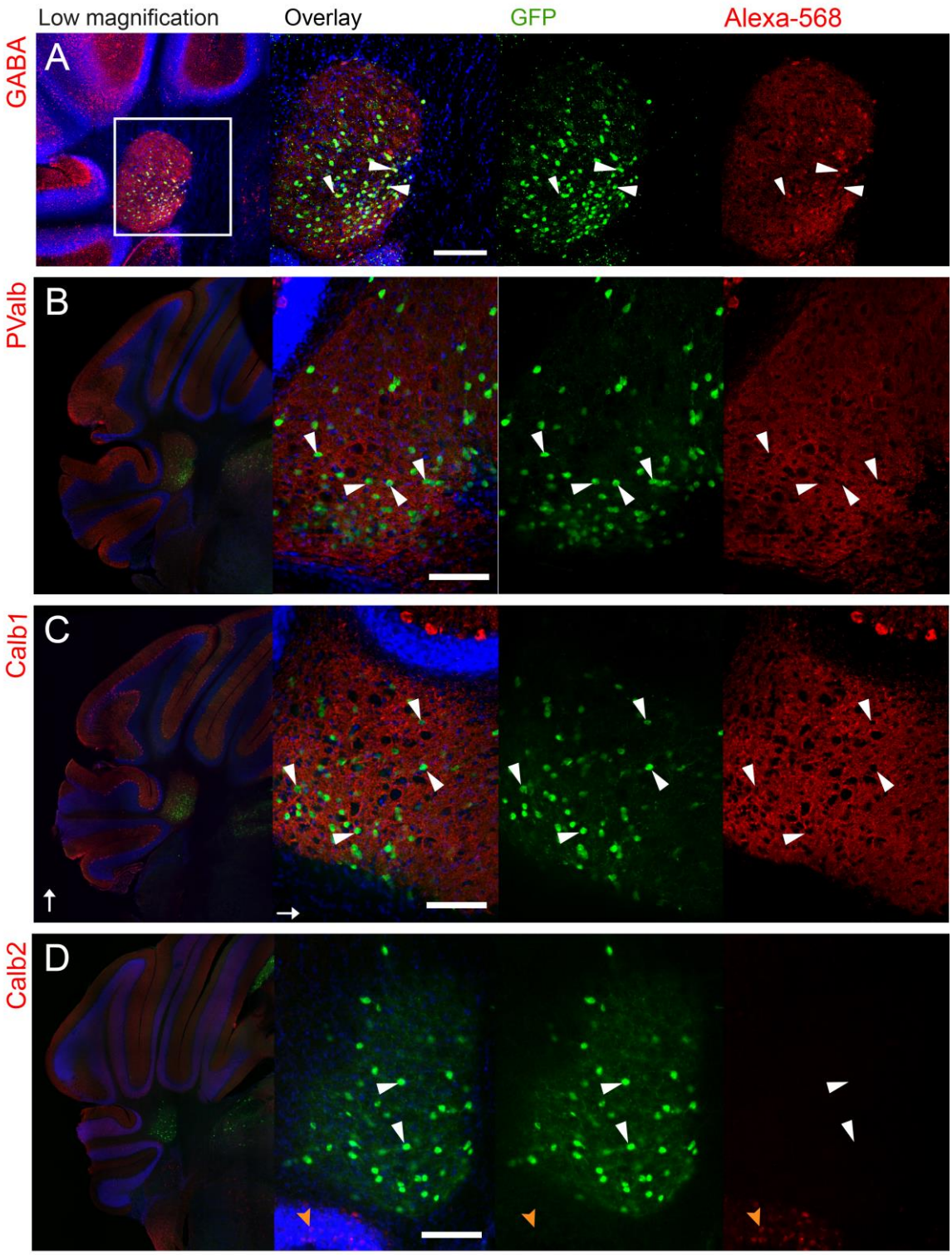

Figure 2-6 Immunostaining Sox14$^{Gfp/+}$ cerebellar coronal slices

*Immunostaining for GABA (**A**), PValb (**B**), Calb1 (**C**) and Calb2 (**D**). The far left column shows the low magnification image, while the three other columns show the lateral nucleus in higher magnification, with the overlay, then GFP only and Alexa-568 only. Visibility of GFP$^+$ cells was improved by immunostaining against GFP and specific examples of the GFP$^+$ cells are denoted by white arrowheads. Orange arrowheads highlight*

*immunoreactive neurons in the cerebellar cortex, showing Purkinje cells that express PValb (**B**) and Calb1 (**C**), and granular layer cells that express Calb2 (**D**). Scale: A: 200 µm, B-D: 100 µm*

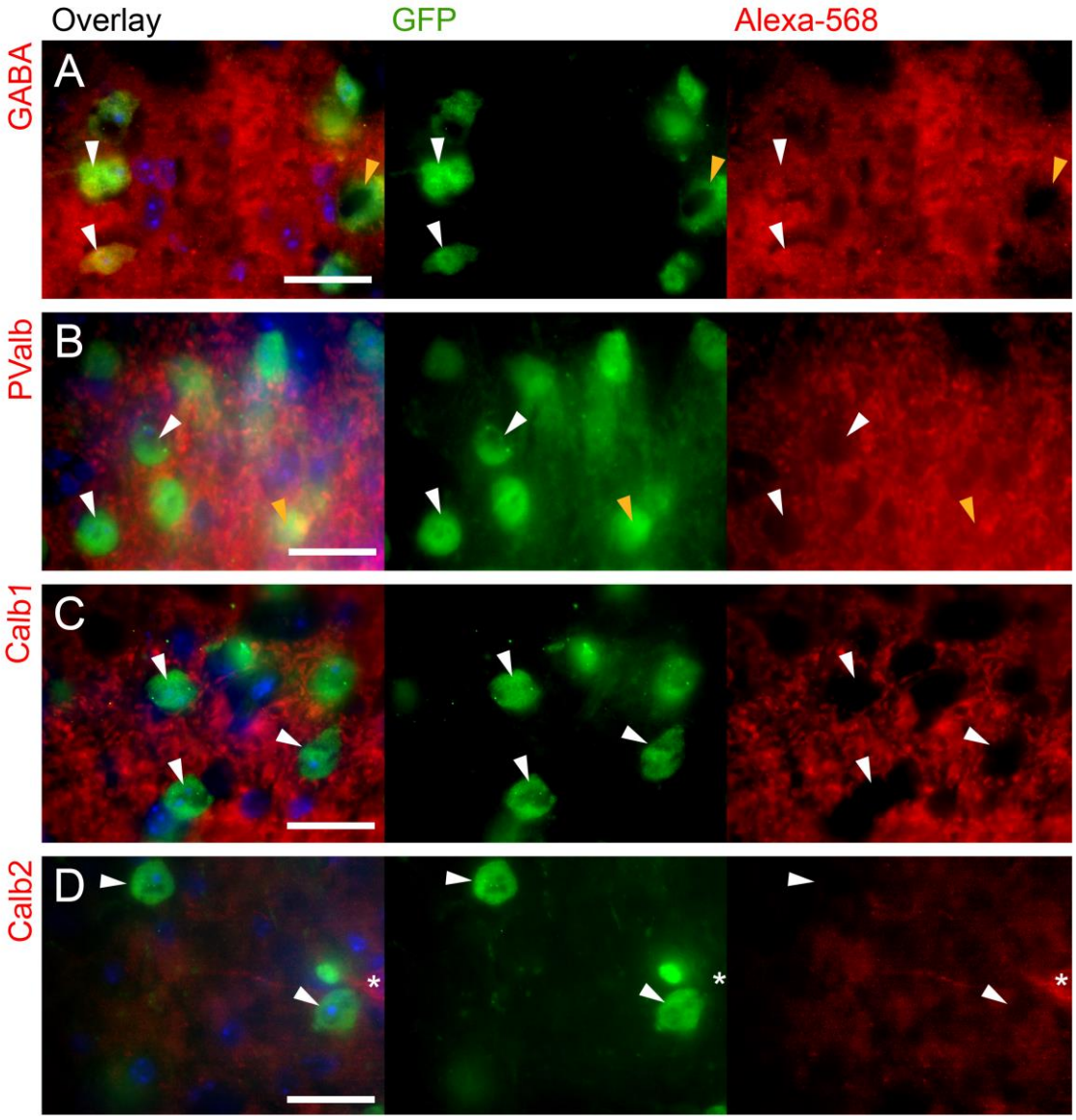

Figure 2-7 Immunostaining Sox14$^{Gfp/+}$ cerebellar coronal slices

*Immunostaining for GABA (**A**), PValb (**B**), Calb1 (**C**) and Calb2 (**D**), imaged at 100x magnification of the lateral nucleus. The columns show the overlay, then GFP only and Alexa-568 only. The white arrowheads show examples of GFP$^+$ cells that colocalise with GABA, but not PValb, Calb1 or Calb2. Orange arrowheads show ambiguous cases. There is little immunoreactivity for Calb2 within the cerebellar nuclei, but a single GFP$^-$/Calb2$^+$ cell is seen, denoted with an asterisk (*). Scale: 20 µm*

2.2.2.1 PRIMARY CELL CULTURE USING SOX14$^{GFP/+}$ MICE

In order to see colocalisation accurately, cerebellar cells were dissociated from a *Sox14*$^{Gfp/+}$ P0 brain and plated onto poly-D-lycine coated glass coverslip and maintained in a tissue culture incubator **(Figure 2-8A**). After one night in culture, the cells form a monolayer, with GFP$^+$ cells dispersed across the coverslip. In all instances, GFP co-localised with GABA and the pan-neuronal marker MAP2 in cultured cells (n=21). **Figure 2-8B** shows 11 examples of this colocalisation in individual GFP$^+$ cells. The morphologies of the cells were variable, presumably since the dissociation process causes the neurites to retract and the short culture time did not allow for complete recovery. These data confirm that all the *Sox14*$^+$ cells are GABAergic; however, it did not determine whether all GABAergic cells in the cerebellar nuclei express *Sox14*.

Figure 2-8 Primary cell culture of brain tissue from Sox14$^{Gfp/+}$ P0 neonates.

A) *schematic of the process in which the cerebellar tissue was extracted from a neonate pup, homogenised using papain enzyme and seeded onto poly-D-lycine coated coverslips. After one day, the coverslips were fixed for immunostaining.* ***B i-xi)*** *Immunostaining Sox14$^{Gfp/+}$ primary cell culture for GFP, GABA and MAP2. The overlay is shown on the left most column and each channel shown separately on the right. Each image shows an individual GFP$^+$ cell that colocalises with both GABA and MAP2. Scale: 40 µm*

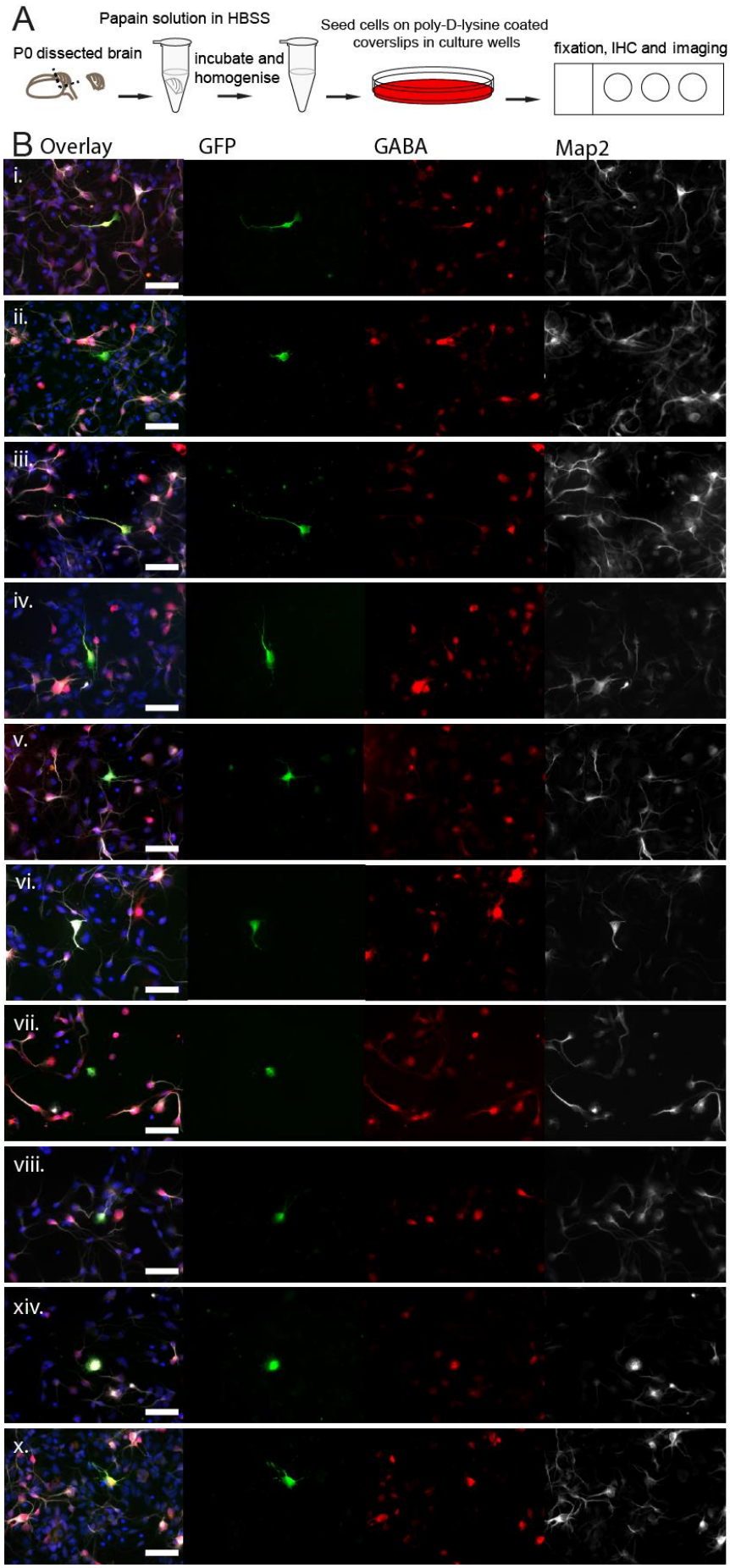
A
Papain solution in HBSS
P0 dissected brain
incubate and homogenise
Seed cells on poly-D-lysine coated coverslips in culture wells
fixation, IHC and imaging
B Overlay
GFP
GABA
Map2
i.
ii.
iii.
iv.
v.
vi.
vii.
viii.
xiv.
x.

2.2.3 IDENTIFICATION OF *SOX14*+ CELLS BY IN SITU HYBRIDIZATION

Neither the immunohistochemistry in serial brain sections nor primary cell culture could confirm whether there are other GABAergic populations besides the *Sox14*$^{+}$ cells within in the cerebellar nuclei. To resolve this question, I carried out *in situ* hybridization using riboprobes against *Gad1* and *Gad2* mRNA, which encode the GABA synthesising GAD67 and GAD65 enzymes, respectively, and are therefore valid markers for GABAergic neurons. *In situ* hybridization was conducted on long-fixed sections of *Sox14*$^{Gfp/+}$ P14 and P21 brain. Fast red was used as a substrate over NBT/BCIP as it is fluorescent and thus can be visualised alongside other fluorophores and GFP.

Figure 2-9 summarises the *in situ* hybridization and histochemical data for all the riboprobes in the lateral nucleus. *Gad1* (**Figure 2-9A**) and *Gad2* (**Figure 2-9B**) staining shows that GFP^{+} cells express both mRNA for GAD67 and GAD65 proteins. *In situ* hybridization with riboprobes against *PValb*, *Calb1* and *Calb2* confirmed that GFP^{+} cells are negative for PValb (**Figure 2-9C**) and Calb1 (**Figure 2-9D**) and are mostly negative for Calb2 (**Figure 2-9E**). While this largely concurs with the immunohistochemistry reported above, GFP^{+}/Calb2^{+} cells were observed in the ventral part of the lateral nucleus.

Figure 2-10-13 show each mRNA expression pattern throughout the cerebellar nuclear mass across rostral to caudal sections.

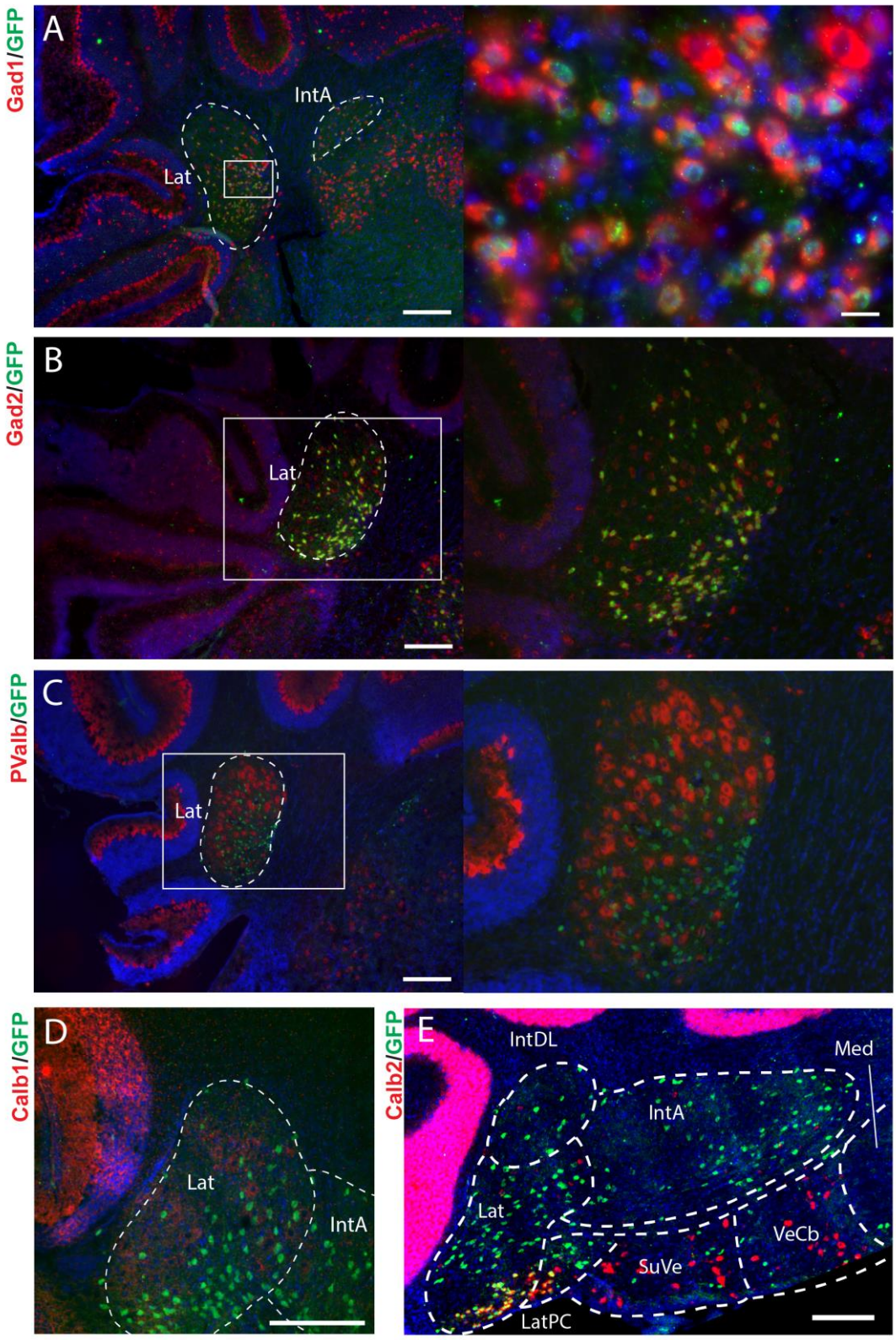

Figure 2-9 In situ hybridisation in Sox14$^{Gfp/+}$ cerebellar coronal slices at P14 and P21

*ISH against Gad1 (**A**), Gad2 (**B**), PValb (**C**), Calb1 (**D**) and Calb2 (**E**). The right hand side shows higher magnification images of the lateral nucleus. Scale: A: 200µm, inset: 20µm, B-E: 200 µm*

2.2.3.1 GAD1 MRNA IS FOUND THROUGHOUT SMALL CELLS OF THE CEREBELLAR NUCLEI

Figure 2-10A shows the GFP and *Gad1* colocalisation in the lateral and anterior interposed nuclei. As expected, *Gad1* expression is also observed within Purkinje cells as well as the molecular layer of the cerebellar cortex and in scattered cells within the granule cell layer. Large and small *Gad1*$^{+}$ cells are seen in the vestibular nuclei inferior to the anterior interposed nucleus (**Figure 2-10B**).

Figure 2-10E shows a higher magnification image of **Figure 2-10B** and shows that both GFP^{+} (**white arrowheads**) and GFP^{-} (**orange arrowheads**) cells are *Gad1*$^{+}$. This suggests that not all GABAergic cells of the cerebellar nuclei express *Sox14*. The co-expression of GFP and *Gad1* is consistent throughout the cerebellar nuclei (**Figure 2-10B,D,E**). Small *Gad1*$^{+}$ cells are seen in the medial nucleus (**Figure 2-10B,E, orange arrowheads**), where GFP^{+} cells are absent.

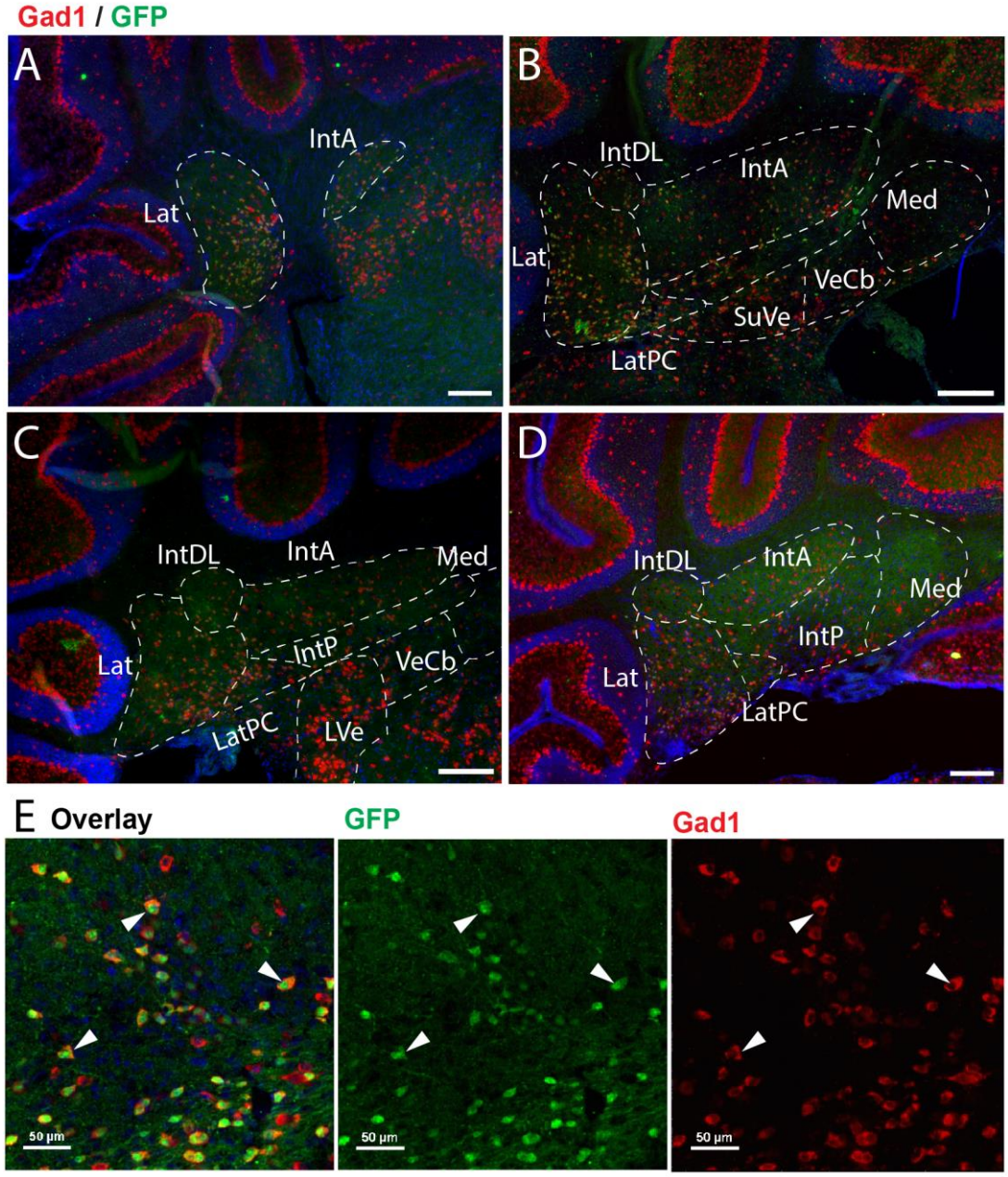

Figure 2-10 In situ hybridisation against Gad1

*$Sox14^{Gfp/+}$ cerebellar coronal slices at P14 and P21 arranged from rostral (**A**) to caudal (**D**). **E**) a higher magnification image to show that all the GFP^+ cells are positive for Gad1 (white arrowheads), and in addition, there are $Gad1^+$ cells that are not GFP^+. Scale: A-D 200 µm, E: 50 µm*

2.2.3.2 GAD2 LABELLING CORRESPONDS WITH GAD1 LABELLING

Figure 2-11 shows *Gad2* labelling throughout the cerebellum. Hybridisation of the riboprobe at 65˚C resulted in unspecific binding so that even the oligodendrocytes in the white matter are labelled (**Figure 2-11A**). This prompted an optimization of the protocol where the hybridisation temperature was incrementally increased to suppress non-specific hybridisation. Labelling of *Gad2* similar to that of the *Gad1* expression pattern was seen following hybridization at 72 ˚C. Small *Gad2*$^+$ cells are seen throughout all the sub-regions of the cerebellar nuclei, most of which co-localised with GFP expression. Since there were no GFP single positive cells, I conclude that all the *Sox14*$^+$ cells express *Gad2*.

As with *Gad1* expression, there are *Gad2*$^+$ cells that are not GFP$^+$, implying the existence of at least two distinct GABAergic populations. This is most clearly seen in **Figure 2-11B**, where instances of co-labelling are marked with white arrowheads and *Gad2*$^+$ only cells are marked with an orange arrowhead. Again, *Gad2*$^+$ only cells are seen in the medial nucleus, where there are no GFP$^+$ cells (**Figure 2-11C,D**). Looking at the cerebellar cortex, it is evident that the Purkinje cell layer and some cells in the granule cell layer are *Gad2*$^+$, as well as some cells in the molecular layer. In addition, large GFP$^-$/*Gad2*$^+$ cells are seen in the vestibular and cochlear nuclei, as well as some GFP$^+$/*Gad2*$^+$ cells in the vestibulocerebellar nucleus (**Figure 2-11C**).

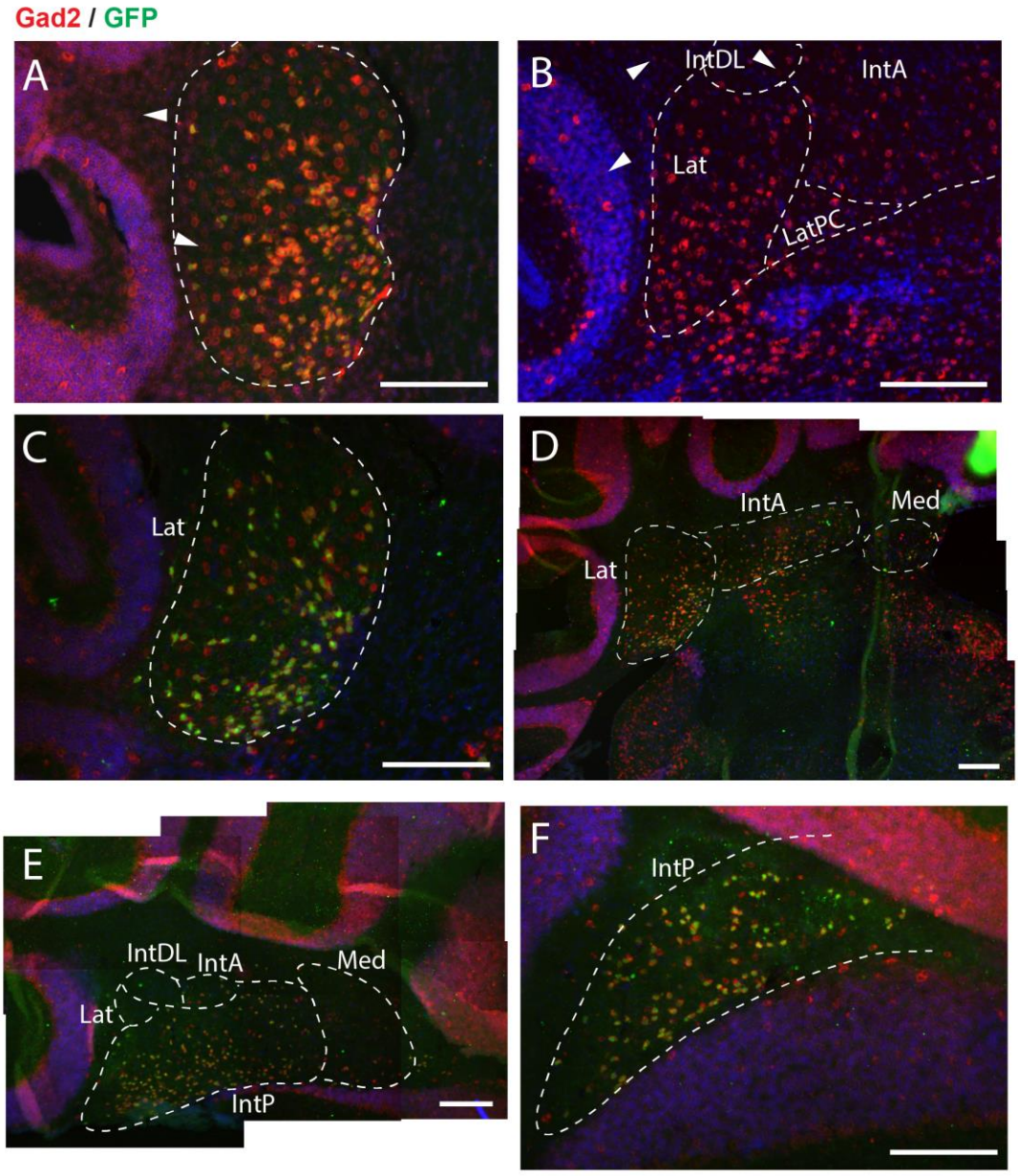

Figure 2-11 In situ hybridisation against Gad2

$Sox14^{Gfp/+}$ cerebellar coronal slices at P14 and P21. ***A&B****) An example unspecific binding when the probe was hybridised at 65˚C, showing many more "labeled" cells (white arrowheads), including small oligodendrocytes in the white matter, cortex and nucleus.* ***C-F****) The distribution of $Gad2^{+}$ cells in the cerebellum as compared to the Sox14 expression from rostral (****C****) to caudal (****F****) sections. Scale: 200 µm*

2.2.3.3 *PVALB* MRNA REVEALS A POPULATION THAT IS MUTUALLY EXCLUSIVE OF SOX14 GENE EXPRESSION

The expression pattern of *PValb* differs substantially from that of *Gad1* and *Gad2* (**Figure 2-12**). Notably, *PValb* and *GFP* labelling is restricted to different domains throughout the cerebellum. Within the cerebellar cortex, the Purkinje cells and molecular layer cells are $PValb^{+}$, while there are no $PValb^{+}$ in the granule cell layer. $PValb^{+}$ cells are seen throughout the cerebellar nuclei, but do not overlap with the distribution of GFP^{+} cells. Much of the rostral tip of the lateral nucleus is comprised of $PValb^{+}$ cells where few GFP^{+} cells are found (**Figure 2-12A**). More caudally in the lateral nucleus, the highest density of $PValb^{+}$ cells is found in the dorsal part of the nucleus, forming a C-shape that cups the majority of ventrally located GFP^{+} cells (**Figure 2-12B,C,D**). Correspondingly, there are many $PValb^{+}$ cells in the GFP-sparse dorsolateral and anterior interposed nuclei (**Figure 2-12C,D,**E). Most caudally, there are $PValb^{+}$ cells in the posterior interposed and medial nuclei (**Figure 2-12E,F**).

Cells that express *PValb* are consistently larger than both GFP^{+} cells and GFP^{-} cells that express $Gad1^{+}$ and $Gad2^{+}$ (noted in **Figure 2-10** and **Figure 2-11**). There is therefore a distinct population of large, $GFP^{-}/PValb^{+}$ cells which are both $Gad1^{-}$ and $Gad2^{-}$.

Comparing *PValb* (**Figure 2-9C**) and *Calb1* (**Figure 2-9D**) expression patterns in the lateral nucleus, the two are alike in location and size and appear to mark the same population. Neither of these genes co-express with GFP but they differ in

cerebellar cortical expression, where *Calb1* expression is observed in the granule cell layer. It was not possible to obtain consistent staining against *Calb1* mRNA.

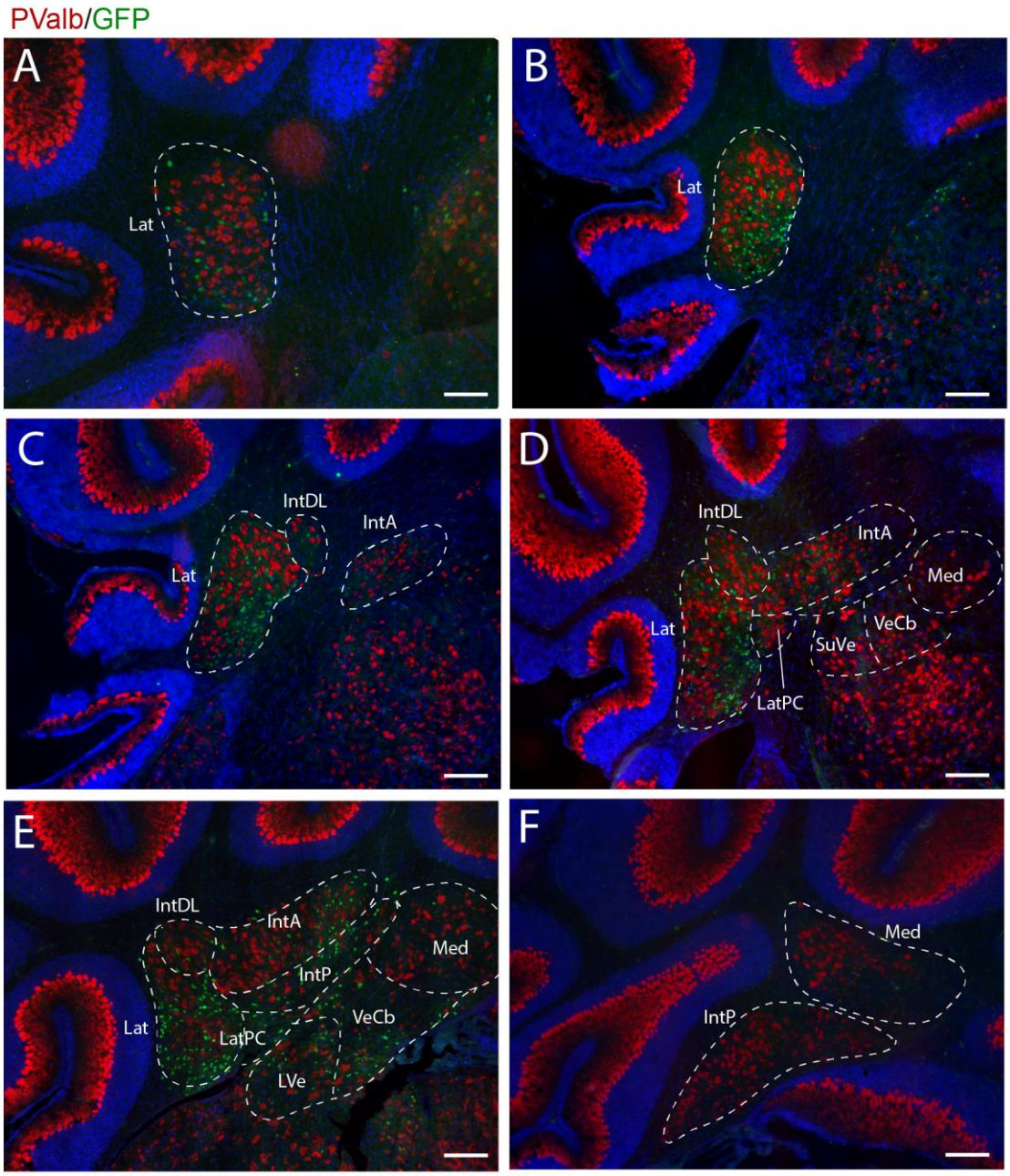

Figure 2-12 In situ hybridisation against PValb

*$Sox14^{Gfp/+}$ cerebellar coronal slices at P14 and P21 from rostral (**A**) to caudal (**F**) sections. Consistently throughout the cerebellum, the PValb and GFP expression patterns are mutually exclusive. Scale: 200 µm*

2.2.3.4 CALB2 LABELLING DIFFERENTIATES SOX14 EXPRESSION INTO TWO POPULATIONS

Figure 2-13 shows *in situ* hybridization against *Calb2* in the central cerebellum. The expression pattern highlights two distinct groups: a small subset of GFP^{-}/*Calb2*$^{+}$ cells scattered across dorsally in the lateral and anterior interposed nuclei (**Figure 2-13B**), and a cluster of GFP^{+}/*Calb2*$^{+}$ cells in the ventral lateral nucleus (**Figure 2-13C**). The ventral segment of the lateral nucleus is very densely populated, and the co-localised cells form a tight-knit group that are geographically distinct from the other lateral nucleus GFP^{+} cells. Within this group, all GFP^{+} cells appear to be *Calb2*$^{+}$. This localised group of cells was consistently observed in repeated staining across different brains (n=5). The remaining GFP^{+} cells did not express *Calb2* throughout the rest of the cerebellar nuclei. The majority of other *Calb2*$^{+}$ cells in the slice are seen in the superior vestibular nuclei and vestibulocerebellar nuclei, as well as the cochlear nuclei more ventrally (**Figure 2-13A**). The scattered GFP^{-}/*Calb2*$^{+}$ cells may be a sub-population of the GFP^{-}/*Gad1*/*2*$^{+}$ remnant (**Figure 2-10, Figure 2-11**); however, this would need to be confirmed with a double ISH experiment against both *Calb2* and *Gad1*/*2*. It would appear, therefore, that there are *Calb2*$^{+}$and *Calb2*$^{-}$ populations within the *Sox14*$^{+}$ population and possibly more sub-populations of GFP^{-}/*Gad1*$^{+}$ neurons, some of which are *Calb2*$^{+}$.

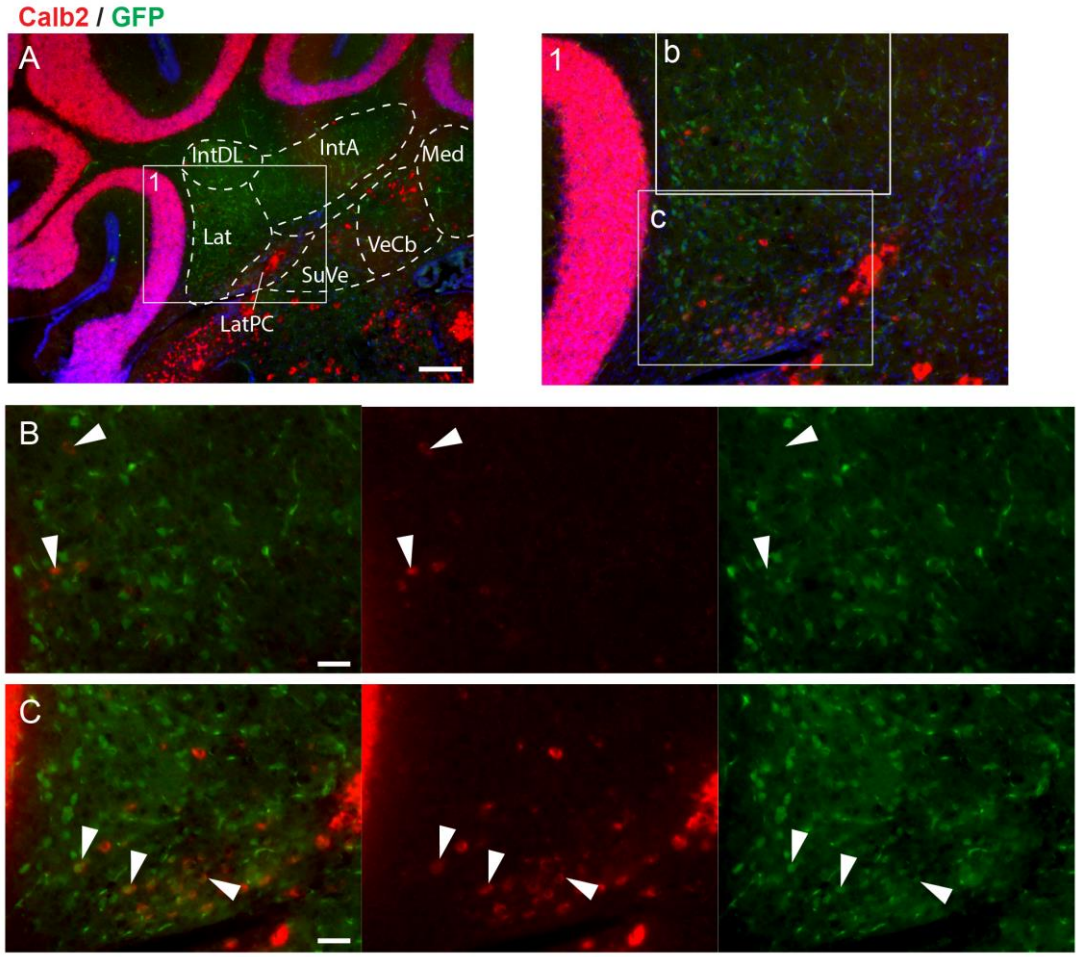

Figure 2-13 In situ hybridisation against Calb2.

A) *A Sox14$^{Gfp/+}$ cerebellar coronal slice at P14. The panels (**B**) and (**C**) show the dorsal and ventral parts of the lateral nucleus in higher magnification. Two distinct populations within the Sox14^{+} cells of the cerebellar nuclei. Sox14^{-}/Calb2^{+} are seen in the central parts of the lateral nucleus, while Sox14^{+}/Calb2^{+} exist in a dense cluster in the ventral parts of the lateral nucleus. Further afield, Calb2^{+} are seen in the vestibular nuclei, medial nucleus and cochlear nuclei. Scale: A: 200 µm, B-C: 40 µm*

2.2.4 THE *SOX14* GENE IS EXPRESSED IN THE MAJORITY, BUT NOT ALL GABAERGIC CELLS

The GFP, *Gad1*, *Gad2* and *PValb* labelling described above was quantitatively analysed to describe the different cell populations identified. The numbers of cells across the cerebellar nuclei that were GFP^+ only, fast-red^+ only or both were counted across the brain slices that were stained (n=5). It was found that while 97% of GFP^+ cells were $Gad1^+$, only 27% of $Gad1^+$ cells were GFP^- (**Figure 2-14A**). A similar result was seen for counts comparing GFP and *Gad2* expression, with 80% of cells co-expressing *Gad2* and GFP. This suggests that *Sox14* expression only represents a portion of GABAergic nuclear neurons. In contrast, 100% of GFP^+ cells were $PValb^-$ and vice versa, verifying the mutual exclusion of the two genes.

In order to gauge the size of the $Sox14^+$ cells relative to the cell types described in other literature (summarised in **Table 2-1**), a sample of these cells were measured for soma size as defined by the cross-sectional area of the cell body on the image plane, and the mean diameter. This was calculated by measuring the maximum and minimum diameter of each soma and taking the average of the two values. The average sizes of $GFP^+/Gad1^+$, $GFP^-/Gad1^+$ and $GFP^-/PValb^+$ cells are charted in **Figure 2-14**. The mean soma cross-sectional area for the three different cell types measured 153.4 ± 5.8 μm^2, 170.7 ± 8.5 $\mu m^2$and 381.4 ± 10.4 μm^2, respectively. The mean soma diameter for the three different cell types measured 14.1 ± 0.3 µm, 15.1 ± 0.4 µm and 22.3 ± 0.3 µm, respectively. As I did not take z-stacks of the cells, the measurements underestimate the true size of the cell soma, since the image plane is likely above or below the widest point of the cell. In addition, the $PValb^+$ cells had an elongated shape so depending on the slice angle, the cross-sectional area varies

over a large range. The GFP$^+$ and GFP$^-$/*Gad1*$^+$ populations largely overlap in both measurements and are not significantly different, while the *PValb*$^+$ cells have little overlap in size with the other two populations. It is unclear whether the distribution is bimodal, with a smaller peak around 280µm^2 in area and 19µm in diameter. This may be due to the elongated profile of the cells (seen in **Figure 2-12**) that would give a large range in cross-sectional area and diameter.

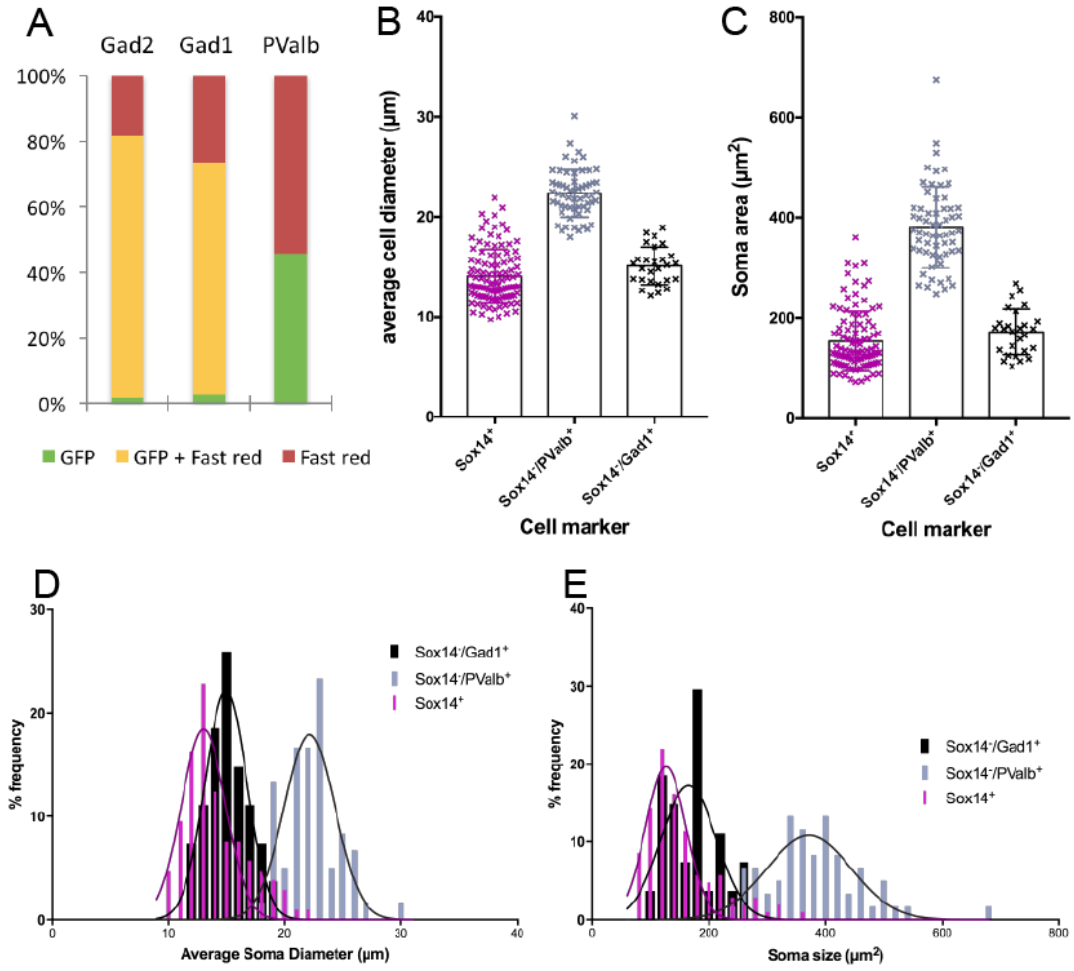

Figure 2-14 Nuclear co-labelling and size analyses.

A*) Cell counts of GFP only, fast-red only and co-labelling from in situ hybridisation data for Gad1, Gad2, and PValb (n=5).* ***B and C****) Scatterplots of soma size as measured by mean soma diameter (µm) (****B****) and by mean soma cross-sectional area (µm^2) (****C****). The mean soma diameters are as follows: GFP$^+$ 14.1 ± 0.3 µm; GFP$^-$/Gad1$^+$ 15.1 ± 0.4 µm; and GFP$^-$/PValb$^+$ 22.3 ± 0.3 µm. The mean soma cross-sectional areas are as follows: GFP$^+$ 153.4 ± 5.8 µm^2; GFP$^-$/Gad1$^+$ 170.7 ± 8.5 µm^2; and GFP$^-$/PValb$^+$ 381.4 ± 10.4 µm^2 (mean±SEM).* ***D and E****) Histograms representations to show peak frequencies of the two Gad1$^+$ populations are also similar.*

2.3 DISCUSSION

Using a *Sox14*$^{Gfp/+}$ mouse line, I found that GFP^{+} cells are found in the cerebellar nuclei. While within the cerebellum, expression is limited to the cerebellar nuclei, this expression pattern is not exclusive within the hindbrain, with other populations found in the medulla. This is the first time that *Sox14* expression has been recorded in the cerebellum and, here, I describe that its expression may define specific sub-populations that can drive forward much needed research on the development and function of cell types in the cerebellar nuclei.

While it is assumed that like the cerebellar cortex, there are many sub-type of nuclear cells, research has been lacking in how to separate and investigate individual groups besides morphological differences, particularly in terms of the GABAergic cells. The results of this chapter sheds light into the possibility of *Sox14* being a marker for a sub-population of GABAergic cells, as well as *PValb* being another specific nuclear marker. *Sox14* is a good candidate as a specific marker due to its limited expression. However, it is important to note that the expression of *Sox14* in vestibular nuclei directly adjacent to the cerebellar nuclei as a caveat to future studies. In addition, while the dramatic loss of GFP^{+} cells in the *Sox14*$^{Gfp/Gfp}$ mouse is not observe in the *Sox14*$^{Gfp/+}$ mouse, haploinsufficiency has not been sufficiently determined. It is known that circadian entrainment and other behavioural phenotypes observed in the knockout mice is not observed in the heterozygous mice. At a broad behavioural level, the heterozygous mice are indistinguishable from wildtype mice. The evidence so far suggests that a 50% reduction in *Sox14* does not lead to any major defect. There is still the possibility that a minor effect is present, perhaps this

could be measured once direct transcriptional targets of *Sox14* are known. A comparison of *Sox14* RNA or protein expression could be made between postnatal heterozygous and wildtype mice to ensure functional expression of the gene.

As described in **Chapter 1.4**, the composition of various cell types can differ across the nuclear mass. Different nomenclature has been used throughout the literature to refer to sub-regions of the cerebellar nuclei. For consistency, I will use the terms outlined in "The Mouse in Stereotaxic Coordinates" Atlas (Paxinos and Franklin, 2004) for guidance. Where necessary, I have interpreted different nomenclature to match this atlas so results are comparable, but it should be noted that some maps are more detailed (Ruigrok, 2011) than the atlas, while others refer only to lateral, interposed or medial nuclei.

2.3.1 HETEROGENEITY OF *SOX14* EXPRESSION ACROSS THE CEREBELLAR NUCLEI

The cerebellar nuclei are irregular in shape and size and its cells also appear to be heterogeneously distributed. The organization and cytology of the nuclei are therefore difficult to describe and ascribe. Chan-Palay made very detailed accounts of morphologically defined cell types and their organizational patterns in her seminal work (Chan-Palay, 1973c). This heterogeneity has been further described in terms of expression patterns of various antigens and transgenes, revealing further subdivisions (Chung et al., 2009).

The present characterization across the cerebellar sub-nuclei reveals heterogeneity not only in clustering of cell types, but also in gene expression. Specifically, the

distribution of *Sox14* expression differs across each nucleus, and for the medial nucleus, it appears to be very limited or completely missing. This distribution is complementary to the distribution of *Zac1*, which is exclusively expressed in GABAergic neurons of the medial nucleus during development, and also in a subset of Golgi cells and within the EGL (Chung et al., 2011).

The highest density of *Sox14*$^+$ cells is found at the ventromedial, parvicellular portion of the lateral nucleus. This distribution matches the description of nucleo-olivary neurons labelled in retrograde tracing experiments from the inferior olive (Brown et al., 1977; Buisseret-Delmas and Batini, 1978; Legendre and Courville, 1987; Tolbert et al., 1976), which found more labelled cells in the ventral regions of the cerebellar nuclei. Labelled cells were located mostly in the lateral parts of the anterior and posterior interposed and in the medial hilus, i.e. the ventromedial portion of the lateral nucleus. In this portion of the lateral nucleus, there is a *Sox14*$^+$/*Calb2*$^+$ population that is distinct from the main *Sox14*$^+$ population. It is not known what the significance of this population is, since no such population has ever been reported until now.

The Purkinje cells of the cerebellar cortex and cerebellar nuclei are topographically connected to form cerebellar modules, which differ in neocortical connectivity and so there may be functional implications for the distribution of these cells (De Zeeuw et al., 1994). Similarly, there is a sub-set of Purkinje cells that project to the vestibular nuclei, which also contain *Sox14*$^+$ neurons, paralleling the connectivity to the cerebellar nuclei. Given the similarities between these two nuclear groups, *Sox14*

expression in the adjacent superior vestibular and vestibulocerebellar nuclei is not surprising.

2.3.2 CHARACTERISING THE *SOX14*$^{+}$ POPULATION

2.3.2.1 SOX14^{+} *CELLS ARE GABAERGIC*

Since *Sox14*$^{+}$ cells in the thalamus are GABAergic interneurons, my first hypothesis was that these are GABAergic interneurons. This is supported by the absence of observable axonal projections that extended beyond the nuclei in the *Sox14*$^{Gfp/+}$ mice. The fact that few or no GFP^{+} cells exist in the medial nucleus also strengthens the case for them being interneurons, since projection neurons are known to extend from all the nuclei.

The staining of cerebellar cells in primary cell culture shows that GFP^{+} cells are invariably GABAergic. In addition, only very occasional GFP^{+} cells were *Gad1*$^{-}$, which are likely to be outliers. This opposes findings by Najac & Raman (2015) where only around 60% of cells retrogradely labelled from the inferior olive were positive for GAD67.

Chan Palay (1973c) noted that there is an array of GABAergic nuclear interneurons, distinguishable by morphology, but there is currently no defined number of interneuronal types. With this in mind, the GFP^{+} cells could be one or more of several interneuronal types. However, based on the large number of GFP^{+} cells, it is possible that these are GABAergic nucleo-olivary projection neurons, since no large population of interneurons have yet been identified and it is thought that nucleo-

olivary neurons are the majority of GABAergic neurons in the cerebellar nuclei (Fredette and Mugnaini, 1991). From the cell counts of *Gad1* and GFP colocalisation, it would seem that the minority GFP^{-}/*Gad1*$^{+}$ population is more likely to be the less frequently reported interneuronal population(s). It is known that glycinergic nuclear interneurons also express GAD67 (Husson et al., 2014; Tanaka and Ezure, 2004). If this is the case, *Sox14* expression may be crucial in distinguishing nucleo-olivary neurons from interneuron; soma size analysis and electrophysiological studies have not shown two discrete GABAergic populations (Uusisaari and Knöpfel, 2008). The present soma size analysis of *Gad1*$^{+}$ cells also shows that GABAergic populations are not significantly different even though they are genetically discrete. It is still to be confirmed whether the *Sox14*$^{+}$ cells represent nucleo-olivary neurons, so the focus of the next chapter looks at potential projections of these cells.

2.3.2.2 SOX14+ CELLS HAVE A UNIFORM SOMA SIZE

The size measurements of the cell types defined by unique marker expression patterns showed results comparable to those reported in previous studies (De Zeeuw et al., 1997; Legendre and Courville, 1987; Teune et al., 1998; Tolbert et al., 1976). Soma size analysis showed that all the GFP^{+} cells are within the 70 to 360µm^{2} range in soma cross-sectional area and 10 to 22µm range in diameter. GFP^{-}/*Gad1*$^{+}$ cells had a similar mean cross-sectional area. While it has previously been pointed out that cell types cannot be determined based on soma size alone (Uusisaari and Knöpfel, 2010; Uusisaari et al., 2007), the measurements in the current study match those of nucleo-olivary neurons measured in previous studies (De Zeeuw et al., 1997; Legendre and Courville, 1987; Teune et al., 1998; Tolbert et al., 1976).

Correspondingly, Uusisaari *et al.* (2007) measured the soma cross-sectional area and obtained similar averages for cells that were GAD^+. The average cell diameters measured also matched those of the small neurons observed in Chan-Palay's work. Chan-Palay (1973c) found that cells could be grouped either above or below 180μm^2 cross-sectional area, with the larger neurons comprising projection neurons.

2.3.2.3 ARE SOX14+ CELLS A SINGLE CELL TYPE?

The histogram of soma sizes of GFP^+ cells is unimodal, and mostly showed the same pattern of expression: they are GABA, *Gad1* and *Gad2* positive, and *Calb1* and *PValb* negative. However, a very small subset of GFP^+ cells in the ventral domain of the lateral nucleus is *Calb2*$^+$, while all other GFP^+ cells are *Calb2*$^-$. This is an additional population, which has not been previously identified. From this finding, it is confirmed that *Sox14* expression defines at least two groups of neurons within the cerebellar nuclei.

2.3.2.4 SOX14+ CELLS DO NOT REPRESENT ALL GABAERGIC POPULATIONS IN THE CEREBELLAR NUCLEI

Since *Gad1*$^+$ and *Gad2*$^+$ also characterise cells that are GFP^-, *Sox14* is not a universal marker gene for GABAergic cell types in the cerebellar nuclei. It is not clear whether the GFP^-/*Gad1*$^+$ and GFP^-/*Gad2*$^+$ populations are one and the same. Some papers suggest that GAD65 and GAD67 are co-expressed in GABAergic populations in the cerebellar nuclei (Esclapez et al., 1994; Greif et al., 1991; Ji and Obata, 1999). In addition, there are *PValb*, *Calb1* and *Calb2* expressing cells that are not part of the GFP^+ population, indicating the presence of *Sox14* negative GABAergic neurons.

2.3.2.5 PVALB MAY BE A MARKER FOR LARGE GLUTAMATERGIC PROJECTION NEURONS

PValb expression identified another nuclear population. The soma size of the *PValb*$^+$ cells matches the measurements for the "large GAD$^-$ cells" or "large columnar neurons" within the literature, which are assumed to be the glutamatergic projection neurons (Aizenman et al., 2003; Chan-Palay, 1973c; Uusisaari et al., 2007). These cells also fit the description of Chan-Palay's large columnar cells, in placement and orientation of cells, as elongated cells that point towards and enclose the medial hilus.

The fact that the glutamatergic neurons express *PValb* is unexpected, since it is a well-known GABAergic interneuron marker. The *PValb*$^+$ cells observed were a different size to those reactive to *Gad1* and *Gad2* staining, showing that they are not GABAergic. While most cells that express *PValb* have been cortical GABAergic interneurons, there is precedent in the literature for *PValb* expression in excitatory corticostriatal projection neurons, pyramidal cells across the neocortex, and a large number of thalamic neurons (Jinno and Kosaka, 2004; Tanahira et al., 2009).

I would posit that the glutamatergic projection neurons express *PValb,* at least transiently in the first 21 postnatal days that were investigated here. This unexpected marker for the glutamatergic neurons could play a significant part in development of circuitry. For example, the expression pattern may relate to the connectivity between *PValb*$^+$ Purkinje cells, *PValb*$^+$ nuclear projecting neurons and *PValb*$^+$ thalamic neurons and the formation of a homotypically mapped circuit between these

structures, not dissimilar to the “Core and matrix” theory described by Jones *et al.* (2001).

2.3.3 CONCLUSIONS

The results in this chapter show that there is a widespread, heterogeneously distributed population of *Sox14*$^{+}$ cells identified by GFP labelling in the *Sox14*$^{Gfp/+}$ mouse line.

Several conclusions can be made from my IHC and ISH experiments:

i. The *Sox14*$^{+}$ cells are GABAergic but do not represent all GABAergic populations in the cerebellar nuclei
ii. The *Sox14*$^{+}$ cells have uniformly small sized soma and their distribution matches that of nucleo-olivary projection neurons
iii. The medial cerebellar nucleus is largely devoid of *Sox14*$^{+}$ cells
iv. *PValb* may be a marker for large glutamatergic projection neurons

It is yet to be determined whether the *Sox14* expressing GABAergic cells are the nucleo-olivary neurons, interneurons, or an unidentified projection cell type that targets another area of the brain. Thus, in the next chapter, I will discuss how Cre-dependent viral vectors expressing fluorescent proteins were used in conjunction with the *Sox14*$^{Cre/+}$ line to investigate the efferent projections of these cells and confirm if this is the case.

3 CONNECTIVITY

3.1 INTRODUCTION

The previous chapter highlighted that *Sox14*$^{+}$ cells represent some but not all of the GABAergic cells in the cerebellar nuclei. By their preponderance in the lateral and interposed nuclei, it is likely that the main (*Sox14*$^{+}$/*Calb2*$^{–}$) population is the nucleo-olivary neurons that have been reported in many past neuronal tracing experiments (Graybiel et al., 1973; Martin et al., 1976; Ruigrok and Voogd, 1990). By contrast, *Sox14*$^{+}$/*Calb2*$^{+}$ cells are found in the ventral part of lateral nucleus, which also has the highest density of *Sox14*$^{+}$ cells. This region is known to be the origin of cerebello-pretectal projections (Kawamura et al., 1982; Nakamura et al., 2006). While Nakamura *et al.* (2006) found that these projections were derived from both GAD^{+} and GAD$^{–}$ cells, the smaller GAD^{+} cells, mostly found in the ventral part of lateral nucleus, most closely match the observed distribution of *Sox14*$^{+}$ cells. It therefore seems possible that there is a second population of *Sox14*$^{+}$ cells that project to the pre-tectum. This chapter aims to determine whether these *Sox14*$^{+}$ cells are exclusively, projection neurons of a single or diverse type, or a mixture of projection neurons and local interneurons.

The availability of *Sox14*$^{Cre/+}$ mice offers the advantage of being able to conditionally target only the *Sox14*$^{+}$ cells within the cerebellar nuclei. Using the *Sox14-Cre* line, the Cre/LoxP recombinase system was used to induce specific expression with stereotaxically injected rAAVs. Additionally, the *Sox14-Gfp* reporter line was used to trace candidate target regions of nuclear *Sox14*$^{+}$ nuclei with fluorescent RetroBeads.

3.1.1 THE HISTORY OF AXONAL TRACING TECHNIQUES

Neuronal tracing techniques have existed since the 19th century (Cowan, 1998) and for decades, the main efferent projections of the cerebellar nuclei have been known from tracing experiments that were performed in larger animals such as the opossum, cat, ferret and rat. Early techniques relied on either chromatolysis in Nissl statins or the labelling of specific myelin degeneration following targeted axonal lesions to trace connectivity. In the 1970s, retrograde and anterograde tracers based on axonal transport mechanisms allowed the labelling of intact axons (Wingate and Kwint, 2006). Early retrograde tracing experiments using horseradish peroxidase (HRP), then HRP conjugated to certain plant lectins such as wheat germ agglutinin (WGA) into the inferior olive (Dom et al., 1973; Martin et al., 1976). Meanwhile, autoradiographic injections of radioactively tagged amino acids into the cerebellar nuclei provided concurring anterograde evidence for nuclear projections (Angaut and Cicirata, 1982; Graybiel et al., 1973; Legendre and Courville, 1987).

As technological knowledge improved and methods expanded to biocytin, Phaseolus vulgaris-leucoagglutinin (PHA-L) (Ruigrok and Voogd, 1990) and biotinylated dextran amine (BDA), allowing the morphology of labelled neurons to be seen better. In addition, inorganic fluorescent dyes such as Fluoro-gold and fast blue made visualisation easier without the need for histochemical processing (Legendre and Courville, 1987).

Ideal tracers conform to the following ideals: 1) selective and efficient up-take by intact neurons, and not cut fibres that pass the injection site; 2) targeting of specific intracellular proteins to transport a tracer protein in either an anterograde or

retrograde direction; 3) amplification of visible particles with minimal histological processing to fill the cell so morphology can be analysed; 4) a variety of different colours for multiple tracers to be used together; 5) the speed of transport, which determines the time between injection and observation; and 6) the potential to cross synapses to label higher-order neurons if needed (Nassi et al., 2015). These ideals can be fully realised with molecular techniques that enable selective labelling of genetically defined populations. In recent years, genetic reporter mouse lines have been coupled with viruses that are engineered to cause biological production of fluorescent proteins to investigate specific populations.

3.1.2 Adenoassociated viruses can be used as non-trans-synaptic tracers

Advances in neuronal tracing techniques have cumulated in viral tracing, which allows delivery of genes by manipulating neurotropic viruses to act as vectors. There are many different classes of viruses, which vary in replication competency, the target cell type, whether the viral genome is DNA or RNA, whether the vector genome integrates into the host genome, the limits of vector genome size, stability and duration of gene expression levels, the vector concentration, speed of expression after infection, ease of altering the genome and capsid, cytotoxicity and safety to the user. A review of the different types of viral vectors can be found in Nassi *et al.* (2015). The usefulness of a specific virus can only be determined by weighing up which aspects of a viral vector are important for the experiment. Recombinant Adenoassociated viruses (AAVs) have been used for anatomical and functional circuit mapping in a large number of studies (Betley and Sternson, 2011). AAVs are a class of parvoviridae, which can be used as non-transsynaptic, low

immunogenicity vectors to deliver recombinant genes. AAVs do not integrate its DNA into the genome, but rather the recombinant AAV (rAAV) vectors deliver a single stranded DNA into the host cell. Targeted injections of AAVs have been successfully used to trace the long-range axons (Chamberlin et al., 1998).

The naturally occurring AAV has the *Rep* and *Cap* genes flanked with inverted terminal repeats (ITR) (**Figure 3–1A**), which are needed for the synthesis of the complementary DNA strand. In contrast to these AAVs, which integrate their genome into the host chromosome at a specific locus, tracing experiments use modified AAV vectors carrying a deletion of the rep genes so that integration, which can disrupt normal gene function, will not occur (McCarty et al., 2004). Transcription of the transgene is driven by the constitutive ubiquitous promoter EF1a and the whole genome is flanked by ITRs. The *Rep* and *Cap* genes are put into a separate plasmid, which specifies the serotype. In rAAV production, this Rep-Cap plasmid is transfected along with the AAV expression plasmid that has the transgene and ITRs, and a helper plasmid that have the adenovirus genes E2a, E4 and VS that are found in the helper virus that is normally required for infection (**Figure 3–1B**).

Following infection, host cell-mediated DNA synthesis processes the single strand transgene DNA into a circular double-stranded episome, which can concatemerise and exist extra-chromosomally because of its high molecular weight as concatermers or episomes. These episomes are chromatin-like and so are stable, non-damaging to the host cells and can remain in non-dividing cells for long periods of time while enabling transgene expression. AAVs are therefore unsuitable for use in dividing cells.

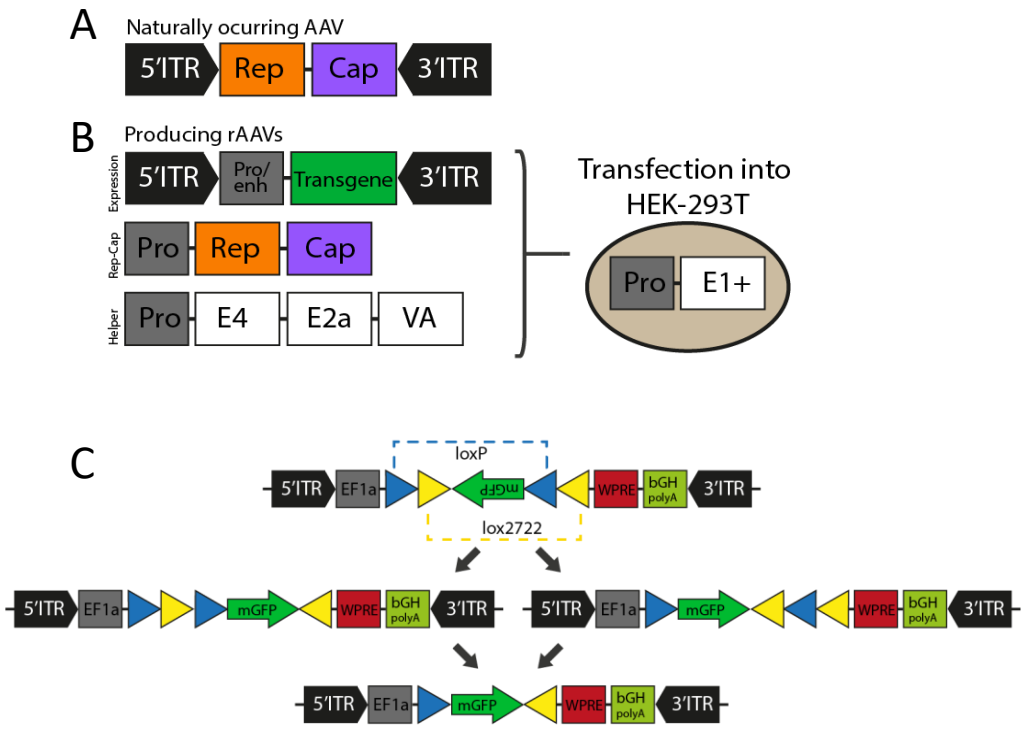

Figure 3–1 DNA plasmids in AAV production

A*) The DNA of a naturally occurring AAV* ***B****) The expression plasmids needed to produce rAAVs by transfection into HEK293T cells.* ***C****) Schematic of the double-floxed inverted ORF (DIO) system. The reverse-complemented desired transgene is flanked by oppositely oriented LoxP and Lox2272 sites. When Cre acts on either pair of anti-parallel lox sites, it forms intermediate configurations that inverts the transgene, but are unstable and can return back to the original orientation. However, from the intermediate configurations, Cre can act on the now parallel lox sites to excise the other lox site. This prevents further recombination, and thereby ensures stable expression of the transgene.*

The size of the viral genome is limited to ~4.7Kb, which is a major disadvantage of AAVs since this means the delivery of short genes as compared to adenoviruses that have a packing capacity of 36Kb, or retroviruses that can pack up to 12Kb. However, this is counteracted to some extent by the high titres of AAVs that can be made, which means that several AAVs can be co-injected with good rates of co-infection.

The different types of naturally occurring AAVs are referred to as serotypes. Different serotypes vary in their capsid protein and their ITR sequences. As a result, choice of serotype needs to be considered as it confers the AAVs tropism to specifically infect certain cell types and also the speed of onset of the desired gene expression (Aschauer et al., 2013; Burger et al., 2004). In this chapter, I use AAVs that are pseudotype AAV2/1 (ITR sequence from AAV2 and the capsid protein from AAV1). By utilising a hybrid serotype, we can take advantage of the tropism and infection efficiency conferred by AAV1 while keeping the speed of infection, which is limited by the time it takes to produce the second strand for double stranded DNA. AAV2 ITRs have been the most extensively used serotype, and yet the AAV2/2 serotype has been shown to be least effective at transduction compared to pseudotypes that combine the AAV2 ITR with the capsid from another serotype (Holehonnur et al., 2014; Wang et al., 2003).

3.1.2.1 CONDITIONAL ACTIVATION OF AAVS ALLOWS GENETIC TARGETING OF SUBSETS OF NEURONS

In this chapter, I used AAVs that express a fluorescent reporter protein to investigate whether the cerebellar nuclear *Sox14*$^{+}$ cells have processes that exit or remain within the nuclei, using the Cre-lox system (Sauer and Henderson, 1988) and the *Sox14*$^{Cre/+}$ mouse. This enabled visualization of the morphology of the cells and their projections. To ensure that the recombination of the transgene is not reversed, the recombinant DNA uses the double-floxed inverted system (**Figure 3–2C**). The inversed desired transgene is flanked by oppositely oriented LoxP and Lox2272 sites. When Cre acts on either pair of anti-parallel lox sites, it forms intermediate configurations that inverts the transgene but are unstable and can return back to the

original orientation. However, from the intermediate configurations, Cre can act on the now parallel Lox sites to excise the other Lox site. This prevents further recombination, and thereby ensures stable expression of the transgene (Betley and Sternson, 2011).

3.1.3 RETROGRADE TRACING USING FLUORESCENT MICROSPHERES (RETROBEADS)

RetroBeads (Lumafluor) are retrogradely transported fluorescent latex microspheres approximately 0.02μm in diameter. First described by Katz *et al.* (1984) to trace the visual cortex and thalamus, both red and green beads are available and are observed with rhodamine and fluorescein filters, respectively. Injections result in distinctive punctate fluorescence within the cell soma. Unlike other available retrograde fluorescent tracers such as carbocyanine dyes, fast blue, fluorogold, fluororuby and nuclearyellow (Bentivoglio et al., 1980; Honig and Hume, 1989; Schmued and Fallon, 1986), RetroBeads do not readily diffuse from the injection site. Like other fluorescent tracers, they do not require any histochemical processing to visualise, in contrast to retrograde techniques based on the transport of HRP or WGA. RetroBeads do not appear to cause cytotoxicity or phototoxicity and can remain in the *in vivo* animal for months without detrimental effect. Since the RetroBeads are exclusively transported in a retrograde direction and must be actively endocytosed by axonal endings, and so do not carry the risk of being uptaken by damaged projections made by the injection (Apps and Ruigrok, 2007), we can be sure that the traced cells are specific to the injection and are upstream of the injection site. In addition, both colours of RetroBeads have been shown to have high transport efficiency (Apps and Garwicz, 2000; Schofield et al., 2007).

However, the beads are not permanent and that the fluorescence is easily quenched. This was addressed by minimising the amount of processing performed on injected tissue samples and by using Fluoromount mounting agent, since contact with glycerol causes quenching (Katz and Iarovici, 1990).

Using *Sox14*$^{Gfp/+}$ mice, RetroBeads were injected into the inferior olive, the hypothesised target of the *Sox14*$^{+}$ cerebellar nuclear neurons if they are projection neurons, then observed for bead fluorescence at the nuclei, which are retrogradedly transported from the injected areas. If the *Sox14*$^{+}$ neurons are indeed the nucleo-olivary neurons that project to the inferior olive, the beads would fluoresce in the same cells expressing endogenous GFP. RetroBeads have been used previously to label the climbing fibre connectivity of the olivocerebellar system to look at topography of the projections (Apps and Garwicz, 2000). Injections into the cerebellar cortex found that the numbers of retrogradely labelled olive cells corresponded closely to the density of Purkinje cells at the injection sites. I expect that injections into the inferior olive will highlight the nucleo-olivary neurons, and their distribution across the cerebellar nuclei.

3.1.4 AIMS OF THE CHAPTER

Using the two methods outlined above, the aim of this chapter was to investigate whether the *Sox14* expressing cells of the cerebellar nuclei are projection neurons. Injections of AAVs into the nuclei identified axons that reach the inferior olive, and thus are nucleo-olivary projection neurons. RetroBead injections into the midbrain and inferior olive further defined the two *Sox14*$^{+}$ nuclear populations that I identified in the last chapter.

3.2 RESULTS

AAVs were used to specifically target the *Sox14*$^{+}$ cells using the Cre-Lox recombination system, promoting expression of membrane GFP to visualise cell projections. Here, I describe: 1) the process of optimising targeted injections into the cerebellar nuclei, oculomotor nucleus and inferior olive; 2) the production of AAVs; and, 3) the results of the AAV infection and RetroBead tracing experiments.

3.2.1 THE CEREBELLAR NUCLEI CAN BE SPECIFICALLY TARGETED BY STEREOTAXIC INJECTION

Since *Sox14*, and therefore *Cre*, expression declines before adulthood, stereotaxic injections into the nuclei were performed at P14 (**Figure 3–2A**). At this age, it is possible to carry out consistently targeted injections. As the brains at this age are much smaller than adult mice brains, I could not rely on adult brain atlas coordinates for the injections. I acquired my own coordinated by using dye injections into the wild-type mice. I initially used fast green dye (**Figure 3–2B&C**) and subsequently an ink (**Figure 3–2D-G**), which diffused less readily into the surrounding tissue, making it easier to deduce the precise injection site. In this manner, I acquired the coordinates for all the brain regions I injected throughout this thesis (**Table 7-7**). For each of the following experiments, I first carried out trial injections on the wild-type littermates to make minor adjustments for small variations due to different birth times.

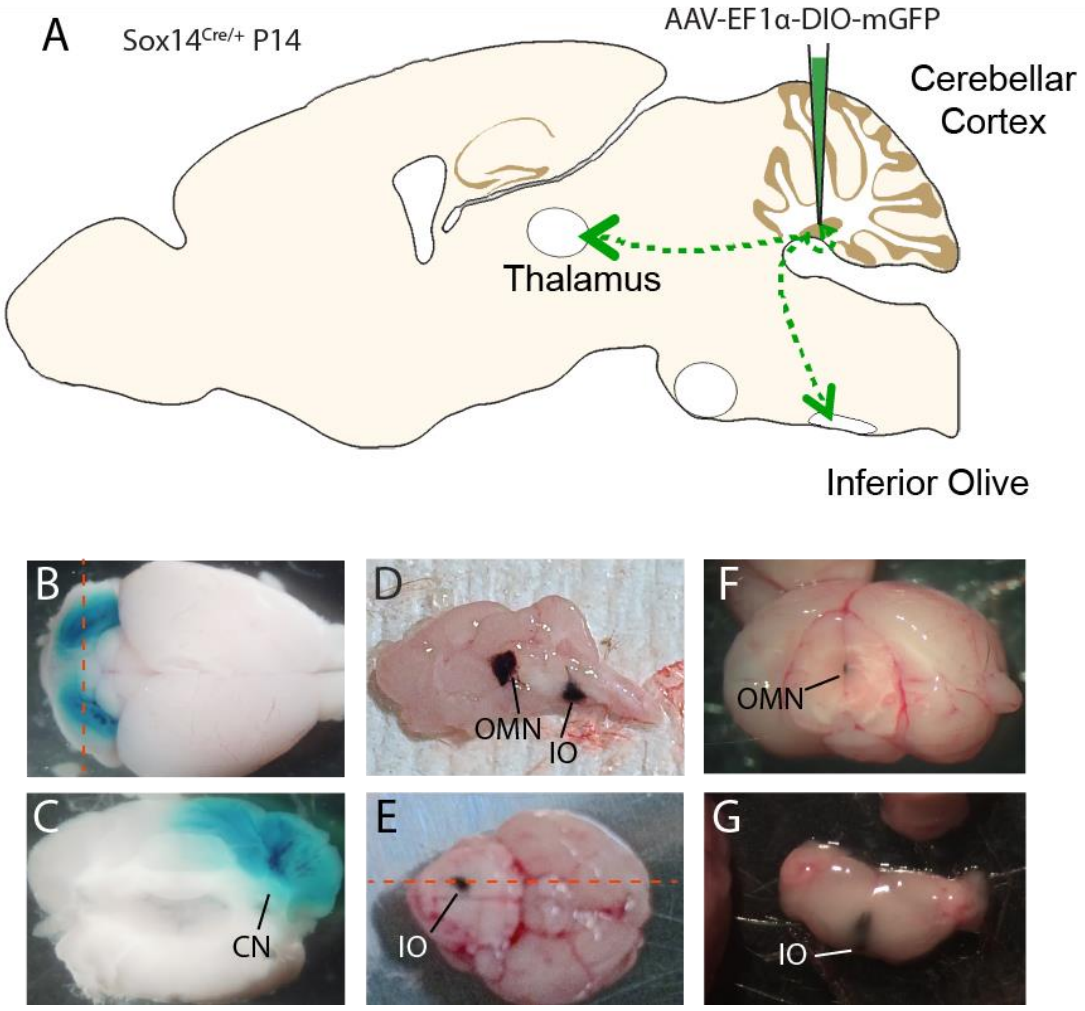

Figure 3–2 Stereotaxic injections into the cerebellar nuclei

A) *schematic of an experiment where a floxed fluorescent reporter AAV is injected into the cerebellar nuclei and thus may mark the projections of Cre-expressing Sox14⁺ cells.* ***B-G)*** *Injection site coordinates were tested on wildtype littermates of the same age. Initially the trial injections were carried out using Fast green dye but this diffuses into the surrounding tissue readily making the injection site difficult to identify (**B&C**).* ***B)*** *dorsal view of mouse brain with bilateral injection of Fast green dye* ***C)*** *a coronal section cut through the cerebellum. The dye spread towards the cerebellar nuclei but the centre of the injection is in the cerebellar cortex, where the dye is most concentrated. Later on, I used ink, which gave a clearer, well-defined injection site (**D-G**). The brains show trial injections for the oculomotor cortex (sagittal:* ***D****, coronal:* ***F****) and the inferior olive (dorsal side of whole brain:* ***E****, sagittal:* ***D****, coronal:* ***G****).*

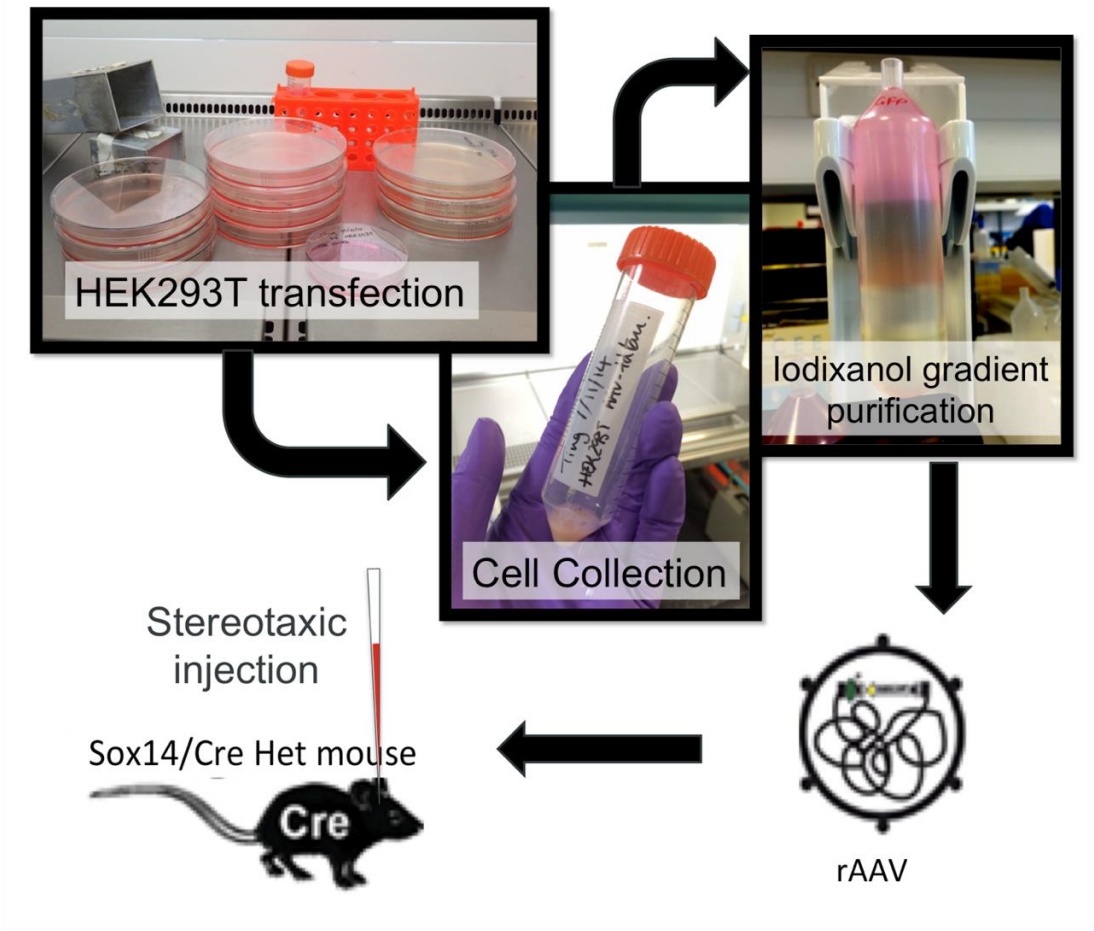

Figure 3–3 Schematic showing the production of AAVs

E. coli containing recombinant DNA plasmids was cultured and the DNA extracted by maxi prep. The rDNA was then transfected into HEK293T cells alongside the adenoviral helper plasmid (pHGT1-adeno) and the AAV serotype 2.1 plasmid using polyethylenimine assisted transfection. 60 hours post transfection, the cells were harvested by centrifugation into a pellet. rAAVs were isolated from the cells by freeze-thaw break down, and precipitated. The virus was then purified and concentrated by ultracentrifugation through an Iodixanol gradient and the fraction was collected and kept at -80˚C until use for stereotaxic injection.

3.2.2 AAV PRODUCTION WAS OPTIMISED IN CELL CULTURE

I produced my own AAV viruses using plasmids bought on Addgene. **Figure 3–3** shows the work flow of AAV production carried out in the lab. The AAVs were quantitatively titred by qPCR to give a measure of vector genomes in each ml (vg/ml) and these titres can be found in **Table 7-5**. The AAVs were also tested *in vitro* for infectivity. Since the AAVs are Cre-dependent, I generated two *Cre*-expressing cell line, firstly using primary cells of *Sox14*$^{Cre/+}$ mice and secondly by stable transfection of the *Cre* gene into HEK293T cells.

3.2.2.1 CRE-EXPRESSING PRIMARY CULTURE CELLS SHOW THAT AAV CAN SPECIFICALLY TARGET CRE EXPRESSING CELLS

Cerebellar cells were dissociated from *Sox14*$^{Cre/+}$ P0 pups was described in the last chapter. After an overnight culture, the primary culture was infected with AAV-EF1a-DIO-TdTomato. The cells were fixed 8 days post infection and stained against MAP2 as a nuclear marker. **Figure 3–4A&B** show the results of testing infectivity of rAAV-EF1a-DIO-TdTomato. The red fluorescence confirms infection by the AAV and successful expression of transgene was consistently limited to MAP2 immunoreactive neuronal cells, shown in green. The co-localisation of TdTomato, GFP and DAPI can be seen at higher magnification (**Figure 3–4B**). This demonstrates that the AAVs are able to infect the neuronal *Cre*-expressing cells targeted, seemingly with selectivity. In addition, the morphology of the cells is clearly exhibited by the expression of the fluorescent protein, making it apt for axonal tracing.

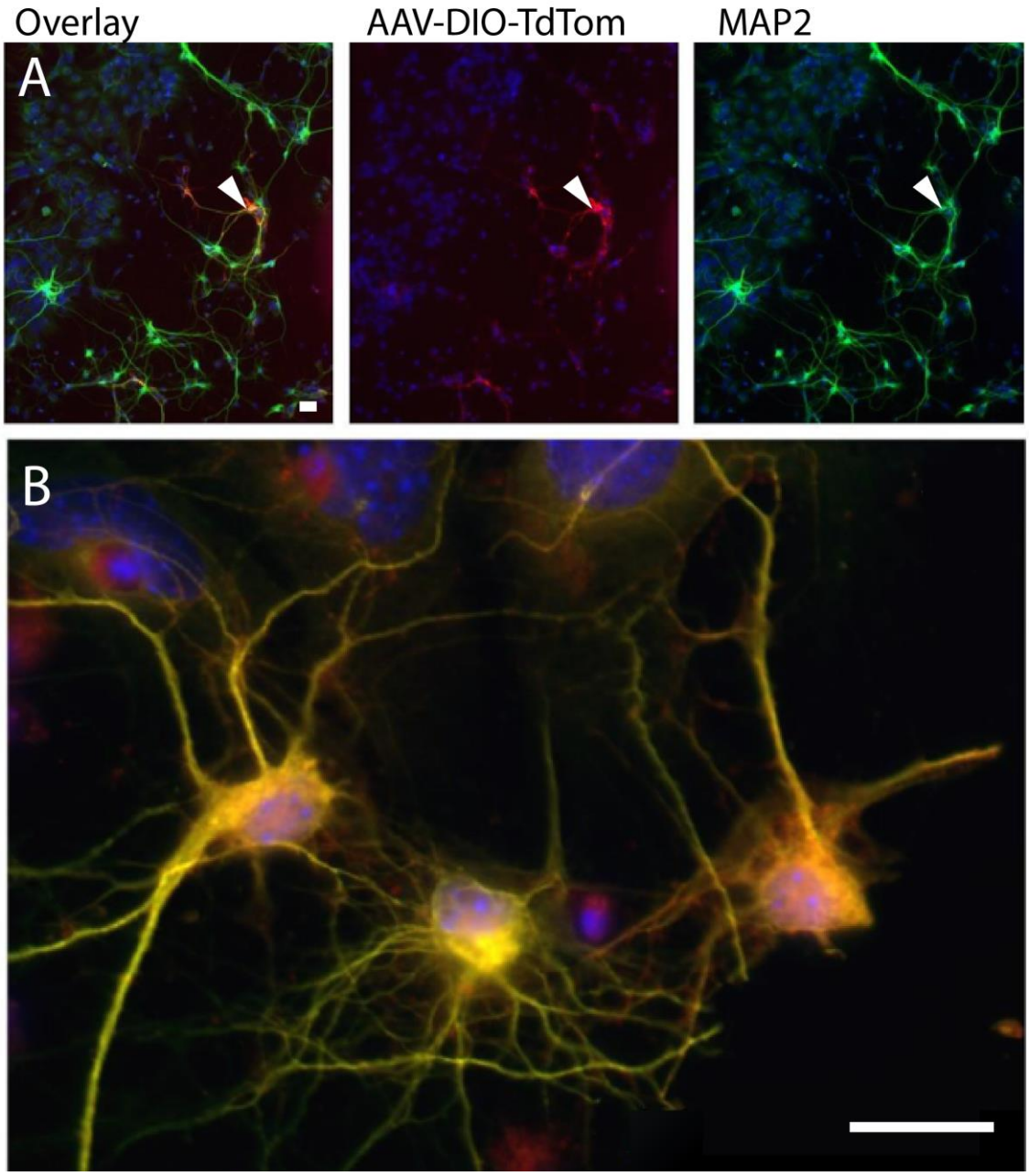

Figure 3–4 In vitro infection of AAVs into primary cell culture

A) *Sox14$^{Cre/+}$primary culture infected with AAV-EF1a-DIO-TdTomato, fixed 8 days post infection and stained with MAP2 as a nuclear marker. The red fluorescence confirms infection by the rAAV-EF1a-DIO-TdTomato and successful expression of transgene (white arrowhead) is limited to MAP2 immunoreactive neuronal cells, shown in green.* ***B)*** *The co-localisation of TdTomato, GFP and DAPI can be seen at higher magnification (40x). Scale: 20 µm*

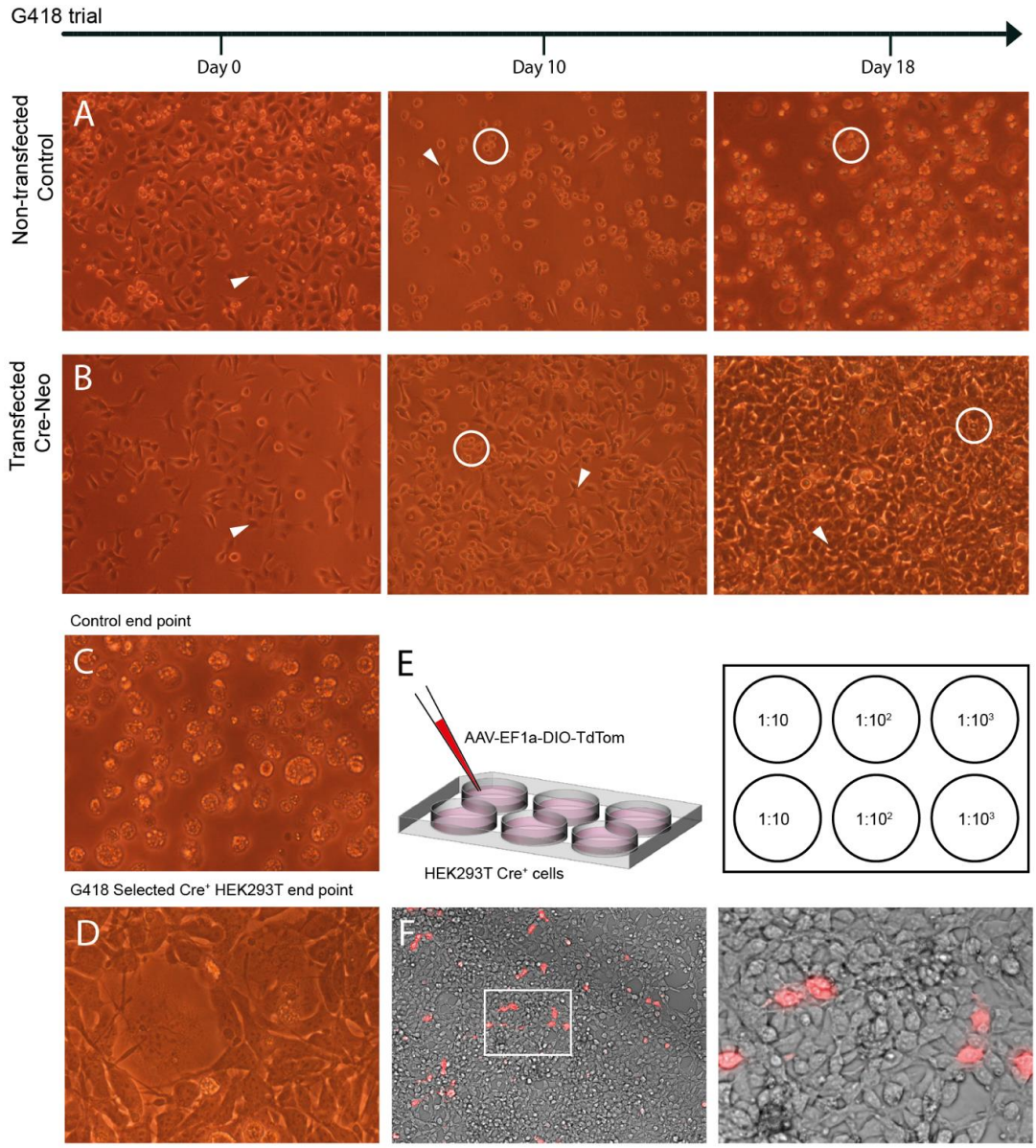

Figure 3–5 Production of Cre-expressing cells by G418 selection

A) *Non-transfected control are the cells without Cre-Neo plasmid and are seen disintegrating with G418. The cells become clumped and detach from the plate, a sign of cell death.* ***B)*** *The transfected cells appear resistant to G418 due to presence of Cre-Neo plasmid which confers resistance to Neomycin. The majority of cells survive in spite of G418 and proliferate by day 18 of the G418 treatment, though other cells do also seem to die. These are presumed to be the cells that have not been transfected with the plasmid.* ***C&D)*** *Magnified images of the end-point cells for both control (**C**) and transfected, G418 resistant cells (**D**). The healthy HEK293T cells reach high confluency and adhere to the surface of the well to form a smooth monolayer, while dying or dead cells form small particles that detach and clump together. These clumps can be seen moving around the culture medium when the plate is agitated. E) HEK293 Cre⁺ cells infected with serial dilutions of rAAVs stock.* ***F)*** *HEK293 Cre⁺ cells infected with AAV-EF1a-DIO-TdTomato, expressing the TdTomato fluorescence, indicating positively infected cell by a viral particle.*

3.2.2.2 PRODUCTION OF CRE-EXPRESSING CELLS BY G418 SELECTION

In order to generate a Cre-expressing immortalised cell line, the Cre-Neo plasmid was transfected into HEK293T cells. Non-transfected cells lack the neomycin resistance conferred by the Cre-Neo plasmid and therefore cannot survive when G418, specific analogue of neomycin, is applied. Through application of G418 every 4 days, cells without neomycin resistance were killed while those resistant and expressing *Cre* survived and continued to divide. **Figure 3–5A&B** shows the selection process compared to a non-transfected control, in which all the cells eventually died. The white arrowheads exemplify healthy looking cells while instances of dead cell clusters that float are circled. After 18 days of G418 selection, the transfected cells appear resistant to G418 and proliferate to high confluency (**white arrowheads** and **Figure 3–5D**), though some cells do also die (**circled** and **Figure 3–5C**). These are presumed to be the cells that have not been transfected with the plasmid. In contrast, the control plate that had no plasmid transfection had dying or dead cells, which form small particles that detach and clump together.

In order to test that the cell culture was expressing *Cre*, a serial dilution of *Cre*-dependent AAV virus was added as shown in **Figure 3–5E** and left to infect. Some HEK293 Cre^{+} cells were successfully infected with AAV-EF1a-DIO-TdTomato (**Figure 3–5F**), expressing the TdTomato fluorescence, indicating positively infected cell by a viral particle. However, unexpectedly, the majority of surviving HEK293T cells from the G418 selection were not infected by the virus. It is not known why this is the case, but the serotype of the AAV is chosen to infect neuronal cells, not immortalised human embryonic kidney cells.

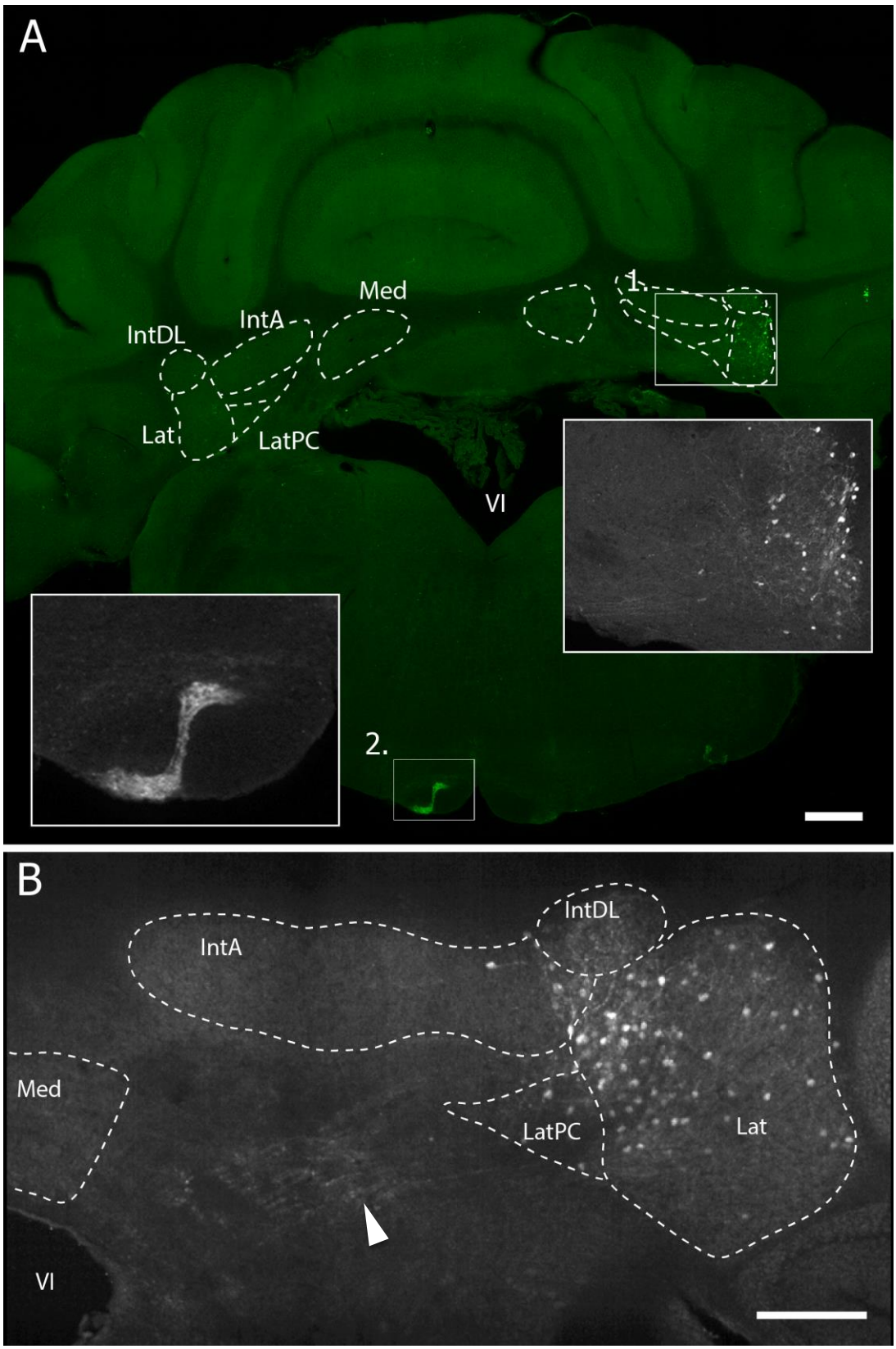
A
Med
IntA
IntDL
Lat
LatPC
VI
1.
2.
B
IntDL
IntA
Med
LatPC
Lat
VI

Figure 3–6 An example of an injection of AAV-EF1a-DIO-mGFP into the lateral nucleus.

A*) image showing the full coronal slice of the hindbrain. It shows the GFP$^+$ targeted cells in the right lateral nucleus and projections seen in the ventro-medial portion of the contralateral medulla, at the most rostral end of the inferior olive. Higher magnification of the two GFP dense areas are shown inset. It is likely that the inferior olive projections are in the principle olive (IOPr), though the slice angle makes it unclear.* ***B****) A more rostral section of the same brain shows that the injection site continues to target predominantly the lateral nucleus. In addition, projections are seen going from the hilus of the lateral nucleus, in the ventromedial part of the lateral nucleus, towards the 4th ventricle (VI), denoted by the white arrowhead. Scale: A: 400 µm, B: 200 µm*

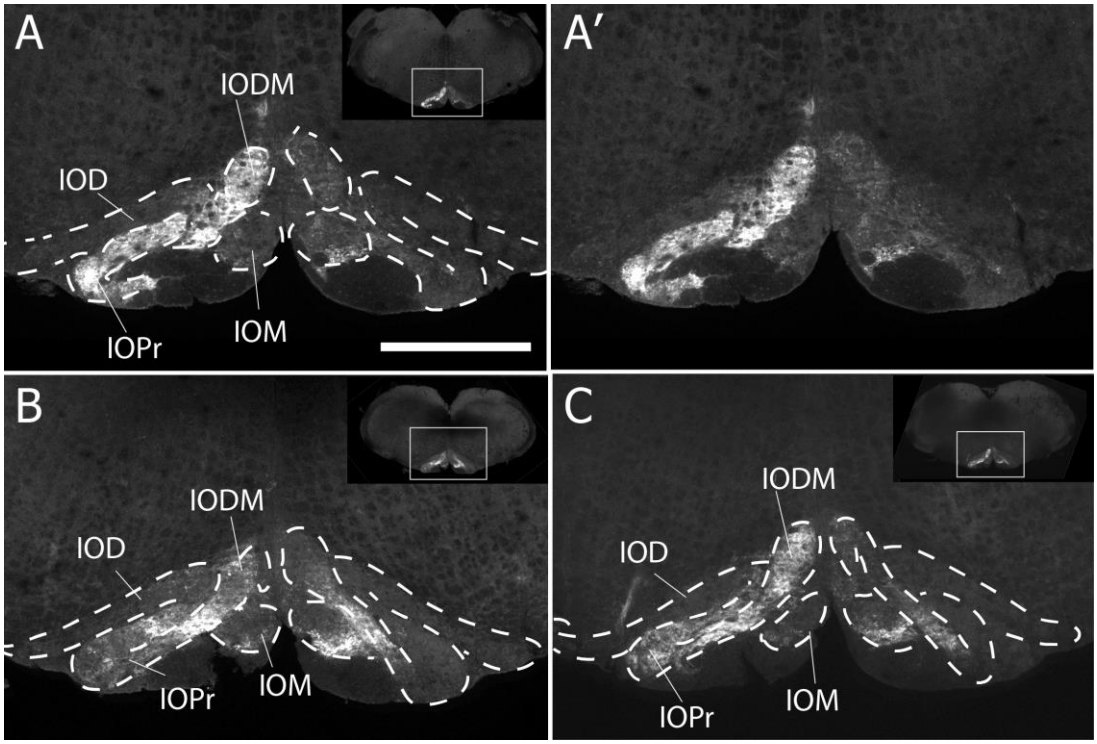

Figure 3–7 AAV-mGFP expression is found in the inferior olive

A-C*) Three select caudal sections of the brainstem, where projections terminate in the inferior olive. Projections were mainly, but not exclusively, found in the contralateral principle olive (IOPr) and rostral medial nuclei of the olive (IOM).* ***(A')*** *shows the same image as* ***(A)*** *without the subnuclear outlines. IOA= inferior olive subnucleus A of medial nucleus; IOB= inferior olive subnucleus B of medial nucleus; IOBe= inferior olive beta subnucleus; IOC= inferior olive subnucleus C of medial nucleus; IOD= inferior olive dorsal nucleus; IODdf= dorsal fold of the IOD; IODM= inferior olive dorsomedial cell group; IOK= inferior olive cap of Kooy of the medial nucleus; IOM= inferior olive medial nucleus; IOPr= inferior olive principal nucleus; IOVL= inferior olive ventrolateral protrusion. Scale: 200 µm*

3.2.3 AAV VIRUS TRACING DEMONSTRATES THAT *SOX14*$^{+}$ CELLS OF THE CEREBELLAR NUCLEI INNERVATE THE INFERIOR OLIVE

The cerebellar nuclei of *Sox14*$^{Cre/+}$ heterozygous mice were unilaterally stereotaxically injected with AAV-EF1a-DIO-mGFP tracers at P14 and collected for analysis at P28 (*n*=14). Injections were able to label the *Sox14*$^{+}$ cells of the lateral cerebellar nucleus specifically. An example of such is shown in **Figure 3–6** and **Figure 3–7**. The distribution and size of labelled cell soma are similar to the cells seen in *Sox14*$^{Gfp/+}$ sections (**Chapter 2.2.1**), with a higher density of cells found in the ventromedial portion of the lateral nucleus (**Figure 3–6B**). Injections into the lateral nucleus also traced projections travelling medially the cerebellar peduncles that comprise the lateral and superior walls of the fourth ventricle (**Figure 3–6B**, **white arrowhead**).

In the coronal slice shown in **Figure 3–6A**, GFP labelling was observed in the ventral medulla on either side of the midline. Since I believed this could be the very rostral tip of the inferior olive, the rest of the brain stem was analysed. These axonal tracts were found to predominantly target the contralateral inferior olive (**Figure 3–6A**, **inset**, and **Figure 3–7**). **Figure 1–7** shows the brainstem sections from most rostral (**A**) to caudal inferior olive (**C**) from a single animal. No labelled axon terminals were detected in the most caudal inferior olive. Terminals are mainly, but not exclusively, found in the contralateral principle olive (IOPr), and inferior olive dorsomedial cell group (IODM), while no projections are seen in the dorsal olivary nucleus (IOD). Careful examination reveals ipsilateral terminations in similar regions, but also, additionally, in the medial olivary nucleus (IOM), seen clearly in

Figure 1–7A', (which is the same image as **Figure 1–7A** without the atlas guide lines). This pattern of labelling with strongest targeting of the principal olivary nucleus was confirmed through repeated injections targeting lateral nucleus (n = 14).

3.2.4 *SOX14*$^{+}$ CELLS OF THE LATERAL CEREBELLAR NUCLEUS PROJECT TO BOTH CONTRALATERAL AND IPSILATERAL INFERIOR OLIVE

To investigate bilateral connectivity, the lateral nuclei on either side of the brain were injected with AAV driving expression of contrasting membrane-bound GFP and tdTom fluorescent proteins (**Figure 3–8** and **Figure 3–9**). **Figure 3–8A** shows the injected cerebellar nuclei. Fluorescence is seen in both lateral nuclei, although only the rostral lateral nucleus is depicted. AAV-GFP infection is found not only in the lateral nucleus, but also in the dorsolateral and anterior interposed nuclei. Red and green fluorescent axons are seen extending medially towards the ventricle (**Figure 3–8A**, **white arrowheads**) and they reappear in the contralateral ventromedial portion of the medulla of the same slice.

Figure 3–8B shows the inferior olive of the same brain, where distinct patterns of fluorescent label are seen bilaterally. Both AAV expression patterns are strongest in the contralateral inferior olive compared to the ipsilateral contribution. Again, the most intense expression is found in the principal olive, but since more regions of the cerebellar nuclei were infected on both sides, faint expression is also seen in the other regions of the olive, such as the medial nuclei and the dorsomedial cell group. In addition, fainter ipsilateral projections appear to mirror the contralateral targeted regions.

High magnification images were taken of the inferior olive axonal terminals in order to examine the differences between contralateral and ipsilateral connections (**Figure 3–9**). **Figure 3–9A** shows the labelled axons more caudally in the inferior olive. As well as the principal olive, there is strong expression at the ventrolateral protrusion (IOVL) and the cap of Kooy of the medial nucleus (IOK). The contralateral fibres are seen to form a dense mesh around presumptive cells (spherical inclusions that are devoid of any axons). This is seen in the higher magnification column in **Figure 3–9B** with axons expressing tdTomato. The GFP expressing fibres (**Figure 3–9C**) come from the ipsilateral cerebellar nuclei and are seen to target the same areas. While these axons span the same regions as the contralateral axons, there are far fewer projections and individual axonal varicosities can be seen. This is not related to the effectiveness of the two different AAVs since the corresponding pattern is observed in the opposite inferior olive. Thus the projections extend with bilateral symmetry, though the contralateral side is always more densely populated with axonal boutons.

Figure 3–9D-F show three instances of nucleo-olivary axons expressing mGFP within the inferior olive, bypassing "spaces" where olivary cells reside, confirmed by nuclear DAPI staining (**asterisk, ***). Interestingly, synaptic boutons do not seem to contact the boundaries of the cell, but rather are gathered in bundles (**Figure 1-9E**, **white arrowheads**) where there are no visible cells.

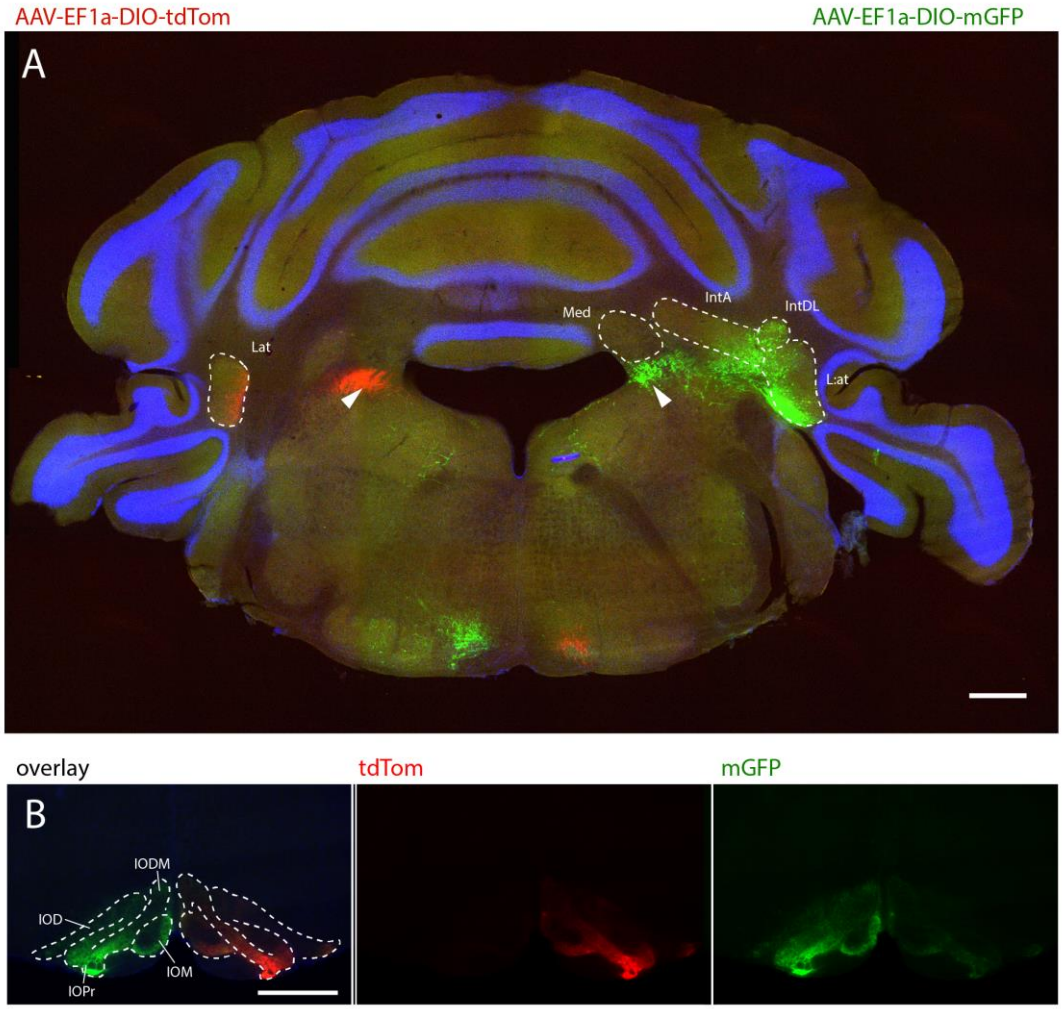

Figure 3–8 Bilateral stereotaxic AAV injections

A) *Injections of AAV-EF1a-DIO-mGFP and AAV-EF1a-DIO-TdTomato into the lateral nuclei of Sox14$^{Cre/+}$ heterozygous mice at P14 and collected for analysis at P28 (n=7). Injections into the lateral nucleus traced projections travelling medially towards the ventricle before heading dorsally to target the inferior olive.* ***B)*** *Axonal tracts target both the ipsilateral and contralateral inferior olive. For the mGFP, it is clear that the projections are bilateral, though denser fluorescence is seen on the contralateral side. Scale: A: 500 µm, B: 200 µm*

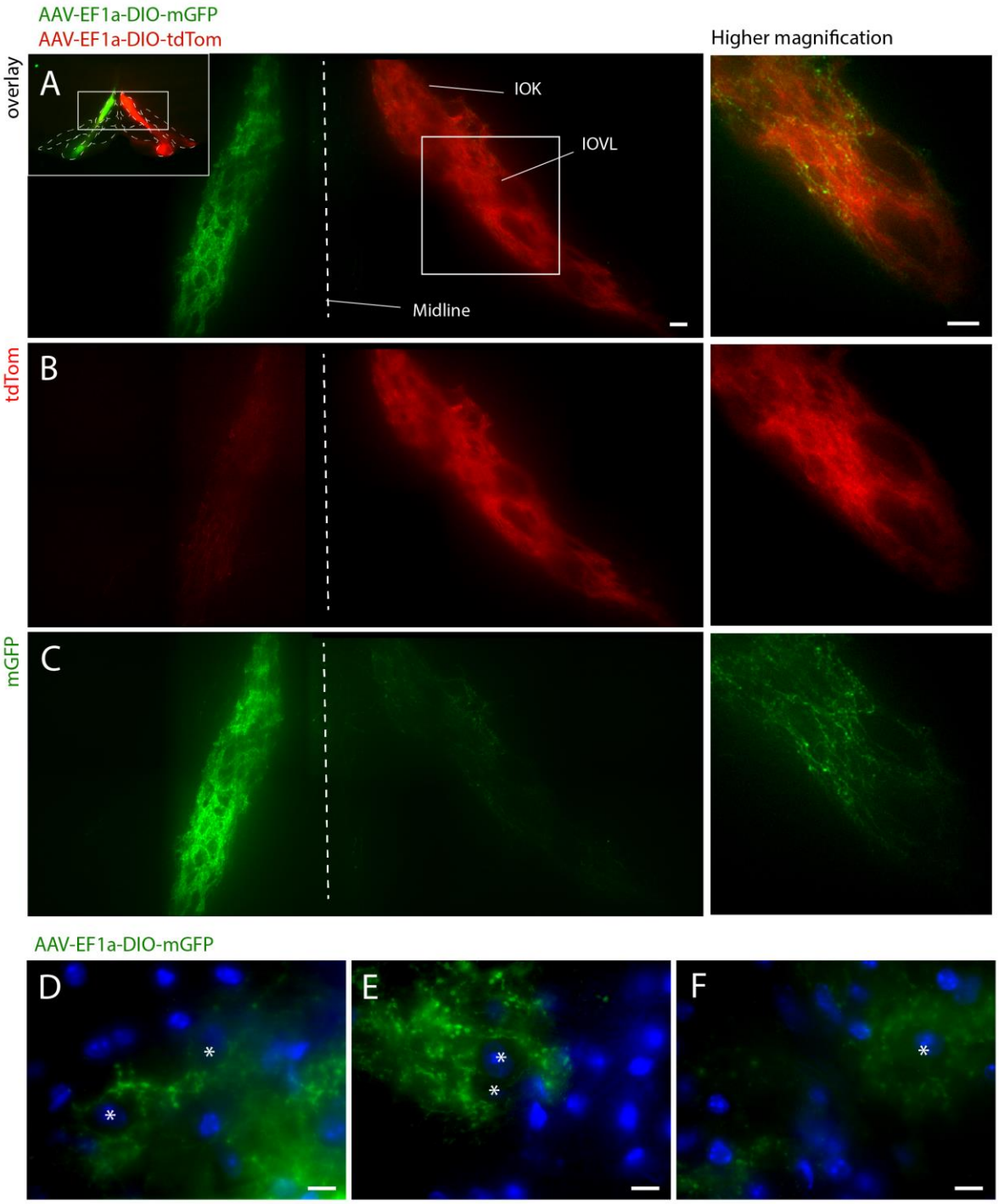

Figure 3–9 Detailed images of the inferior olive of the bilaterally injected brain from Figure 3–8

A-C) *The panels show Although the projections clearly terminate in the contralateral olive, axons with synaptic boutons can be seen in the ipsilateral side contacting the same range of cells. Higher magnification view is shown on the right hand side.* ***(D-F)*** *mGFP expressing axons imaged at high magnification show axons bypassing spaces where olivary cells reside (asterisk, *). DAPI staining in blue shows each space has a nucleus in the centre. Scale: 20 µm*

3.2.1 INJECTIONS OF CRE-DEPENDENT AAV MEMBRANE MARKERS ALSO LABEL IPSILATERAL OCULOMOTOR NUCLEUS.

In addition to projections of *Sox14*$^{+}$ cells to the inferior olive, a small proportion of brains showed projections that extend from injection sites into the midbrain. **Figure 3–10** and **Figure 3–11** show various coronal brain slices of one particular example of this. The cerebellar nuclei were widely targeted ipsilaterally to cover all the cerebellar nuclei except the medial nucleus (**Figure 3–10A-C**). As expected, this resulted in widespread targeting across the inferior olive (**Figure 3–10D-F**). While the majority of axonal tracts descend after the decussation to travel caudally back towards the inferior olive (**Figure 3–10G&I**), a few fibres with axons (**Figure 3–10H**, **white arrowhead**) are seen separating from the tract before the decussation and head towards the ipsilateral oculomotor nucleus, which lies dorsal to the recognisable medial longitudinal fasciculus. More rostrally, these axons are more clearly seen in the oculomotor nucleus, which lies on the ventral edge of the periaqueductal grey, below the cerebral aqueduct (**Figure 3–11A&B**, **inset**). In the same section, GFP expressing axons are also detected just lateral of the contralateral pontine nucleus (**Figure 3–11A**, **bottom inset**). Presumably, these are the continuation of the descending tracts after the decussation seen in **Figure 3–10G&I**, which travel back caudally towards the inferior olive along the ventral flank of the brain.

Figure 3–12 parallels the bilateral injection experiment shown in **Figure 3–8**, where either side of the brain was injected with AAV driving expression of contrasting membrane-bound GFP and tdTom fluorescent proteins, this time targeting the interposed nuclei using more medial-caudal coordinates (n=4). **Figure 3–12A** and **B**

show the left and right injected cerebellar nuclei, respectively. The AAV-DIO-mGFP targeted the cerebellar nuclei more effectively than the AAV-DIO-tdTomato. On both sides, fluorescence is seen in the parvicellular portion of the lateral nuclei, where the separate *Sox14*$^{+}$/*Calb2*$^{+}$ population is located, as well as the anterior interposed nuclei. It is also worth noting that *Sox14*$^{+}$ cells are also found in the underlying vestibular nuclei and AAV expression is found in these cells too, denoted by white arrowheads.

Red and green axons from these injections are found in the respective ipsilateral oculomotor nuclei (**Figure 3–12C**). The more limited AAV-DIO-tdTomato injection provides a clue that these midbrain projections are perhaps derived from the anterior interposed cerebellar nucleus or the vestibular nuclei. However, it was not possible to make small targeted injections to definitively identify the precise source of these projections. In order to answer this question, I used an alternative axon tracing method described in the next section. As expected, projections were also seen in the inferior olive. In these injections, nucleo-olivary neurons are shown to target the inferior olive cap of Kooy of the medial olivary nucleus as well as the principle olive (**Figure 3–12D**). As before, these axons extend bilaterally but are most intense in the contralateral inferior olive.

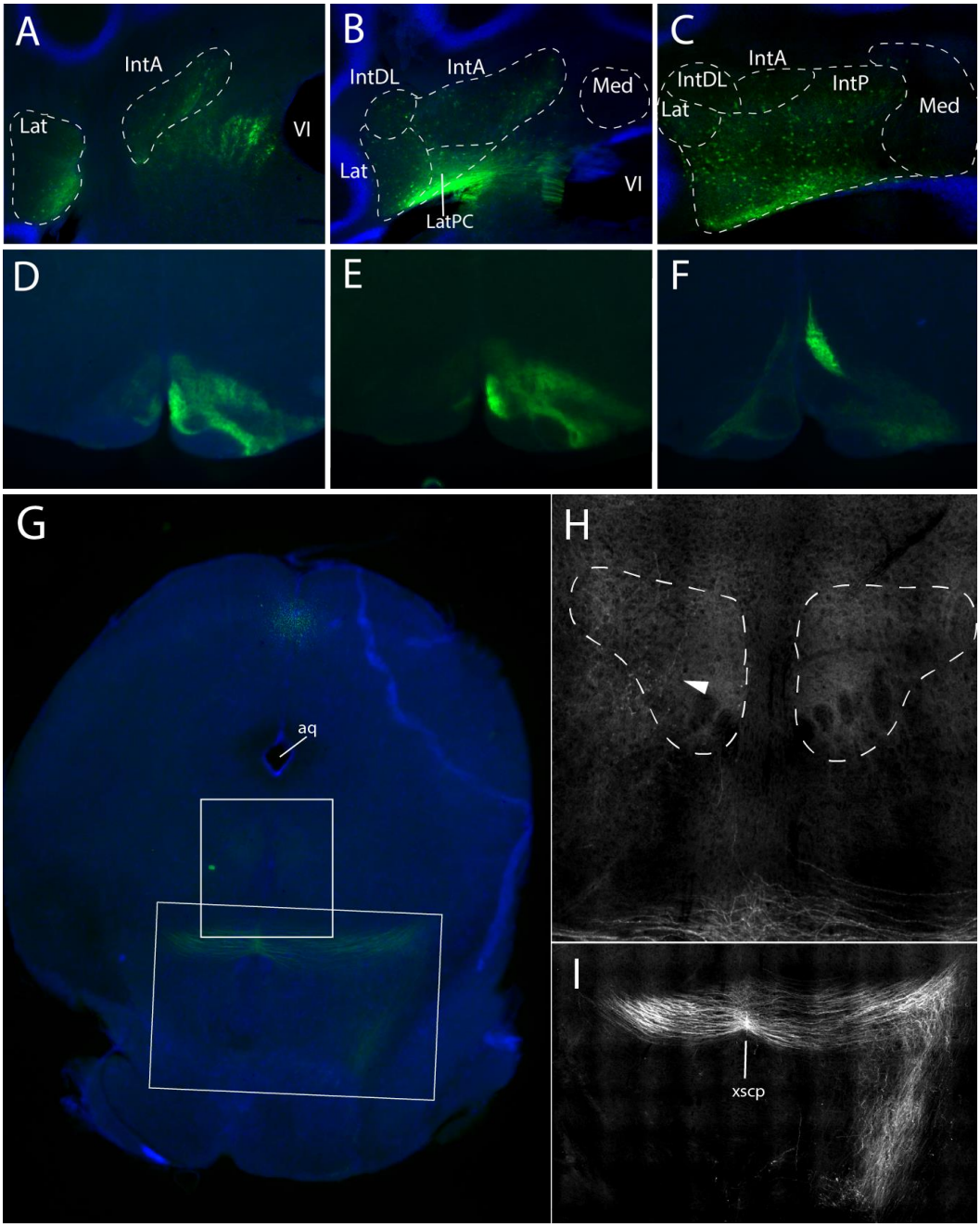

Figure 3–10 An example injection of AAV-EF1a-DIO-mGFP targeting the lateral and interposed nuclei of a Sox14$^{Cre/+}$ heterozygous mouse.

A-C*) The broad unilateral targeting across all the cerebellar nuclei, except the medial nucleus shown in coronal slices from rostral (**A**) to caudal (**C**). **D-F**) Axonal tracts target both the ipsilateral and contralateral inferior olive. The projections were observed in the medial, principle and dorsal nuclei of the inferior olive, shown in rostral (**D**) to caudal (**F**) slices. **G**) An overview of a midbrain slice. Axons are seen crossing at the decussation of the superior cerebellar peduncle. (**H**) and (**I**) show higher magnification images of the boxed regions. **H**) a very small number of tracts are seen heading up into the ipsilateral oculomotor nucleus. **I**) The majority of axons are seen to cross at the decussation of the superior cerebellar peduncle and descend towards the ventral portion of the slice.*

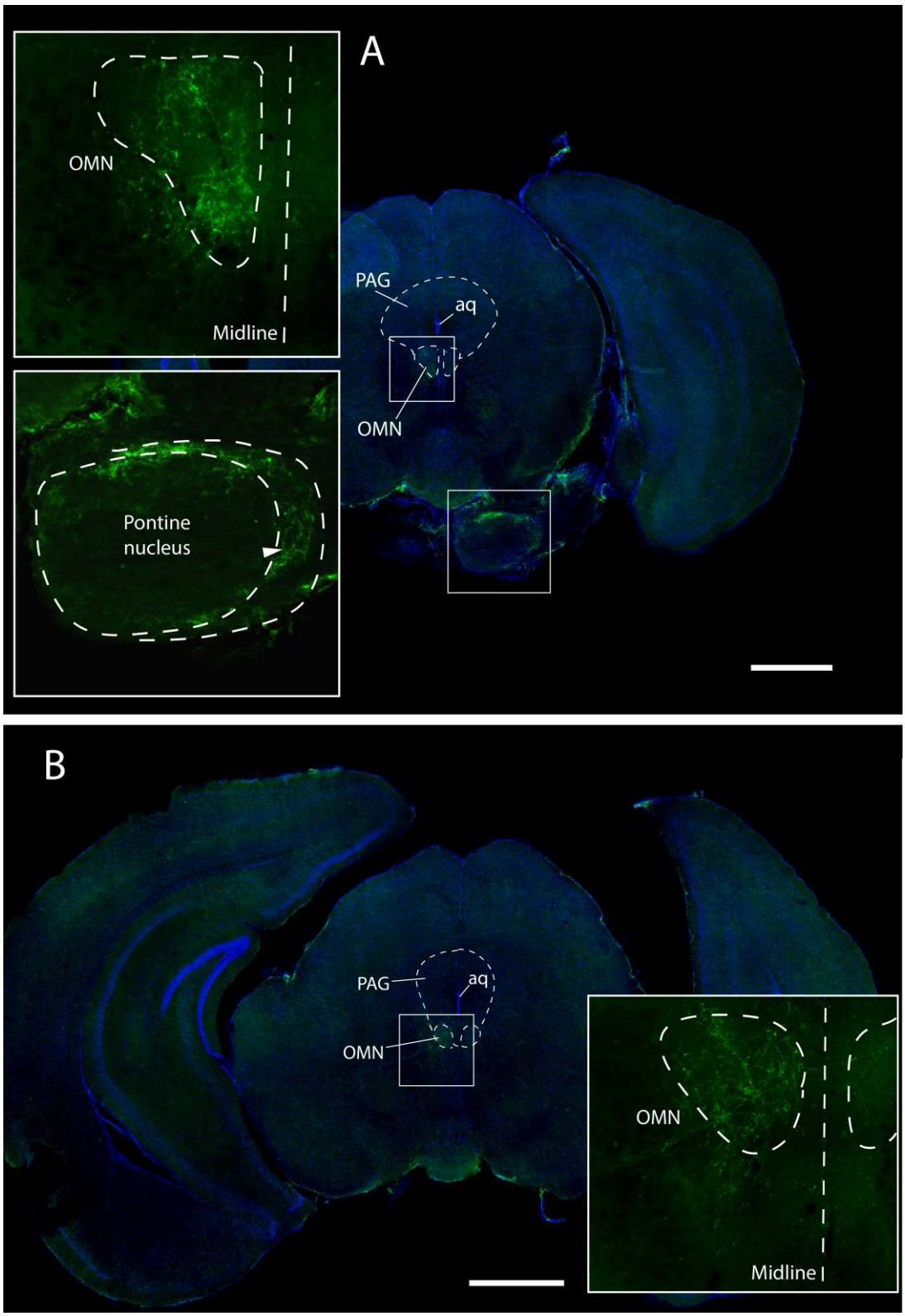

Figure 3–11 Midbrain sections of the injection shown in Figure 3–10

A) *Axons are seen in two regions of this slice. Firstly, axon terminals are seen in the oculomotor nucleus (upper inset). Secondly, passing axons are seen latera of the contralateral pons, where the middle cerebellar peduncle is known to traverse (lower inset).* ***B****) Axons continue to be detected in more rostral parts of the oculomotor nucleus, but no further projections were seen beyond this section. Scale: 1000 µm*

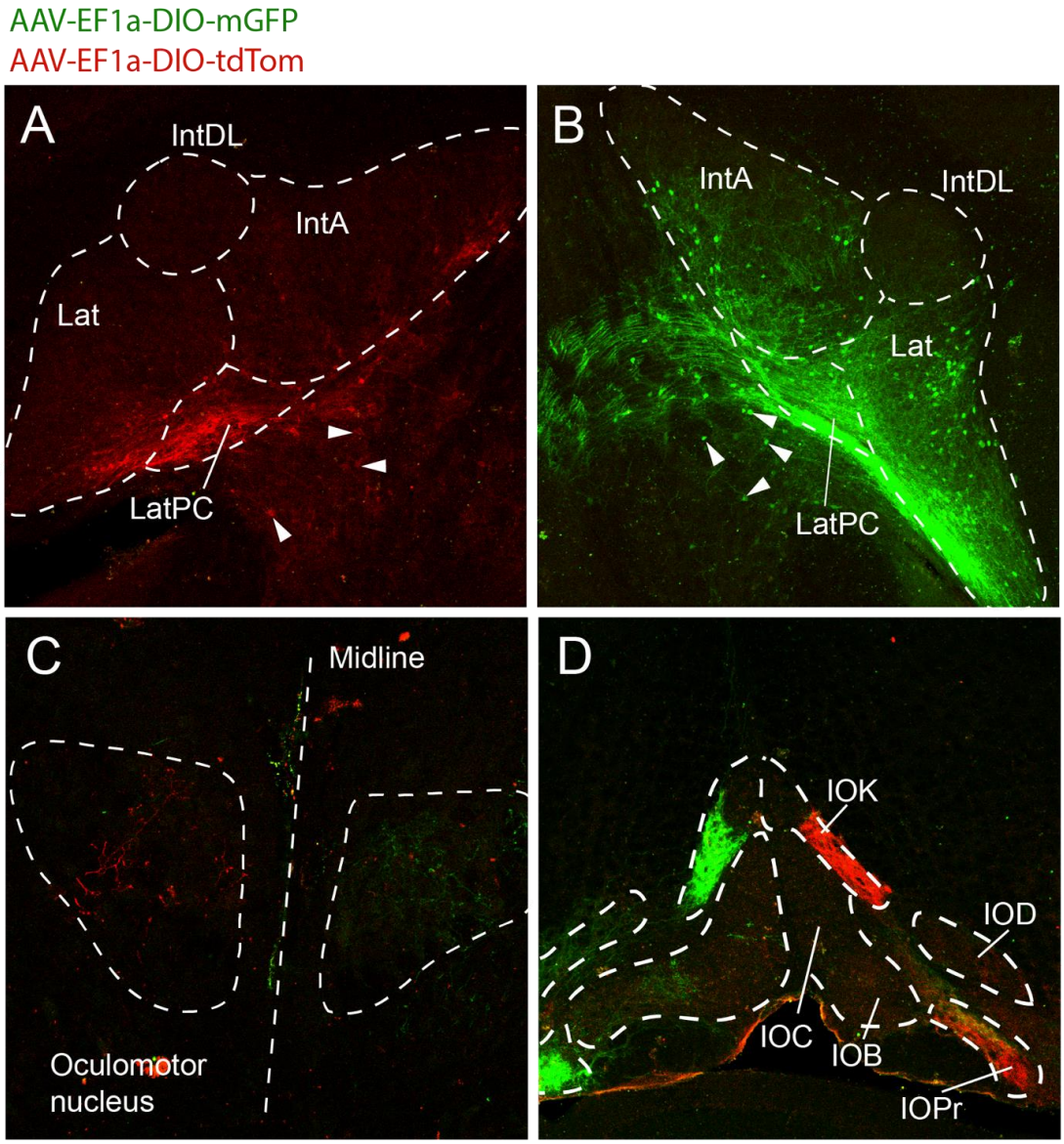

Figure 3–12 Projections of Sox14 expressing cells in the oculomotor nuclei.

Bilateral stereotaxic injections of AAV-EF1a-DIO-mGFP and AAV-EF1a-DIO-TdTomato into the interposed nuclei on either sides of Sox14$^{Cre/+}$ heterozygous mice at P14 and collected for analysis at P28 (n=4). ***A&B****) The resultant fluorescence in the cerebellar nuclei of one mouse. Note that in addition to the lateral and interposed nuclei, the virus also infected more ventral cells in the adjacent vestibular nuclear area (white arrowheads). The fluorescent axons of both injections are seen in the ipsilateral oculomotor nuclei (****C****) and contralateral inferior olives (****D****). In these injections, axons were seen in the principle olive (IOPr) and inferior olive cap of Kooy of the medial nucleus (IOK), but not the dorsal nucleus (IOD) nor the B and C subnuclei of the medial inferior olive nuclei (IOB and IOC).*

3.2.2 RETROGRADE BEAD TRACING REVEALS THAT THE OCULOMOTOR NUCLEUS IS INNERVATED BY NEURONS IN THE VESTIBULAR NUCLEI: FIVE EXAMPLES OF INJECTIONS

The last chapter demonstrated the existence of a small subset of genetically distinct *Calb2*$^{+}$/*Sox14*$^{+}$ cells in the cerebellar nuclei. To investigate whether the projections to the oculomotor nucleus are derived from a distinct population of *Sox14*$^{+}$ cells, green and red latex RetroBeads were injected into the oculomotor nuclei and inferior olive of *Sox14*$^{Gfp/+}$ mice (n=10). Five individual injected mice are described in **Figure 3–13**, **Figure 3–14**, **Figure 3–15** and **Figure 3–16**. Each injection targeted slightly different areas with varying degrees of precision and together they comprise a map of projections from the cerebellar nuclei to midbrain and medulla.

Unlike the AAVs, the RetroBeads are not selective for a particular cell type so common trends must be identified across many injections. In addition, the beads are only available in two colours, green and red. Since I used the *Sox14*$^{Gfp/+}$ mouse to identify *Sox14* expressing cells, the green bead labelled cells had to be distinguished from the endogenous GFP expressing cells. The beads give a punctate, bright appearance, in contrast to the endogenous GFP, which fills the cytoplasm in a uniform manner.

Figure 3–13B-D shows a brain where green RetroBeads were injected into the oculomotor nucleus and red RetroBeads were injected into the inferior olive to see if these any cerebellar nuclear cells could project to both target regions or if the nucleo-olivary neurons could be distinguished from the projection neurons that target the oculomotor nucleus. The beads are seen in the cerebellar nuclei following

retrograde transport from the injection sites. As expected, the beads injected into the inferior olive consistently co-express with the endogenous GFP^+ cells of the contralateral cerebellar nuclei and represent the nucleo-olivary neurons (**Figure 3–13D'**, **white arrowheads**). The beads injected into the oculomotor nuclei labelled cells that exist in a region directly below the medial hilus of the lateral cerebellar nucleus, near the vestibular populations (**Figure 3–13D, D'**). Most of the labelled cells were too large to be any of the *Sox14*$^+$ population in the area (**Figure 3–13D'**, orange arrowheads). However, there were some cells that have a smaller cell soma (**Figure 3–13D'**, **blue arrowheads**) and that may be the *Sox14* expressing cells in the vestibular nuclear area.

In order to accurately visualise the endogenous GFP expression, I subsequently stained the cerebellar slices against GFP to bind a far-red (Cy5) secondary antibody that could then be detected using a different fluorescence. In addition, I used PValb antibody to stain midbrain sections in order to clearly define the boundaries of the oculomotor nuclei. **Figure 3–13E&F** show the two staining procedures to identify the injection site of the green RetroBeads into the oculomotor nuclei (**E**) and the endogenous GFP alongside the retrogradely transported beads in the cerebellum (**F**). The injection only just encroached onto the oculomotor region along the midline and may actually have targeted the Edinger-Westphal nucleus that sits medial to the oculomotor nuclei. As with before, the transported beads are seen in the region just ventral of the cerebellar nuclei. There are no large cells labelled, only small cells that are similar to the Cy5 labelled endogenous GFP^+ cells, but these two populations do not colocalise (**Figure 3–13F**, **inset white arrowheads**).

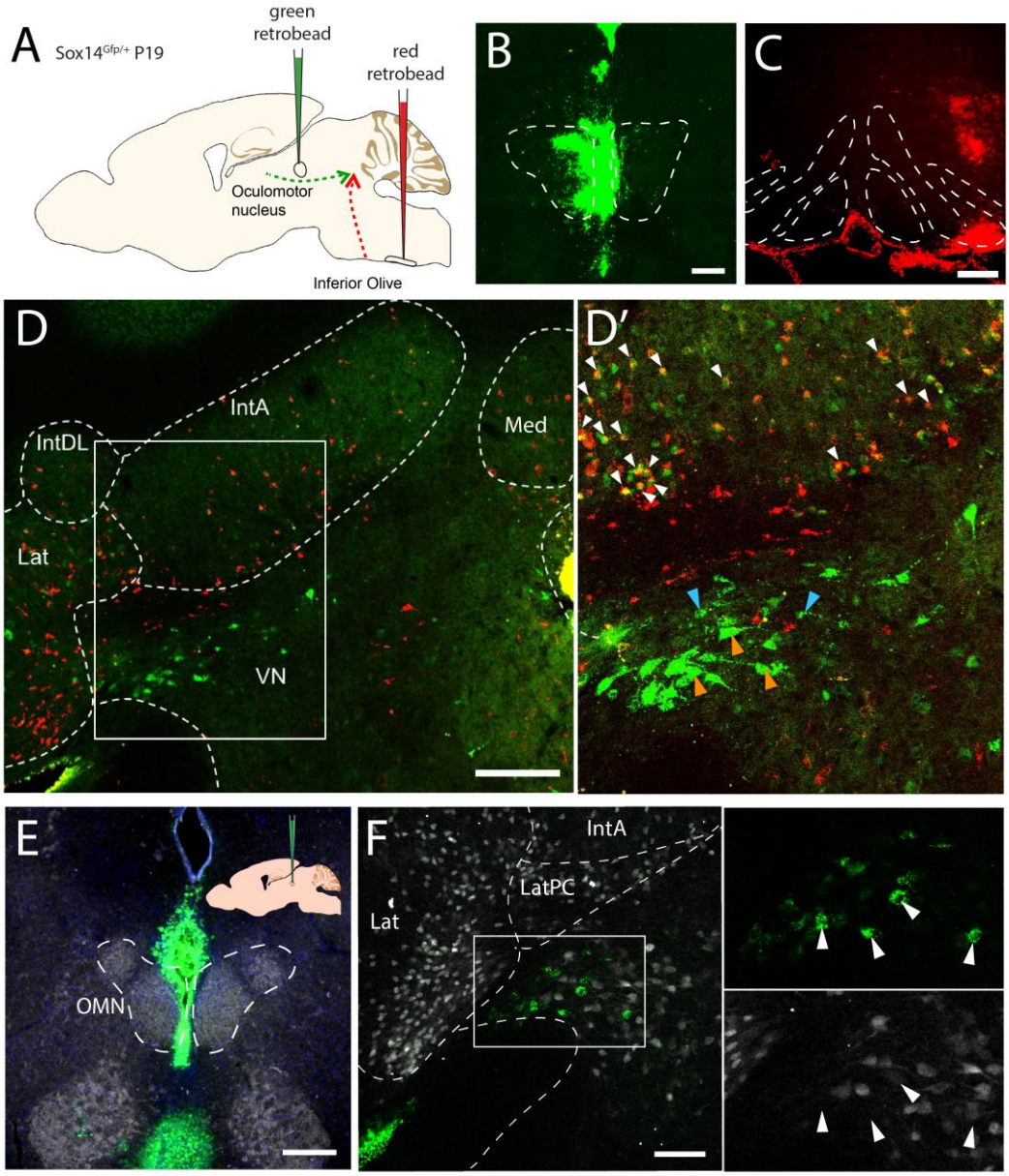

Figure 3–13 RetroBead injection example #1 and #2

A) *schematic showing the green and red RetroBead injections into the ipsilateral oculomotor nucleus and contralateral inferior olive of Sox14$^{Gfp/+}$ mice at P19 (n=10).* ***B&C)*** *Example injection #1 where green RetroBeads were injected into the oculomotor nucleus and red RetroBeads were injected into the inferior olive. The injection targeted the principle olive of the inferior olive.* ***D)*** *Red beads were retrogradedly transported back to the cerebellar nuclei and are seen to co-localised with the endogenous GFP signal (**D'**, white arrows). Green beads are found throughout the vestibular nuclei, distinct from endogenous GFP signal with a punctate, bright appearance. The beads are found in large (**D'**, orange arrows) and small (**D'**, blue arrows) cells that are ventral to the cerebellar nuclei.* ***E&F)*** *Example injection #2 where only green RetroBeads were injected into the oculomotor nucleus. The midbrain slices were stained against PValb antibody to better localise the oculomotor nucleus (**E**, PValb in white), while cerebellar slices were stained against GFP along with a Cy5 secondary antibody so endogenous GFP is distinct from the green RetroBeads (**F**, Cy5 in white). RetroBeads were found ventral to the cerebellar nuclei. Staining against GFP showed that these cells did not express endogenous GFP (**F**, inset white arrowheads). Scale: B: 50 µm, C:200 µm, D: 200 µm, E: 100 µm, F: 100 µm*

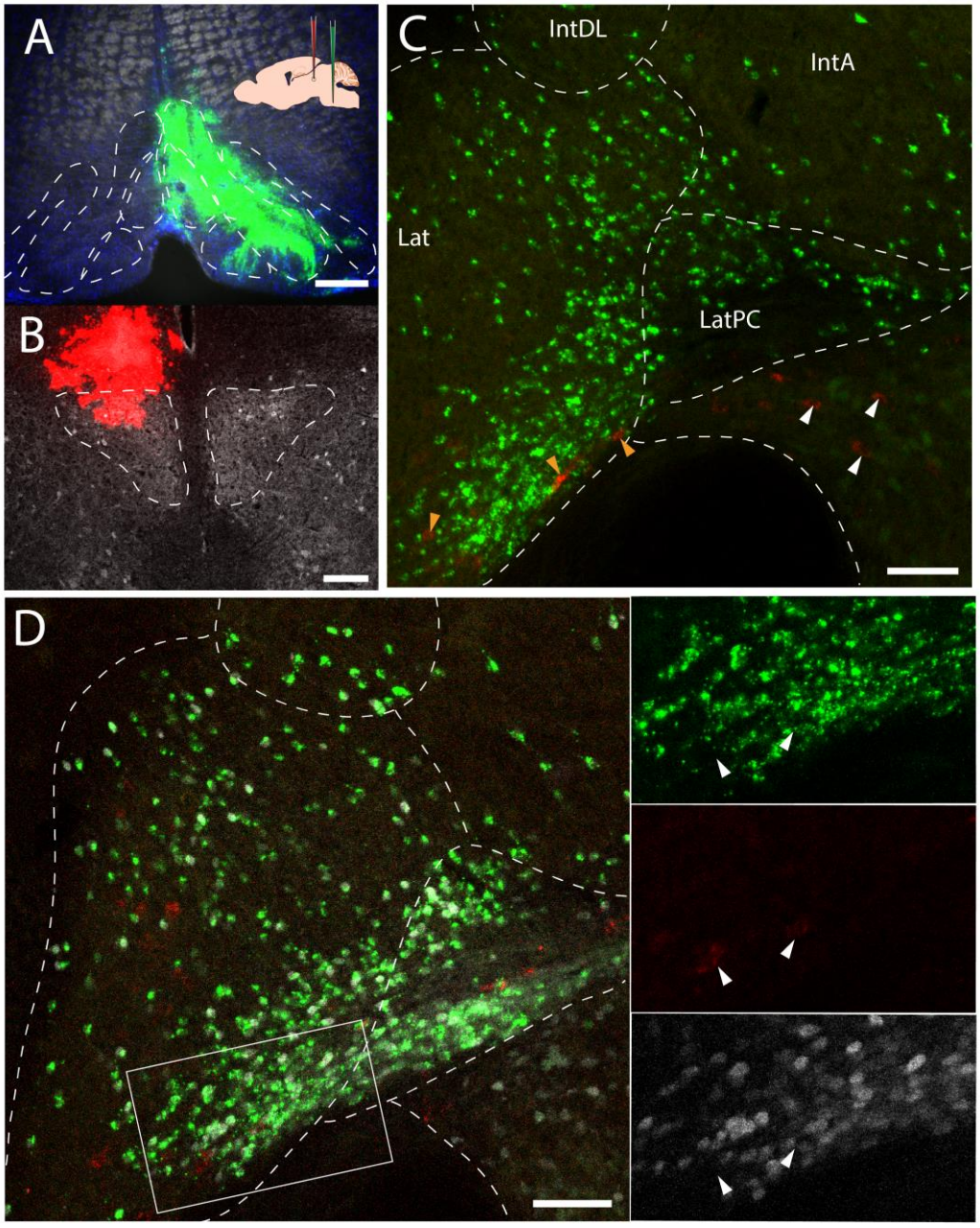

Figure 3–14 RetroBead injection example #3

Green RetroBeads were injected into the Inferior olive ***(A)*** *and red RetroBeads were injected into the oculomotor nucleus* ***(B)****.* ***A)*** *The regions of the inferior olive are better visualised by imaging a brightfield image of the same slice. The injection targeted most of the right inferior olive except the dorsal nucleus****. B)*** *The oculomotor nucleus (PValb in white). The injection hit the region dorsal of the oculomotor nucleus as well as the nucleus itself.* ***C)*** *The cerebellar slice shows that beads from the inferior olive are found in the cerebellar nuclei, while the beads from the oculomotor nucleus are found in the vestibular nuclei immediately below. (white arrowheads). In addition, some red beads are seen in the cerebellar nuclei (orange arrowheads).* ***D****) another cerebellar slice from this brain was stained against GFP along with a Cy5 secondary antibody to visualise Sox14-GFP expressing cells (Cy5 in white). While the RetroBeads ventral to the cerebellar nuclei could not be seen, the red beads in the cerebellar nuclei were not found to colocalise with the endogenous GFP, nor the green beads from the inferior olive (inset, white arrowheads). Scale: A: 200 µm, B: 50 µm, C-D: 100 µm*

I reversed the colours of the beads for the next injection since immunostaining quenches some of the bead fluorescence. Green RetroBeads were injected into the inferior olive, hitting the medial nucleus and principle olive on the right side (**Figure 3–14A**), while red RetroBeads were injected into the oculomotor nucleus and the region just dorsal to it (**Figure 3–14B**). **Figure 3–14C** shows the left cerebellar nuclei without any staining procedure. The green beads are recognisably distributed in the same way as the *Sox14*$^{+}$ population. Red beads are found in the region under the parvicellular lateral nucleus (**Figure 3–14C**, **white arrowheads**) and also in the ventral portion of the lateral nucleus (**Figure 3–14C**, **orange arrowheads**), where *Sox14*$^{+}$/*Calb2*$^{+}$ cells were noted in the last chapter. Beads of the two different colours never coincide within the same cell. The red beads in the vestibular nuclear area do to appear to be taken up by cells expressing endogenous GFP. On staining against GFP with a Cy5 secondary antibody (**Figure 3–14D**), I was not able to locate red beads in the vestibular nuclear area. Red beads present in the lateral nucleus did not appear to be in cells that expressed endogenous GFP (**Figure 3–14D**, **inset white arrowheads**). Thus, these are unlikely to be the *Sox14*$^{+}$/*Calb2*$^{+}$ cells.

3.2.1 RETROGRADE TRACING REVEALS THAT OCULOMOTOR NUCLEI ARE INNERVATED BY SOX14⁺ NEURONS OF THE VESTIBULAR NUCLEI

Figure 3–15D shows that green RetroBeads injected into the oculomotor nucleus are taken up by cells that lie ventral to the parvicellular lateral cerebellar nucleus. This region (**Figure 3–15D**, **inset**) appears to consist of many types of neurons: cells that project to the inferior olive (red beads), cells that project to the oculomotor nucleus (green beads), *Sox14* expressing cells (white cells). Importantly, endogenous GFP is expressed in cells that project to both the inferior olive (**Figure 3–15D**, **inset blue arrowheads**) and the oculomotor nucleus (**Figure 3–15D**, **inset white arrowheads**), but no single cell projects to both regions. Additionally, cells with green beads from the oculomotor nucleus do not necessarily express *Sox14*. This pattern of expression was also seen in **Figure 3–13F** (**inset**), showing there are at least two distinct populations that project to the oculomotor nucleus. Here, the few cells with green beads that do express Sox14-GFP are the probable source of the AAV-expressing projections seen in the oculomotor nucleus.

Across all the experiments, RetroBeads from the oculomotor nucleus are consistently seen in the region just lateral to the superior vestibular nucleus, directly ventral to the parvicellular lateral cerebellar nucleus. This region contains both *Sox14* positive and negative cells that project to the oculomotor nucleus.

3.2.1 IPSILATERAL NUCLEO-OLIVARY CONNECTIVITY IS DERIVED FROM A RESTRICTED SUBSET OF SOX14^{+} NEURONS

In a separate experiment, injection of green RetroBeads was made on only one side of the inferior olive. **Figure 3–16A** shows that the injection targeted the caudal end of the principle olive, which is known to connect with the lateral cerebellar nuclei, while **Figure 3–16B** shows the caudal inferior olive. Green beads are seen bilaterally in the cerebellar nuclei (**Figure 3–16C&D**), illustrating that bilateral nucleo-olivary neurons contribute to signalling in one half of the inferior olive. While the topographic distribution of the green beads in both the contralateral and ipsilateral lateral nuclei are roughly equivalent, the number of cells in which beads are detected are noticeably fewer in the ipsilateral nucleus (**Figure 3–16D'**).

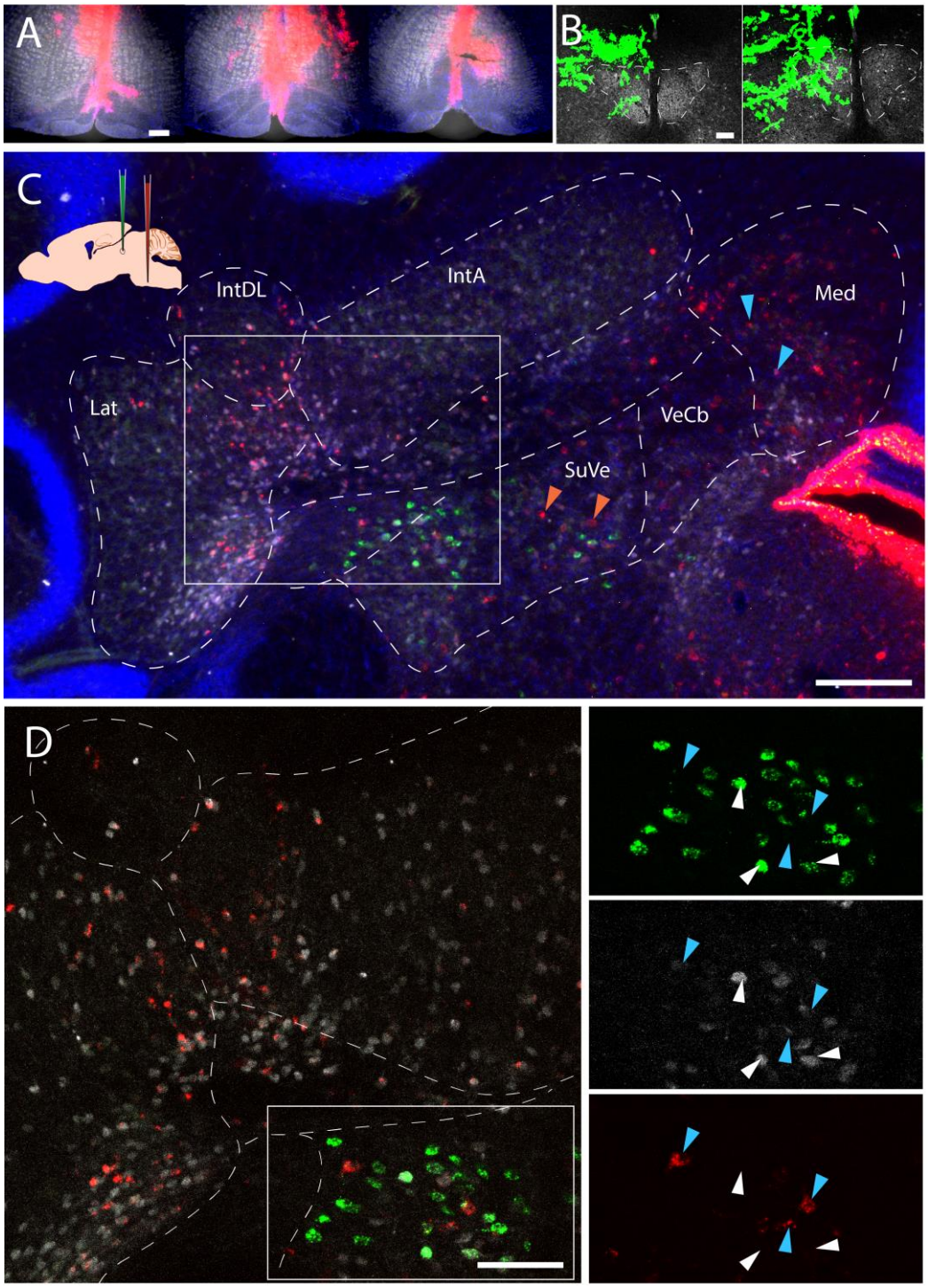

Figure 3–15 RetroBead injection example #4

Red RetroBeads were injected into the inferior olive ***(A)*** *and green RetroBeads were injected into the oculomotor nucleus* ***(B)****.* ***A****) The regions of the inferior olive are better visualised by imaging a brightfield image of the same slice. The injection targeted mainly the medial nucleus of the inferior olive and the region just dorsal of it.* ***B****) The oculomotor nucleus (PValb in white).* ***C&D****) the cerebellar nuclei (GFP-Cy5 in white). Red RetroBeads were found in the cerebellar nuclei and the region ventral to the nuclei. Green RetroBeads were found in the region ventral to the nuclei and the cells did also express endogenous GFP (inset white arrowheads), while the cells with red RetroBeads did not colocalise with endogenous GFP (blue arrowheads). Scale: A: 200 µm, B: 50 µm, C : 200 µm, D: 100 µm*

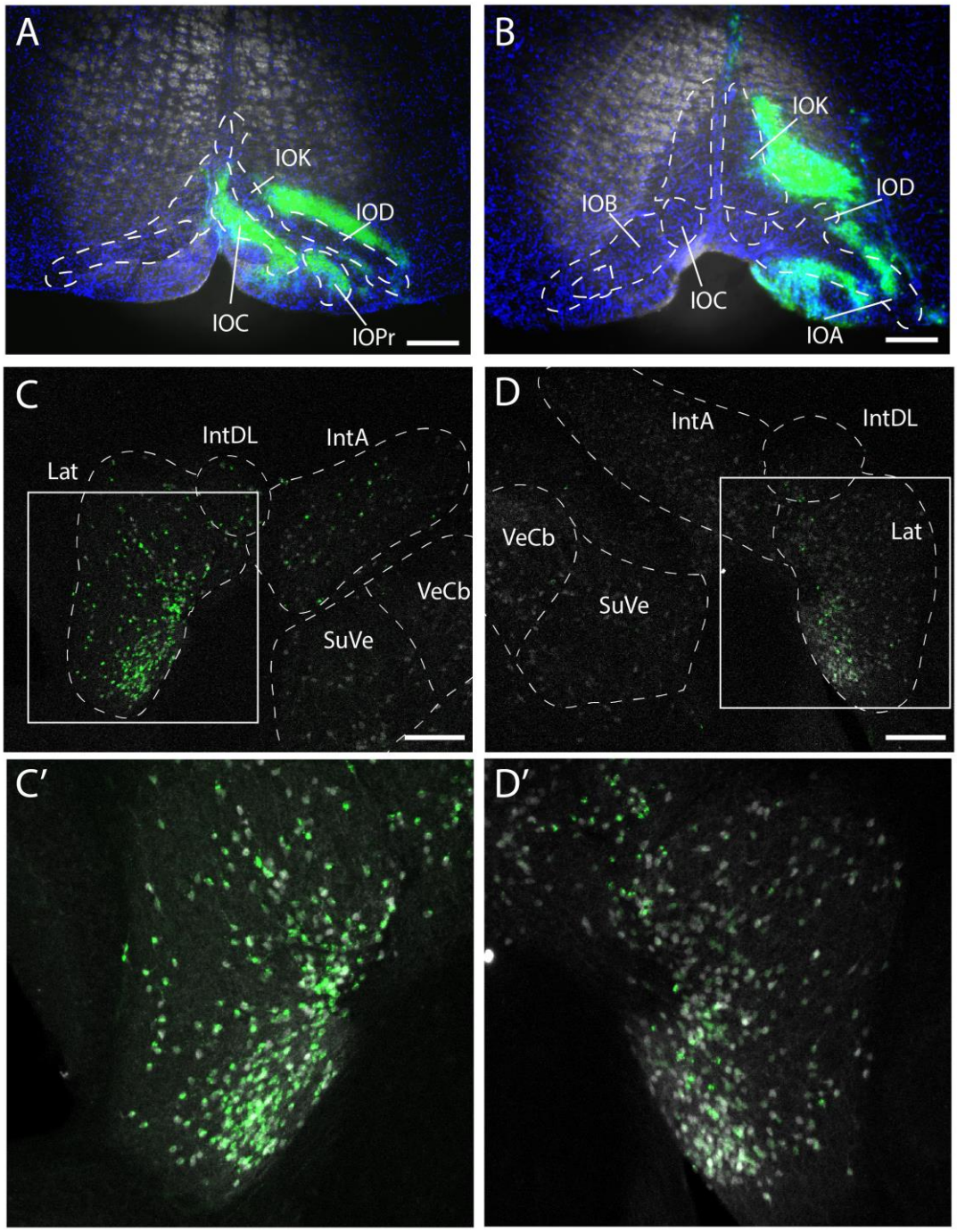

Figure 3–16 RetroBead injection example #5

A&B) *Green RetroBeads were injected into the inferior olive.. The injection targeted mainly the medial nucleus of the inferior olive as well as the caudal end of the principle olive.* ***C&D)*** *As a result, green RetroBeads are observed in the lateral cerebellar nuclei. The cerebellar slices were stained against GFP along with a Cy5 secondary antibody (shown in white) to show Sox14-GFP expressing cells.* ***(C)*** *shows the contralateral cerebellar nuclei (where all cells are double labeled) while* ***(D)*** *shows the ipsilateral cerebellar nuclei (where only a subset of GFP$^+$ cells are labeled). Scale: 200 µm*

3.2.2 IPSILATERAL NUCLEO-OLIVARY CONNECTIVITY IS DERIVED FROM A RESTRICTED SUBSET OF SOX14^{+} NEURONS

Drawing together the results of all the RetroBead injections, injections into the inferior olive label small cells, which were mostly in the contralateral cerebellar nuclei. The RetroBeads that are transported from the inferior olive co-label with endogenous GFP (*Sox14*$^{+}$) in the cerebellar nuclei. Furthermore, within a contralateral region labelled by RetroBeads from the inferior olive, all *Sox14*$^{+}$ cells contain RetroBeads. This is clearly shown in **Figure 3–14D** and **Figure 3–16C**, where RetroBeads are appear to be present in all GFP expressing cells contralateral to the injection site. Since no additional GFP^{-} cells in lateral and interposed cerebellar nuclei contain beads, it is reasonable to conclude that *Sox14* expressing cells are the only cerebellar nuclear cell type that project to the inferior olive.

Table 3-1 and **Figure 3–17** summarise the findings in this chapter. I classified the injections by targeted region and consider on the topographical distributions of the projections revealed by similarly targeted injections. Taking into account both AAV and RetroBead injections, it is clear that the lateral cerebellar nucleus is linked to the principle olive (IOPr) and the dorsomedial cell group (IODM); the interposed nuclei are linked to the medial olivary nucleus (IOM) and the dorsal olivary nucleus (IOD); and the vestibular nuclei are linked to the cap of Kooy of the medial nucleus (IOK) and the ventrolateral protrusion (IOVL).

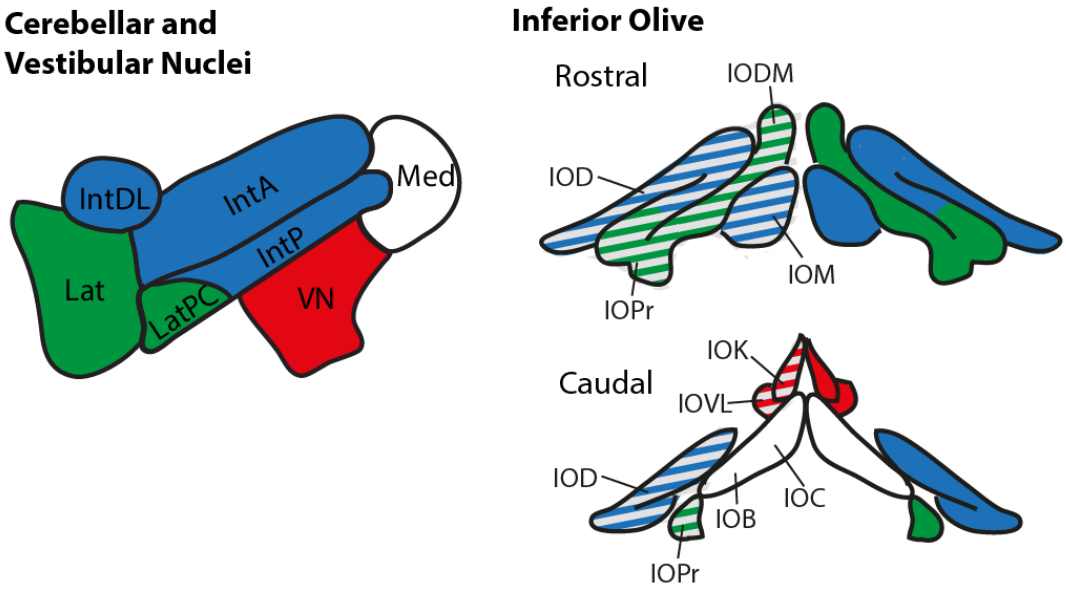

Figure 3–17 Summary of Sox14⁺ nucleo-olivary topography shown in AAV and RetroBead injections.
The nucleo-olivary neurons of the lateral cerebellar nucleus (green) project to the principle olive (IOPr) and the dorsomedial cell group (IODM). The nucleo-olivary neurons of the interposed cerebellar nuclei (blue) project to the medial olivary nucleus (IOM) and the dorsal olivary nucleus (IOD). The Sox14⁺ neurons of the vestibular nuclei (red) project to the cap of Kooy of the medial nucleus (IOK) and the ventrolateral protrusion (IOVL). No Sox14⁺ were observed from the medial cerebellar nucleus. All the projections were seen bilaterally in the inferior olive, but the contralateral contribution was consistently more intense.

Table 3-1 Summary of injection sites, and collective observations.

n numbers represent the number of injections where regions were targeted, which may overlap with other regions. ***Bold*** *= intense label; Normal = weaker label; Italics – possible off-target label where injection site has spread into neighboring territory*

Injection paradigm	**Cell labelling**		***n***
	Contralateral	**Ipsilateral**	
AAV unilateral into lateral CN of *Sox14$^{Cre/+}$*	**IOPr** **IODM** *IOVL*	IOPr IOM *IODM* *IOVL* *oculomotor nucleus*	14
AAV unilateral into interposed CN of *Sox14$^{Cre/+}$*	**IOD** **IOM** IOVL IOK	IOD IOM IOVL IOK *oculomotor nucleus*	12
AAV unilateral into dorsal vestibular nuclei of *Sox14$^{Cre/+}$*	IOVL **IOK**	oculomotor nucleus	6
RetroBeads into oculomotor nucleus of *Sox14$^{Gfp/+}$*		**Large cells of nucleus Y** *Large cells of the CN*	6
RetroBeads into IOPr of *Sox14$^{Gfp/+}$*	**Small GFP$^+$ cells in Lat and LatPC CN** *Medial vestibular nuclei*	Small GFP$^+$ cells in Lat and LatPC CN	5
RetroBeads into IOD of *Sox14$^{Gfp/+}$*	**Small GFP$^+$ cells in IntA and IntP CN** *Medial vestibular nuclei*	Small GFP$^+$ cells in IntA and IntP CN	3
RetroBeads into caudal IOD of *Sox14$^{Gfp/+}$*	*Large cells of the Lat and Med CN*		1
RetroBeads into caudal IOB, IOC and IOK of *Sox14$^{Gfp/+}$*	**Medial vestibular nuclei** **Med CN** *Medial parts of IntA CN*		3

3.3 DISCUSSION

From the various neuronal tracing experiments described in this chapter, three main conclusions can be made:

1. The *Sox14*$^{+}$ cerebellar nuclear cells project to the inferior olive
2. These projections target symmetric areas in the contralateral and ipsilateral inferior olive, but differ in the projection density.
3. Populations of *Sox14*$^{+}$ and *Sox14*$^{-}$ cells in the vestibular nuclei target the ipsilateral oculomotor nucleus.

3.3.1 THE *SOX14*$^{+}$ CEREBELLAR NUCLEAR CELLS PROJECT TO THE INFERIOR OLIVE AND FOLLOW PREVIOUSLY NOTED TOPOGRAPHIC MAPPING

The principal goal of these experiments was to address the question from the previous chapter: do *Sox14*$^{+}$ GABAergic neurons project beyond the cerebellar nuclei? The injections of AAV-EF1α-DIO-mGFP and AAV-EF1α-DIO-tdTom have proved that the *Sox14*$^{+}$ neurons of the cerebellar nuclei are nucleo-olivary neurons.

It is known that the nucleo-olivary connectivity follows a rough topographical mapping that matches the olivo-cerebellar circuitry. The lateral nucleus projects to the principal olive, the anterior interposed nuclei project to the dorsal nucleus of the inferior olive, the dorsolateral interposed nuclei project to the dorsomedial cell group of the inferior olive, the posterior interposed nuclei project to the rostral half to the medial subnuclei of the inferior olive (Angaut and Cicirata, 1982; Ruigrok and Voogd, 1990). A small number of cells from the caudal parts of the medial

cerebellar nucleus have been reported to send fibres to the olive, where they target the caudal medial subnuclei of the inferior olive (Legendre and Courville, 1987).

In the tracing experiments reported here, targeted injections into the lateral or interposed nuclei resulted in projections to different parts of the inferior olive (**Table 3-1, Figure 3–17**). The nucleo-olivary cells in the lateral nucleus project mainly to the principle olive (IOPr), and also the dorsomedial cell group (IODM) and to some extent, the rostral end of the medial nuclei of the olive (IOM). The inclusion of targets outside the IOPr may reflect spread of the tracer injection site to label nucleo-olivary neurons in the dorsolateral interposed nucleus.

For injections targeting the anterior and posterior interposed nuclei (**Table 3-1, Figure 3–17**), projections were seen in the dorsal olivary nucleus, the dorsal fold of the olive, and the medial olivary nucleus especially in the rostral regions, and also in the cap of Kooy (IOK). Overall, the results concur largely with the known topography of the nucleo-olivary connectivity, though the injection sites were too large to confirm precise topography. For example, projections observed in the principle olive from injections targeting the interposed nuclei are probably due to AAV infection of caudal parts of the lateral nucleus. Often the injections also encompassed regions of the vestibulocerebellar nuclei and it is known that the dorsal vestibular nuclei also contain nucleo-olivary neurons, resulting projections observed in the dorsal fold of the inferior olive and the cap of Kooy (Fredette and Mugnaini, 1991).

3.3.2 THE MEDIAL CEREBELLAR NUCLEUS CONTAINS *SOX14* NEGATIVE NUCLEO-OLIVARY PROJECTION NEURONS

As anticipated from the previous chapter, we did not find any *Sox14*$^{+}$ cells in the medial nucleus even though nucleo-olivary neurons have been observed in the ventro-lateral region of the medial nucleus in other retrograde labelling experiments (Fredette and Mugnaini, 1991). RetroBead injections that targeted the caudal inferior olive revealed the presence of *Sox14*$^{-}$ nucleo-olivary projections. While the majority of beads are found in the lateral and interposed nuclei, beads were also found in the medial cerebellar nuclei in a small number of experiments.

The significance of a medial cerebellar nucleo-olivary connection, which is genetically distinct from the lateral and interposed nuclei, is unclear. However, across different species, the number of cerebellar nuclei vary, with the lateral nucleus being later evolved and specific to mammals (Green and Wingate, 2014). Historical tracing experiments suggested that while the projections from the lateral and interposed nuclei travelled down the superior cerebellar peduncle, medial nuclear neurons target the inferior olive by a different route (Martin et al., 1976). This difference is further discussed in **Chapter 6.4.3**.

3.3.3 NUCLEO-OLIVARY PROJECTIONS TARGET SYMMETRIC AREAS OF THE CONTRALATERAL AND IPSILATERAL INFERIOR OLIVE, BUT DIFFER IN PROJECTION DENSITY.

The nucleo-olivary neurons innervate mainly the contralateral inferior olive, but ipsilateral terminations can also be seen. **Figure 3–9** shows that the density, but not the territory occupied by the ipsilateral axons is drastically different. While they reach the same space of the contralateral axons, the ipsilateral connection is at a far

lower density. Ipsilateral axons have well defined varicosities, but at a much lower density that the contralateral counterparts. This bilateral connectivity has been previous noted (Ruigrok and Voogd, 1990; Ruigrok, 1997) and may play a part in cerebellar function. It is known that the climbing fibres only innervate the contralateral cerebellum, yet synchrony of Purkinje cell firing has been shown to exist between the two cerebellar hemispheres. Bilateral nucleo-olivary connection could be a significant mechanism in achieving this synchrony.

3.3.4 NUCLEO-OLIVARY PROJECTIONS DO NOT APPEAR TO TARGET OLIVARY CELL SOMA, PREFERRING TO MAKE SYNAPTIC CONTACTS DISTALLY

High magnification imaging of AAV expressing projections enable the visualization of the nucleo-olivary terminal endings. Asterisks in **Figure 3–9D-F** mark examples of spherical voids where the olivary cell somas are. The densely packed fluorescent axons establish the boundaries of the cell bodies and yet axonal boutons seldom make contact at these borders. Instead, nucleo-olivary neurons likely make synaptic connections with the olivary dendrites that exist in between somas. It has been previously observed that synaptic contacts from nucleo-olivary neurons are more density packed on dendrites than the cell bodies of olivary neurons (De Zeeuw et al., 1989; De Zeeuw et al., 1990; Lefler et al., 2014; Ruigrok and De Zeeuw, 1993; Sotelo et al., 1986). It is thought that these distal contacts are crucial in the modulatory function of nucleo-olivary neurons on olivary coupling, since gap junctions between cells occur in glomeruli. Accordingly boutons that cluster together, and may be part of glomeruli, are seen in high magnification images of the axonal projections (**Figure 3–9E**, **white arrows**).

3.3.5 AAV TRACING SHOWS PROJECTIONS THAT EXTEND ROSTRALLY ALONG THE SUPERIOR PEDUNCLE

Injections resulted in projections that lead from the cerebellar nuclei, gathering at hilus of the lateral nucleus, and travel along the ventral edge of the cerebellum, towards the 4th ventricle. From there, the tracts travel rostrally towards the midbrain, where they appear along the superior cerebellar peduncle (brachium conjunctivum) and cross the midline. Glutamatergic cerebellar nuclear cells that connect the cerebellum to the midbrain initially travel along the same path as nucleo-olivary neurons. While glutamatergic cells project along the ascending limb of the superior cerebellar peduncle to form cerebello-thalamic and cerebello-rubral tracts, nucleo-olivary olivary projections join the descending limb of the superior cerebellar peduncle (brachium conjunctivum descendens). This tract has been recognised since the 1840s and was originally known as the 'horseshoe-shaped commissure of Wernekinck" (Voogd and van Baarsen, 2014). When the nucleo-olivary tract tracing was originally identified, it was however unclear whether this tract was truly part of the superior cerebellar peduncle or was a separate fibre tract that lies ventral to the superior cerebellar peduncle and crosses the midline at the same point as the decussation of the superior cerebellar peduncle (Ban and Ohno, 1977; Graybiel et al., 1973; Legendre and Courville, 1987; Martin et al., 1976; Svensson et al., 2006; Tolbert et al., 1976).

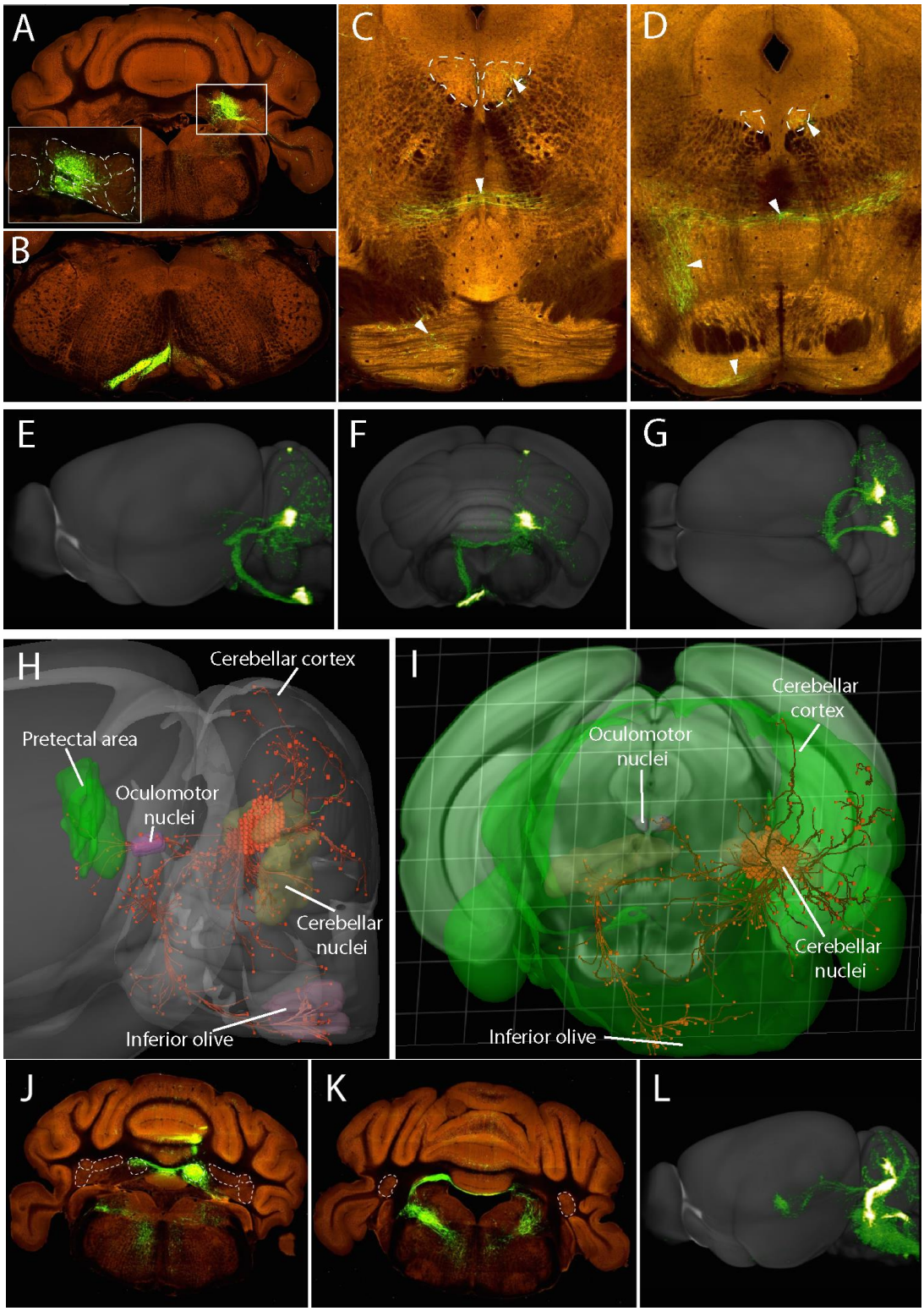
A
B
C
D
E
F
G
H
Cerebellar cortex
Pretectal area
Oculomotor nuclei
Cerebellar nuclei
Inferior olive
I
Cerebellar cortex
Oculomotor nuclei
Cerebellar nuclei
Inferior olive
J
K
L

Figure 3–18 Allen Mouse Brain Connectivity Atlas Projection data

*Images of an injection of (**A-I**) Cre-dependent AAV expressing GFP into the Slc32a1-IRES-Cre mouse (Experiment 304537794) and (**J-L**) of AAV-EGFP into the wild-type C57BL/6J mouse (Experiment 127650431) from the Allen Mouse Brain Connectivity Atlas Projection data. **A**) This injection targeted the interposed nucleus. Projections were observed in the inferior olive (**B**), crossing at the decussation of the superior cerebellar peduncle and within the oculomotor nucleus and pons (**C&D**, white arrowheads). **E-G**) The projection data as a stacked and rendered 3-D image, showing the intensity of the axonal projections as viewed from the sagittal (**E**), coronal (**F**) and axial (**G**) perspectives. **H&I**) The summarised data with the main projection targets as coloured regions. The 3-D neuronal projections are displayed in orange with the injection site shown as a cluster of spheres, re-sampled to a 100 micron grid resolution. Each line traces the fluorescent projection signal with a cube to indicate the termination of signal. **J**) A separate injection of AAV-EGFP into the wild-type C57BL/6J mouse, targeting the right side medial nucleus. Projections are seen decussating at the cerebellar commissure and descending into the medulla via the uncinate fasciculus of Russell. **L**) The projection data viewed from the sagittal perspective shows the difference in route taken by medial cerebellar neurons compared to those in the interposed nucleus in (**E**).*

The "horseshoe-shaped commissure of Wernekinck" is seen clearly in following an injection by Allen Mouse Brain Connectivity Atlas (Allen Brain connectivity.brain-map.org) of Cre-dependent AAV into the interposed nucleus of the Slc32a1-IRES-Cre (**Figure 3–18A**). The *Slc32a1* gene (*VGat*) codes for a GABA vesicular transporter, so the AAV targets all GABAergic nuclear neurons. **Figure 3–18B-D** shows the brainstem and midbrain coronal sections of the injected brain and illustrates the similarity between this injection and the injections described in my results. **Figure 3–18D-G** shows a 3-D reconstruction of the tract. It travels rostrally, decussates and extends caudally to the inferior olive. A small projection to the oculomotor nucleus is also seen in (**Figure 3–18C&D**). I have now identified this connection to be from the vestibular nuclei.

In contrast, an injection of AAV into the medial cerebellar nucleus of a wild-type C57BL/6J mouse shown in AAV infects all cell types (**Figure 3–18J-L**). Axons from the medial cerebellar nucleus take a different route to the inferior olive

crossing the midline at the cerebellar commissure (**Figure 3–18J**) and joining the uncinate fasciculus of Russell (**Figure 3–18K**), seen in the medulla as a diagonal tract projecting medially towards the inferior olive. **Figure 3–18L** shows the projection data viewed from the sagittal perspective. Compared to the nucleo-olivary tract seen in lateral and interposed nuclei injections, the route does not travel into the midbrain. This diversity has been noted in previous neuronal tracing experiments (Dom et al., 1973; Fink et al., 2006). There is also a subset of medial axons that target the thalamus, which are likely derived from glutamatergic projection neurons.

The variation in axonal path suggests that (*Sox14*$^{-}$) olivary projection neurons of the medial cerebellar nucleus are developmentally distinct from the other cerebellar nuclear (*Sox14*$^{+}$) populations, whose nucleo-olivary projections run parallel to the glutamatergic cerebello-thalamic and cerebello-rubral tracts (Ruigrok and Voogd, 1990).

3.3.6 A POPULATION OF *SOX14*$^{+}$ CELLS IN OR AROUND THE CEREBELLAR NUCLEI TARGET THE IPSILATERAL OCULOMOTOR NUCLEUS.

When injections of *Cre*-dependent AAV tracers targeted not only the cerebellar nuclei, but also included targeting of the dorsal vestibular nuclei, axon terminals were observed in the ipsilateral oculomotor nuclei in addition to the inferior olive. The axons of the cerebellar nuclei travel rostrally along the superior cerebellar peduncle and but do not cross the midline at the decussation of the superior cerebellar peduncle. Instead, the axons continue to extend dorsally into the oculomotor nucleus on the ipsilateral side.

In order to locate the origins of these oculomotor nuclei projections, I injected RetroBeads into *Sox14*$^{Gfp/+}$ mice. The beads labelled cells that exist in a region just below the medial hilus of the lateral cerebellar nucleus near the vestibular populations (**Figure 3–13**). While some of the labelled cells were too large to be any of the *Sox14*$^{+}$ population, there were some cells that have a smaller cell soma. When the slices were stained against GFP to compare the RetroBead tracing to the endogenous GFP, it was clear that a subset of these cells are part of a *Sox14* expressing population. However, there is no mention in literature of a GABAergic projection cell type that is unique to the lateral nucleus.

Conversely, projections to the oculomotor nucleus have been found originating from the vestibular nuclei as part of the VOR network. Since *Sox14*$^{+}$ cells also exist in the vestibular nuclei, it is possible that cells containing RetroBeads from the oculomotor nucleus are a vestibular population. Comparing the location of these cells to an atlas, the cells may be part of the infracerebellar nucleus, nucleus Y or the paracochlear glial substance. These areas, also known as the "subpeduncular corner", are not well characterised, particularly in rodents (Diño and Mugnaini, 2008; Mugnaini et al., 1980; Paxinos, 1985; Paxinos and Franklin, 2004).

In particular, the nucleus Y, also known as "group Y", has been shown to project to the ipsilateral oculomotor nucleus and interstitial nucleus of Cajal, which lies just rostral of the oculomotor nucleus (Graybiel and Hartwieg, 1974; Stanton, 1980; Steiger and Büttner-Ennever, 1979; Yamamoto et al., 1986). It sits ventral to the parvicellular region of the lateral nucleus, but there is no consensus where the boundaries lie between nucleus Y, the infracerebellar nucleus and the parvicellular

region of the lateral nucleus (Paxinos, 1985). The nucleus Y is much more prominent in cats, rabbits and monkeys; in these animals, the structure is separate from that of the lateral nucleus and exists right under the rostral pole of the lateral nucleus, between the lateral nucleus and the superior vestibular nucleus. In the mouse, however, nucleus Y is a very small triangular group of cells that exists in the space between the lateral cerebellar nucleus, lateral vestibular nucleus and dorsal cochlear nucleus (Frederickson and Trune, 1986). The group is made up of small neurons (10-20µm diameter) and fewer larger neurons (20-30µm diameter) (Frederickson and Trune, 1986). This is consistent with the cell sizes observed from the RetroBead tracing, where both large and small neurons are labelled in some brains, while only small *Sox14*$^{+}$ cells were observed in both cerebellar nuclei and vestibular nuclei in the *Sox14*$^{Gfp/+}$ mouse characterisation of the last chapter. Nucleus Y has been the subject of smooth eye movement and vertical vestibulo-ocular reflex (Chubb and Fuchs, 1982; Highstein et al., 1997) and has been shown to receive afferents from the flocculus (Langer, 1985).

3.3.7 IMPLICATIONS FOR THE *SOX14* GENE AS A GENETIC TOOL

The results of this chapter has demonstrated that the *Sox14* gene is a marker for nucleo-olivary neurons in the cerebellar nuclei. While Cre-dependent AAV injection using the *Sox14*$^{Cre/+}$ mouse has proved to be a reliable way to deliver genes specifically into this cell population, presumed vestibulo-oculomotor connectivity was also observed, showing that nearby *Sox14* expressing cells can also be affected if the injections extend ventrally beyond the cerebellar nuclei. Also, it is still unknown if the *Sox14*$^{+}$/*Calb2*$^{+}$ cells in the ventral part of the lateral cerebellar nucleus function differently to the other *Sox14*$^{+}$ cerebellar nucleo-olivary neurons.

They do not appear to be related to the oculomotor projections and AAV injections did not suggest for any other projections to other targets.

Subsequent chapters will use the *Sox14*$^{Cre/+}$ and *Sox14*$^{Gfp/+}$ mice to investigate the development and function of the nucleo-olivary neurons. The projections of these neurons form the vital link to send feedback (or perhaps feedforward) information from the cerebellum to the inferior olive. This is known to inform the subsequent firing of climbing fibres and so is thought to be important in how the climbing fibre firing pattern represents motor error.

Not only is this the case on a general systems level, but the olivo-cerebellar loops are known to be closed loops with architecture that has precise compartmentalisation. As the cerebellar cortical Purkinje cells are compartmentalised into lobules along the rostral-caudal axis, then into sagittal zones along the medial-lateral axis, and the inferior olive into various sub-nuclei, so the cerebellar nuclei are divided into sub-nuclei also. These different sub-regions are delineated by differential gene expression patterns from early on in embryogenesis (Apps and Hawkes, 2009). The sub-regions have corresponding relationships so that the reproducible micro-zones are formed where genetically specified Purkinje cells are innervated by climbing fibres with the complementary genetic expression pattern (Reeber and Sillitoe, 2011; Sawada et al., 2008). How are these precise micro-circuitries formed in development? Are they functionally distinct? These questions are the basis for many investigations on the functional organisation of the olivo-cerebellar loops. While these studies have been able to help us understand the relationship between climbing fibres and Purkinje cells, it has been limited to the

molecular and cellular mechanisms by which climbing fibres invade the cerebellar cortex, recognise their corresponding Purkinje cells and are synaptically pruned.

There is a lack of knowledge, however, about how specific connections are made between micro-zonal Purkinje cells and cerebellar sub-nuclei, and between cerebellar sub-nuclei and inferior olive sub-nuclei. The progress so far has been made possible by the discovery of distinct markers for subsets of Purkinje cells and climbing fibres (Reeber et al., 2012) such as corticotrophin releasing factor (CRF) (Sawada et al., 2008) and zebrin II (Brochu et al., 1990). Thus in the following chapter, I will use the *Sox14*$^{Cre/+}$ mouse line to address questions on the development of the nucleo-olivary neurons.

4 DEVELOPMENT

4.1 INTRODUCTION

Understanding the developmental origins of the cerebellar nuclei neurons have presented a historical challenge. Birth-dating and Nissl studies of the mid 1980's identified the important role of a nuclear transitory zone (NTZ) as a point at which the nuclei are developmentally assembled but little of their ultimate origins (Altman and Bayer, 1985). It was only with the application of genetic fate maps exploiting *Atoh1* that substantial progress was made in identifying the origins of *Lhx9* and *Tbr1* positive glutamatergic projection neurons (Fink et al., 2006; Machold and Fishell, 2005; Wang et al., 2005). By contrast, the origins of GABAergic nuclear cells remain relatively obscure. Our discovery that *Sox14* is a developmental marker for nucleo-olivary neurons forges new ground for understanding cerebellar nuclear development. Until now, no specific marker has been found and the knowledge we have about how nucleo-olivary neurons form is based either on assumptions (i.e. that because they are GABAergic, they are ventricular zone derivatives) or by process of elimination (ie. temporary markers that do not fit any other possible known cell types).

The fact that inhibitory cerebellar cortical neurons do not express *Sox14*, while neurons in the cerebellar nuclei do, suggests that the nucleo-olivary cell population may be derived through separate lineages as compared to the other inhibitory cortical cells. This chapter aims to look at the *Sox14*$^{+}$ expression pattern in order to identify the progenitor pool that nucleo-olivary cells are born from, and to establish the timeline for the cells' birth, differentiation, and migration.

4.1.1 BIRTH-DATING CEREBELLAR DEVELOPMENT

There are several methods to establish the birthdate of cell types, or to follow the sequence of progeny from a specific progenitor zone using labelling methods. Classical birth-dating uses an analogue of nucleoside Thymidine to look at timings of cell birth (Angevine and Sidman, 1961). Tritiated H^3-Thymidine is injected at a specific timepoint. As cells divide and undergo mitosis, the H^3-Thymidine is incorporated into the newly synthesised DNA. This H^3-Thymidine can be traced by autoradiography since the tritiated isotope is radioactive. Since a limited amount of H^3-Thymidine is injected, the cells undergoing S-phase of the cell cycle at the injection time-point will have the heaviest labelling. The proliferative cells that are labelled will split the amount of DNA with every division, while cells that commit to a post-mitotic state will retain high levels of labelling. Therefore, the later born cells will have increasingly less labelling as labelled DNA dilutes with each stem cell division.

Since the radioactive H^3-Thymidine is visualised via a lengthy, process of autoradiography, which can take weeks, safer and easier alternatives are now used. The synthetic analogue of the nucleoside Thymidine such as bromodeoxyuridine (BrdU) is preferentially used because there are monoclonal antibodies to BrdU (Gratzner, 1982; Miller and Nowakowski, 1988). This means faster processing without the need for exposure to radioactivity. However, BrdU has since been shown to be toxic and have mutagenic effects on the cells that incorporate it (Rowell and Ragsdale, 2012; Taupin, 2007). Analysis of the results therefore needs to be considered cautiously to not exclude possibility of cell death or changes in neurogenesis.

To tackle the ambiguity caused by the cumulative labelling in the above methods, the "window-labelling" technique was developed, which is based on sequential administration of H^3-thymidine and BrdU (Belecky-Adams et al., 1996; Repka and Adler, 1992). This meant that the cells born between the two injections would be the only cells labelled by the first, but not second nucleotide analogue.

Altman & Bayer (1978) used autoradiography to look at birthdates of "nuclear cells". They found that the majority of cells (95%) were labelled with H^3-thymidine when injections were administered into the mother at E13 and E14, and after that time, the proportion of nuclear cells tagged decreased. No nuclear cells were tagged after injections from E16-E18. However, no injections were made prior to E13, limiting the results to cells born after that time. When the results were sorted by cell size, they found no difference in the birthdate results, though they excluded cells smaller than 200μm^2, arguing that these are probably glial cells. The threshold placed to differentiate "small" from "large" cells was 650μm^2. Combining this with our current knowledge of cell cytology, it is likely that both "large" and "small" cells were the elongated glutamatergic and glycinergic projection neurons viewed from different slice planes, and that the nucleo-olivary neurons and interneurons were omitted from this analysis. They also found a lateromedial gradient of birth order, whereby the lateral nuclei cells are born first compared to medial nuclei cells. This has also been shown in the chicken (Green and Wingate, 2014).

Another cerebellar birth-dating experiment using H^3-Thymidine found that only large "roof nuclei" (cerebellar nuclei) cells are early born from E11-13, while the smaller cells in the same region are born from E13-17 (Miale and Sidman, 1961). While another similar investigation came to similar conclusions, Pierce (1975)

found that the development of cerebellar nuclei starts earlier at E10, which is the lower limit for H^3-Thymidine labelling. She also saw that from E10, small neurons were labelled and continued to be labelled until late embryogenesis (E17). At that time, the cytology of the cerebellar nuclei was only beginning to be described, and it is now known there are many cell types under the umbrella term of "small morphology". It has since been shown that all the interneurons of the cerebellum are born from E14 onwards and it is likely that the early-born small cells noted by Pierce are the nucleo-olivary neurons (Carletti and Rossi, 2008; Fink et al., 2006).

The *Sox14*$^{Gfp/+}$ mouse can now confirm whether nucleo-olivary neurons are indeed the early born small nuclear cells observed in Pierce's study by injecting BrdU into pregnant dams at different gestation stages from E10.5-E18.5. Co-localisation of BrdU labelling and endogenous GFP indicates that cells are broadly-speaking born on the day of injection, assuming that the labelling "dilutes" out after a few divisions. BrdU immunoreactivity might still be picked up in cells born later, but never earlier, than the injection time-point.

4.1.2 ADDING NUCLEO-OLIVARY NEURONS TO CEREBELLAR FATE MAPS

Fate-mapping of the cerebellum has been done in a variety of ways, ranging from chick-quail homotypic grafts (Hamburger and Hamilton, 1951; Martinez and Alvarado‐Mallart, 1989; Millet et al., 1996; Otero et al., 1993; Wingate and Hatten, 1999) to genetic fate-mapping (Florio et al., 2012; Machold and Fishell, 2005; Obana et al., 2015; Sgaier et al., 2005; Zervas et al., 2004). The results of these are reviewed in the **Chapter 1.6**. Though early birth-dating experiments would

suggest that the nucleo-olivary neurons are early-born, the lack of a specific developmental marker for this cell type has meant that we know nothing about the lineage of these cells. In this chapter, I used *Sox14* as a marker in order to add to the limited knowledge we have about where the nucleo-olivary neurons fit with current cerebellar fate maps.

Clonal analyses, using the LaacZ technique, have shown that nuclear neurons have a common lineage with Purkinje cells and cortical interneurons (Mathis et al., 1997; Mathis and Nicolas, 2003). While these nuclear neurons are most probably, like Purkinje cells and interneurons, GABAergic, there is no further analysis to distinguish whether these cells are late-born interneurons or nucleo-olivary neurons. Since the methodology used is one of random, low-frequency recombination to include a laacZ reporter gene into a small group of cells at any time, it is unable to identify when the clones are marked. Interestingly, a few clones labelled only nuclear neurons and otherwise, only large clones that had dispersed cells over many cerebellar lobules had cells in the cerebellar nuclei as well as the cortex (Mathis and Nicolas, 2003). For small clones, related cells were either exclusively in the cortex or in the cerebellar nuclei. This result implies that though the two groups have a common lineage, there may be a segregation limiting the multipotency of cell fate determination, perhaps by temporal control, so that nuclear precursors have a potential to divide to only produce other nuclear neurons. If the nuclear cells are early born nucleo-olivary cells, it would suggest that there is a separate progenitor pool that only forms nuclear cell types since a common progenitor pool would show clonally related, later-born cortical cell type. However, if they are the later-born

nuclear interneurons, it is conceivable that the recombination event happens at a later enough stage that only nuclear interneurons are produced.

4.1.2.1 ARE ALL CEREBELLAR GABAERGIC NEURONS FROM THE PTF1A LINEAGE?

One possibility is that the nucleo-olivary neurons are akin to the other GABAergic cells in the cerebellum; thus far, all have been found to be derived from the *Ptf1a*$^{+}$ progenitor pool (Hoshino et al., 2005; Martinez et al., 2013; Seto et al., 2014). The most convincing evidence of this hypothesis is from the c*erebelless*, *cbll*, mutant (Hoshino et al., 2005). The homozygous mutant mouse lacks a cerebellum and show ataxic gait. It was found that the mutant is deficient in *Ptf1a* only in the cerebellum and not the pancreas, enabling the mouse to survive to adulthood, unlike another *Ptf1a* mutant that cannot survive past birth (Pascual et al., 2007). They observed that in the *cbll* adult, the GABAergic nuclear neurons were completely absent in the mutant, while glutamatergic nuclear neurons remained, though were fewer in number. Likewise, during development, GABA immunoreactivity is completely missing throughout the whole cerebellar plate at E14 and E16. In the *Ptf1a* complete knock-out mice, Pascual *et al.* (2007) did not report any deficits in the cerebellar nuclei, instead, focusing on the cerebellar cortex.

These results suggest that the GABAergic nuclear neurons share a common *Ptf1a* lineage with the other GABAergic cerebellar neurons. However, it is seen that while ISH against GAD65/GAD67 mRNA showed a dramatic reduction of expression in the *Ptf1a* null mutant cerebellum at E18, this reduction did not terminate all GABAergic expression (Pascual et al., 2007). Instead, some labelling is seen in the

intermediate zone where the cerebellar nuclei would be, although this is not discussed in the paper. Furthermore, since *Ptf1a* expression is limited to the hindbrain and spinal cord, it cannot define the precursors of *Sox14*$^{+}$ cells in the diencephalon, which by contrast are derived from the *Ascl1* (*Mash1)* lineage (Delogu et al., 2012).

We expect that like the diencephalic *Sox14*$^{+}$ population, the expression of *Sox14* is post mitotic (Delogu et al., 2012), while *Ptf1a* expression is known to be down regulated after cell division. This presents a problem in showing that the two expressions coincide within one neuron. Lineage can be confirmed by labelling a progenitor cell with an incorporated reporter gene that will be passed onto its progeny, thereby showing which cell-types are derived from the same cell. These genes can be delivered using retroviruses, or electroporation of plasmids. In order to definitively affirm that *Sox14*$^{+}$ neurons are derived from the *Ptf1a* progenitor pool, I would need to deliver a reporter gene that targets *Ptf1a*$^{+}$ cells before mitosis and differentiation, then observe whether any marked cells are in the *Sox14*$^{+}$ population.

Our initial method of investigating the hypothesis was to electroporate embryos to deliver expression plasmids that would cause *Ptf1a*$^{+}$ cells to produce a reporter protein that outlasts the endogenous *Ptf1a* expression. We could then see if these marked cells coincide with later *Sox14* expression. The construct had the mouse 2.3 kb *Ptf1a* enhancer from Meredith *et al.* (2009), which also drives expression of a red fluorescent reporter protein. I first tested the construct in chicken electroporation experiments as well as in the E13.5 mouse to show that it is able to mark ventricular zone progeny.

Electroporations were not successful in mouse from E10.5-E11.5, having tried *in utero* electroporation and *exo utero* electroporation. The methodology required plasmid delivery before E10/E11 but correct injection of the plasmids and electroporation into the ventricular zone proved too difficult to achieve at these early stages and very few embryos survived the procedure and none showed reporter protein fluorescence. Yoshida *et al.* (2011) showed that *in utero* electroporation into the telencephalon and thalamus is possible from E9.5, but I was not able to target the cerebellar primordium at this timepoint due to visibility problems as the uterine wall is not stretched enough to see the embryo. I also tried *exo utero* electroporation (Ngô-Muller and Muneoka, 2010), which is to open the uterine wall while keeping the embryos and placentas intact. However, the embryos are obscured by a surrounding decidual layer of tissue over the amniotic sac at E10.5. Removal of this layer compromises embryo survival (Ngô-Muller and Muneoka, 2010), so I was not able to improve visibility to target the r1 ventricular zone while maintaining viability.

4.1.2.2 DOWNSTREAM MOLECULAR MARKERS FOR VENTRICULAR ZONE PROGENY

As well as *Ptf1a*, other molecular markers in the cerebellum have been found, and together, they have helped to define the precise spatiotemporal sequence of GABAergic neurogenesis (Leto et al., 2012). Temporal sequences of gene expression are known that follow the migratory pattern of cells as they leave the cycle cycle and translocate dorsally from the ventricular zone. In particular, the *Lhx1/5* and *Corl2* gene expression from E12.5 represents the Purkinje cell population that are born from the ventricular zone and migrate radially outwards

towards the cortical transitory zone (CTZ) (Chizhikov et al., 2006; Minaki et al., 2008; Morales and Hatten, 2006; Zhao et al., 2007). In addition, *Pax2* expression from E13 in the anterior portion of the ventricular zone is thought to give rise to a separate set of GABAergic progenitors that become interneurons, perhaps including nuclear interneurons (Leto et al., 2006; Maricich and Herrup, 1999).

The only genetic marker that has been shown to result in confirmed GABAergic nuclear cells is *Zac1* (Chung et al., 2011). *Zac1* is expressed in the ventricular zone during early development, then continues to be expressed in postmitotic GABAergic neurons in the medial cerebellar nuclei. Though *Zac1* cells have been identified as interneurons due to their small size, the *Zac1* expression begins earlier than interneuron production and $Zac1^{+}$ cells are already seen in the CTZ as well as in the ventricular zone by E12. It may be that early $Zac1^{+}$ expression delineates medial nucleo-olivary projection neurons, which form an early sub-nucleus just ventral to the NTZ. If this is the case, the *Sox14* expressing nucleo-olivary neurons may do likewise.

Thus, I investigated how the expression of *Sox14* relates to known markers of cerebellar neurogenesis. Immunohistochemistry and *in situ* hybridization was performed against *Lhx1*/5, and against known markers for the NTZ: *Pax*, *Lhx9* and *Tbr1*.

4.1.3 NUCLEOGENESIS

Insight into cerebellar nucleogenesis currently stems from following the glutamatergic *Lhx9*$^{+}$/*Tbr1*$^{+}$ nuclear cells, which transit via the NTZ to finally reside in the white matter. It is not known how the NTZ moves to the final location of the cerebellar nuclei. This translocation may be due to morphogenic changes in the cerebellar structure as granule cells precursors in the EGL proliferate and displace the NTZ, or it may reflect an active migration inwards towards the ventricular zone (Altman and Bayer, 1985). How GABAergic projection neurons and interneurons from the ventricular zone are incorporated into the cerebellar nuclei, however, is still completely undefined. It is not known at which stage nucleo-olivary neurons join the glutamatergic projection neurons. Through following the developmental expression patterns of *Zac1*, it is known that some GABAergic cerebellar nuclear cells migrate into the CTZ and sit under the NTZ (Chung et al., 2011).

In this chapter, *Sox14*$^{Gfp/+}$ heterozygous mice are used to reveal patterns of *Sox14* expression across embryonic and postnatal time-points, as the cerebellum continues to mature beyond birth into adulthood. In particular, the distribution of endogenous GFP fluorescence compared to rhombic lip derivatives will help explain how nucleo-olivary neurons migrate into their final position and, in particular, whether they enter the NTZ. Correspondingly, the availability of the *Sox14* knock-out mouse allows a direct assessment of the function of *Sox14* in the development of nucleo-olivary neurons.

4.1.4 AIMS OF THE CHAPTER

There are three key aims to the experiments described in this chapter:

- Determination of birthdates of *Sox14*$^{+}$ nucleo-olivary cells by BrdU injections
- Examination of *Sox14* expression throughout embryonic developmental stages
- Analysis of nucleus assembly in the *Sox14*$^{-/-}$ mouse to assess the role of the *Sox14* gene in nucleogenesis.

4.2 RESULTS

4.2.1 DISTRIBUTION OF *SOX14*$^{+}$ CELLS DURING EMBRYONIC AND POST-NATAL PERIOD

Sox14$^{Gfp/+}$ Embryos from timed pregnancies were collected at time-points from E10.5 to E15.5. The E11.5 and E12.5 embryos were flat mounted by dissecting the hindbrains, then opening up the neural tube to mount the cerebellar plates with the ventricular surface facing downwards (**Figure 4–1A**). Though *Sox14* expression is seen in the E10.5 (not shown) and E11.5 embryos (**Figure 4–1B**), expression in the cerebellar plate is first seen in E12.5 embryos (**Figure 4–1C&D**). The expression is spread across the rostrocaudal axis of the cerebellum distal to the rhombic lip (**Figure 4–1D**). This expression also indicates that at least some *Sox14*$^{+}$ cells are born prior to E12.5. From this perspective, it is unclear whether cells have migrated to this position from the rhombic lip, or are derived from the underlying ventricular zone.

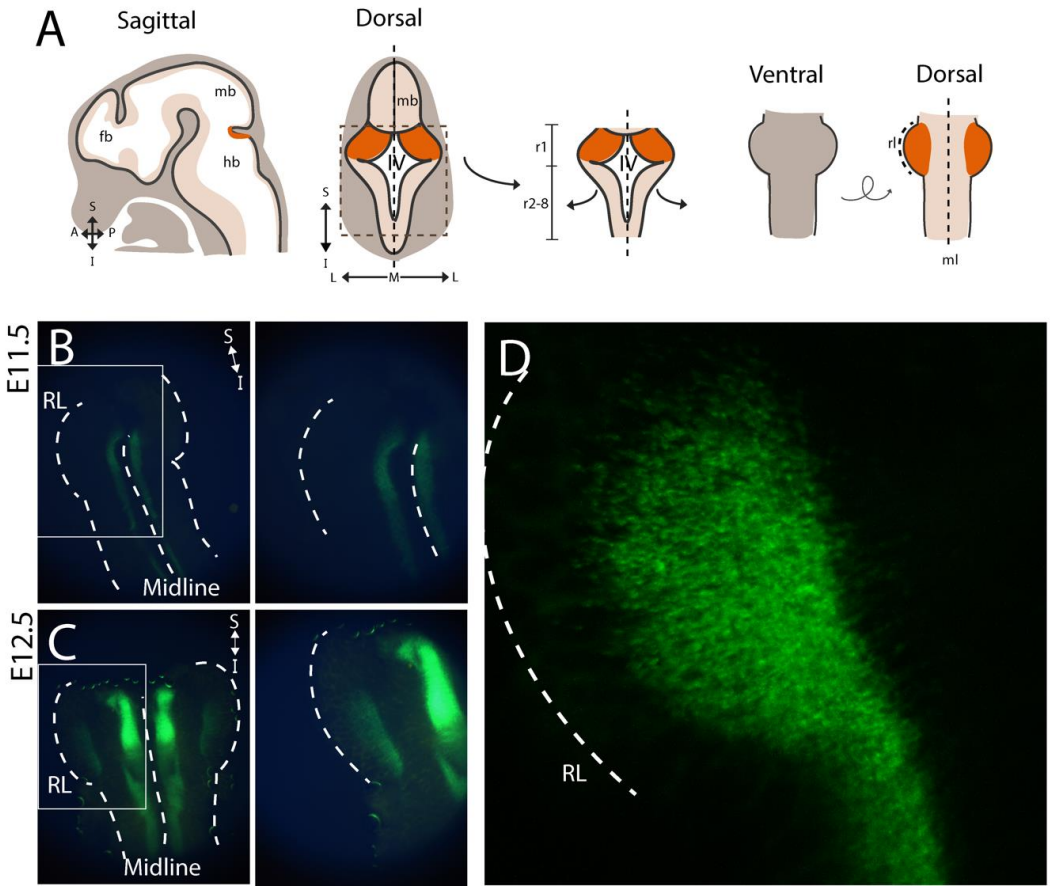

Figure 4–1 Flat-mount of the Sox14$^{Gfp/+}$ hindbrain

***A**) schematic of the embryonic mouse brain shown in the sagittal and dorsal view. The cerebellar primordium is shown in orange. In order to image the whole cerebellar primordium at an early embryonic stage (E10.5-E12.5), the hindbrain is dissected out, then opened up dorsally along the midline and mounted flat so the rhombic lip, which originally lined the intersection between the cerebellum and roof plate, is the most lateral edge. **B-D**) Flat-mount of Sox14$^{Gfp/+}$ brains at E11.5 (**B**) and E12.5 (**C**). In both, GFP expression is seen on either side of the midline, while expression in the cerebellar plate is only seen from E12.5 onwards (**C**). **D**) A large number of cells express Sox14, as seen in the higher magnification confocal microscope image, which is a flattened z-stack. While there is no Sox14 expression at the rhombic lip, the Sox14^{+} cells span the length of the cerebellar plate along the anterior-posterior axis.*

4.2.1 CEREBELLAR *SOX14*$^{+}$ NEURONS ARE BORN AROUND E10.5-E11.5

BrdU was injected into pregnant dams at different embryonic stages from E10.5-E18.5. The *Sox14*$^{Gfp/+}$ brains of the mice pups were collected and analysed at P7 (**Figure 4–2** and **Figure 4–3**). GFP^{+} neurons had incorporated BrdU for injections administered at E10.5 (**Figure 4–2A&G**, **Figure 4–3A**) and E11.5 (**Figure 4–2B&H**). For injections made E12.5 or later, no BrdU staining was seen in GFP^{+} cells (**Figure 4–2C-F**, **I&J**, **Figure 4–3B**). At the cerebellar cortex, BrdU was detected in Purkinje cells for injections made at E11.5, E12.5 and E13.5, showing the nucleo-olivary neurons are born prior to GABAergic Purkinje cells and interneurons. GFP^{-}/BrdU^{+} cells are seen in the cerebellar nuclei throughout all the injections, showing that the other nuclear cell types are also generated during this time window.

Figure 4–2 BrdU birthdating analysis

*BrdU was injected in the pregnant dam at time points from E10.5-E18.5. The Sox14$^{Gfp/+}$ pups were collected and analysed at P7. **A-F)** BrdU^{+} cells are seen in the CN throughout all the injection timepoints. **G-J)** Higher magnification images to show co-labellng of GFP and BrdU when injection is at E10.5 (**G**, white arrowheads), and E11.5 (**H**, white arrowheads), but not E12.5 (**I**) or E13.5 (**J**). The majority of double-labelled cells were found with BrdU injected at E10.5 as this will also have BrdU incorporated into cells born at E11.5. The BrdU^{+} expression pattern concurs with known knowledge of cerebellar developmental timelines, with Purkinje cells labelled from injections at E11. 5-13.5, and interneurons labelled from injections at E13.5-18.5. Scale: A-F: 100 µm, G-J: 20 µm*

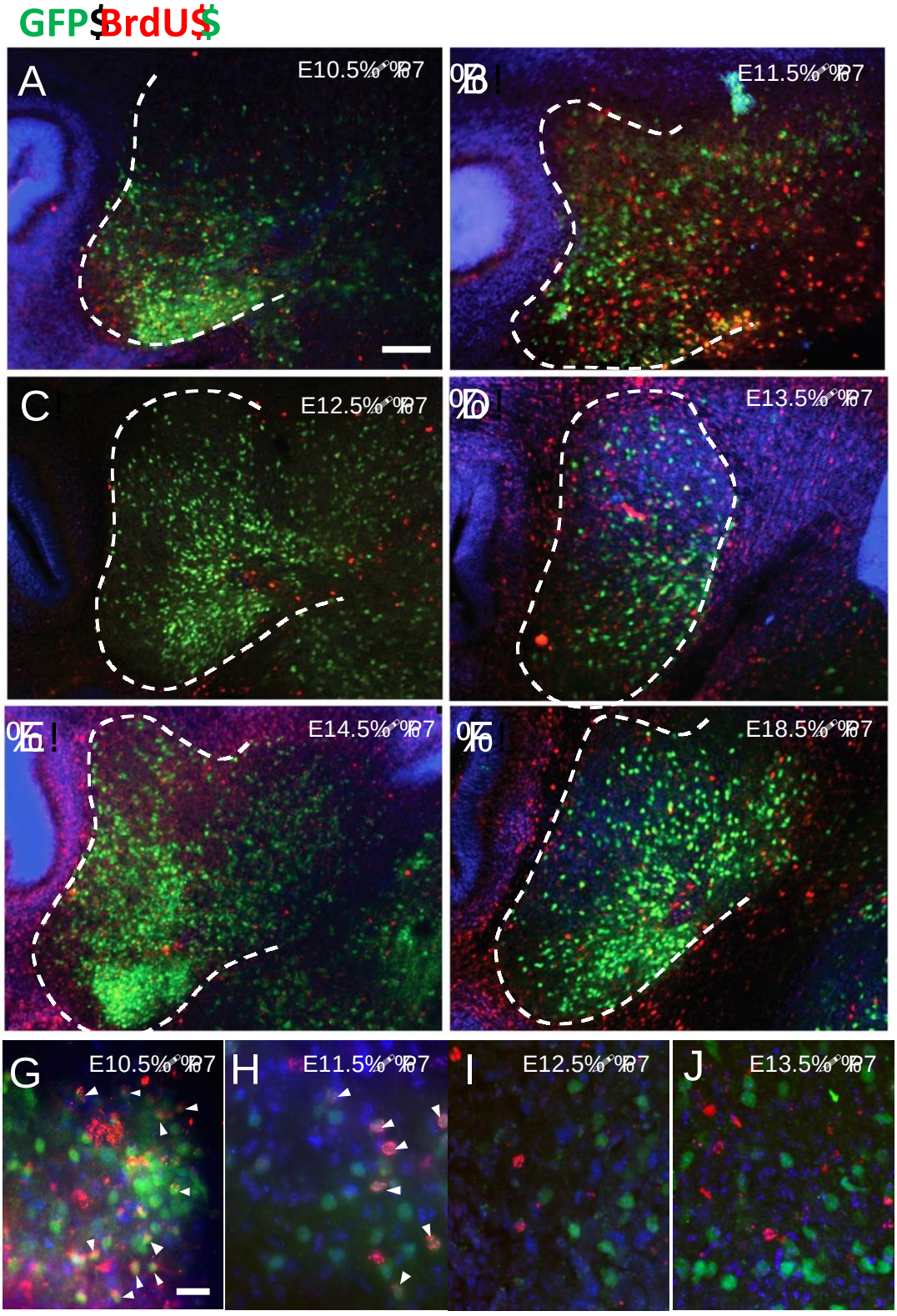
GFP$BrdU$
A
E10.5
B
E11.5
C
E12.5
D
E13.5
E
E14.5
F
E18.5
G
E10.5
H
E11.5
I
E12.5
J
E13.5

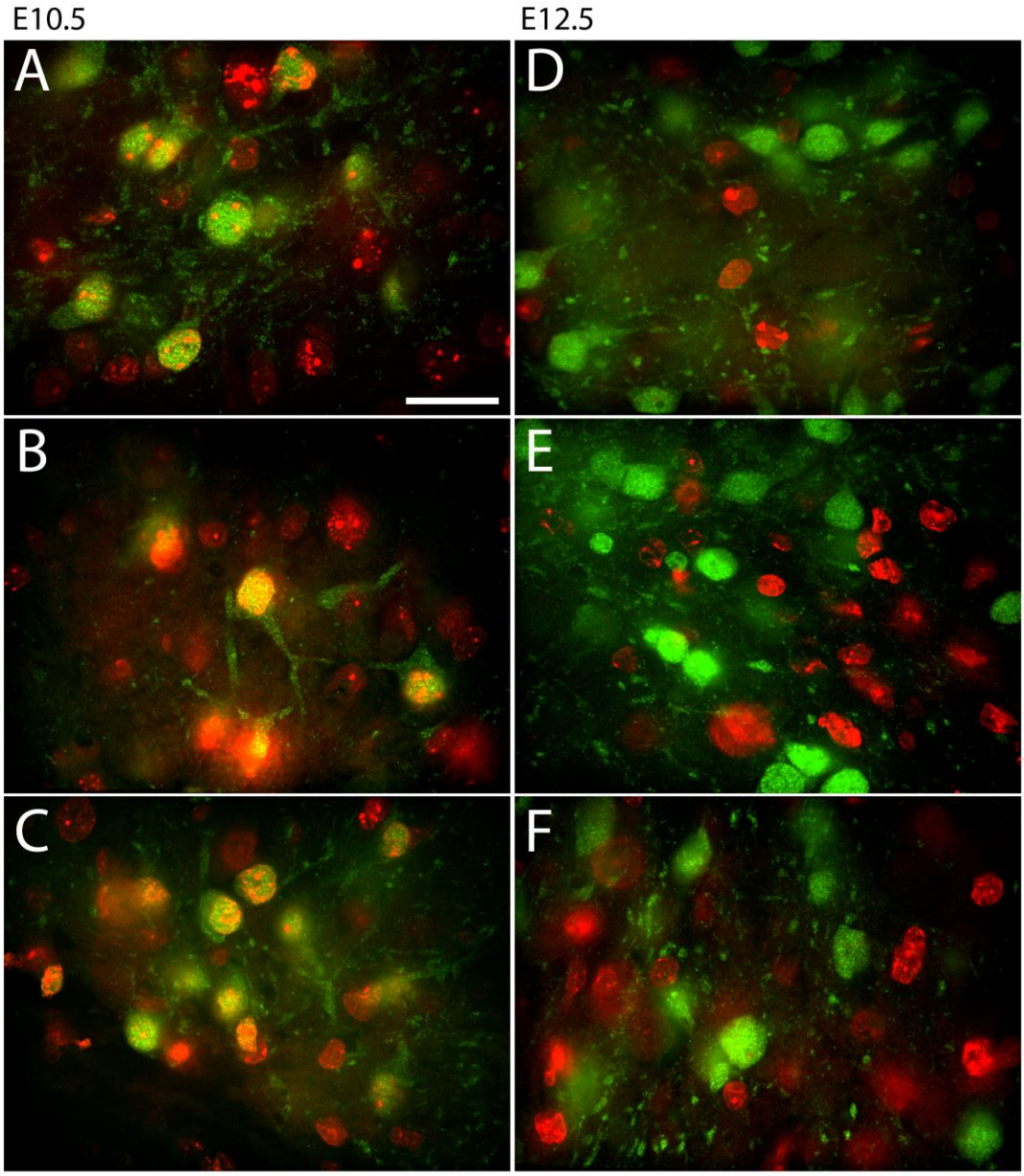

Figure 4–3 BrdU birthdating analysis.

Images at high magnification shows almost all GFP$^+$ cells are born after injection of BrdU at E10. 5 (A-C), while BrdU injected at 12.5 shows no colocalisation, showing all the GFP$^+$ cells are born before E12.5 (D-F). Scale: A-F: 20 µm

4.2.2 *SOX14*$^{+}$ CELLS CONGREGATE ADJACENT TO GLUTAMATERGIC CELLS OF THE NTZ

Figure 4–4 shows *Sox14*$^{Gfp/+}$ E12.5, E13.5 and E15.5 sagittal slices that were stained against *Pax6*, *Tbr1* and *Lhx9*, both by IHC and ISH to compare the GFP^{+} population with rhombic lip derived cerebellar nuclear cells. While *Pax6* expression defines the cell populations that are migrating from the rhombic lip (**Figure 4–4E-G**), *Lhx9* (**Figure 4–4A-D**) and *Tbr1* (**Figure 4–4H**) defines only the glutamatergic nuclear population that migrate from the rhombic lip, and reach the NTZ. There is no co-localisation between GFP and any of these markers, so *Sox14*$^{+}$ cells are distinct from the glutamatergic projection neurons, which are also early born but migrate from the rhombic lip to gather at the nuclear transitory zone. At E12.5, GFP^{+} cells occupy an anterior-posterior strip that lies just beneath the subpial rhombic lip migratory stream (**Figure 4–4B&E**). From E13.5 onwards, it is apparent that the GFP^{+} cells do not travel to the NTZ, but instead are spread throughout the cortical transitory zone (**Figure 4–4C,D,F,G,H**).

4.2.3 *SOX14*$^{+}$ NEURONS EXPRESS LHX1/5

Figure 4–5A&B shows two sagittal sections of the *Sox14*$^{Gfp/+}$ E12.5 brain. The GFP^{+} neurons are a subset of Lhx1/5^{+} neurons, which are known to be expressed in Purkinje cells that are derived from the ventricular zone. Lhx1/5 is therefore a marker for nucleo-olivary neurons as well as Purkinje cells, which are the GFP^{-} /Lhx1/5^{+} cells that sit ventral to the GFP^{+} cells. Comparing the Lhx1/5 and Pax6 immunoreactivity (**Figure 4–5C**), the GFP^{+} population sits between the nuclear transitory zone and the radially migrating Purkinje cells. Since the GFP^{+} cells also express Lhx1/5, it would seem likely that they come from the same progenitors in

the ventricular zone, preceding the birth of Purkinje cells. However, the processes protruding from the GFP$^+$ cells are tangentially orientated (**Figure 4–5A&B**, **inset white arrowheads**). It is therefore unclear whether the GFP$^+$ cells are tangentially migrating along the subpial rhombic lip migratory stream, or radially migrating before the Purkinje cells (**Figure 4–5D**).

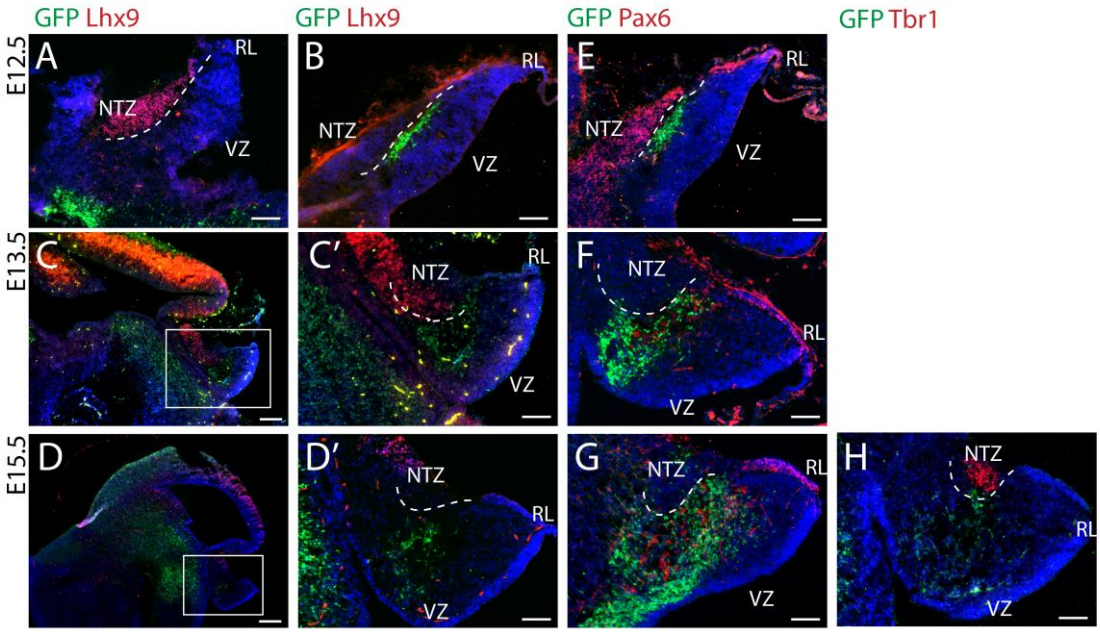

Figure 4–4 Immunohistochemistry and in situ hybridisation of Sox14$^{Gfp/+}$ sagittal sections at E12.5, E13.5 and E15.5 against known markers for the nuclear cells migrating from the rhombic lip.

A) *Lhx9 is seen in medial sections of the E12.5 brain, while GFP was only found in more lateral sections (**B**). At this time-point, no single section was found to cover both expression zones.* ***C)*** *At E13.5, strong Lhx9 expression is seen in the midbrain. In the cerebellum (**C'**), it defines a rostrodorsal population, clustered to form the nuclear transitory zone (NTZ). The GFP$^+$ expression at this time spans the region ventral to the NTZ, defined as the cortical transitory zone (CTZ). No expression is seen at the rhombic lip nor the ventricular zone. The two populations are more disparate at E15.5 (**D**) as the cerebellar primordia grows and GFP$^+$ cells stay in the CTZ of the anterior part of the cerebellum.* ***E-G)*** *Pax6 is seen from the rhombic lip in cells as they translocate across the subpial rhombic lip migratory stream at E12.5 to the NTZ.* ***F-G)*** *Unlike Lhx9 and Tbr1, Pax6 expression fades after the cells arrive at the NTZ but is still seen migrating from the rhombic lip.* ***H)*** *Like Lhx9, Tbr1 is seen at the NTZ at E15.5 while GFP expression sits ventral to the Tbr1$^+$ cluster. Scale: A, B, C', D', E-H: 100 µm, C-D: 200 µm*

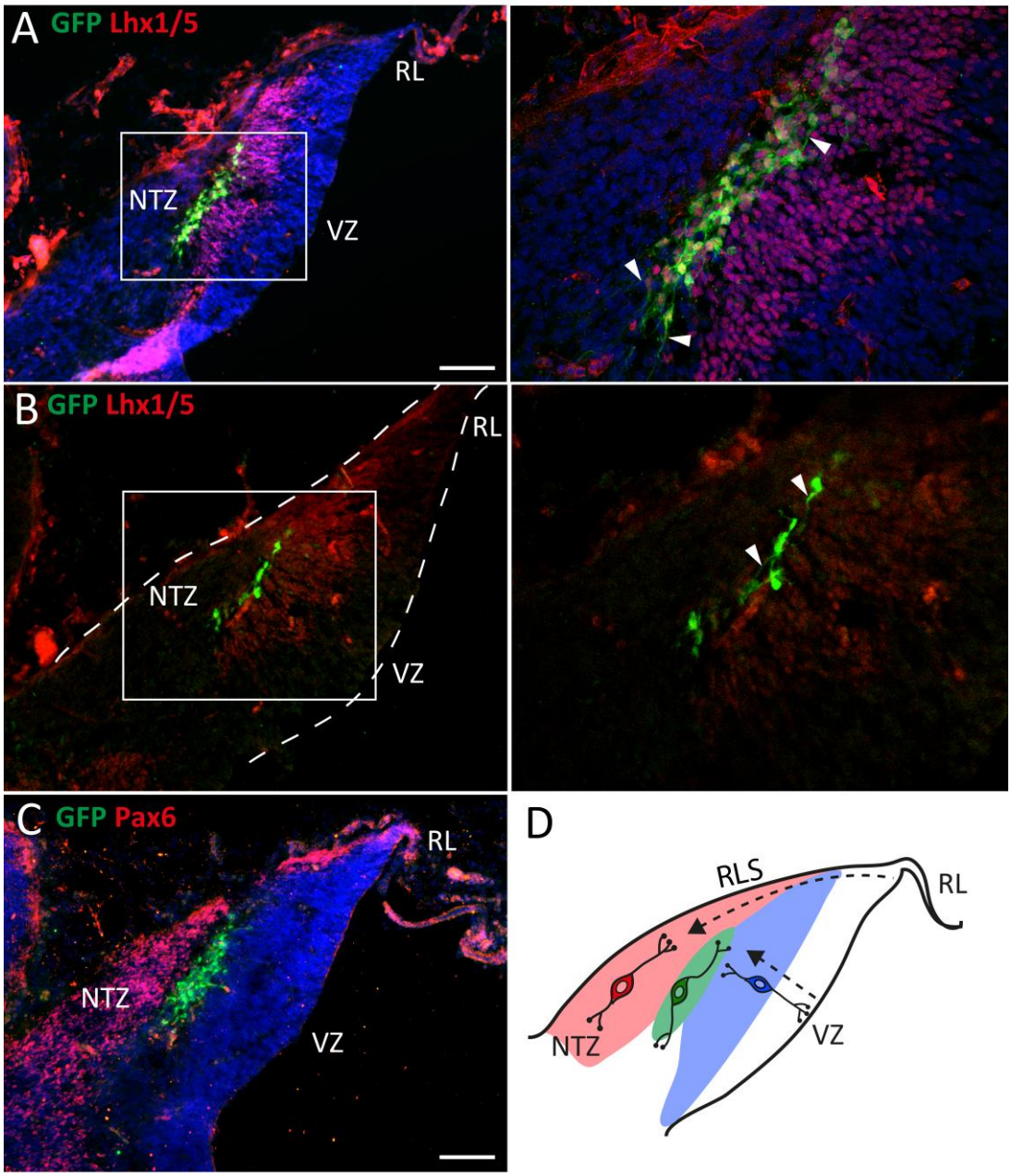

Figure 4–5 Immunohistochemistry of Sox14$^{Gfp/+}$ sagittal sections at E12.5 against Lhx1/5

A&B) *IHC against Lhx1/5 and GFP in the Sox14$^{Gfp/+}$ E12.5 sagittal brain sections. The Lhx1/5 expressing cells span the anterior-posterior axis of the cortical transitory zone, and are mostly Purkinje cell precursors. However, there is a dorsal layer of Lhx1/5^{+} and GFP^{+} population that are genetically distinct, seen in the higher magnification images (**inset**). These cells appear to be in a tangential orientation (white arrowheads), unlike the GFP^{-}/Lhx1/5^{+} Purkinje cells which appear to be radiating from the ventricular zone.* ***C)*** *The space above the GFP^{+} cells is filled with Pax6^{+} cells coming from the rhombic lip.* ***D)*** *a schematic to show the tangential orientation of the GFP^{+} cells, seen in green, alongside the Pax6 excitatory cells migrating tangentially along the subpial rhombic lip migratory stream (RLS) in red, and the GFP^{-}/Lhx1/5^{+} Purkinje cells that are migrating radially from the ventricular zone. Scale: 100 µm*

4.2.4 MIGRATION OF *SOX14*$^{+}$ NEURONS TO FORM DIFFERENT CEREBELLAR NUCLEI IS NOT CORRELATED WITH GROSS CEREBELLAR MORPHOGENESIS

I looked at patterns of *Sox14* expression in P0-P5 *Sox14*$^{Gfp/+}$ mouse, imaging systematically along the rostrocaudal axis (**Figure 4–6**). The aim was to see when the nuclei form and if the morphological changes occurring in the cerebellar cortex could be involved in nucleogenesis. At P0, no GFP^{+} cells are observed in the rostral sections, although nearby vestibular populations are seen (**Figure 4–6Ai,ii**). The lateral nucleus can be seen in **Figure 4–6Aiii**. The cerebellum is small as the cortex has not expanded. In more caudal sections, the shape of the nuclei can already be detected and resemble the distribution of GFP^{+} cells in the adult as cells are more dense ventrally (**Figure 4–6Aiv-vi**) the dense masses also appear to outline migration paths. As the cerebellar cortex expands and becomes foliated at P1- P3 (**Figure 4–6B-D**), the nuclei continue to be populated and the rostral lateral nucleus becomes defined (**Figure 4–6Diii**). The GFP^{+} cells also appear more dispersed as the spaces between the more densely populated "streams" become more occupied. The cerebellar cortex at P4 and P5 is not fully matured (**Figure 4–6E&F**), but the main structures of the cerebellar nuclei are can be distinguished. The density of GFP expression is much higher than the nuclei in P14 and P21 brains observed in **Chapter 2.2**. This may be due to the small size of the brain. It may be that as the cerebellum continues to grow and mature, these cells become more dispersed. It is clear from these images that the morphological changes of the cerebellar cortex are not the driving force that forms the contours of the nuclei.

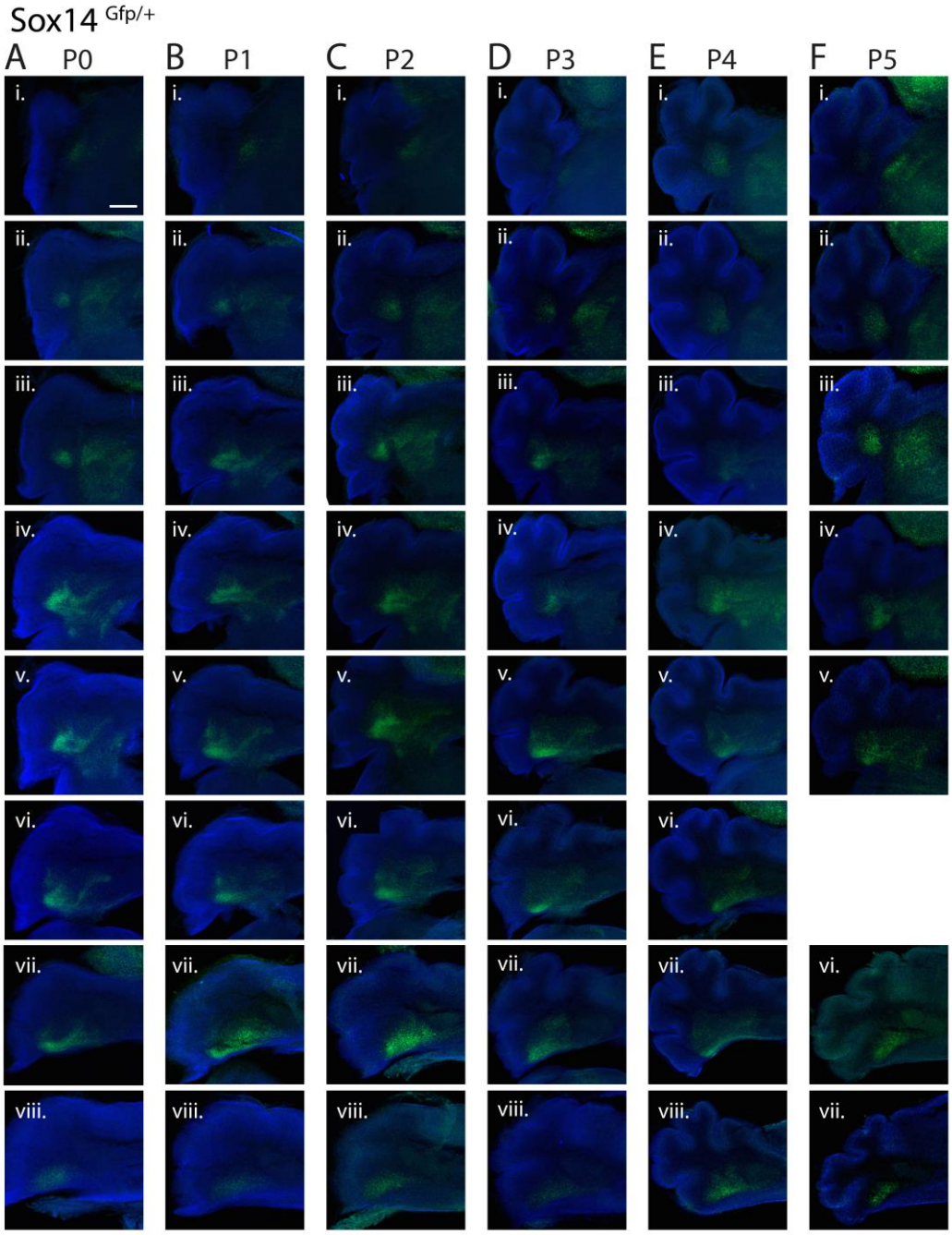

Figure 4–6 Postnatal development of the nucleo-olivary neurons of the cerebellar nuclei

*Sox14$^{Gfp/+}$ mice cerebellar sections at P0 (**A**), P1 (**B**), P2 (**C**), P3 (**D**), P4 (**E**) and P5 (**F**). By P0, although the foliation of the cerebellar cortex has not fully expanded, the Sox14^{+} neurons already have a heterogeneous distribution with defined populations at the lateral nucleus (**A ii&iii**), while the interposed nuclei appears to be formed in migratory streams (**A iv-vi**). These streams spread to become defined anterior and posterior interposed nuclei and this is already apparent by P2, before the foliation of the cerebellar cortex is prominent. There are many more Sox14^{+} cells in the nuclei at these early postnatal timepoints as compared to the adult brain. Scale: 300 µm*

4.2.5 *SOX14* IS NECESSARY FOR ASSEMBLY OF THE GABAERGIC CELL COMPONENT OF THE CEREBELLAR NUCLEI

The possible functions of *Sox14* gene in development were assessed by examining the mature distribution of GABAergic cells in the *Sox14* knock-out mouse. **Figure 4–7** shows the $Sox14^{Cre/Cre}$ mouse at 4 weeks post-birth compared to two $Sox14^{Cre/+}$ mice at the same age. As the cells no longer express *Sox14* at this stage, I used *Gad1* ISH to visualise the nucleo-olivary cells, as validated by the experiments in **Chapter 2.2.3.1**. As seen in **Figure 4–7A&B**, the overall contours of the cerebellar nuclei in the knock-out do not appear to be malformed compared to the heterozygous mice (**Figure 4–7C-F**). It would appear that the formation of distinct lateral and interposed nuclei is independent of *Sox14* function. However, while the $Gad1^{+}$ cells mainly reside in the ventral parts of the nuclear mass of the $Sox14^{Gfp/+}$ mouse, $Gad1^{+}$ cells are more sparsely and evenly distributed throughout the nuclei of the knock-out animal. Overall, there appear to be lower numbers of $Gad1^{+}$ neurons in the nuclei of the knock-out. This is particularly evident in the ventromedial portion of the lateral nucleus, where $Sox14^{+}$ cells are denser in number, suggesting that *Sox14* deletion results in a repositioning, respecification or loss of nucleo-olivary neurons.

A comparison of $Sox14^{Gfp/Gfp}$ (**Figure 4–8A**) and $Sox14^{Gfp/+}$ mice (**Figure 4–8B&C**) at P0, shows a change in distribution of GFP^{+} cells within the cerebellar nucleus as a result of the deletion of *Sox14*. At high magnification, it appears that GFP^{+} cells fail to migrate to occupy the dorsolateral portion of the white matter to become the dorsal part of the lateral nucleus (**Figure 4–9**). Instead, gaps are seen where GFP^{+} cells are observed in the heterozygous mouse (**Figure 4–9A**, **marked by ***). **Figure 4–9B&C** show the normal distribution of GFP^{+} cells. The presumptive cerebellar

nuclear boundaries can already be traced as the cells form distinguishable contours (**Figure 4–9C**). While a role for *Sox14* in postnatal cell survival cannot be ruled out, it is clear that a large number of neurons survive to at least P0 but display altered migration paths. Clusters of GFP^+ that form in the knockout also are also suggestive of other migration cues that are able to instruct cells to reach goalposts (**Figure 4–9A**, **white arrowheads**).

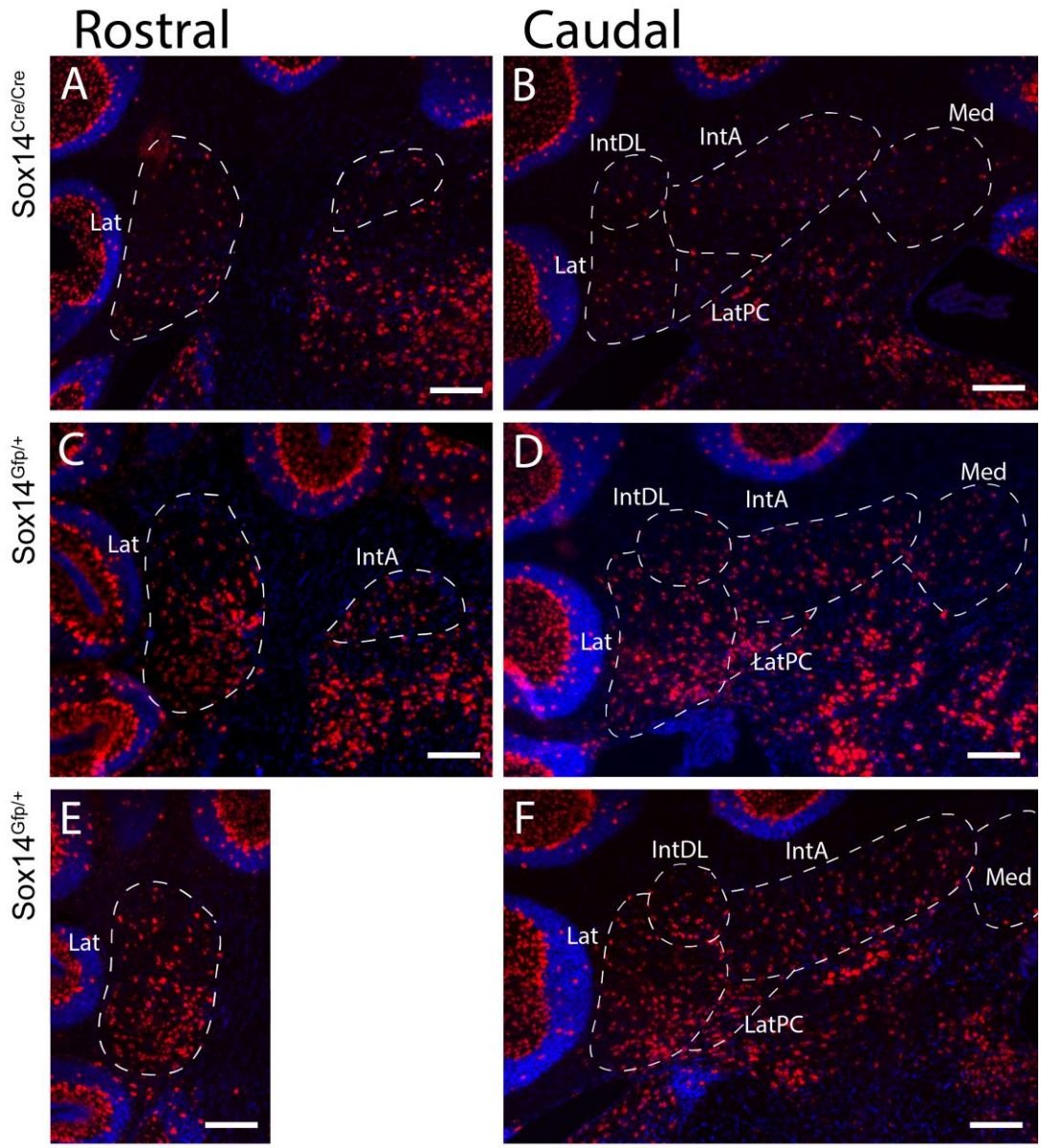

Figure 4–7 Gad1 ISH in adult Sox14$^{Gfp/Gfp}$ knock-out mouse

*Gad1 ISH in cerebellar nuclei of the Sox14$^{Gfp/Gfp}$ P28 knock-out mouse **(A&B)** compared to two Sox14$^{Gfp/+}$ mice **(C-F)**. The left column shows more rostral sections of the lateral and anterior interposed nuclei, while the right column shows comparable sections that include the caudal lateral nucleus, the anterior interposed nucleus, and the medial nucleus. Compared to the heterozygous mice, the knock-out had less cells that were immunoreactive for Gad1, particularly in the ventromedial parts of the lateral nucleus and the parvicellular portion of the lateral nucleus. In addition, although the morphology of the nuclei is similar between the two sets of mice, the distribution of Gad1^{+}cells differs. Scale: 100 µm*

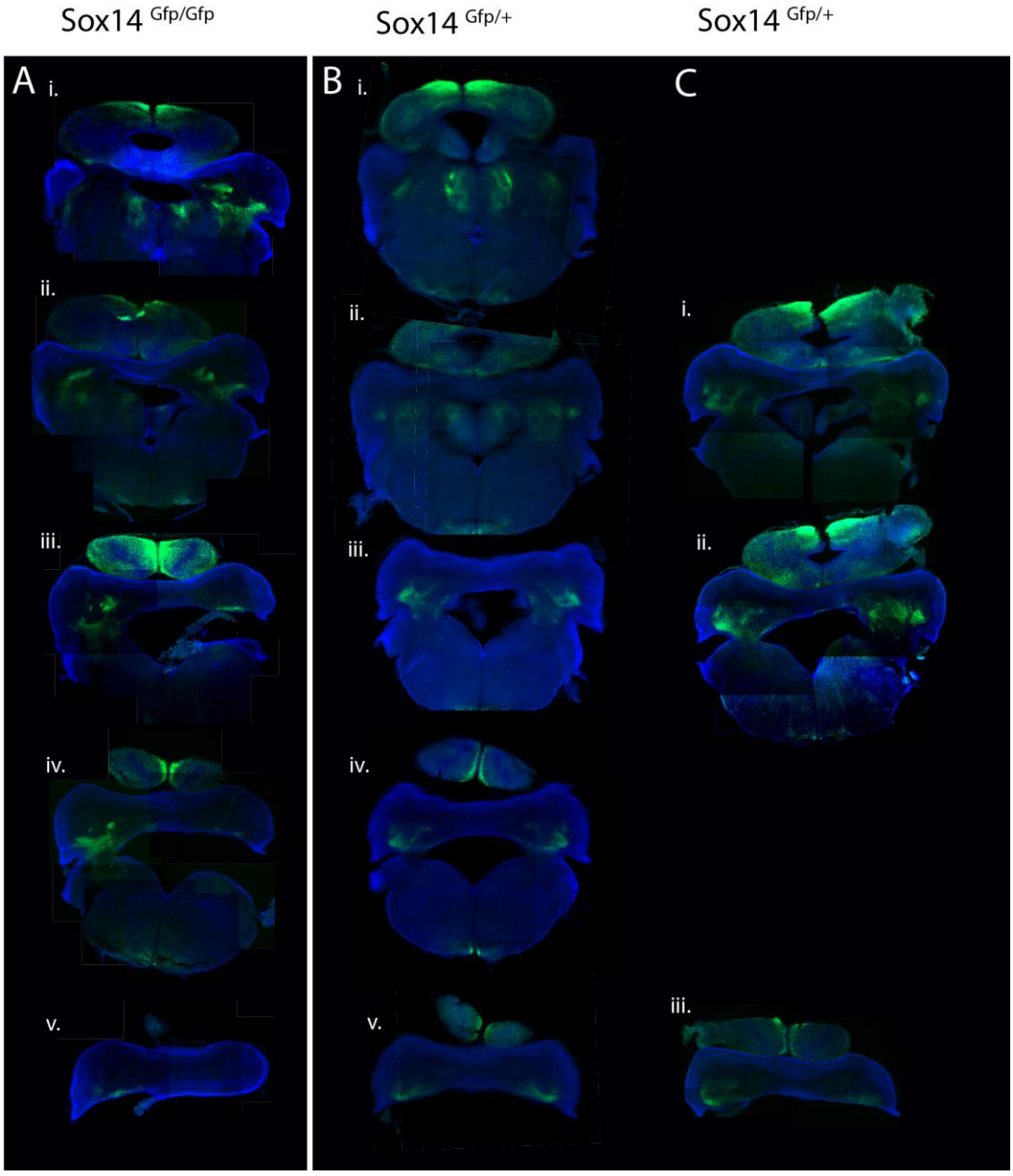

Figure 4–8 The P0 Sox14$^{Gfp/Gfp}$ knock-out mouse

*Coronal sections of the P0 Sox14$^{Gfp/Gfp}$ knock-out mouse (**A**) compared to two Sox14$^{Gfp/+}$ mice (**B**&**C**) arranged from rostral to caudal sections (**i to v**). The sections are matched approximately to the nearest section using morphological features of the slices such as the connection between the cerebellum and the medulla, and the shape of the cerebellar cortex. Note that for the Sox14$^{Gfp/+}$ mouse, the migratory streams already resemble the future boundaries between the sub-nuclei, while for the knock-out, the cells fail to populate some areas, leaving large gaps and deviant clusters of cells. Particularly, the lateral nuclear cells fail to reach their targets. There are still some likenesses between the two brains, which suggests that there are other migratory mechanisms at work in the development of nucleo-olivary neurons.*

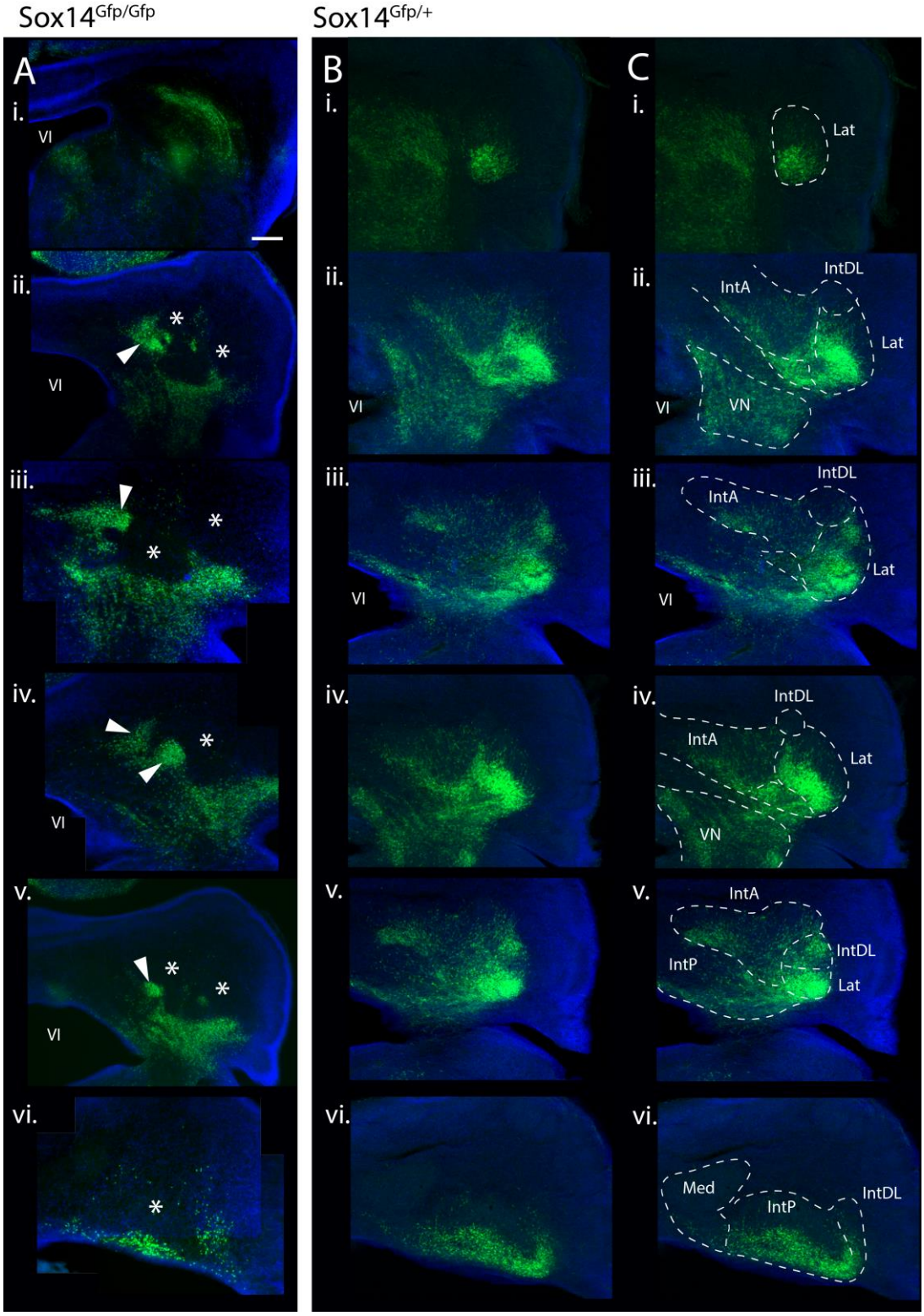
Sox14Gfp/Gfp
Sox14Gfp/+
A
B
C
i.
ii.
iii.
iv.
v.
vi.
VI
Lat
IntDL
IntA
VN
IntP
Med

Figure 4–9 The P0 Sox14$^{Gfp/Gfp}$ knock-out mouse

*Close-up view of the Sox14^{+} cells in the developing CN of the Sox14$^{Gfp/Gfp}$ knock-out mouse (**A**) compared to the Sox14$^{Gfp/+}$ mouse (**B&C**) arranged from rostral to caudal sections (**i to vi**). The sections are matched approximately to the nearest section using morphological features of the slices such as the connection between the cerebellum and the medulla, and the shape of the cerebellar cortex. (**C**) shows the same images as (**B**), outlining the presumptive cerebellar nuclear boundaries. Note that for the Sox14$^{Gfp/+}$ mouse, the migratory streams already resemble the future boundaries between the sub-nuclei, while for the knock-out, the cells fail to populate some areas, leaving large gaps (marked by *) and deviant clusters of cells (white arrowheads). Particularly, the lateral nuclear cells fail to reach their targets. There are still some likenesses between the two brains, which suggests that there are other migratory mechanisms at work in the development of nucleo-olivary neurons. Scale: 200 µm*

4.3 DISCUSSION

The following conclusions can be made from the experiments in this chapter:

1. *Sox14* expression is first observable in the cerebellar nuclei at E12.5
2. Nucleo-olivary neurons are early-born (E10-E11)
3. Nucleo-olivary neurons sit adjacent to do not enter the glutamatergic nuclear transitory zone
4. The *Sox14* gene is needed for nucleo-olivary neurons to integrate correctly into the nuclei

4.3.1 ARE *SOX14*$^+$ NUCLEO-OLIVARY NEURONS DERIVED FROM VENTRICULAR ZONE PROGENITORS?

From **Figure 4–5**, it is clear that the *Sox14*$^+$ neurons are in fact a subset of *Lhx1*/5$^+$ neurons, which previously was thought to only represent ventricular zone derived Purkinje cells, which migrate radially outwards towards the dorsal cerebellar anlage (Chizhikov et al., 2006; Minaki et al., 2008; Morales and Hatten, 2006). *Lhx1*/5 is therefore a marker for nucleo-olivary neurons as well as Purkinje cells.

Since *Lhx1/5*$^+$ Purkinje cells are known to be *Ptf1a*$^+$ ventricular zone derivatives, this finding suggests that *Sox14*$^+$/Lhx1/5$^+$ could also be ventricular zone derivatives. BrdU analysis shown here corroborates previous birth-dating that shows nucleo-olivary neurons are among the first-born of the cerebellar cell types. Co-localisation between GFP and BrdU is observed in injections administered at E10.5 and E11.5, but not E12.5. By E12.5, GFP$^+$ cells are observed across the cerebellar plate. However, it is debatable whether *Ptf1a* is expressed at this early stage. Liu *et al.* (2010) did not detect *Ptf1a* expression at E10.5 in rhombomere 1 (r1), only seeing

expression in the spinal cord at the time of the birth of *Sox14*$^{+}$ cells. They found that *Ptf1a* is first detected in r1 at E11.5 in the dorsal ventricular zone adjacent to the rhombic lip. If Ptf1a is not expressed from E10.5, it is conceivable that the nucleo-olivary neurons may be unique, being a GABAergic cell type that is not derived from the *Ptf1a* progenitor domain. On the contrary, Hoshino *et al.* (2005) claim that *Ptf1a* is expressed in the ventricular region of the cerebellar primordium at E10.5, but data was not shown. It has also been shown that the *Ptf1a* mutant lacks nuclear GABAergic cells (Hoshino et al., 2005; Pascual et al., 2007) and loss of *Ptf1a* results in misspecification of ventricular zone cell fate to produce both rhombic lip (more dorsal) and extra-cerebellar (more ventral) derivatives (Millen et al., 2014). However, staining for GABAergic markers reveal a very small number of GAD65/67 or GABA positive cells in the cerebellum of Ptf1a::Cre and *cerebelless* mutant mice (Hoshino et al., 2005; Pascual et al., 2007). Thus the loss of *Ptf1a* does not abolish all GABAergic cells. Future fate-mapping will hopefully be able to determine if *Ptf1a* expression is upstream of *Sox14* expression to confirm the lineage of the nucleo-olivary neurons.

4.3.1.1 SOX14^{+} CELLS APPEAR TO TANGENTIALLY MIGRATE ACROSS THE CEREBELLAR PRIMORDIUM AT E12.5

My finding that nucleo-olivary neurons also express *Lhx1/5* has major implications for the results found by Miyata *et al.* (2010), who identified early-born Purkinje cells at E10 based on Lhx1/5 immunoreactivity. They correctly identified glutamatergic nuclear cells that were in the subpial rhombic lip migratory stream, but until now, it had been assumed that all *Lhx1/5*$^{+}$ cells in the cerebellar primordium are Purkinje cells. They showed unexpected the leading processes in the

tangential orientation in these early-born *Lhx1/5*$^{+}$ cells, compared to cells closer to the ventricular surface, and therefore are later-born, that have radially orientated processes. From this difference in morphology found at E12.5, they concluded that Purkinje cells born at E10.5 initially migrate radially, but then migrate tangentially from the posterior periventricular region of the lateral cerebellum towards the anterior. It is probable that the cells found with this different orientation are nucleo-olivary neurons, consistent with the tangential orientation seen here in Lhx1/5^{+}/*Sox14*$^{+}$ cells. This distinction also strengthens the case for nucleo-olivary neurons coming from a different non-*Ptf1a* progenitor zone.

4.3.1.2 OTHER POSSIBLE LINEAGES FOR SOX14+ CELLS

Sox14^{+} cells in the midbrain are derived from progenitors that express *Ascl1* (Delogu et al., 2012). This is has shown to be part of an expression cascade where *Ascl1* and *Helt* (also known as *Heslike*) are expressed first from the onset of neurogenesis in uncommitted progenitors (Achim et al., 2014; Song et al., 2015). Expression of *Ascl1* and *Helt* is transient and expression fades by E14.5. This then induces the expression of *Tal1* in intermediate progenitors, but not in the most differentiated stages. The onset of *Sox14* expression correlates with cell-cycle exit in cells that have already initiated transcription of the *Gad1* gene. Perhaps a similar genetic cascade upstream of *Sox14* also exists in the cerebellum. *Ptf1a* is the best candidate as a hindbrain functional analogue of *Helt*, since both act alongside *Ascl1* to determine an inhibitory subtype (Hori et al., 2008; Sudarov et al., 2011). *Ptf1a* expression is restricted to the developing hindbrain and spinal cord (Glasgow et al., 2005), while *Helt* expression is restricted to the forebrain and midbrain (Miyoshi et

al., 2004; Nakatani et al., 2007). Both genes encode for bHLH transcription factors with similar functions in GABAergic specification(Nakatani et al., 2007).

It may be possible that other pro-neural genes first define the progenitor domain, which then becomes further redefined as the expressions start to overlap with the *Ptf1a* domain from E11.5. The pro-neural gene *Ascl1* is expressed along the ventricular zone, greatly overlapping with *Ptf1a* expression (Dastjerdi et al., 2012), but expression is found in r1 at E10.5 (Liu et al., 2010; Sudarov et al., 2011; Zordan et al., 2008). While *Ptf1a* is necessary for cerebellar GABAergic fate, *Ascl1*$^{+}$ cells that do not express *Ptf1a* become extra-cerebellar cells (Millen et al., 2014). Gain or loss of *Ascl1* function results in an increase or decrease of *Pax2*$^{+}$ and *Olig2*$^{+}$ precursor cells, respectively (Dastjerdi et al., 2012; Grimaldi et al., 2009).

Neurogenin (Ngn)1 and 2 have also been implicated in inhibitory specification (Florio et al., 2012; Kim et al., 2008; Lundell et al., 2009; Zordan et al., 2008). *Ngn2*$^{+}$ precursors give rise to Purkinje cells and GABAergic nuclear neurons, which could be nucleo-olivary neurons (Florio et al., 2012; Zordan et al., 2008). Likewise, Zordan *et al*. (2008) found that *Ngn2* and *Ascl1* expression at E10.75 is located dorsally, nearby the location that *Sox14* expression is observed at E12.5. The *Ngn2* expression is still detected at E11.5 but fades by E12.5, making it a potential cerebellar analogue of *Tal1*, which marks an intermediate progenitor domain.

Together with the literature, the findings here suggest that nucleo-olivary neurons may be derived from a *Ascl1*$^{+}$ progenitor zone that is established early on. This supports the findings of the clonal analyses that show some lineage divergence

between cortical and nuclear GABAergic neurons (Hoshino et al., 2005; Mathis and Nicolas, 2003).

In the future, it would be informative to compare *Sox14* and *Corl2*/*Skor2* expression patterns, which are also known Purkinje cell markers, to see if these are truly exclusive markers for Purkinje, and are not also expressed in nucleo-olivary neurons (Seto et al., 2014). Minaki *et al.* (2008) have shown that although *Corl2* and *Lhx1/5* expressions mostly overlap, there is a section of *Corl2*$^{-}$/*Lhx1/5*$^{+}$ cells in the "c2" domain of the cortical transitory zone (**Figure 4–10**).

Furthermore, this residual population appear to be *Pax2*$^{+}$, suggesting that *Pax2* expression is not only found in cerebellar interneuronal populations. I tried to stain against Pax2 but the antibody needed more optimisation and it was not possible to visualise both the GFP and Pax2 expression patterns reliably. A future investigation could look at *Pax2*$^{+}$ population, which is known to define a rostral portion of the ventricular zone that produces nuclear interneurons (Seto et al., 2014). Together with glutamatergic nuclear cell markers *Lhx9* and *Tbr1*, this could show more fully how the different nuclear populations come together during nucleogenesis.

Lmx1a is another marker that would be interesting to compare with *Sox14* expression. There are *Tbr1*$^{+}$/*Lmx1a*$^{+}$ cells being born from the rhombic lip which is often labelled c1, but there is another *Lmx1a* population more ventrally (c3) seen at E12.5 near where *Sox14*$^{+}$ cells are found (**Figure 4–10**) (Chizhikov et al., 2006). Chizhikov *et al.* also found that, at E17.5, *Lmx1a*$^{+}$ cells are found in the cerebellar nuclei. Some papers say these become extracerebellar cells that originate from outside the cerebellar primordium (Millen et al., 2014; Yeung et al., 2016), but

others suggest that these could become cerebellar nuclear neurons (Marzban et al., 2015; Zordan et al., 2008).

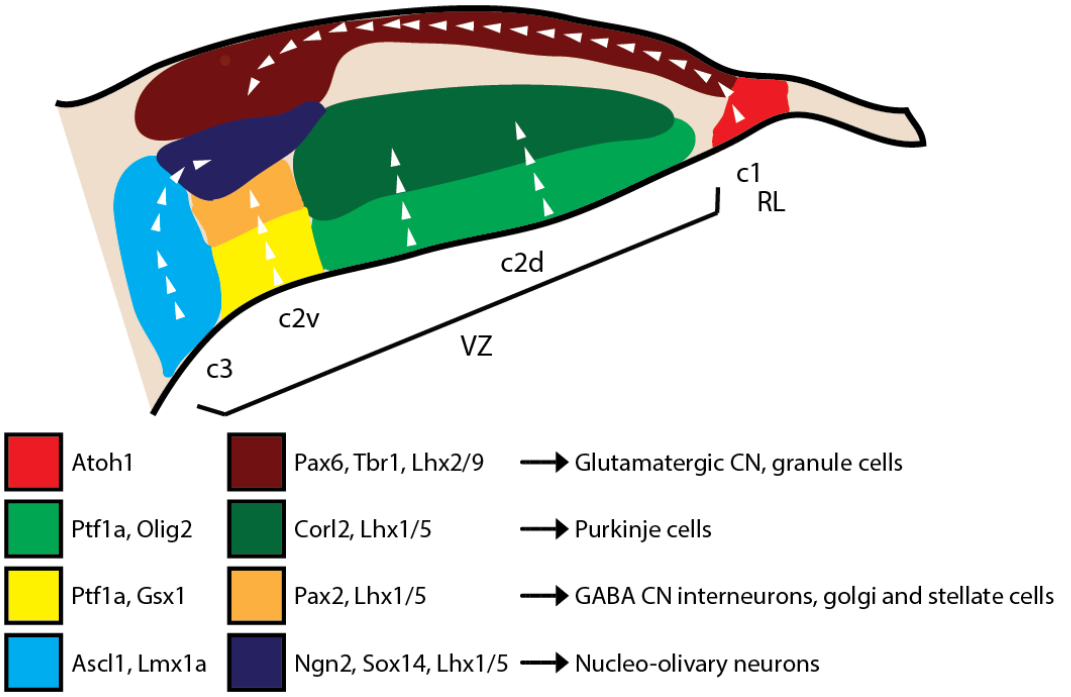

Figure 4–10 Prospective progenitor domains of the cerebellar primordium

This schematic is a modified version of that suggested by Hoshino et al. (2012). The c1 domain corresponds to the rhombic lip, which is characterised by Atoh1 expression. This progenitor zone produces all types of glutamatergic neurons in the cerebellum, the most early born being the glutamatergic nuclear projection neurons, which express Pax6, Tbr1 and Lhx9 sequentially as they migrate across the subpial rhombic lip migratory stream to reach the nuclear transitory zone. The c2 domain is the Ptf1a-expressing ventricular zone that generates most, if not all, types of GABAergic cerebellar neurons. At E12.5, the c2 domain is subdivided dorsally and ventrally into c2d and c2v, based on En1/2 staining, as well as Gsx1 and Olig2 expression patterns. The whole c2 domain produces Lhx1/5 expressing cells, but this population can then be subdivided corresponding to c2d and c2v, which produce corl2-expressing Purkinje cells, and Pax2-expressing GABAergic interneurons, respectively. The c3 domain is Lmx1a-expressing, and could potentially derive nucleo-olivary neurons, which are also Lhx1/5-positive. The resultant intermediate progenitors sit ventral to the NTZ. The c4 domain (not shown) is Lhx1/5-positive, but it is not known what cell types are produced from this area and whether this is still cerebellar.

The distribution of *Sox14*$^{+}$ cells at E15.5 is similar to the pattern of *Irx3* expression shown by Yeung *et al.* (2016). This expression was found to persist even in the

Sey/Sey cerebellum, which lacks *Pax6* expression, and therefore also lacks *Tbr1*$^{+}$ cells. This shows that *Irx3* expression does not define glutamatergic nuclear cells, but rather GABAergic nuclear cells, contrary to the findings of Morales and Hatten (2006), who postulated that *Irx3*, *Meis2* and *Lhx2/9* expression defined one single population of postmitotic nuclear progenitors. It is likely that *Meis2*, *Lhx2/9* and *Tbr1* expression denotes glutamatergic projection nuclear cells, while *Sox14*, *Irx3* and *Lmx1a* expression represents GABAergic nucleo-olivary cells.

4.3.2 THE *SOX14* GENE IS NECESSARY FOR CEREBELLAR NUCLEOGENESIS

It has previously been shown in *Sox14*$^{Gfp/Gfp}$ knock-out animals, where replacement of the *Sox14* gene by GFP cDNA results in *Sox14* deficiency, that GFP^{+} cells of the diencephalon and midbrain display migration errors since they fail to reach the ventral and dorsal lateral geniculate nucleus (Delogu et al., 2012; Jager et al., 2016). In *Sox14*$^{Gfp/Gfp}$ mice, nucleo-olivary cells also fail to reach their normal destination by adulthood. At P0, the GFP^{+} cells in knock-out mouse cerebellum appear in clusters, suggesting recognition of extrinsic guidance cues, but are unable to integrate into nuclei and instead form there are large voids where GFP^{+} cells are usually found. This raises the possibility that cells that initially lie outside the glutamatergic NTZ remain excluded as a result of the loss of *Sox14* function.

By adulthood, the nucleo-olivary neurons of the knock-out mouse appear to be largely missing or non-functional as shown by the lack of *Gad1* immunoreactivity compared to heterozygotes. The mechanisms for neuronal survival and pruning are

currently not known, but it seems that the migratory errors seen during development may ultimately lead to extinction of the cells.

Alternatively, the apparent lack of nucleo-olivary neurons in the adult knock-out mice may be due to secondary effects downstream of the loss or misspecification of *Sox14*$^{+}$ cells elsewhere in the brain. It should be noted that GFP^{+} cells within the ventral medulla also display migratory errors in the knock-out (**Figure 4–8A iv**). The tightly clustered GFP^{+} cells become broadly dispersed across the ventral portion of the medulla. Although these cells are proximal to the inferior olive, they are unidentified as a cell type and it is not known what function they perform. The large scale remodeling of *Sox14*$^{+}$ neurons in the caudal hindbrain, close to the inferior olive, may affect network function within the cerebello-olivary loop and hence cells in the cerebellar nuclei. It is conceivable that if they are involved in olivo-cerebellar function, their inability to reach the correct destination may in turn affect the survival of other neurons that depend on synaptic feedback. In either case, cells lacking *Sox14* gene function may not able to make the correct synaptic connections that are needed for survival into adulthood.

The mechanisms underlying integration of GABAergic and glutamatergic neurons during nucleogenesis are completely unknown. From observing the *Sox14*$^{+}$ cell distribution during morphogenesis it seems that passive translocation is unlikely to explain the timing of GABAergic integration. By E13.5 and E15.5, *Sox14*$^{+}$ cells are spread throughout the cortical transitory zone suggesting an active migration away from the NTZ boundary. It is known that Bergmann glia, which are specialised radial glia, arise from the VZ and send apical processes to the subpial surface with

their soma beside the Purkinje cells (Bellamy, 2006; Yamada and Watanabe, 2002). The Bergmann fibres traverse across the cerebellar primordium towards the external germinal zone by E15 (Del Cerro and Swarz, 1976; Yuasa, 1996), and Purkinje cells as well as other GABAergic precursor cells migrate along these fibres to populate the cortical transitory zone (Hatten and Heintz, 1995). It would be interesting to investigate whether *Sox14*$^{+}$ nucleo-olivary neurons use the radial glial fibres to traverse away from the pial surface towards a deeper cerebellar position as the nucleus forms.

I also observed the structure of the nuclei in early postnatal stages using the *Sox14*$^{Gfp/+}$ mouse. **Figure 4–6** shows that at P0, prior to cortical expansion and foliation, the boundary between the lateral and interposed nuclei is already somewhat distinct. This suggests that cortical morphogenesis is not required for the formation of the nuclear mass. Of course, it is possible that both environmental and genetic cues are needed in combination as the two are not mutually exclusive.

5 FUNCTION

5.1 INTRODUCTION

Given that *Sox14* can be used to identify and mark nucleo-olivary neurons, I used a conditional expression model to study function relating to cerebello-olivary circuitry. Loss of function experiments were carried out using AAVs that not only express a fluorescent reporter, but express proteins that effectively ablate the cells.

Previously, lesion experiments, electrical stimulation, and chemical modulation of signalling have revealed functions of the cerebellum and inferior olive (Bradley et al., 1991; Cerminara and Apps, 2011; Horn et al., 2010; Llinás et al., 1975; McCormick and Thompson, 1984; O'hearn and Molliver, 1993; Pijpers et al., 2008; Strick et al., 2009; Willson et al., 2007). Until now, specific targeting of the nucleo-olivary neurons was achieved either by retrograde injections into the inferior olive (Najac and Raman, 2015), or targeting the cerebellar nuclei with AAVs then selecting fibres that reach the inferior olive (Lefler et al., 2014). The latter of these was used to investigate the electrophysiological function of the nucleo-olivary neurons in slice, but the method cannot be used to look at *in vivo* function. The researchers found no significant difference in results when targeting only Cre-expressing cells of the *Gad2-Cre* mouse compared to targeting all cells of the cerebellar nuclei in the wild-type mouse, since the channelrhodopsin produced by the AAV was activated not in the cerebellar nuclei, but at the inferior olive.

5.1.1 FUNCTIONS OF CEREBELLO-OLIVARY CIRCUITRY

The nucleo-olivary neurons are just one component of the loop that connects the cerebellum with the inferior olive. Its hypothesised role is to provide feedback from the cerebellum to modulate the signals that are sent back via the climbing fibres. Since the climbing fibres have such a strong influence on the firing pattern of the cerebellar cortex, this feedback could refine such an influence and therefore be an error-correction circuit for motor control. The inferior olivary neurons are electrically coupled through gap junctions to enable synchronous firing, aided by the spontaneous generation of subthreshold oscillations (Blenkinsop and Lang, 2006; Lampl and Yarom, 1997; Llinás, 2011). Studies that have specifically manipulated nucleo-olivary neural firing using electrophysiology in slice have shown that the feedback is capable of decreasing firing rates and reducing spike synchrony in the olivary neurons (Lefler et al., 2014). Furthermore, activation of GABA nucleo-olivary cells inhibit their inferior olive targets by releasing GABA asynchronously (Best and Regehr, 2009).

Two theories have been put forward for nucleo-olivary feedback: the first is that these cells are crucial for determining the clustering of group synchrony in the olive, since inhibition from the cells onto the gap junctions can shunt coupling and reduce spike synchrony of the associated olivary cells (Best and Regehr, 2009; Leznik et al., 2002; Llinas, 2014; Llinás, 2011); the second is a dynamic role of this feedback, which is weak at the beginning of motor learning, and as the cerebellar cortex undergoes synaptic modulation, the feedback strengthens so that once the motion is learnt, the climbing fibre signals are weakened by decoupling (**Figure 5–1**) (Schweighofer et al., 2013).

Synchrony of climbing fibre firing underlies both of these theories, and nucleo-olivary activity works only to weaken coupling and therefore spike synchrony. Indeed, Lang *et al.* (1996) showed the potential role of the nucleo-olivary neurons physiologically by manipulating the GABA transmission to the inferior olive. They injected picrotoxin (PIX), a GABA-A antagonist, into the inferior olive, blocking the GABA receptors at the gap junctions. The result was increased firing rate, synchrony and rhythmicity at the cerebellar cortex as measured by complex spiking in Purkinje cells using a multielectrode. Chemical lesions of the lateral cerebellar nucleus were performed using NMDA and kainic acid injections and these resulted in the similar effects, showing that these changes are due to the blocking of nucleo-olivary projections.

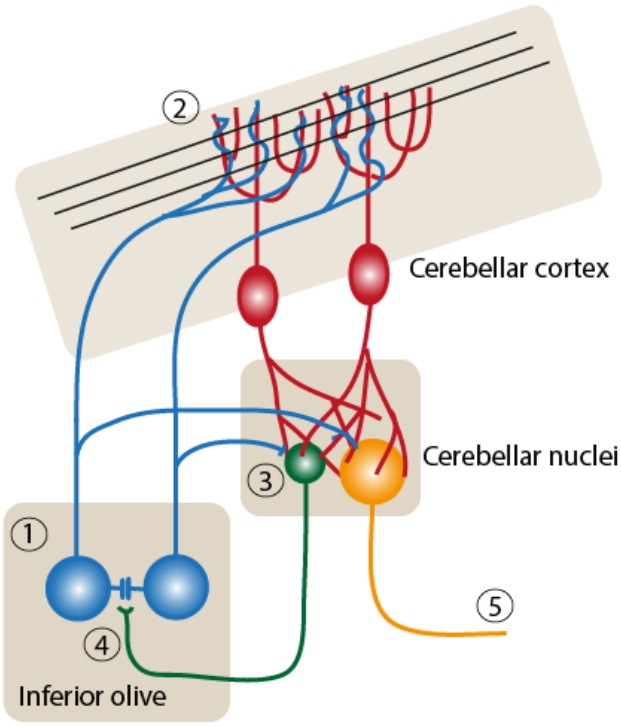

1) Coupling between olivary neurons results in synchronous sub-threshold oscillations and therefore concurrent climbing fibre signalling to the cerebellum.
2) Synaptic changes as the climbing fibre signals are compared to mossy fibre signals.
3) Purkinje cells disinhibit the nucleo-olivary neurons in the cerebellar nuclei
4) The nucleo-olivary feedback results in decoupling of olivary neurons and thus less spike synchrony in the climbing fibres.
5) Glutamatergic projection neurons send signals to the motor cortex and other areas to execute for motor commands.

Figure 5–1 Dynamics of electrotonic coupling in the inferior olive and its role within the olivocerebellar loop.

Additionally, mutants lacking gap junction protein Cx36 as well as injections of blockers into the inferior olive result in reduced synchrony and a corresponding deficiency in motor learning behaviour (Lefler et al., 2014; Van Der Giessen et al., 2008). Here, the specific ablation of nucleo-olivary neurons creates the opposite condition: reduced feedback that should result in increased coupling. Is the deletion of inhibitory feedback also detrimental to motor learning? If the circuitry is fully reliant on all the individual components, it would be expected that the lack of nucleo-olivary input into the olive would result in over-rigid synchronous firing. Perhaps the olivary clustering would be affected, or it would be impossible to break synchrony after a motor command has been learnt?

5.1.2 NUCLEO-OLIVARY ROLE IN MOTOR LEARNING?

It is thought that the nucleo-olivary neurons work to modulate the amount of electrotonic coupling that exists between olivary neurons. The coupling is facilitated by gap junctions between cells that occur at glomeruli. The inhibitory feedback from nucleo-olivary neurons is thought to act as a shunt, essentially short-circuiting the current passing through the gap junction and thus reduce the level of coupling (Llinas et al., 1974).

It is known that nucleo-olivary neurons show physiological differences compared to other nuclear neurons. Particularly, they are sensitive to small Purkinje cell inputs and do not exhibit rebound firing properties (Najac and Raman, 2015). While other nuclear cells have prolonged rebound periods of increased firing rate in response to inhibition (Hoebeek et al., 2010; Zheng and Raman, 2009), the nucleo-olivary neurons resume baseline firing rates quickly and so faithfully integrate and process

instantaneous Purkinje cell signals. This property adds to theories about their instant feedback role in motor learning (Medina et al., 2002; Rasmussen and Hesslow, 2014).

Bengtsson *et al.* (2007) found that stimulation of the nucleo-olivary pathway can block an impending unconditioned stimulus signal and cause extinction of a trained conditioned response. It has also been shown that once a conditioned response has been acquired the nucleo-olivary neurons are responsible for feedback that suppresses the inferior olive so that the climbing fibre signal weakens (Hesslow and Ivarsson, 1996; Rasmussen et al., 2008; Sears and Steinmetz, 1991). Thus the nucleo-olivary circuitry is crucial for associating the conditioned and unconditioned stimuli and maintaining conditioned responses.

5.1.3 NUCLEO-OLIVARY ROLE IN MOTOR TIMING?

Ito's theory of the function of the olivo-cerebellar system is that it provides both sensory feedforward control and motor feedback control by conveying error signals and inducing plasticity by LTD and LTP based on how the signals from the mossy fibres and climbing fibres relate to each other. However, Llinas (1974; 1991) has suggested that while error detection is very important as an aspect of cerebellar function, it may not be the only, or primary cerebellar function. He argues that the rhythmicity (around 10Hz) guided by oscillatory activity in the olive is crucial to cerebellar function, particularly for movements that are non-continuous. These subthreshold oscillations have a phase, which determines the timing of action potentials, since depolarization is more likely to occur when the membrane potential is closer to the threshold. When the olivary cells are also coupled to one another, this

results in spike synchrony that is thought to be important for gating and synchronising cortical motor output (Lang et al., 1992).

The phase of the oscillations has been found to be reset following input to the olive, either from intracellular or extracellular stimulation (Leznik and Llinás, 2005; Llinás et al., 2002). However, these have all been done on rodent brainstem slices, with artificial stimulation. It is not known whether such re-setting of oscillations occurs organically in vivo. If phase shifts do occur, we can imagine that the nucleo-olivary neurons play an important role in generating the shifts. Lesions to the cerebellar nucleus also cause the 10Hz rhythm to disappear, and this is rescued by PIX or harmaline injections (Lang et al., 1996). This shows that cerebellar feedback to the inferior olive is crucial for olivary rhythmicity.

Thus, rather than looking at individual error signals that result in single synaptic changes, Llinas' theory is one of population clustering, where large populations of Purkinje cells cause inhibition of the nucleo-olivary neurons, which in turn disinhibit the olivary neurons to increase electrical coupling at the olivary gap junctions. The coupling mediates synchronous activation of olivary neurons, and thus causes climbing fibre stimulation to arrive back the cerebellar cortex synchronously. The nucleo-olivary connection is thought to enable dynamic shifts in olivary coupling. If nucleo-olivary input to the olive is able to modulate the grouping of coupled cells, then differentially recruited cohorts are essential for different motor commands. Under this theory, the inferior olive is a motor time keeper while the nucleo-olivary input is a decoupling pattern generator.

5.1.4 TWO SIDES OF THE SAME COIN?

It has been shown that mice which lack the connexin-36 protein at gap junctions, which is essential for electrotonic coupling, show deficits in motor learning tasks like the conditioned eyeblink response, while not showing any general motor deficits (Kistler et al., 2002; Van Der Giessen et al., 2008). In humans, administration of the drug mefloquine also results in reduced coupling at the inferior olive. Patients show no deficits in general motor function but appear to have impairments in motor learning ability (Van Essen et al., 2010). Since the olivary neurons of the *Cx36*$^{-/-}$ mutants also have altered subthreshold oscillations, spike latency and spike synchrony, these motor learning deficits are likely linked to the role of the cerebello-olivary loop in motor timing. The mutants showed more variable latencies of olivary spike activity in response to unconditioned stimuli than in control animals. Thus motor learning and motor timing appear to be two perspectives of the common goal: accurate and anticipated movement.

5.1.5 ABLATION OF *SOX14*$^{+}$ CELLS

The experiment described in this chapter investigates the functional significance of the nucleo-olivary neurons. There have been cerebellar nuclear lesions (Clark et al., 1984; Mccormick et al., 1981; Yeo et al., 1985), simulations based on anatomy (Herreros and Verschure, 2013) and slice electrophysiology (Lefler et al., 2014; Najac and Raman, 2015), but the present findings are the first to specifically ablate nucleo-olivary neurons while preserving adjacent cells to observe *in vivo* behavioural changes.

Using the same technique as the previous AAV viral tracing experiments, I wanted to investigate the loss of function phenotype of the cerebellar nuclear *Sox14*$^{+}$ cells. I produced the AAV-flex-taCasp3-TEVp, which encodes a pro-caspase 3 protein with a specific cleavage site that is cleaved by the tobacco etch virus protease (TEVp), which is also encoded to result in an activated caspase 3 that induces apoptosis in *Cre*-expressing cells (Gray et al., 2010; Yang et al., 2013). The advantage of this system is specificity in ablation that preserves the surrounding cells, unlike past methods of laser ablation or mechanical disruption. Similar to these methods is the fact that this ablation is non-reversible. This avoids any need to make adjustments to cell firing, unlike optogenetic or pharmacogenetic DREADD technologies.

To confirm the efficacy of the AAV-flex-taCasp3-TEVp, I injected a small sample of mice into the lateral nuclei at P14 (♀ unilateral AAV-Casp3 n=4; ♂ bilateral AAV-Casp3: n=2; ♂ bilateral Sham: n=1). The hypothesis was that the number of *Sox14*$^{+}$ cells, approximated by *Gad1 in situ* hybridization labelling, would decrease significantly in comparison to similarly sham injected littermates. In the trial, only one mouse displayed a significant decrease in number of *Gad1*$^{+}$ cells on one side, while another mouse had a drop in *Gad1*$^{+}$ cells not in the cerebellar nuclei, but in the medial vestibular nucleus (**Appendix D**). Thus it is possible to effectively ablate the *Sox14*$^{+}$ cells using AAVs.

As there is no way to identify the injection site, given the virus produces no expression marker, I decided to produce another AAV that causes ablation, the AAV-mCherry-flex-dtA. The AAV-mCherry-flex-dtA encodes a subunit of the

diphtheria toxin in the Cre-expressing cells while also promoting the non-Cre-dependent production of a mCherry red fluorescent protein in all cells infected by the virus, thus allowing me to observe the site of injection postmortem.

5.1.6 BEHAVIOURAL ASSESSMENT OF CEREBELLAR FUNCTION

I carried out preliminary tests in order to identify suitable behavioural assays to measure motor learning and motor coordination. Of the options available to me, I chose to test the mice using Rotarod and the Erasmus ladder.

5.1.6.1 ROTAROD

The Rotarod is the most commonly used apparatus for looking at motor behaviours. It consists of a rotating drum on which the mouse is placed. When the trial begins, the rotation speed increases so the task of remaining on the drum becomes increasingly difficult. The task measures the latency to fall on sequential trials, three each day, one hour apart, for three days. A sham animal is expected to display prolonged latency to fall each subsequent trial as it learns new motor skills in order to stay on the accelerating rod to the trial end at 300s. However, ablated mice on the pilot study revealed some deficit in prolonging latency to fall. In severely ataxic mice, the animals struggle to remain on the Rotarod, demonstrating impaired motor skills rather than a lack of motor learning (Long et al., 2014). Thus the Rotarod can also act as a measure of motor coordination. I hypothesised that mice with effective cerebellar nucleo-olivary cell ablation would have motor learning phenotypes and so while the sham mice would learn to remain in the Rotarod longer after each trial, the ablation would cause the mice to stay at a baseline level of latency, unable to learn to improve.

I confirmed in an independent Rotarod trial that the heterozygous mice behaved in the same way as their wildtype counterparts without the changes caused by AAVs. The heterozygous *Sox14*$^{Cre/+}$ is behaviourally comparable to a wildtype animal and can therefore be a useful tool to study *Sox14*$^{+}$ neurons during their normal development (Delogu et al., 2012).

5.1.6.2 ERASMUS LADDER

I was also given the opportunity to trial the Erasmus ladder, a horizontal ladder with pressure sensors on two levels of rungs on both left and right sides that can assess how a mouse travels from one end to the other (**Figure 5–2A,B**). The Erasmus ladder has been used in cerebellar function studies (Cupido, 2009; Schonewille et al., 2011; Van Der Giessen et al., 2008; van der Vaart et al., 2011) and it is known that the obstacle is able to evoke complex spikes in Purkinje cells of the lateral vermis(Van Der Giessen et al., 2008).

The mouse is put into a box at the end of the ladder and is required to sit in the box until a light cue notifies the mouse to leave the box. In the first few sessions, the mouse is trained to do this. If the ladder senses a weight prior to the cue, a front wind blows from the other end of the ladder to encourage the mouse back in the box and the resting period until the cue resets. Once the mouse correctly steps on the ladder on cue, a tail-wind ensures that it moves forward without retreating back to the box. The types of steps the mouse uses to traverse the ladder are categorised (**Figure 5–2C**), where short steps are consecutive rung steps, long steps skip one rung and jumps skip two or more rungs. Back steps are also counted, as well as

missteps, where the mouse places a paw onto the lower set of rungs, which is more uncomfortable for it and is considered a mistake.

The Erasmus ladder not only measures motor learning by evaluating a mouse's ability to walk correctly on a ladder, but also assesses conditioned learning by being able to introduce obstacles paired with a conditioned stimulus once the mouse has learned to walk on the ladder. The mouse undergoes four days of training, where all trials are undisturbed and the mouse simply improves its ability to traverse the ladder. On the fifth to eighth days, unexpected perturbations, in which an obstacle rung suddenly lowers, occur as the unconditioned stimulus, which may or may not be paired with a conditioned stimulus, an auditory tone. The fixed 250ms pause between the tone and the perturbation allows mice that are conditioned to anticipate the obstacle and jump over the obstacle. Thus, there are four types of trials that are given randomly after training sessions:

- Undisturbed — With no tone and perturbation.
- Unconditioned Stimulus (US)-only — With perturbation (US) only.
- Conditioned Stimulus (CS)-only — With tone cue (CS) only.
- Paired — With both tone cue (CS) followed by a perturbation (US) after 250ms.

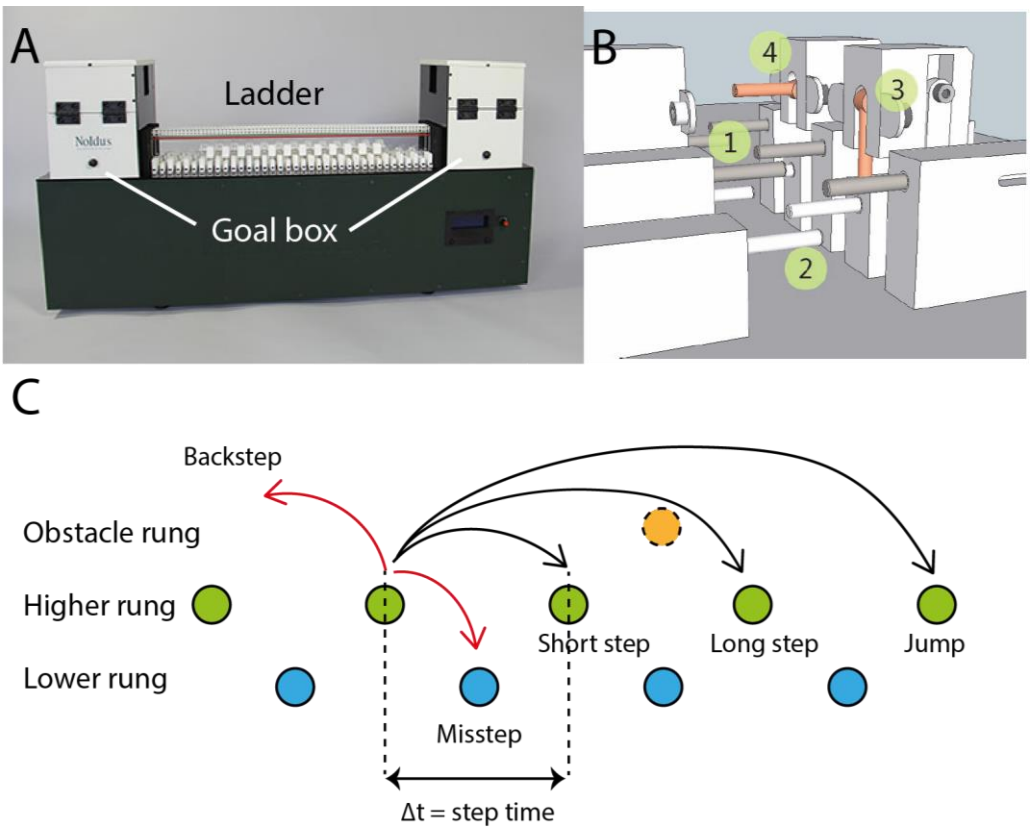

Figure 5–2 The Erasmus Ladder

A*) Overview of the Erasmus ladder with two goal boxes on either end and a series of rungs that have pressure sensors.* ***B****) The structure of the ladder consists of three sets of rungs on each side, which alternate. The middle set of rungs (1) is where the mouse walks normally. If the mouse misplaces a paw, it will land instead on the lower rung (2). A top rung acts as an obstacle on specific trials. It is hidden by default (3), but swings out when activated (4).* ***C****) The various types of steps that are measured. Step time is recorded for short and long steps as the time between activation of one rung to the next. (images provided by Noldus)*

5.1.6.3 CEREBELLAR NUCLEAR INVOLVEMENT IN LOCOMOTION

Both the Rotarod and Erasmus ladder assess locomotive coordination, balance and adaptation. While the medial cerebellar nucleus plays a large role in locomotion (Thach et al., 1992), the circuitry directly influences important vestibulospinal and reticulospinal motor pathways for walking. Damage to the medial and vestibular nuclei causes changes in posture, balance and pattern generation (Chambers and Sprague, 1955a; Chambers and Sprague, 1955b; Sprague and Chambers, 1953). Since there are no *Sox14*$^{+}$ cells in the medial nucleus, I do not expect any ataxic phenotypes.

The interposed and lateral cerebellar nuclei are thought to play different functions in locomotion that require integration of spinal and cortical inputs to influence the cortical motor areas (Dum and Strick, 2003; Middleton and Strick, 2001). Lesions to the interposed nuclei in cat have shown that they are able to walk on the ground, but have difficulty walking on a treadmill (Yu and Eidelberg, 1983) or a ladder (Chambers and Sprague, 1955a). The connection between the lateral nucleus and premotor cortical areas suggest a role in motor planning and voluntary control (Morton and Bastian, 2004). While damage to the lateral nucleus has a minimal impact on locomotion, it has been shown that lateral nuclear cells of decerebrate cats are activated by perturbations in locomotion (Schwartz et al., 1987). Thus, as the mouse responds to perturbations on the Erasmus ladder, there will be recruitment of the lateral cerebellar nucleus to modulate cell firing in order to adapt. The specific contribution of the nucleo-olivary neurons in the signal integration for these tasks is not known. Ablation of the nucleo-olivary neurons in both the interposed and lateral nuclei may reveal the importance of the cerebello-olivary feedback in locomotive adaptation.

5.1.7 AIMS OF THE CHAPTER

The aim of this chapter was to specifically ablate *Sox14* expressing nucleo-olivary neurons and to investigate the effect of ablation on motor performance using the Rotarod and Erasmus ladder apparatus. In order to ensure that injection of the AAVs were correctly targeted, I also performed post-mortem evaluations of injection targets.

5.2 RESULTS

5.2.1 ASSESSMENT OF THE INJECTION SITES

I performed a trial injection using AAV-mCherry-flex-dtA to confirm the efficacy of the virus and to test methods with which I can assess the extent of ablation. **Figure 5–3** shows the injection of the AAV-mCherry-flex-dtA into the wildtype mouse (**left column**) and two *Sox14*$^{Cre/+}$ mice (**middle and right columns**). The top row shows *Gad1* labelling as a measure of *Sox14*$^{+}$ cells, which make up the majority of GABAergic cells in the cerebellum. There are far more *Gad1* labelled cells in the wildtype compared to the heterozygous mice, particularly in the lateral nucleus. The site of the injection is visualised by looking at mCherry fluorescence, shown on the second row. However, it is not a reliable way to assess true ablation as it is not quantifiable. The bottom row looks at fluorescence of mCherry in the inferior olive. Since the nucleo-olivary projections can be tracked here, mCherry fluorescence is observed in the inferior olive of the wild-type mouse, in which the *Cre*$^{+}$ cells are targeted but not ablated. In the *Sox14*$^{Cre/+}$ mice, this fluorescence is no longer visible since any *Cre*$^{+}$ nucleo-olivary cell would also express the diphtheria toxin subunit and thus become ablated.

Sox14$^{Cre/+}$ heterozygous males were mated with wild-type females. The litter was genotyped and only males were selected for the functional experiment to control for possible sexual dimorphic behaviours. All of the brains were injected with *Cre*-dependent, apoptosis inducing AAV-mCherry-flex-dtA (*Sox14*$^{Cre/+}$: n= 16; *Sox14*$^{+/+}$: n= 12), or control marker AAV-DIO-tdTom (*Sox14*$^{Cre/+}$: n= 4; *Sox14*$^{+/+}$: n= 8).

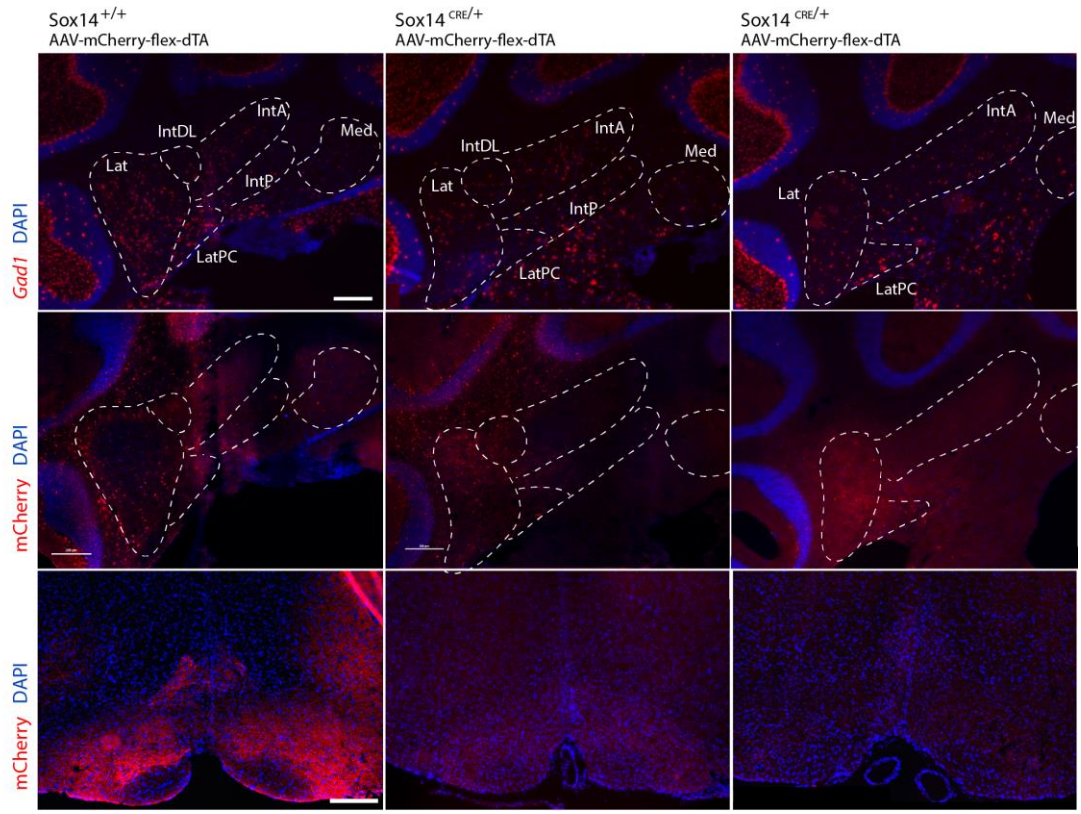

Figure 5–3 Trial injections of AAV-mCherry-flex-dtA into Sox14$^{Cre/+}$ and controls demonstrate specific ablation can be achieved.

The left column shows injection into the wild-type mouse while the central and right columns show two instances of injections into Sox14$^{Cre/+}$ mice. The top row shows Gad1 labelling as a measure of Sox14^{+} cells, while mCherry fluorescence on the second row indicates the region targeted by the injection. The bottom row looks at fluorescence of mCherry in the inferior olive, which is only present in the wild-type mouse, in which nucleo-olivary cells are targeted but not ablated. In the Sox14$^{Cre/+}$ mice, this fluorescence is no longer visible since any Cre-expressing nucleo-olivary cell would also express the diphtheria toxin subunit and thus become ablated. Scale: 200 µm

Figure 5–4 demonstrates the two methods by which I assessed the success of each individual injection in the post-mortem animals following behavioural tests. The simplest way to evaluate the injections is to look at the distribution fluorescence label. AAV-mCherry-flex-dtA induces mCherry fluorescence in all cells infected by the virus (**Figure 5–4A& B**), while *Gad1* labelling by in situ hybridization shows the remaining number of GABAergic cells in the nuclei (**Figure 5–4C&D**). By mapping the regions in which mCherry positive cells can be seen, the injection site can be charted. This was only possible for the sham controls in which I injected

AAV-mCherry-flex-dtA into *Sox14*$^{+/+}$ or *Sox14*$^{Cre/+}$ mice, and not for *Sox14*$^{+/+}$ mice injected with AAV-DIO-tdTom. For each individual mouse that was injected with AAV-mCherry-flex-dtA, but not the AAV-DIO-tdTom controls, the mCherry fluorescence was mapped onto a standard atlas. Schematic diagrams in **Figure 5–5A** and **Figure 5–6A** highlight the cerebellar nuclei sub-regions infected by the virus in each individual injected mouse, while **Figure 5–6B** summarises the areas in which the injections are seen in the experimental group.

The anterior interposed nucleus was the most frequently targeted nucleus (n=26/32), while fewer injections hit the medial (n=13/32) and posterior interposed nuclei (n=14/32). All of the injections correctly targeted the cerebellar nuclei on at least one side, and the mCherry fluorescence was consistently found in the rostral end of the nuclear mass. However, often the injections also targeted the vestibular nuclei (n=17/32), which is undesirable. In addition, the mCherry fluorescence was not as dense as anticipated, showing that infectivity was low. The serotype of the AAV-mCherry-flex-dtA was the same as those used in **Chapter 3.2.3**, and the AAV was of a higher titre, so it is unclear why so few cells expressed fluorescence. In addition, mCherry signal was often detected in the oligodendrocytes in the white matter surrounding, a relatively sparsely labeled, adjacent nuclear region. It is not known whether this is due to selectivity in infection and expression, or due to how the viral injectate moves through the tissue initially. However, **Figure 5–4B&D** clearly shows that the lack of mCherry fluorescence in the cerebellar nuclear region cannot predict the extent of cell loss as measured by *Gad1* labelling.

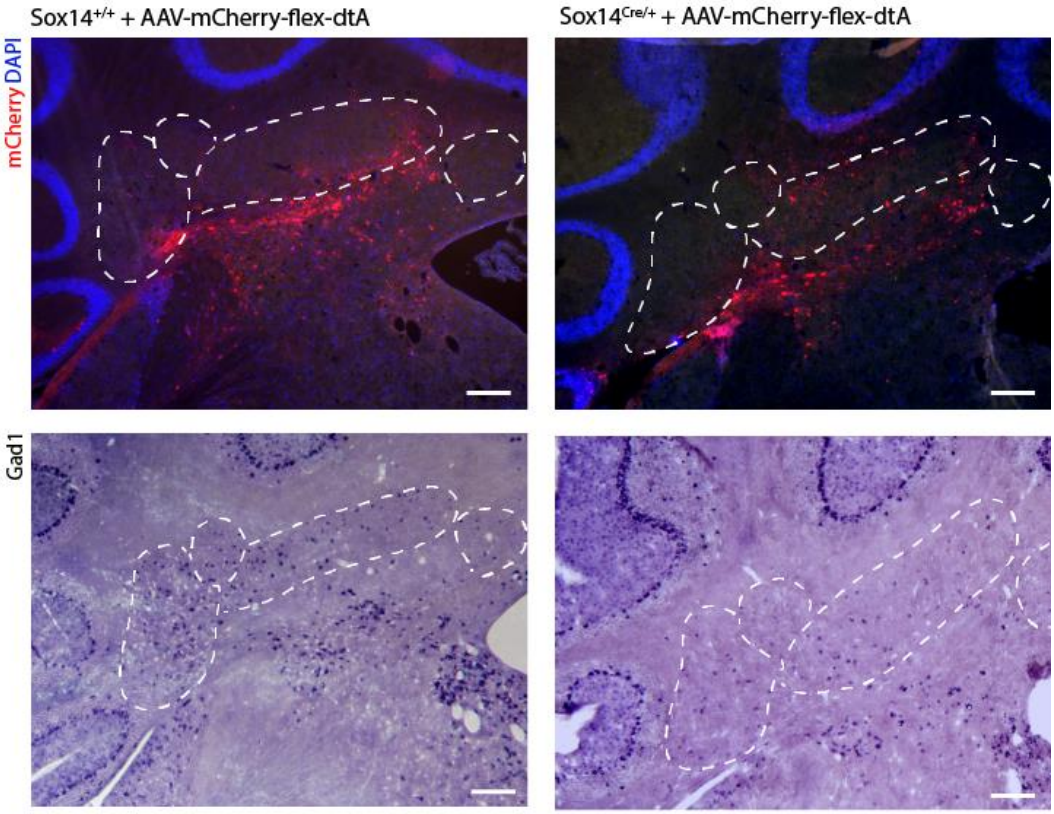

Figure 5–4 Assessing the extent of ablation

*Assessment using mCherry fluorescence (**A&B**) as a gage for injection targeting and Gad1 labelling (**C&D**) as a measure of nucleo-olivary cell loss. The left side shows injection into the wild-type mouse while the right column shows the injection in the Sox14$^{Cre/+}$ mouse. In both mice, the mCherry fluorescence signifies viral infection within the cerebellar nuclei, while the Gad1 labelling of the sequential sections reveals nuclear cell loss in the Sox14$^{Cre/+}$ mouse. Scale: 200 µm*

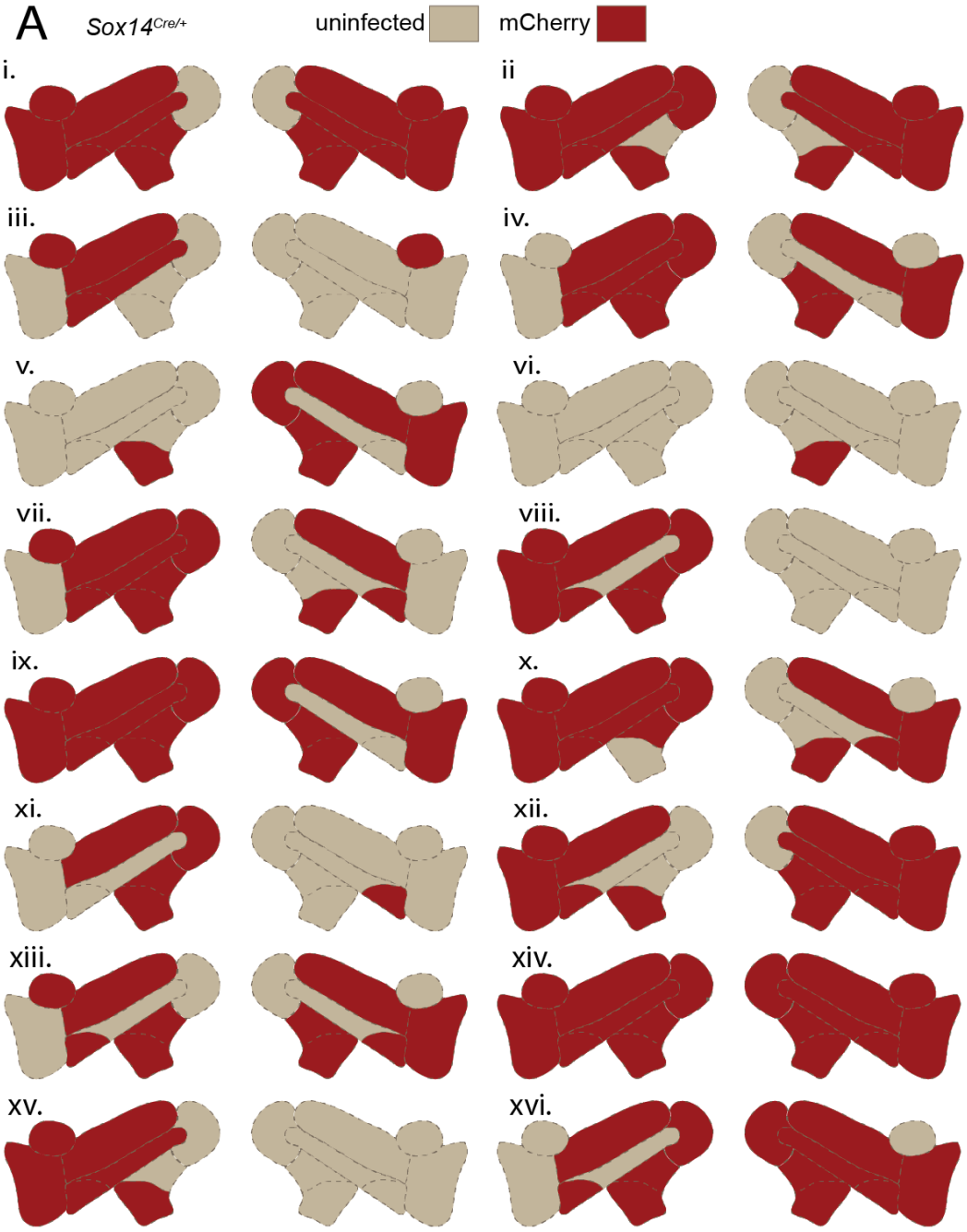

Figure 5–5 Extent of injection sites assessed using mCherry fluorescence

mCherry fluorescence across the experimental mice was assessed to gage injection targeting, thereby informing the sub-region in which the virus was most active. ***A****) All the experimental Sox14$^{Cre/+}$ animals that were injected with AAV-mCherry-flex-dtA, represented diagrammatically across 16 experimental animals* ***(i-xvi)****. The location of fluorescence was marked onto individual atlases and summarised in these schematics, where red shading denotes the sub-regions in which mCherry expression was found over the all the representative coronal sections analysed. Axonal mCherry expression was ignored.*

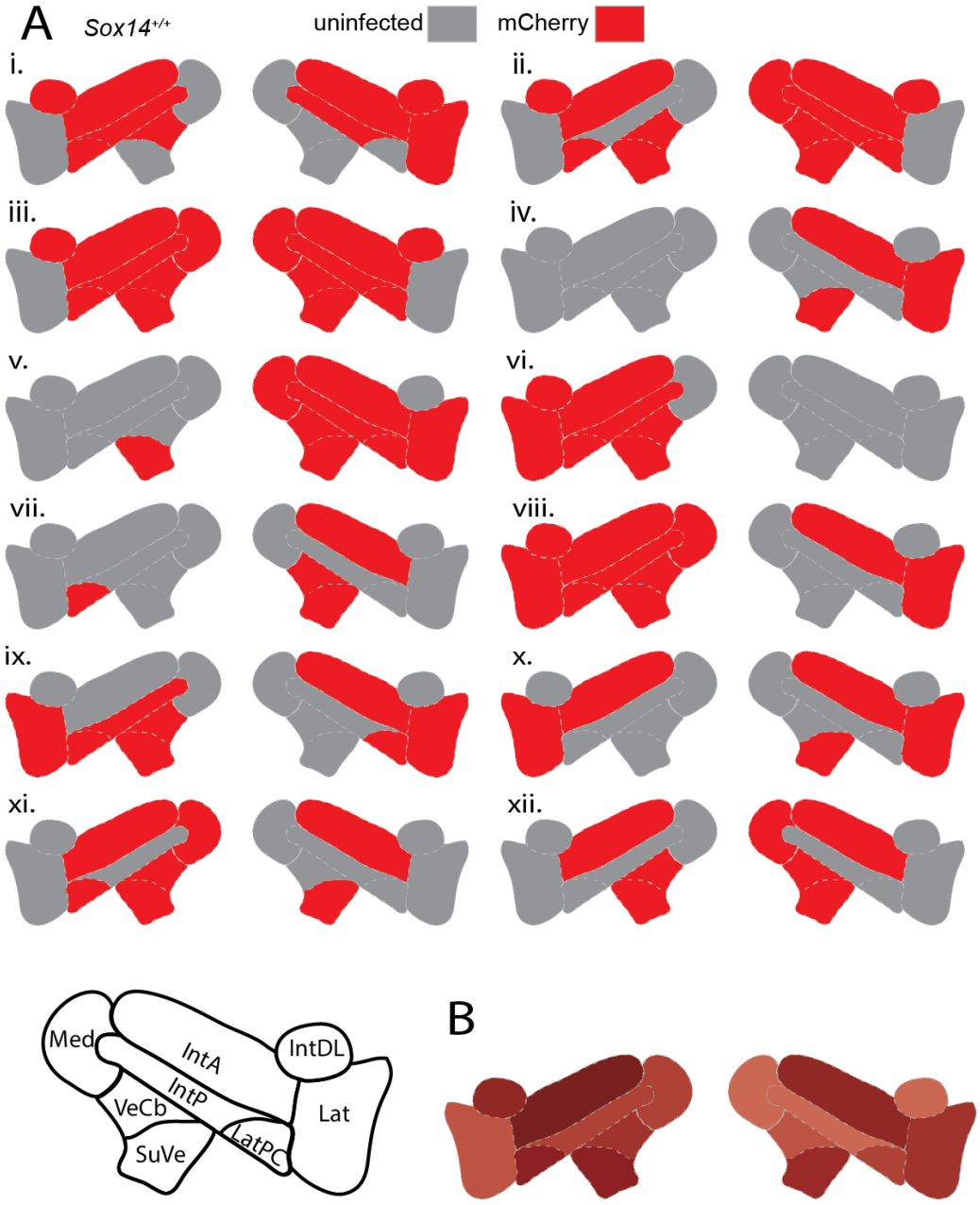

Figure 5–6 Extent of injection sites assessed using mCherry fluorescence

A*) All the wild-type littermates that were injected with AAV-mCherry-flex-dtA as one of the sham groups, represented diagrammatically across 12 animals* ***(i-xii****). **B**) A summary of the grouped injections in the experimental animals listed in (**Figure 5–5A**), where the darkness of shades represents the frequency of targeting each area. The anterior interposed nuclei on both sides were frequently infected, as were the two vestibular nuclei that lie beneath the interposed nuclei in central regions.*

For the majority of animals, cell loss was quantified by counting the number of *Gad1*$^{+}$ cells labelled by *in situ* hybridisation (**Figure 5–4C&D**). As seen in **Chapter 2.2.4**, around 80% of *Gad1*$^{+}$ cells in the cerebellar nuclei are *Sox14*$^{+}$ cells. Regions of interest were defined for different sub-nuclei (**Appendix B**) and a bespoke macro on ImageJ software was written to automatically count the number of high intensity cellular profiles, or spots, within the drawn regions of interest (**Appendix C**). The images were manually checked for errors and if necessary, the threshold value for spot detection was amended for individual sets of images since there was variability in the quality of *in situ* hybridisation staining. The main source of error was from high density labelled areas where individual spots merged and could not be detected, thus resulting in an underestimate of cell count or occasionally from detection of artefacts in the image such as bubbles in the mounting medium or folds in the tissue. Random spot checking of images showed that the automated count system could reliably quantify the number of cells compared to manual counting. However, this does not take into account the variability in tissue integrity, riboprobe labelling and imaging. I averaged the number of *Gad1* cells seen in each region within 3 control animals, then found the percentage change in cell number for each experimental mouse. **Figure 5–7** shows a diagrammatic representation of this estimated percentage change. The percentage changes have been binned into 5 bands, where darker cells represent higher levels of cell survival while lighter cells highlight areas of discernible ablation. From this, it is clear that many of brains had ablation, some with very significant cell loss.

While **Figure 5–7** shows absolute cell numbers as a percentage of control brains, the analysis was performed on every 8th serial 20µm thick section and thus may differ in

the size of the regions of interest for each sub-region due to the irregular form of the nuclei. As a complementary quantification of cell loss, I divided the number of cells by the area of each region of interest to calculate a relative density of cells. These values were also binned into 5 bands and are shown in **Figure 5–8** for the same mice. Though the heterogeneous distribution of cells shown in **Chapter 2.2.1** means that the density of cells can vary across each sub-nuclei, I found that these values are useful alongside the absolute cell counts to evaluate ablation in the mice. Based on these two measurements, I selected 6 mice that had the most obvious cell loss to analyse the behavioural data: i, ii, vii, xi, xiii, xiv (*nb*: xi was not assessed on the Erasmus ladder).

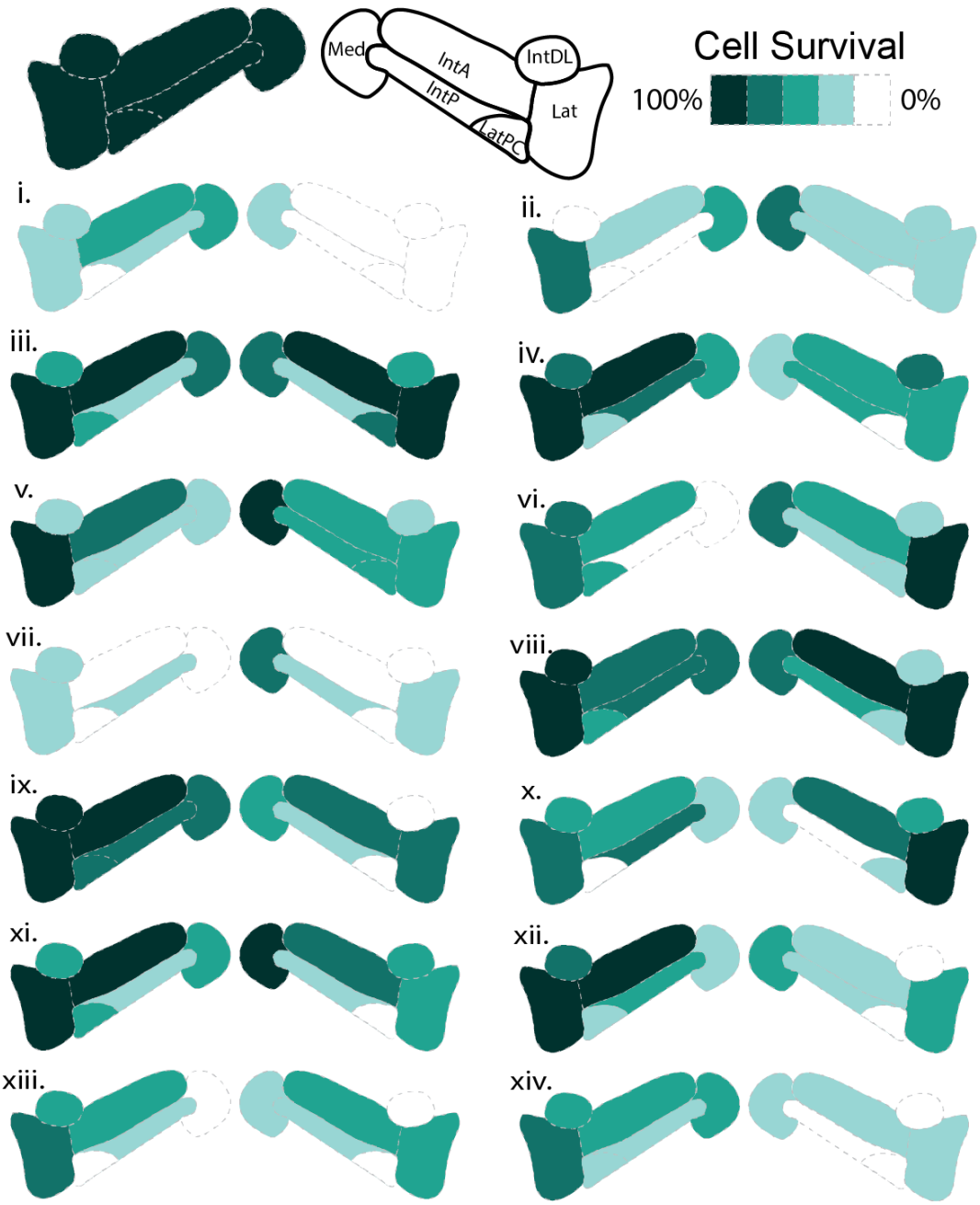

Figure 5–7 Extent of ablation assessed by relative change in Gad1 count

The number of Gad1$^+$ cells in different sub-regions of cerebellar nuclei were counted in the ablated and control mice. The extent of cell loss in each experimental mouse is presented here as a percentage change from the averaged cell numbers across the control animals. The percentage change is binned into 20% groups and coloured as shown in the key, represented diagrammatically across 14 experimental animals ***(i-xiv)****.*

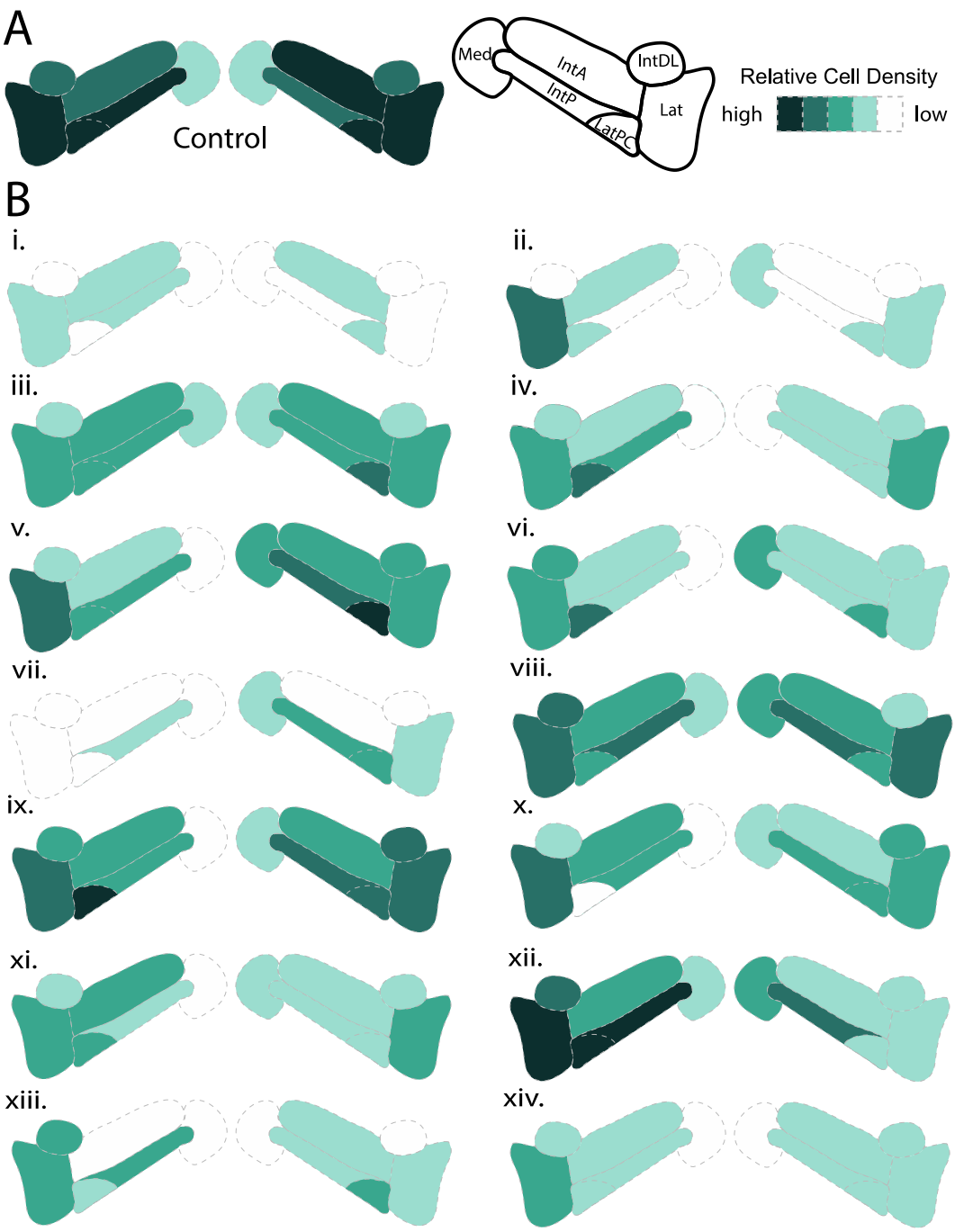

Figure 5–8 Extent of ablation assessed by density of Gad1 labelling

*The relative density of Gad1^{+} cells as calculated by divided the number of cells by the area of each region of interest throughout all the sections analysed. The relative densities are shown binned into 5 bands and group average (**A**) can be compared to the experimental mice (**B i-xvi**).*

5.2.2 ROTAROD RESULTS

All the injected animals were tested for motor phenotypes on the Rotarod. The mice were tested three times each day, with one-hour intervals, for three days. **Figure 5–9A** shows the data averaged over each day for all the sham controls together compared against all the experimental animals. As expected, sham injected animals acquire the motor skills to prolong their latency to fall. After repeated trials, many of the animals were able to stay on the accelerating rod over 290s to the trial end at 300s consistently over all 3 trials on day 3 (sham: n=16/24; experimental animals: n= 6/16). While the experimental animals show a similar acquisition curve, and start from similar levels of latency on day 1, the latency to fall in this group was significantly shorter at day 2 and at day 3 compared to sham scores on those days (p=0.0324 and p=0.0374, respectively).

Figure 5–9B shows the same data, but selecting only the 6 mice that were identified as having extensive cell loss as measured by the number of remaining *Gad1*$^{+}$ cells. Again, ablation was shown to have a significant effect on latency (two-way ANOVA: main effect of ablation, $F(1,120) = 4.479$, $P = 0.0064$). These results show that ablation of *Sox14*$^{+}$ cells reduces the ability to acquire the motor skills needed to stay on the accelerating rod.

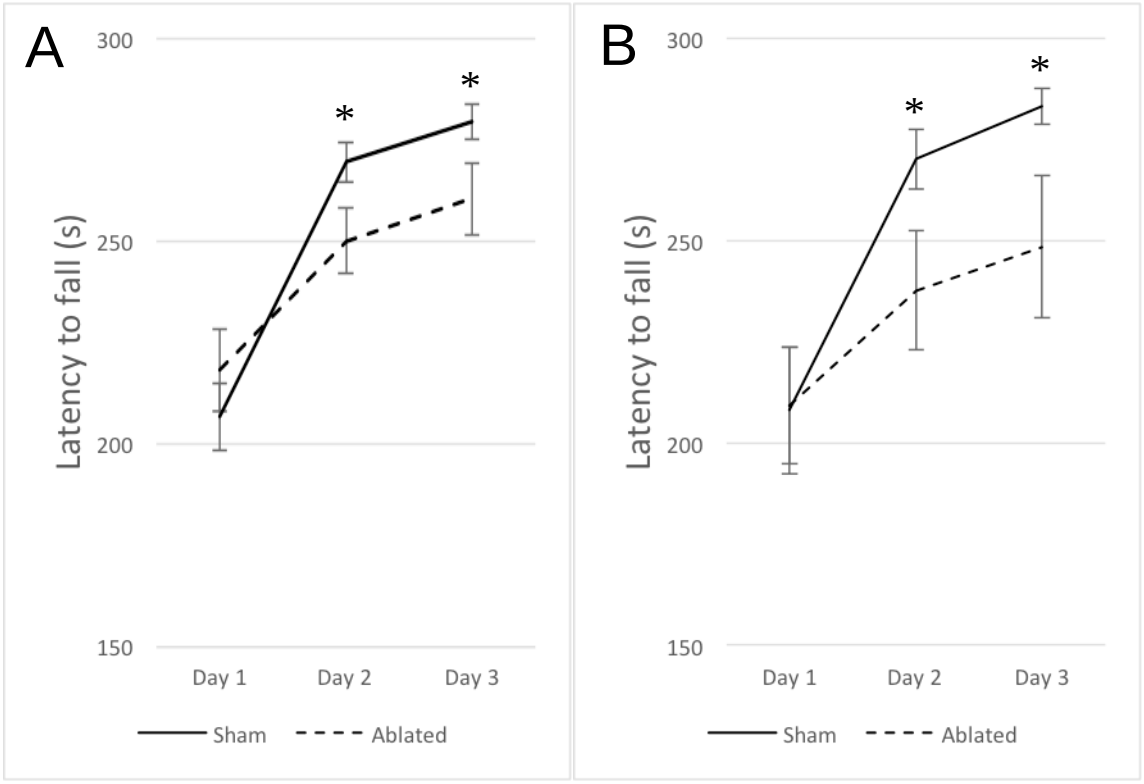

Figure 5–9 Rotarod results

A*) Averaged data for all experimental animals on the accelerating Rotarod against the sham group. The ablated group show significantly reduced latencies for both day 2 (p=0.0324) and day3 (p=0.0374).* ***B****) Selecting only for the 6 mice that showed extensive cell loss (more than 70%) loss compared to WT: i, ii, vii, xi, xiii, xiv. The selected group perform worse with significantly reduced latencies for both day 2 (p=0.041) and day3 (p=0.036). Mean ± SEM. Two-way ANOVA followed by Bonferroni post-tests: main effect of trial time, F (2,120) = 1122, P < 0.0001; main effect of ablation, F (1,120) = 4.479, P = 0.0064; ablation × trial time interaction, F (2,1.20) = 1.25, P = 0.2903).*

5.2.3 ERASMUS LADDER RESULTS

A selection of experimental mice (n=12) and wild-type littermates (n=10) were trained to walk on the Erasmus ladder. Each rung on the ladder is equipped with a pressure sensor, with 30 mm gaps between rungs. The ladder can perform instantaneous analysis of the sensor activation and predict the walking pattern of the mice within in the millisecond range based on the previous steps. This is crucial for the placement and timing of perturbations in later trials.

The mice were initially trained on the ladder without perturbations for 4 days. Each day, the mouse would be placed in the goal box and carry out 42 consecutive trials, resting in the goal boxes in between each trial. The experimental animals and wild-type littermates showed a similar overall step time averaged over these first 4 days, which was defined as the time needed to place the front paw from one rung to the other (sham: 339 ms ± 23.5; experimental animals: 358 ms ± 29). The step time can be considered a measure of competence in motor performance. Over the whole 8 day experiment, the step times, shown as pre-perturbation step time, of the both groups decrease as the mice become familiar to walking on the ladder (**Figure 5–10A**).

5.2.3.1 OUTCOMES OF TESTS FOR ASSOCIATIVE LEARNING

While the pre-perturbation step time and percentage of missteps in the training days give indication to the motor performance, the latter four days of the trial test associative learning. Using the pre-perturbation step time to predict the future location of the mouse (**Figure 5–10A**), the ladder is able to deliver a perturbation by lowering an obstacle rung immediately before the mouse reaches the location of the

obstacle. This acts as an unconditioned stimulus and in some trials, it is preceded by an auditory tone that acts as a conditioned stimulus.

The post-perturbation step time measures the step time directly after the conditioned stimulus as a gauge of associative learning. The averages of these values across all paired trials are shown in **Figure 5–10B**. When the animal is unprepared for the obstacle, the post-perturbation step time increases to overcome the obstacle. This is seen clearly in the increase on day 5 for both groups in paired and unconditioned stimulus only ("US-only") trials. The averaged data for all trials is shown in **Figure 5–11A&B**, which highlights the change in step time from pre-perturbation and post-perturbation on day 4 (no difference) and day 5 (increase). Comparing all experimental animals (**Figure 5–11A**, ○) and the mice selected for extensive ablation (**Figure 5–11B**, ○) to the sham group (**Figure 5–11A&B**, ●), no significant difference is detected. A decrease in post-perturbation step time over the sessions was seen for both groups in both paired, CS and US-only trials (**Figure 5–10B**) suggests that the mice are able adjust their stepping pattern to overcome the obstacle. This demonstrates associative motor learning in both control and experimental groups.

5.2.3.2 MOTOR LEARNING OVER TIME (NOT ASSOCIATIVE LEARNING)

The percentage of missteps made by the mouse is indicative of motor performance. While, as expected, the percentage of missteps would increase from post-training (day 4), to "1st perturbation" (day 5) due to the introduction of obstacle trials, it was expected that the percentage of missteps would accordingly decrease by "final

perturbation" (day 8) as the mice learn to predict the obstacle and adapt their step pattern to avoid missteps. However, the percentage of missteps in the both groups stays high at final perturbation (**Figure 5–11C-E**). There is no significant difference in the percentage of missteps between the groups, whether the experimental group was sorted by ablation targeting (**Figure 5–11C&D**) or extent of ablation (**Figure 5–11E**). **Figure 5–11C** compares the sham (●) with only the experimental mice that had injections which included the lateral nucleus either unilaterally (◐) or bilaterally (○), while **Figure 5–11D** shows experimental mice selected for unilateral or bilateral targeting of the anterior interposed, since these two cerebellar nuclei are most likely to encode circuits for locomotive error correction. **Figure 5–11E** shows experimental mice selecting the 5 mice that were identified as having extensive cell loss.

The experimental group performed less well on initial introduction to the ladder, with a significantly higher percentage of missteps (**Figure 5–11F**, $p = 0.0433$), suggesting that some motor function is compromised by the ablation. However, this difference is ameliorated over the training days and there is no significant difference median percentage of missteps after training by day 4 between the two groups (**Figure 5–11C-E**).

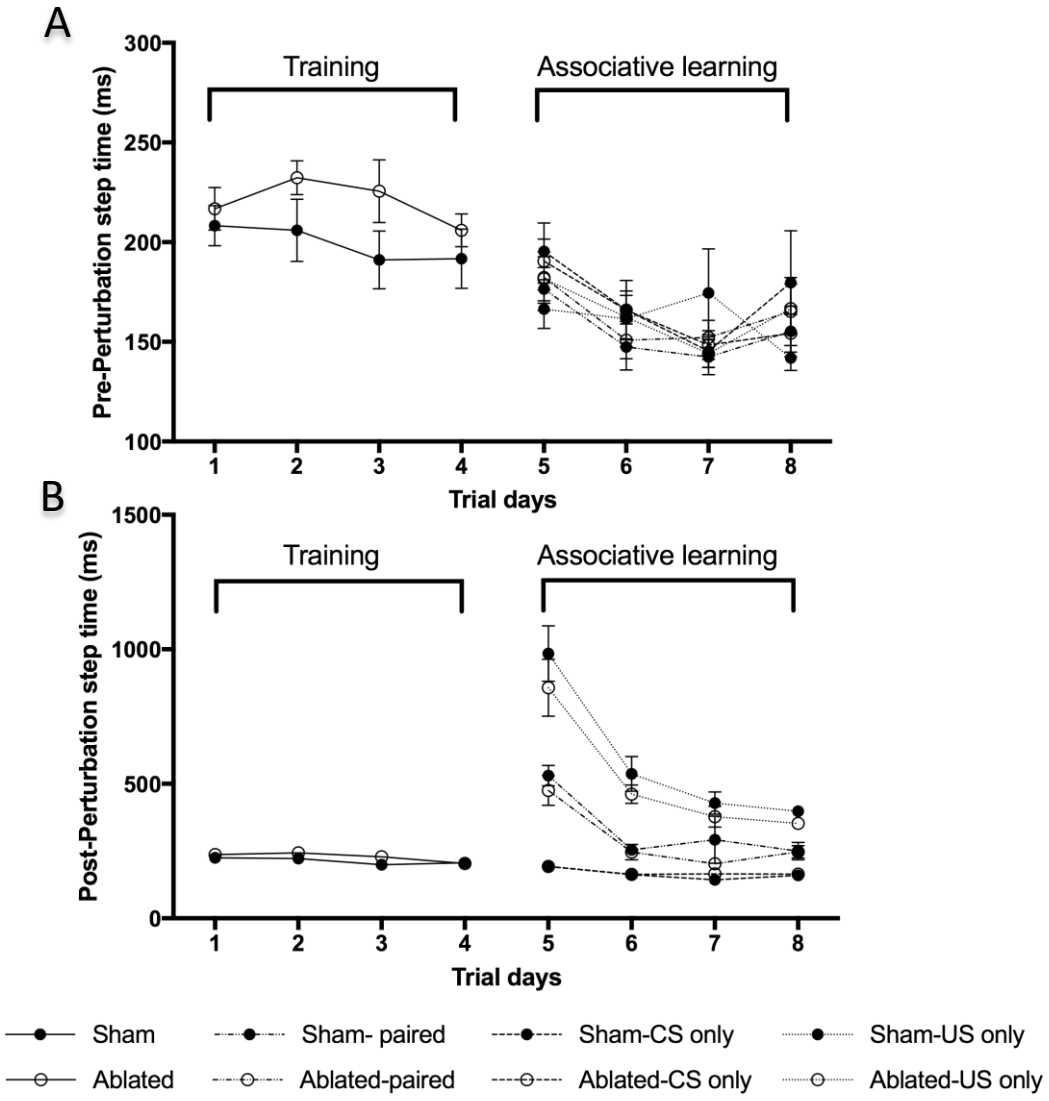

Figure 5–10 Pre and post-perturbation step-times of the sham and ablated groups as measured on the Erasmus ladder over 8 trial days.

*During the first 4 days, only undisturbed trials were run to train the mice to traverse the ladder. Since there is no perturbation in these trials, there is no difference between the pre- (**A**) and post- perturbation (**B**) step-times. On days 5-8, trials are run so that the mouse is presented with either CS only, US only or paired CS-US stimuli. Where there is an US presented in the trial, the post perturbation step-time will increase if the mouse is not anticipating the obstacle. In all trial types, there was no significant difference in pre- and post-perturbation step time between the two groups.*

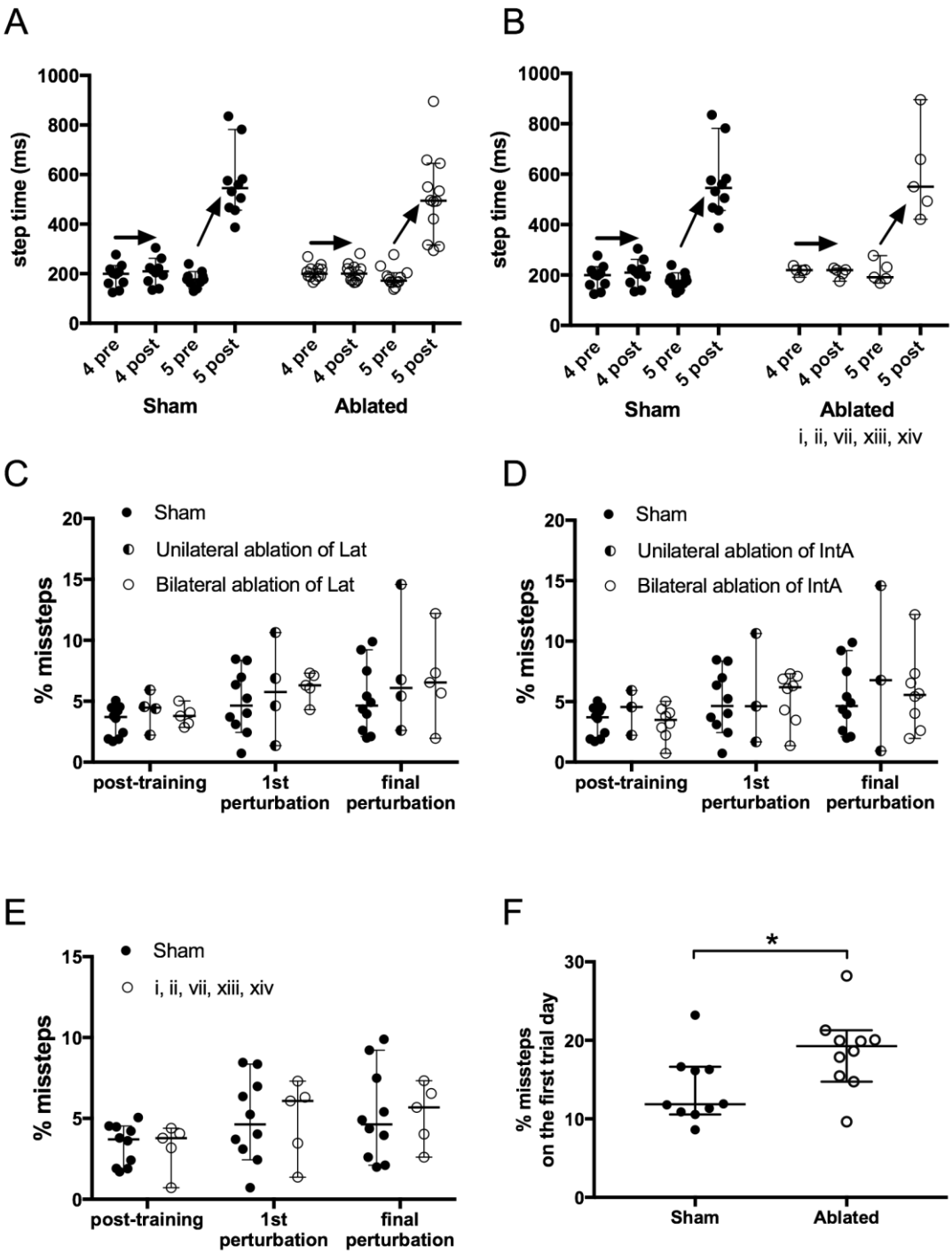
A
B
step time (ms)
1000
800
600
400
200
0
4 pre
4 post
5 pre
5 post
Sham
Ablated
i, ii, vii, xiii, xiv
C
D
% missteps
20
15
10
5
0
Sham
Unilateral ablation of Lat
Bilateral ablation of Lat
Unilateral ablation of IntA
Bilateral ablation of IntA
post-training
1st perturbation
final perturbation
E
F
i, ii, vii, xiii, xiv
% missteps on the first trial day
30
*

Figure 5–11 Erasmus ladder outcomes.

A&B) *Pre and post-perturbation step-times of the sham and ablated groups averaged over all trial types. The comparison between day 4, before introduction of the obstacle, and day 5, when the obstacle is first introduced, reveals the large increase in step time pre and post-perturbation, a measure of locomotion adaptation. Both groups react equally badly to the obstacle since the post-perturbation step time is long. (**A**) compares the entire experimental group while (**B**) compares only the 5 mice that showed severe ablation. **C-E**) Percentage of missteps measured at 3 time-points: "Post-training" represents day.4, the last day of the training period, while "1st perturbation" represents day 5, when the mice are introduced to the US. "Final perturbation" represents day 8, after 4 days of associative learning trials. (**C**) compares the experimental group with injections that cover the lateral nucleus either unilaterally or bilaterally. (**D**) compares the experimental group with injections that cover the anterior interposed nucleus either unilaterally or bilaterally. (**E**) compares only the 5 mice that showed severe ablation. **F**) Percentage of missteps measured on the introduction onto the Erasmus ladder apparatus shows the experimental group initially made more mistakes compared to the sham group. Median percentage of missteps in sham and experimental groups were 11.85 and 19.26%, thus the distributions in the two groups differed significantly (Mann-Whitney U = 23, n_1 =10 n_2 = 10, p = 0.0433 two-tailed). Median with 95%Cl*

5.2.3.3 STEPPING PATTERNS REVEAL SIGNS OF ADAPTIVE MOTOR CONTROL

Differences emerged between the stepping patterns of experimental group and the sham group, suggesting that locomotion was modified to adapt to the ladder task over time (**Figure 5–12** and **Table 5-1**). Assessments on the proportion of step types using two-way ANOVAs show that ablation has a significant effect on the step times of long steps (p = 0.01) as well as the proportion of jumps made (p= 0.0005). Those in the experimental group made consistently quicker long steps while some of the sham animals displayed hesitance by resting on the ladder for long periods of time. The experimental group jumped significantly fewer times than the sham group in both undisturbed and US-only trials. It may be that jumping is a sign of motor competence, since it takes motor coordination to achieve, and the proportion of jumps increase in both groups over undisturbed trials. Accordingly, the proportion of short steps (p=0.024) and backsteps (p=0.026) decreased significantly over

training sessions while the proportion of long steps increased significantly over training sessions ($p < 0.0001$). The proportion of back steps over the sessions also significantly decreased for both groups during paired ($p = 0.0009$) and US-only ($p < 0.0001$) trials. This is evidence of increasing competence to overcome the perturbations, since the sudden appearance of the obstacle initially caused back steps.

Thus, along with the results of the Rotarod assessment, these results suggest that experimental mice display impaired motor skills and impaired, but not abolished, motor learning.

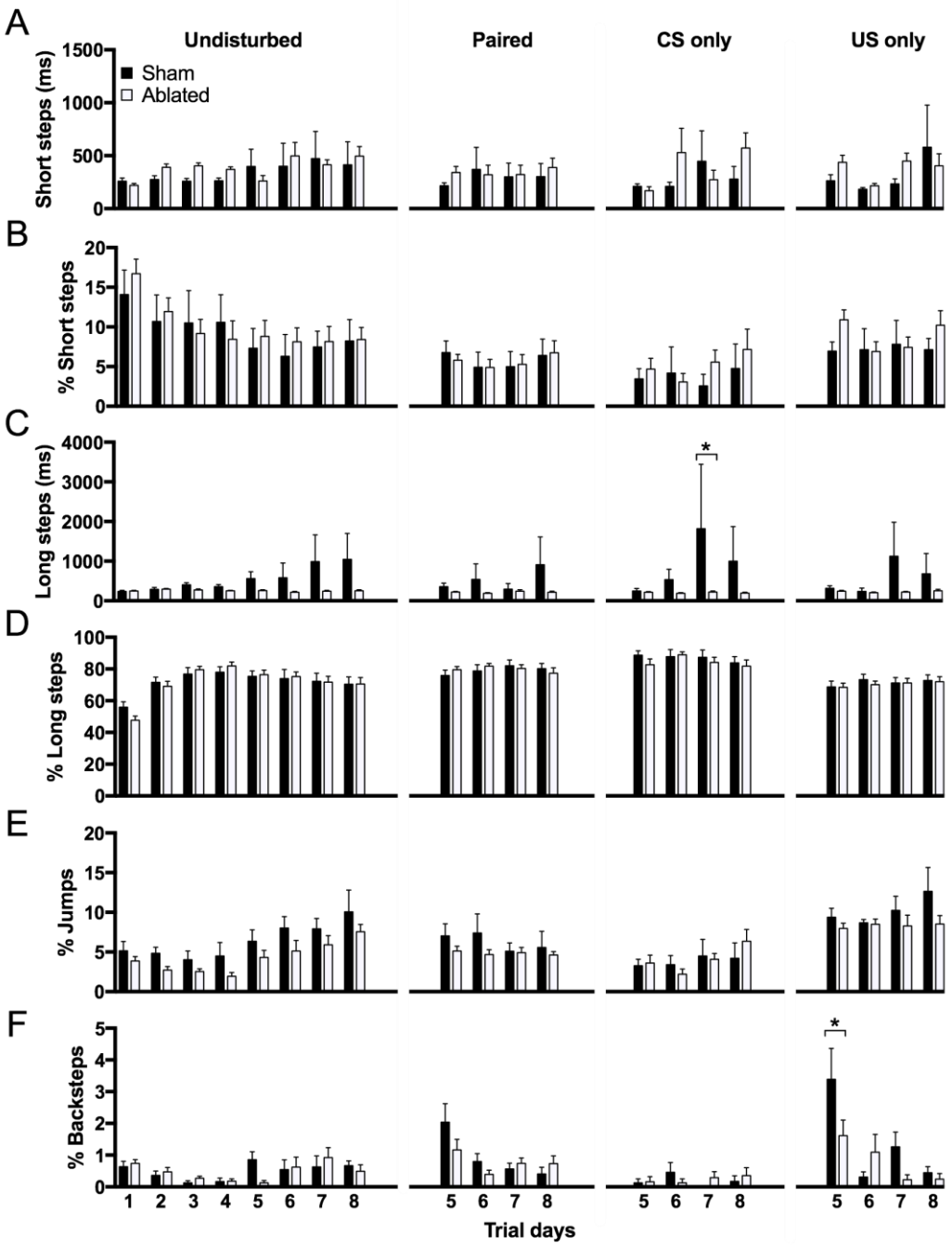

Figure 5–12 Usage of various step types, as classified in Figure 5–2, over the different trial days by trial type ***A)*** *The lengths of the step time of short steps,* ***B)*** *The percentage of steps that were short steps used in each trial day.* ***C)*** *The lengths of the step time of long steps. Ablation group had significantly increased step time compared to sham in CS-only trials (adjusted p=0.0340, Two-way ANOVA followed by Bonferroni's Multiple comparison test).* ***D)*** *The percentage of steps that were long steps used in each trial day.* ***E)*** *The percentage of steps that were jumps used in each trial day.* ***F)*** *The percentage of steps that were back steps used in each trial day. Ablation group had significantly decreased percentage of back steps compared to sham in US-only trials (adjusted p=0.0345, Two-way ANOVA followed by Bonferroni's Multiple comparison test). Mean ± SEM.*

Table 5-1 The results of two-way ANOVAs performed for the data shown in Figure 5–12.

	Ablation			Trial days			Ablation x Trial days		
	F	*df*	*p*	*F*	*df*	*p*	*F*	*df*	*p*
Short steps (ms)									
Undisturbed	0.50	1, 160	0.48	1.00	7, 160	0.43	0.43	7, 160	0.88
Paired	0.36	1, 80	0.55	0.17	3, 80	0.92	0.25	3, 80	0.86
Conditioned stimulus only	0.97	1, 66	0.33	1.02	3, 66	0.39	1.48	3, 66	0.23
Unconditioned stimulus only	0.37	1, 80	0.55	1.40	3, 80	0.25	0.77	3, 80	0.52
Short steps (%)									
Undisturbed	0.22	1, 160	0.64	2.39	7, 160	**0.024**	0.22	7, 160	0.98
Paired	0.01	1, 80	0.92	0.62	3, 80	0.60	0.08	3, 80	0.97
Conditioned stimulus only	0.87	1, 79	0.35	0.49	3, 79	0.69	0.38	3, 79	0.77
Unconditioned stimulus only	1.58	1, 80	0.21	0.50	3, 80	0.69	0.77	3, 80	0.52
Long steps (ms)									
Undisturbed	6.80	1, 157	**0.01**	0.83	7, 157	0.56	0.93	7, 157	0.48
Paired	2.71	1, 78	0.10	0.52	3, 78	0.67	0.59	3, 78	0.63
Conditioned stimulus only	6.04	1, 63	**0.017**	1.50	3, 63	0.22	1.46	3, 63	0.23
Unconditioned stimulus only	3.64	1, 77	0.060	1.19	3, 77	0.32	1.18	3, 77	0.32
Long steps (%)									
Undisturbed	0.02	1, 160	0.89	11.97	7, 160	**<0.0001**	0.55	7, 160	0.79
Paired	0.07	1, 80	0.80	0.53	3, 80	0.67	0.61	3, 80	0.61
Conditioned stimulus only	1.01	1, 79	0.32	0.79	3, 79	0.50	0.34	3, 79	0.80
Unconditioned stimulus only	0.22	1, 80	0.64	0.58	3, 80	0.63	0.12	3, 80	0.95
Jumps (%)									
Undisturbed	12.50	1, 160	**0.0005**	5.59	7, 160	**<0.0001**	0.10	7, 160	1.00
Paired	2.59	1, 80	0.11	0.43	3, 80	0.73	0.38	3, 80	0.77
Conditioned stimulus only	0.06	1, 79	0.81	1.42	3, 79	0.24	0.64	3, 79	0.59
Unconditioned stimulus only	3.68	1, 80	0.06	0.85	3, 80	0.47	0.68	3, 80	0.57
Backsteps (%)									
Undisturbed	0.04	1, 160	0.85	2.35	7, 160	**0.026**	1.24	7, 160	0.28
Paired	0.94	1, 80	0.34	6.09	3, 80	**0.0009**	1.85	3, 80	0.14
Conditioned stimulus only	0.10	1, 79	0.76	0.35	3, 79	0.79	1.01	3, 79	0.39
Unconditioned stimulus only	2.86	1, 80	0.09	8.60	3, 80	**<0.0001**	2.78	3, 80	**0.046**

5.3 DISCUSSION

The experiments investigated the functional significance of the nucleo-olivary neurons. *Sox14*$^{Cre/+}$ or *Sox14*$^{+/+}$ mice were injected with AAV viruses that delivered either an apoptosis inducing gene (Cre-dependent), or a fluorescent marker. Following injections, the mice were tested for their ability to acquire motor skills using the Rotarod test and the Erasmus ladder.

My hypothesis was that the nucleo-olivary neurons are crucial feedback cells in the olivo-cerebellar loop: that they modulate error signals sent by climbing fibres from the inferior olive to the Purkinje cells, which then "learn" based on these signals. Following the ablation of nucleo-olivary neurons by inducing apoptosis, behavioural studies revealed specific deficits in motor performance and motor learning:

1. On the Rotarod balance test, experimental animals start from similar levels of latency on day 1 to controls and demonstrate an ability to improve their performance. However, learning is significantly impaired at day 2 and 3 when compared to controls ($p=0.0324$ and $p=0.0374$, respectively)
2. The experimental group exhibits a significantly higher percentage of missteps ($p = 0.0433$) on introduction to the Erasmus ladder, this difference disappears over the course of 4 training days
3. The experimental group make consistently quicker “long steps” and fewer jumps compared to controls.

In summary, mice with impaired nucleo-olivary connections show 1) impaired motor learning in Rotarod trials. However, they are 2) able to overcome an initially significantly poorer performance on the Erasmus ladder through training. 3) Associative learning is not disturbed.

5.3.1 AAV-mCherry-flex-dtA was effective in inducing specific ablation in Cre-expressing populations

The mCherry mapping combined with the count analysis of *Gad1* labelling suggests that the majority of injections into the experimental group resulted in targeted cell ablation. Many of the mice had reduced numbers of cells labelled with *Gad1* compared to their sham counterparts, indicating apoptosis had been induced. From previous experiments, *Sox14*$^{+}$ cells make up approximately 80% of the *Gad1*$^{+}$ population in the cerebellar nuclei. This suggests that an 80% loss of *Gad1*$^{+}$ cells in this measure would equate to a complete cell loss of *Sox14*$^{+}$ cells. Unexpectedly, in many of the brains with effective ablation, *Gad1*$^{+}$ cell counts within the medial nucleus also decreased despite a lack of *Sox14*$^{+}$ cells in this domain. This may demonstrate inter-regional dependency for survival where the loss of lateral and interposed nuclear circuitry results in medial nucleus cell loss.

Levels of mCherry fluorescence did not necessarily correlate with reduced levels of *Gad1*, showing that mCherry fluorescence alone cannot be used as a reliable measure of injection efficacy. Decreased levels of *Gad1* labelling also occur in regions that showed little fluorescent expression. The multiplicity of infection (MOI) factor was not measured for the AAV-mCherry-flex-dtA, but it is known that AAVs can show preferences for specific cell types (Watakabe et al., 2015). It may

be that the serotype of the AAV preferentially infects the nucleo-olivary neurons, leading to a loss of both mCherry and *Gad1*, while other nuclear cell types are not infected.

5.3.2 WHY DOES MOTOR LEARNING PERSIST FOLLOWING NUCLEO-OLIVARY ABLATION?

Learning acquisition curves were still observed following ablation in both the Rotarod and Erasmus ladder trials. This was unexpected given other experiments in which cerebellar lesions or inactivation abolished associative learning (Krupa et al., 1993). Below, I consider some of the reasons why associative motor learning is spared following the loss of nucleo-olivary neurons:

1. The current theories for motor learning need to account for different layers of learning
2. The cerebello-olivary feedback is involved in a different aspect of motor control
3. The cerebello-olivary feedback is partially redundant
4. The developmental brain finds a way to compensate for the loss
5. The chosen behavioural tests were not sufficient to detect a phenotype

5.3.2.1 DO DIFFERENT LAYERS OF MOTOR LEARNING ACCOUNT FOR THE MOSAIC BEHAVIOURAL EFFECTS OF NUCLEO-OLIVARY ABLATION?

There are many theories of motor learning but most do not allow for different levels of learned behaviour. Schweighofer *et al.* (2013) proposed that the modulation that the nucleo-olivary neurons play on the inferior olive coupling is dynamic so that coupling is initially strong, but results in fast but coarse learning as many Purkinje

cells are mistakenly recruited by additionally coupled climbing fibres. However, over time, as learning proceeds, the nucleo-olivary feedback causes olivary coupling to decrease in order to give more precise error signals that fine-tune the motion, but this slows learning as a trade-off. This is an interesting concept since nucleo-olivary feedback is not needed for coarse learning acquisition. Lack of nucleo-olivary feedback later on in training would lead to an inability to fine-tune learnt movements. This may explain how latency increases in ablated mice over the trials on the Rotarod task, but are not able to reach the latencies shown by the wild-type unablated littermates.

5.3.2.2 EXPLANATION 1: THE CEREBELLO-OLIVARY FEEDBACK IS INVOLVED IN A DIFFERENT ASPECT OF MOTOR CONTROL

The lower latencies seen in the experiment group Rotarod data suggests that while the mice are still able to learn and improve, there is a subtle motor phenotype whereby motor coordination and overall performance is affected perhaps by the lack of nucleo-olivary feedback. This would also explain the increase in the percentage of missteps executed by the ablated animals compared to control on the first day of the Erasmus ladder. The ablated animals are able to learn, as evidenced by the reduction of percentage of missteps, as well as the conditioned responses where the mice were able to learn to anticipate an obstacle when paired with an auditory tone.

While the overall performance on the Erasmus ladder between the two groups is similar, as measured by the percentage of missteps as well as the post-perturbation step time, the ablated mice consistently use less jumps than the controls. Instead, they choose to travel the ladder using short steps and long steps. This may reflect the

mouse's confidence in traversing the ladder, where control mice with better motor ability would choose to skip more rungs by jumping.

5.3.2.3 EXPLANATION 2: THE CEREBELLO-OLIVARY FEEDBACK IS REDUNDANT IN SOME WAY

It is expected that since the olivo-cerebellar loops could be closed loops, that when one component of the loop is cut off, that the entire circuit would fail to function normally. Experiments activating or mimicking the activation of nucleo-olivary neurons at the inferior olive have proved that the Purkinje cells that feed signals to the nucleo-olivary neurons are desynchronised by the GABAergic input into the olive. Conversely, blocking glutamatergic transmission in the inferior olive results in lower firing rates and smaller cohorts of synchronised Purkinje cells (Lang, 2001, 2002).

It is well known that during movement, the inferior olive is suppressed (Apps, 1999; Gellman et al., 1985; Horn et al., 2004; Lidierth and Apps, 1990). The suppression has been shown to be due to the nucleo-olivary neurons since these projections are inhibitory (Bazzigaluppi et al., 2012; Bengtsson and Hesslow, 2006; Hesslow, 1986; Svensson et al., 2006). However, there have also been other findings in which the red nucleus can play a part in providing inhibitory feedback to the olive via the cunate nucleus (Geborek et al., 2012). This parallel pathway may mask a final motor phenotype, since it, too, can control how the inferior olive feeds back to the cerebellum. In Geborek's study, a decerebration that cuts off nucleo-olivary input into the inferior olive did not significantly affect the amount of suppression caused by stimulation cuneate nucleus just preceding pyramidal tract stimulation.

5.3.2.4 EXPLANATION 3: THE BRAIN FINDS A WAY TO COMPENSATE FOR THE LOSS

There is reason to believe that climbing fibres have a role in the development of cerebellar module microcircuitry by sending out many axons to the Purkinje cells, which are then postnatally eliminated by competition so that by adulthood, each Purkinje cell is innervated by only one climbing fibre (Hashimoto and Kano, 2003; Watanabe and Kano, 2011). Furthermore, if all the climbing fibres that connect to one cerebellar hemisphere are cut off from the Purkinje cells during early development, the inferior olive on that contralateral side completely degenerates. Instead, the other side of the inferior olive will send out ipsilateral climbing fibres to re-innervate the Purkinje cells to compensate and recover some olivocerebellar circuitry, which leads to partial reestablishment of motor abilities (Dixon et al., 2005; Sugihara et al., 2003). Since the mono-innervation of climbing fibres to Purkinje cells is not fully established until 2-3 weeks postnatally, this suggests that the timeframe in which I delivered the AAV viruses could be at a stage in which development, and thus plasticity, is heavily at work. This means that the mice could have a compensatory mechanism at work in which the olivo-cerebellar circuitry is re-established despite a mass – but not necessarily total – ablation.

Of course the studies above are investigating the ability of climbing fibres to re-structure while the current investigation focuses on the nucleo-olivary connections, but if the olivo-cerebellar circuitry is made up of closed loops, and honed by synaptic strength, it is possible that the nucleo-olivary neurons have a similar, complementary mechanism for the development of its connectivity, something that is sadly beyond the scope of my project.

In *Cx36*$^{-/-}$ mutant mice, the rhythmic oscillations of olivary cells are maintained through compensatory mechanisms which change the cytological and electroresponsive properties of olivary neurons (De Zeeuw et al., 2003; Long et al., 2002). The opposite adaptation could occur in mice lacking nucleo-olivary connections, where coupling could be restricted in response to deficient feedback. Perhaps fewer gap junction channels would be expressed by olivary neurons in order to prevent over rhythmic activity.

Experiments that cause a delayed ablation may shed more light onto whether there is some aspect of compensation occurring in the present study. Injections of the AAV could be delivered at P21 rather than P14, as the *Sox14* is still being expressed at this stage and would mean that ablation would take place in the mouse's late adolescent stage. Another method would be to use an inducible form of ablation that would be administered in adulthood, such as using an AAV that expresses not the diphtheria toxin, but its receptor, in the Cre expressing cells. The diphtheria toxin could be delivered in adulthood, with only the cells with receptors being affected by it.

5.3.2.5 Explanation 4: The chosen behavioural tests were not sufficient to detect a phenotype

While the Erasmus ladder has been able to show phenotypic differences in mutant animals, it may not be sufficiently sensitive to reveal subtle phenotypes that are unrelated to the motor control needed to traverse a ladder. Although all cerebellar zones play some part in locomotive activity, walking deficits have been shown to be less pronounced after damage to intermediate cerebellar zones, connected to the

interposed nuclei, compared to more medial zones that connect the vermis and flocculonodular lobe to the medial cerebellar nuclei and vestibular nuclei (Morton and Bastian, 2004). Since *Sox14* is not expressed in nucleo-olivary neurons of the medial nucleus, the ablation of Cre-expressing cells only affects olivocerebellar loops that connect to intermediate cerebellar zones.

Ideally, I would like to be able to repeat the experiment looking at a more precisely defined motion like the conditioned eyeblink reflex, since the cerebellar nuclear location of the cells responsible have been mapped. The paradigm also enables more robust testing of associative learning. Subjects that have a trained conditioned response begin to blink in CS-only trials, and the strength of this response can be correlated to the strength of association. The ladder is unable to provide a parallel response in CS-only trials. In those trials, the animals behaved as in undisturbed trials in the parameters that were measured.

6 GENERAL DISCUSSION

The experiments in this thesis have revealed novel aspects of cerebellar nucleus anatomy, development and function. Most importantly:

1. Within the cerebellar nuclei, *Sox14* gene expression exclusively identifies GABAergic nucleo-olivary projection neurons of the interposed and lateral nuclei. The medial cerebellar nucleus has an anatomically and genetically distinct olivary projection.
2. *Sox14*$^{+}$ cells are early born GABAergic neurons from a yet undetermined lineage and have heterogeneous representation across the cerebellar nuclei and are largely absent from the medial nucleus.
3. Targeted partial ablation of *Sox14*$^{+}$ cells in the cerebellar nuclei leads to significant deficits in motor learning, but not to impaired associative learning.
4. *Sox14* also identifies a vestibulo-oculomotor projection from nucleus Y.

Here, I will discuss the implications of the findings: the role of *Sox14* as a specifier of GABAergic cell fate in brain circuits, the implications of the distribution of *Sox14*$^{+}$ cells for understanding the nucleo-olivary circuit and how the functional analysis of this projection impacts current models of cerebellar function. Finally, having shown the developmental *Sox14* gene to be a valuable tool in specifically targeting this cell group, I will discuss future avenues of research using this genetic tool.

6.1 DOES SOX14 REGULATE THE MIGRATION, DISPERSAL AND SURVIVAL OF GABAERGIC SUB-POPULATIONS IN THE BRAIN?

The conclusions in this thesis can in some ways be likened to previous findings of *Sox14* expressing cells of the diencephalon, where the *Sox14* gene has been shown to be involved in the migratory process during development (Delogu et al., 2012; Jager et al., 2016; Sellers et al., 2014). Delogu *et al.* (2012) demonstrated that there is a significant decrease in GFP^+ cells that are found in the ventral lateral geniculate nucleus in the $Sox14^{Gfp/Gfp}$ knockout mouse at birth, and Jager *et al.* (2016) demonstrated that the dorsal lateral geniculate nucleus is affected by a similar reduction in GFP^+ neurons by P21. The migration failure occurs due to the lack of *Sox14* function, since there was no sign of increased apoptosis in the *Sox14* expressing precursors. Similarly, in **Chapter 4.2.5**, I show that in the P0 $Sox14^{Gfp/Gfp}$ mouse, there is evidence of abnormal migration of GFP^+ cells at the cerebellum. While the GFP^+ cells are present, they fail to disperse to populate the nuclei compared to the $Sox14^{Gfp/+}$ mouse at the same stage. By P28, the null deletion of *Sox14* results in a severe reduction of $Gad1^+$ cells in the cerebellar nuclei. It is not known how *Sox14* affects the survival of these cells. Moving forward, it would be interesting to map precise migration changes by looking at GFP^+ cells in the $Sox14^{Gfp/Gfp}$ mouse over embryonic and early postnatal stages

The *Sox14* gene is also required for the tangential migration of rostral thalamic GABAergic precursors between E14.5-16.5 (Delogu et al., 2012), and postnatally as observed using time lapse imaging and *in utero* labelling using AAVs (Jager et al., 2016). It has been shown that $Sox14^+$ cells of the dorsal lateral geniculate nucleus are derived from midbrain regions and migrate tangentially in a rostral direction,

rather than migrating from the prethalamic sub-ventricular zone, as was previously hypothesised (Golding et al., 2014). It is currently unknown which progenitor zone the cerebellar *Sox14*$^{+}$ cells are derived from. It is assumed that since they are GABAergic, they form part of the ventricular zone progeny that radially migrates into the cerebellar plate. Using the *Sox14*$^{Gfp/+}$ mouse, I was able to identify that, at E12.5, the GFP^{+} cells seen in the sagittal plane have processes that are tangentially orientated. From this, it can be inferred that the cells are following the subpial rhombic lip migratory stream rather than radially migrating from the ventricular zone.

6.2 ARE SOX14+ NUCLEO-OLIVARY NEURONS DERIVED FROM A *PTF1A*$^{+}$ PROGENITOR POOL?

Given the unexpected origins of the *Sox14*$^{+}$ cells in the lateral geniculate nucleus, it is not beyond possibility for cerebellar nuclear *Sox14*$^{+}$ cells to originate apart from the other GABAergic ventricular zone-derived neurons. It is known that the *Sox14*$^{+}$ cells of the thalamus are born from the *Ascl1* progenitor pool. Neurogenesis requires dimerization of Ascl1-Helt, which leads to sequential activation of other transcription factors *Gata2*, *Tal1*, *Tal2*, *Gata3* and *Sox14* (Delogu et al., 2012; Sellers et al., 2014; Song et al., 2015; Virolainen et al., 2012). In the cerebellum, all ventricular zone derived cell types express *Ascl1* and *Ptf1a*, which are required in the generation of Purkinje cells and interneurons (Millen et al., 2014; Pascual et al., 2007; Sudarov et al., 2011). Sudarov *et al.* (2011) showed in *Ascl1*^{CreER} mice that tamoxifen administration at E10.5 resulted in ßGal immunoreactivity in GABAergic cerebellar nuclear cells. It is therefore likely that the *Sox14*$^{+}$ cells are derived from the *Ascl1* progenitor pool. *Ptf1a* expression is limited to the hindbrain and spinal cord (anywhere caudal of the isthmus) and so is not involved in the generation of

more rostral *Sox14*$^{+}$ populations. In the hindbrain, *Ptf1a* plays a similar role to *Helt*, which is expressed in complement, in the forebrain and midbrain (Sudarov et al., 2011). In the dorsal spinal cord, *Ptf1a* and *Rbpj* interact to form a complex that, along with *Ascl1*, is essential for the transcriptional control of downstream genes, such as *Pax2* and *Lhx1/5*, in order to specify inhibitory neurons and repress excitatory neuronal specification (Hori et al., 2008).

There is uncertainty surrounding the onset of *Ptf1a* expression in the cerebellar anlage (Hoshino et al., 2005; Liu et al., 2010), while *Ascl1* is known to be expressed at E10.5 (Liu et al., 2010; Sudarov et al., 2011; Zordan et al., 2008). There is a possibility that nucleo-olivary neurons may be from an *Ascl1*$^{+}$/*Pft1a*$^{-}$ progenitor zone. It has been shown that an *Ascl1*$^{+}$/*Pft1a*$^{-}$ domain does exist in the ventral ventricular zone of rhombomere 1, but this region is known to give rise to extra-cerebellar cells that populate the ventral brainstem (Millen et al., 2014). The loss of *Ptf1a* function shifts ventricular zone-derived cerebellar cells towards the fate of these *Ascl1*$^{+}$/*Pft1a*$^{-}$ cells and results in mass exodus out of the cerebellar anlage and into the ventral brainstem.

There is evidence of *Ascl1*$^{+}$/*Ngn2*$^{+}$ cells in the dorsal parts of the cerebellar plate at E10.75, suggesting that the progenitor pool is distinct from the ventricular zone (Zordan et al., 2008). It has not been shown, however, whether these cells also express *Ptf1a*. Thus, other pro-neural genes may be involved in the specification of nucleo-olivary neurons. If nucleo-olivary *Sox14*$^{+}$ cells come from this domain, the tangential migration seen at E12.5 travels in the opposite direction to the rhombic lip migratory stream.

6.3 DO THE NUCLEO-OLIVARY NEURONS PLAY A ROLE IN CEREBELLO-OLIVARY CIRCUIT FORMATION?

My findings suggest that GABAergic nucleo-olivary projecting neurons are, alongside glutamatergic projection neurons, the earliest born neurons in the cerebellum. The systems by which the cerebellar and pre-cerebellar nuclei develop are surprisingly similar. It is known that the development of climbing fibres occurs early; olivary neurons are produced from E9.5-11.5 (Hoshino, 2012; Pierce, 1973) and reach the developing cerebellum by E14-15, when Purkinje cells are post-mitotic and form clusters that express genetic markers that establish topographic compartments (Reeber et al., 2012). There is literature to suggest that the climbing fibres play a role in the establishment of specific closed-loop micro-circuitry by sending many axons early in development that eventually become pruned down to single-cell innervation (Hashimoto and Hibi, 2012; Reeber et al., 2012; Sotelo et al., 1984). The early birth of nucleo-olivary neurons may enable the nuclear cells to be near the Purkinje cell clusters as climbing fibre projections are established. It would be of interest to determine whether the nucleo-olivary neurons likewise express different expression domains. It has already been suggested that climbing fibre collaterals into the cerebellar nuclei play a role in early postnatal development in the topographic refinement of olivocerebellar modules (Najac and Raman, 2017). This specificity is crucial for working theories of how the olivo-cerebellar loop functions as an error minimiser.

The caudal rhombomeres, which give rise to pre-cerebellar nuclei, are similar to the rhombomere 1 in that it also expresses *Atoh1* and *Ptf1a* in two mutually exclusive zones (Hoshino, 2012; Wullimann et al., 2011). The pre-cerebellar nuclei, which

give rise to the mossy fibres, are derived from the *Atoh1*$^{+}$ lower rhombic lip (Wang et al., 2005), while the excitatory neurons of the inferior olive, which give rise to the climbing fibres, are derived from the *Ptf1a*$^{+}$ lower rhombic lip (Hoshino et al., 2005; Yamada et al., 2007). In the *cerebelless* mutant, which lacks *Pft1a* specifically in the cerebellum, the inferior olivary nucleus and the pontine nuclei are embryonically formed but become absent in adults. This suggests an inter-dependent relationship for survival of these structures that project to the cerebellum (Hoshino et al., 2005). If the nucleo-olivary neurons are truly from the *Ptf1a* progenitor pool and are absent in the *cerebelless* mutant, this would imply a role, not only in the establishment, but in the survival of olivocerebellar modules.

6.4 IMPLICATIONS OF SOX14 EXPERIMENTS FOR UNDERSTANDING CEREBELLAR NUCLEUS FUNCTION

Here, I consider the theories of olivocerebellar circuitry function in light of the findings from the behavioural tests in the last chapter. I will also discuss how the heterogeneous distribution of nucleo-olivary neurons may reflect levels of importance of this feedback for different cerebellar functions.

6.4.1 IMPLICATIONS FOR NUCLEO-OLIVARY CIRCUIT IN MOTOR LEARNING AND MOTOR FUNCTION

Though the ablation targeted all the nucleo-olivary neurons, the behavioural paradigms I chose to perform specifically investigated motor coordination and associative motor locomotion. In the Delogu lab, we have observed that *Sox14*$^{-/-}$ knock-out mice are generally smaller than their heterozygous and wildtype

littermates. They were initially tested for behavioural phenotypes and were shown to have disrupted circadian entrainment (Delogu et al., 2012). The mice were more skittish than their wildtype and heterozygous littermates and showed behaviours such as foot tapping, a persistent postural lean epileptic traits (unpublished data). It is not known whether any of these symptoms are the direct result of non-survival of *Sox14*$^{+}$ cells in the cerebellar nuclei because many *Sox14* expressing populations are affected, particularly in sub-cortical nuclei of the midbrain and brain-stem.

Previous literature showed that lesions to the cerebellar nuclei were able to abolish conditioned learnt responses and prevent the acquisition of further conditioned learning (Mccormick et al., 1981; McCormick and Thompson, 1984), but these crude methods cannot divorce the contributions of the various nuclear cells types. However, specific ablation of the nucleo-olivary projections does not achieve the same drastic changes. From the results of the Erasmus ladder and Rotarod tests, it would seem that on the whole, general motor function and associative motor learning skills are intact. The nucleo-olivary neurons may be primarily responsible for feedback to weaken the climbing fibre signal once a motor command has been learned, while not being necessary to acquire the conditioned response (Hesslow and Ivarsson, 1996; Rasmussen et al., 2008; Sears and Steinmetz, 1991). This would explain why mice are still able to learn to predict the obstacle on the Erasmus ladder in the absence of nucleo-olivary circuitry. I did not look at the maintenance or extinction of these conditioned responses.

The Erasmus ladder only measures the acquisition of conditioned responses while motor learning also requires the ability to break inappropriate associations – i.e.

extinction – and to know when additional conditioned signals cannot further improve prediction of the unconditioned stimulus – i.e. blocking – so that redundant and inefficient learning does not occur. It may be that the nucleo-olivary feedback is not required for the initial associations but is needed for preventing redundant learning by blocking new associations that provide no new information about predicting the obstacle. It has been shown in trained rabbits on an eyeblink conditioning task that olivary administration of picrotoxin (PIX), a GABA antagonist, can prevent blocking (Kim et al., 1998). While normally, the introduction of a second predictive CS (such as light) will not lead to association if an association has already been made (such as an auditory tone) to predict the unconditioned stimulus (the airpuff), PIX injection during a second training session was able to cause association of the second CS to the US.

From previous findings whereby motor function is not grossly affected in *Cx36*$^{-/-}$ mutant mice (Kistler et al., 2002), while conditioned learning is affected (Van Der Giessen et al., 2008), it would appear that gap junction blockade in communication has a more damaging outcome on the ability to acquire new motor skills than lack of activity altogether. It could be argued that excessive activity from inhibitory nucleo-olivary neurons would yield similar effects to a gap junction blockade. Yet here, I demonstrate that disrupting nucleo-olivary circuitry does not lead to drastic loss of cerebellar function. The coupling of olivary populations required to enable appropriate synchrony in climbing fibre and Purkinje cell firing to permit associative learning does not depend on the nucleo-olivary connection. What can this tell us about the function of nucleo-olivary neurons in particular? Perhaps the nucleo-olivary neurons do not play an important role in olivary clustering, as was

hypothesised by Llinas (2014). While it is obvious that climbing fibres have a strong influence on cerebellar function, since it is able to produce complex spiking in the Purkinje cells, the importance of the reciprocal nucleo-olivary connectivity is less clear. It seems that past experiments that manipulate olivary firing as a means of mimicking nucleo-olivary feedback are not sufficient to account for the function of this feedback loop.

Taking everything into account, these findings help us to rethink the role of olivo-cortico-nucleo-olivary loop. Although the olivary input into the cerebellum via climbing fibres is crucial for cerebellar conditioned learning, and electrotonic coupling in the inferior olive is the sole moderator of climbing fibre synchronicity, I have shown that nucleo-olivary feedback is not critical for conditioned learning.

6.4.2 Heterogeneous distribution of *SOX14*$^{+}$ may reflect function

The characterization of *Sox14* expression patterns has provided new insights into cerebellar nucleus function. Here, I discuss the heterogeneous composition of nuclei and the relationship between heterogeneity, connectivity, and function. The cerebellar nuclei sit at the core of cerebellar function, since it is the final output of all cerebellar processing. On the whole, the diversity, connectivity and processing function of nuclear neurons have remained elusive and thus their involvement in cerebellar function models is often inadequately described. Models that include the nucleo-olivary feedback loop assume that the cells function homogeneously across the different cerebellar modules. However, the characterization of nucleo-olivary

neurons have shown that these cells are heterogeneously distributed across the cerebellar nuclei and are genetically distinct in the medial nucleus, even forming a different route to the inferior olive.

Despite the fact that that cells differ along both rostral-caudal and lateral-medial axes in terms of prevalence and the spread of dendritic and axonal trees (Brown et al., 1977; Buisseret-Delmas and Batini, 1978; Chan-Palay, 1973c; Legendre and Courville, 1987; Tolbert et al., 1976), models of cerebellar function assume a homogeneous spread of each nuclear cell type, paralleling the long-assumed homogenous and stereotyped circuitry of the cerebellar cortex, which itself is undergoing re-examination (Cerminara et al., 2015). There is a higher density of nucleo-olivary neurons in the ventral lateral and interposed nuclei (Giaquinta et al., 1999). Accordingly, the Purkinje cell axon terminals spread in a different manner in these parts when compared to more dorsal and medial regions of the nuclei (Sugihara et al., 2009).

It is not known why the distribution of the nucleo-olivary neurons across the nuclei is unequal. As new cerebellar cortical markers have been identified, it has become increasingly clear that individual circuits can be spatially defined in terms of transverse zones and stripes, longitudinal zones. Within these broader maps, detailed maps of microzones and patches have also been identified at a high resolution (reviewed in Apps and Hawkes (2009)).

Given that the topographic loops connecting specific cerebellar subnuclei with inferior olive subnuclei, and also that the glutamatergic projections from the

cerebellar nuclei reach a variety of neocortical targets, the geography of the cerebellar nuclei is closed linked to function (Apps and Garwicz, 2005; Pijpers et al., 2005; Ruigrok, 2011; Sugihara and Shinoda, 2007; Voogd and Ruigrok, 2004). For example, the high density of *Sox14*$^{+}$ cells in the ventromedial lateral nucleus would suggest that feedback to the olive is crucial for visuomotor performance, which is governed by cerebellar modules in this region (Cerminara and Apps, 2011). Yet only specific cerebellar modules have been scrutinised for precise connectivity and linked to functional roles (Sugihara and Shinoda, 2007) and so it is not possible to speculate how the sparseness of nucleo-olivary neurons found in the dorsal parts of the nuclei is connected to functional loops.

Only recently has it been discovered that intrinsic differences exist between the different olivocerebellar modules. Purkinje cells in different zones can display different average firing rates that will affect downstream signals, and also may imply differences in how motor learning could take place across the modules (De Zeeuw and Ten Brinke, 2015).

6.4.3 *SOX14* EXPRESSION HIGHLIGHTS DIFFERENCES ACROSS THE DIFFERENT CEREBELLAR NUCLEI

The olivo-cerebellar modules are precisely topographically organised loops which supply crucial feedback, and so they are considered to be fundamental to cerebellar function (De Zeeuw and Ten Brinke, 2015). Specific lesions or pharmacological blockades into specific subregions of the inferior olive have revealed behavioural correlates with olivo-cerebellar modules (Horn et al., 2010; Llinás et al., 1975; Pijpers et al., 2008; Seoane et al., 2005). As described in **Chapter 1.6.5**, the number

and shape of the various cerebellar nuclei vary across the animal kingdom and the lateral nucleus is the newest addition, only being present in mammals. The evolution in circuitry between the nuclei reveal the approaches to adaptation in circuitry to suit function. Phylogenetically newer parts of the nuclear mass connect to higher order regions in the neocortex to implement complex actions such as grasping, while phylogenetically older parts control shorter reflexive movements such as the VOR, optokinetic eye movement responses and saccades (Ito, 2013). Ito argues that this difference is ultimately seen in the function of the olivo-cerebellar modules, where the modules play a more important, controller role in the medial nucleus, and a supportive role in the lateral nucleus. The fact that *Sox14* is not expressed in the medial nucleus, and that the medial nucleus uses a separate nucleo-olivary axonal tract suggests that the it processes signals differently to the other nuclei.

The heterogeneity in expression patterns is particularly stark when comparing the medial nucleus cytology and connectivity. For example, large glycinergic projection neurons are only found in the medial nuclei (Bagnall et al., 2009; Chung et al., 2009), while its cerebello-olivary circuitry takes a different route to those in the lateral and interposed nuclei (Dom et al., 1973; Legendre and Courville, 1987; Martin et al., 1976), as shown in the last chapter. The glycinergic projection neurons that are exclusively found in the medial nuclei project ipsilaterally to the vestibular nuclei, the ventral brainstem and the ipsilateral ventromedial medullary reticular formation. These are hence the ipsilateral counterparts to the large glutamatergic projection neurons of the same region, which project contralaterally to the same regions. There are suggestions that these projections support the medial nuclear function in posture and balance, since they rely on a system of cross-midline control,

similar system to that of the vestibular control of horizontal eye movements (Bagnall et al., 2009).

That the medial nucleus is, on many aspects, composed differently to the other two cerebellar nuclei is well documented but mostly overlooked in evaluations of the cerebellum. In addition to the lack of *Sox14* expression in the medial nucleus, others have also shown idiosyncratic expression patterns in the medial nucleus. *Zac1* is expressed only in a sub-set of GABAergic medial nuclei neurons (Chung et al., 2011), while *Tbr1* expression is maintained into adulthood exclusively in the glutamatergic projection neurons of the medial nucleus, long after expression is lost in the other cerebellar nuclei (Fink et al., 2006; Green and Wingate, 2014). Conversely, HNK-1 expression is found in the glutamatergic projection neurons in all except the caudal medial nucleus (Chung et al., 2009).

KLC3 immunoreactivity has been claimed as a universal cerebellar nuclei specific marker, since it labels both large and small neurons throughout all the different sub-nuclei (Chung et al., 2007). However, comparing the *Sox14* expression pattern described in the **Chapter 2.2.1** with that of the KLC3 staining in the Chung *et al*. (2007) paper, it would appear that KLC3 is not expressed in the areas where *Sox14*-GFP expression is seen. This is especially evident in areas of high density of GFP^+ cells; the dense collection of ventral $Sox14^+$ cells appear as gaps in the KLC3 immunoreactivity map. I would hypothesise that a double staining against the two proteins would show complementary patterns of expression. KLC3 staining is also observed in the medial nucleus, and it is lost in *Zac1* mutants – *Zac1* is exclusively expressed in a sub-set of early born GABAergic medial nuclei

neurons (Chung et al., 2011). These may be interneurons, but since they are early-born, they could be medial equivalents of the *Sox14*$^{+}$ population, since all projection cell types are born before interneurons.

Additionally, a small number of *Sox14*$^{+}$ cells can be seen in the rostral sections along the ventral edge of the medial nucleus, which have not been identified. There are three possible cell groups that these *Sox14*$^{+}$ cells may be part: 1) they may be an extension of the vestibulo-cerebellar nucleus; 2) in the rat and macaque, a "fifth" cerebellar nucleus known as, the interstitial cell group, has been defined that sits at the border of the medial and posterior interposed nuclei (Buisseret-Delmas and Angaut, 1993; Voogd, 2014); 3) there is also the basal interstitial nucleus, which lies ventral to the posterior interposed in the roof of the 4th ventricle, identified in the monkey (Langer, 1985). Without a vestibular nuclei specific marker, it is not possible to differentiate between the different nuclei and draw boundaries where the posterior interposed, vestibulo-cerebellar and medial nuclei converge based only on morphology.

6.5 FUTURE INVESTIGATIONS ON FUNCTIONAL ROLE OF NUCLEO-OLIVARY CONNECTIVITY

6.5.1 APPROACHES TO DETERMINING CIRCUITRY

AAVs do not transmit across synapses, making them useful for looking at cell morphology and axonal projections but not circuitry. Alternatively, modified rabies viruses can be used to look at trans-synaptic connectivity. In particular, the glycoprotein-deleted (dG) rabies virus transforms the normal rabies virus into a 'single-round' vector that cannot continue to spread due to lack of glycoprotein (G),

thus making it a mono-synaptic retrograde tracer (Wickersham et al., 2010). In order for the rabies to be expressed, it must be trans-complemented in cells that express G, limiting the extent to which the virus can be replicated (Ugolini, 2010). The presence of G in the target cells also allows the virus to be transferred to first-order neurons, where it replicates and also expresses the fluorescent protein. However, as the virus in the first-order neurons lack G, the virus is unable to transfer into second-order neurons, thus only showing monosynaptic connections. Specificity can be achieved by using the avian retrovirus glycoprotein EnvA to coat the virus, making it unable to infect mammalian cells. This ensures that the rabies only infects cells expressing the complementary avian receptor TVA, which is induced by infecting the target cells with AAV-TVA-G-GFP prior to injection of the G-deleted rabies virus. Thus, the virus only successfully infects and replicates in cells that are made to express TVA, and G.

The dG-pseudorabies virus would enable investigation of the cell types that directly synapse onto the *Sox14*$^{+}$ nucleo-olivary neurons. The dG-pseudorabies virus has been used previously to reveal connectivity between the cerebral cortex, basal ganglia, and cerebellum (Bostan et al., 2010; Coffman et al., 2011; Suzuki et al., 2012). By injecting rAAVs that promote expression of TVA-GFP and G into the cerebellar nuclei, then EnVA-SAD-dG-tdTomato into the inferior olive, the nuclear cells that synapse into the inferior olive, and their direct inputs would be visualised. The literature suggests that the cerebellar modules are closed-loops that connect the cerebellar cortex to confined regions of the neocortex, cerebellar nuclei, and inferior olive (Bengtsson and Hesslow, 2013; Dum and Strick, 2003; Ruigrok, 2011; Voogd and Ruigrok, 2004). From this, I would expect that the direct inputs to the neuron-

olivary neurons will include topographic inputs from specific Purkinje cell zones, collaterals from climbing fibres from specific contralateral olivary sub-nuclei as well as mossy fibres and possible interneuronal connections from an internal network. However, connectivity that extends beyond this rigid topography has also been demonstrated (Coffman et al., 2011).

While differential protein and genetic expression patterns can inform us about the specificity of conserved micro-zones (Reeber et al., 2012; Sugihara and Shinoda, 2007), in order to demonstrate truly closed-loop circuitry, one would have to look at single cell connectivity to answer the question: does a nucleo-olivary neuron target the same olivary cell that extends a climbing fibre that feeds back to the it? Kebschull *et al.* (2016) are using DNA sequencing technology to map single neuron projections. This "MAPseq" technique has the power to determine connectivity beyond region to region mapping, and could provide answers to questions about whether truly closed-loop micro-circuits exist between the inferior olive and the cerebellum.

6.5.2 FUTURE DIRECTIONS

The *Sox14-Cre* mouse enables targeting of the cerebellar nuclei, but it requires the stereotaxic targeting of a precise area since vestibular neurons also express *Sox14*. In addition, within the ventral part of the lateral cerebellar nucleus, *Sox14* is expressed alongside *Calb2*, although I was not able to identify if this population are also nucleo-olivary neurons. The limited developmental expression of *Sox14* gene restricts the potential uses of the *Sox14-Cre* and *Sox14-Gfp* mice. The *Sox14-Gfp* mouse is only useful for characterization within the first 4 weeks postnatally while

any genetic modifications using the *Sox14-Cre* mouse must also be performed within that time frame. I have demonstrated that it is possible to stereotaxically target the cerebellar nuclei from P14. The *Gad1* reactivity revealed that the injection of AAVs are able to efficiently deliver Cre-mediated ablation where the injections are targeted correctly. Other pilot injections into the *Sox14-Cre* mice have shown that injections performed at P21 still effectively undergo Cre-dependent recombination**.**

Used with viral methods, such as optogenetics, specific targeting can be achieved to manipulate neural activity *in vivo*. The injections performed in the current experiments were designed to target the whole nucleo-olivary population defined by *Sox14* expression. However, small subsets can be manipulated with precise injections in order to investigate the contribution of specific olivocerebellar modules to motor and non-motor functions.

There are a wide range of genetic tools that can be used together with the *Sox14-Cre* mouse to create manipulations that are permanent, as I have demonstrated in this thesis, long term or acute. Optogenetic technology takes advantage of light-sensitive channelrhodopsins (Fenno et al., 2011), while designer receptors exclusively activated by designer drugs (DREADDs) modulate cellular function pharmacologically (Rogan and Roth, 2011; Roth, 2016). Both technologies promote the expression of specialised ion channel proteins. In the case of optogenetics, the channelrhodopsin is light activated and facilitates acute changes at the firing pattern level. For DREADDs, the synthetic receptor is activated by the administration of a synthetic ligand, clozapine-N-oxide (CNO), either by transfusion into the blood

stream or by localised injections. Both these manipulations can be instigated long after *Sox14* expression has faded and thus can be employed to investigate circuit changes in adulthood, when the brain is less capable of compensatory adaptations. Optogenetic modulation has been used to investigate the role of Purkinje cells in motor coordination (Gutierrez et al., 2011; Tsubota et al., 2013), but no studies have yet been conducted using DREADD technology in the cerebellum.

While the extensive ablation of nucleo-olivary neurons I performed at the developmental stage did not lead to substantial motor function deficits, optogenetics would allow for temporary and acute increases to nucleo-olivary cell firing. It is known that damage to the developing brain compared to changes in the same area during adulthood can result in different observed behaviours. Acute manipulations may reveal nucleo-olivary roles in motor learning ability that were not detected in the current developmental manipulation. DREADDs can be used to increase and decrease cell firing, but since it depends on ligand administration, it proves more useful in investigations looking at semi-long term changes. For example, it may be used in assessing the cerebello-olivary contribution to higher cognitive functional tasks.

It is not known how the nucleo-olivary connection influences other cerebellar functions and there are many behavioural paradigms that can be looked at by applying the range of manipulations. **Table 6-1** shows commonly looked at cerebellar behavioural paradigms with expected phenotypes that may be seen when particular regions of the cerebellar nuclei are targeted in the *Sox14-Cre* mouse.

The eyeblink conditioning paradigm is more useful in precise quantification of acquisition, retention and extinction of conditioned responses since it is able to measure the strength of the eyeblink reflex as well as the precise timing of the responses(Jörntell et al., 2010; McCormick et al., 1985; Medina et al., 2002; Nilaweera et al., 2006). Only one movement is measured compared to the complex coordination that is needed for locomotive adaptation on the Erasmus ladder. Improvements in technology, such as the "Magnetic Distance Measurement Technique" allows precise detection of eyelid movements at a high spatiotemporal resolution, compared to EMGs that were used in the past (Boele et al., 2009; Koekkoek et al., 2002). This enables measurements of the size of the movements, both of the short-latency response and of the unconditioned response, and thus the rate of conditioning can be calculated. Unlike the Erasmus ladder, each trial trace can be compared chronologically so that the speed of acquisition can be accurately quantified.

The vestibulo-ocular reflex (VOR) is the movement of the extraocular eye muscles with counters any movement of the head in order to fix our gaze on an object while our head moves. It has been shown that since this is an open-loop reflex, the cerebellum is able to modify VOR (Broussard et al., 2011; Ezure and Graf, 1984; Ito, 2013; Sekirnjak et al., 2003). This plasticity has been the focus of much of the function of the flocculus and vestibular nuclei. Investigations into the VOR can be achieved by manipulating retinal slip by introducing changes to the visual environment or head movement.

While *Sox14* expression is not found in nucleo-olivary neurons, it is present in the vestibular nuclei and I have shown that at least a subset of these project to the oculomotor nucleus. The vestibular system is involved in many complex circuitries like that of the cerebellar system, therefore there needs to be further characterization of *Sox14*$^{+}$ cells in the vestibular nuclei before being able to hypothesise how the *Sox14-Cre* mouse may be of use. Similarly, the specific contributions of *Sox14*$^{+}$ cells to complex, multi-joint and multi-organ functions, such as posture and locomotion are more difficult to assign without a clear picture of the whole circuitry.

Autistic-like mouse phenotypes have been demonstrated in cerebellar-specific Tsc1 mutants (Tsai et al., 2012) and similar tests can be used to identify cognitive behavioural changes associated with nucleo-olivary ablation during development. A range of social tasks can be used to assess the mouse's tendency to approach other mice, repetitive behaviour, anxiety-like measures and cognitive ability (Moy et al., 2007). A case can also be argued for cognitive assessment using the Erasmus ladder, since measurements can be made of the mouse's reluctance to leave the goal boxes to traverse the ladder. The time it takes for them to leave the box following the light cue, and eventually a strong back-wind cue, can be viewed in terms of motivation, aversiveness and avoidance (Vinueza Veloz et al., 2015).

The understanding of these functions has also been aided by advances in visualising cell activity. This has been achieved using electrophysiology, multielectrode recordings (Lang et al., 1999), calcium flux imaging (Leznik et al., 2002; Sullivan et al., 2005) and fMRI (Kahn et al., 2013). This enables behaviour to be correlated with synchrony in the olive and loop circuitry effects.

Table 6-1 Common cerebellar behavioural paradigms with predicted outcomes to adult or developmental manipulations to nucleo-olivary connectivity using the Sox14-Cre mouse.

** While there are no Sox14$^+$ nucleo-olivary neurons in the medial nucleus, the nucleus is closely linked to the vestibular system for control in these functions. Therefore, disruption of Sox14$^+$ cells in the vestibular nuclei may affect these behaviours.*

Function	***Nucleus***	***Sox14***	***Manipulation***	
			Adult	**Developmental**
Cortical connectivity	Lateral	Y	Higher order cognitive deficits in motor planning	Cognitive deficits/ASD-like phenotypes
Locomotion	Lateral	Y	Ataxia	May have adaptive changes to overcome loss of circuitry
Eye-blink conditioning	Anterior interposed	Y	Deficit in associative learning, extinction and blocking	May have adaptive changes to overcome loss of circuitry
Saccadic and smooth pursuit eye movements	Medial	N*	nothing	nothing
Posture	Medial	N*	nothing	nothing
VOR	Vestibular	Y	Deficit in reflex adaptation	?

6.5.3 FINAL REMARKS

There are still many unanswered questions about the cerebellar nuclei, particularly about, the origins of the diverse range of nuclear cell types and how intra-nuclear networks are formed as well as long range projections. The answers to these questions will be of huge significance for functional models of the cerebellar network. They may also point towards new landmarks for the identification of disease processes in the cerebellum. This somewhat neglected population of brain cells is poised at a threshold of new understanding that offers the promise of new perspectives on the both how the cerebellum works and its clinical vulnerabilities.

7 MATERIALS AND METHODS

7.1 ANIMAL HUSBANDRY

7.1.1 MOUSE LINES

Both the *Sox14-Gfp* (Delogu et al., 2012) and the newly derived knock-in/knock-out *Sox14-Cre* mutant mice lines were generated at Columbia University (Jessell Lab, Columbia) and maintained at KCL. Mice were bred and maintained at KCL under local ethical and legal regulations. The *Sox14* allele coding sequence was replaced with a 5' splice substrate followed by the EGFP or Cre gene, bovine growth hormone polyadenylation sequence and neo cassette. More information can be found at http://www.informatics.jax.org/allele/MGI:3836003

7.1.2 MOUSE MAINTENANCE AND BREEDING

Wildtype C57BL/6 mice for breeding were obtained from Charles River (Margate, Kent, UK). All animal procedures were carried out in accordance with the guidelines and protocols approved by the KCL Ethics Committee and the UK Home Office.

The animals were housed in the Biological Services Unit (BSU) at the Institute of Psychiatry, Psychology & Neuroscience in standard conditions (19-22°C, humidity 55%, 12h:12h light: dark cycle with lights on at 7.30am, food [Rat and Mouse No. 1 Diet; Special Diet Services, Essex, UK] and water ad libitum). Mice were pair-housed with their litter mates in large cages 45x28x13cm with environmental enrichment (small plastic and cardboard houses, cardboard tube, paper sizzle nest material; Datesand Ltd, Manchester, UK). The mice were weaned at P21.

7.1.2.1 GENOTYPING

Ear notches were used to identify mice within a litter and the tissue collected was used to genotype the animal. The tissue was digested at 55ºC in 100 µl of Tissue Lysis Solution (90µl tail buffer + 10µl of Proteinase K) per sample for 3 hr, followed by vortexing and inactivation of the proteinase K at 95ºC for 15 min. Samples were centrifuged for 5min at 4ºC at 14000RPM. 5µl of the sample was transferred into a new tube containing 45µl deionised water and kept on ice before being included in the PCR mix (**Table 7-1**).

Each sample was used to test for both the *Sox14* wild-type gene and the Cre or Gfp transgene using the primers in **Table 7-2**. Thus, the *Sox14* WT Forward primer was used with either the *Sox14* WT reverse, *Sox14* Gfp reverse or *Sox14* Cre reverse primers.

Table 7-1 Master PCR Mix (1 reaction)

Products	*Volume*
My Taq 2x (Bioline)	12.5 µl
Forward Primer	0.5 µl
Reverse Primer	0.5 µl
$H_2O_{deionised}$	8.5 µl
DNA sample	3µl
Total	25µl

Table 7-2 Genotyping primer sets

Primer	**5' to 3' sequence**
Sox14 Wildtype Forward	ATTACCTAGCCACTTAATCCC
Sox14 Wildtype Reverse	CATGAAGGCATTCATGGGCC
Sox14 Gfp Reverse	TGGCCGTTTACGTCGCCGTC
Sox14 Cre Reverse	CATCGACCGGTAATGCAGGC

PCR program =

95°C for 15 min

35 cycles of:

Denature	95°C for 40 s
Anneal	60°C for 30 s
Extend	72°C for 40 s
Final extension	72°C for 10 min (if desired)

The samples were run on a 1% agarose electrophoresis gels with 5% of SYBR-safe (Sigma-Aldrich) were prepared in 1X TBE buffer. 5-10μL of PCR samples were loaded into each well and 150 mV current was applied through the gel during 15 to 30 min, before the gel was analysed under ultraviolet lights.

7.1.3 BRDU INJECTION

Wildtype C57BL/6 dams were mated with heterozygous Sox14 Gfp/+ males. 5-Bromo-2'-deoxyuridine (BrdU, Sigma, B5002) was administered intraperitoneally was administered to pregnant mice (0.2mg/g) at timepoints during gestation between days 10.5 and 18.5, estimated from the occurrence of a vaginal plug (9am of the day that a vaginal plug was detected was designated GD0.5). Dams were allowed to deliver naturally and litters from injected mice were were perfused on postnatal day seven. Only Gfp heterozygous mice were used for analysis. The BrdU is incorporated into newly formed DNA from the stage of injection as a synthetic analogue of the nucleoside Thymidine. Cells that were still undergoing cell division and therefore incorporating BrdU into newly synthesised DNA after the time of injection was visualised by staining against BrdU.

7.2 ADENOASSOCIATED VIRUSES

7.2.1 PRODUCING AAVS IN THE LAB

Over the course of my PhD, I worked with others in the Delogu lab to optimisee the production of AAVs in the lab. This gives us the freedom to produce a vast range of AAVs from bought or cloned plasmids. A list of the AAVs used throughout this thesis is found in **Table 7-3**.

Table 7-3 Plasmids used in AAV production

Plasmid	*Source*
pAAV serotype 2/1	Roska lab
pHGTIadeno1 helper	Roska lab
pAAV-EF1a-DIO-mGFP	Roska lab
pAAV-EF1a-DIO-tdTom	Roska lab
pAAV-flex-taCasp3-TEVp	(Addgene plasmid # 45580)
pAAV-mCherry-flex-dtA	(Addgene plasmid # 58536)

In order to ensure that the AAVs would induce the conditional expression of transgenes, I made my own AAV viruses using plasmids bought on Addgene.

Figure 3–3 shows the work flow of AAV production carried out in the lab. The plasmids were grown in 5 ml starter culture for 5-6 hr in a 15 ml tube containing Leuria Bertini (LB) broth (Sigma) containing 100x Ampicillin. Then the cultures were transferred to 300 ml LB (with 100x Ampicillin) in 1 litre flask and incubated at 37°C overnight, shaking at 213 rpm. DNA was purified from cultures using

QIAfilter Plasmid Maxi Kit (Qiagen) and the purified stock was a quantified on Nanodrop. The purified plasmid was stored at -20°C.

Though there are several protocols on AAV production in the literature which vary in the methods for HEK297T cell transfection (Huang et al., 2013) and viral purification (by using a heparin affinity column, for example) (Grieger et al., 2006; Guo et al., 2012), we decided to follow and optimise a protocol from the Roska lab (FMI, Dr Botond Roska, FMI, Basel), which was used to produce AAVs that have been previously used in the Delogu lab. This method was adopted as it has been shown to yield a higher viral recovery compared to using CsCl for purification.

7.2.1.1 TRANSFECTION OF HEK293T CELLS

The HEK293T cells were maintained in DMEM (Dulbecco's Modified Eagle Medium) (Sigma Lifesciences, 1000 mg/L glucose) containing 10% FBS, 1% Pen/Strep, Sodium Pyruvate and 1% L-Glut at 37 °C in a humidified atmosphere containing 5% CO_2. The cells were passaged at regular intervals on attaining 80-90% confluence, by washing with 1x PBS and dissociating with Trypsin EDTA by incubating with trypsin for 3-4 min. The cells were collected, pelleted by centrifugation and re-suspended in 10 ml medium. The cells were passaged at least 3 times before expanding them for transfection.

One confluent 10cm plate was split onto x3 15 cm plates. 16-24 hr prior to transfection confluent HEK293T cells were passaged at a ratio of ~1:4 onto 10x 15 cm plates so that at the time of transfection, the cells were at 80% confluency.

Plasmids used to co-transfect (1) Vector, pAAV (70µg) carrying the expression cassette flanked by the viral ITRs bought from Addgene. The full list of pAAVs are found in **Table 7-3**; (2) a packaging plasmid (70µg) carrying the serotype 2/1 AAV rep and cap genes; and (3) a helper plasmid (200µg) carrying the adenovirus helper functions was a gift from Basel.

HEK293T cells were co-transfected using linear polyethylenimine (PEI) assisted transfection. A 4:1 (v:w) ratio of DNA to transfection reagent was maintained. The DNA mix was added to 50 ml of pre-warmed serum-free DMEM and mixed. The PEI was added dropwise and mixed gently, then incubated for 15 min at RT. 5 ml transfection mixture was added drop-wise to each culture plate. 60 hr post-transfection, the cells were harvested by centrifugation at 1500 rpm for 5 min into a pellet. The collected cell pellet was stored at -80°C.

7.2.1.2 PURIFICATION OF AAV

The collected cell pellet was re-suspended in 15 ml lysis buffer (150mM NaCl, 20 mM Tris pH 8.0, filter sterilised and stored at 4°C). The virus was subjected to freeze-thaw cycles, 3 times between dry ice/100% EtOH bath and a 37°C water bath. To this, 15µl of 1M $MgCl_2$ and 15µl Benzonase were added and the mix was incubated at 37°C for 30 min to dissolve the DNA or protein aggregates. The cell debris is then centrifuged at 4000 rpm, 4°C for 20 min. This is further purified by Iodixanol method of purification. Specific Iodixanol gradients were prepared using OptiPrep Density Gradient medium (Sigma-Aldrich), found in **Table 7-4**.

Table 7-4 Preparation of iodixanol concentrations

Iodixanol Gradients	17%	25%	40%	60%
10x PBS	5 ml	5 ml	5 ml	-
1M MgCl2	0.05 ml	0.05 ml	0.05 ml	0.05 ml
1M KCl	0.125 ml	0.125 ml	0.125 ml	0.125 ml
5M NaCl	10 ml	-	-	
OptiPrep (Iodixanol)	12.5 ml	20 ml	33.3 ml	50 ml
0.5%phenol red	-	0.1 ml	-	0.025 ml
H2O	Up to 50 ml	Up to 50 ml	Up to 50 ml	-

In a 36 ml OptiSeal tube (Beckman Coulter no.337922), the gradients are formed by adding from the bottom, first 60 % Iodixanol solution, then 40% solution, then 25% solution and then 17% solution, 5 ml of each. This was done using the needle and syringe for injecting the different solutions and then the viral lysate was added on the top of the gradients. The tubes were seal capped and ultracentrifuged for 90 min at 50,000 rpm (Sorvall WX ultra 90 fitted with 70Ti rotor) at 16°C. After that, the viral fraction was harvested. The virus is present in 40% fraction. A 21 gauge needle was inserted 2 mm below intersection of 60% and 40% fractions layers. Most of the 40% fraction was collected avoiding any of the 25% layer. It amounted to roughly 4 ml of liquid, which was then made up to 15 ml by adding 1xPBS and transferred into a pre-wetted Millipore Amicon 100K columns. This was centrifuged for 30 min at 3500 rpm at 4°C. This step removes the Iodixanol and concentrates the virus. After the first centrifuge, the bottom fraction was removed and the top again filled with 15 ml of 1xPBS. This is repeated three times. After the last spin, the virus solution was aliquoted and stored at -80°C.

7.2.2 ASSESSING THE QUALITY OF AAVS

The end goal for the produced AAVs is to infect Cre-expressing *Sox14*$^{+}$ neurons *in vivo*, but this was not possible for me to determine as it required a known number of isolated Cre-expressing neurons in culture to assess the extent of the infection. The AAV was tested in the following ways *in vitro* to check that the virus was present and viable. However, neither of method measures how well the AAV will infect the cerebellar nuclei.

In order to ensure that the transfection of the AAV production plasmids into the HEK293T cells was successful, another plate of the HEK293T cells were transfected with constitutive GFP expression plasmid in parallel as a positive control, using the same PEI as the transfection reagent. The plate was then checked for GFP signal before the virus production HEK293T cells were collected. Although this is not an ideal control, as it does not replicate a triple plasmid transfection, I made sure that an equivalent weight of plasmid was transfected. This plate was also similar in confluence at the time of transfection so that it could be used as a measure of cell health and survival.

Primary neuronal Cre-expressing cells were cultured by using *Sox14*$^{Cre/+}$ brain tissue in primary culture, as described in 7.6. The cells were cultured onto poly-d-lycine coated coverslips, then infected with AAV.

7.2.2.1 PRODUCTION OF CRE-EXPRESSING CELLS BY G418 SELECTION

Since many of the produced AAVs are Cre-dependent, I decided to develop a compatible Cre-expressing HEK293 cell line to test the rAAVs. The Cre-Neo plasmid has Neomycin resistance and can thus be selected for with application of G418 (geneticin), which is an analogue of neomycin that is specific for the eukaryotic ribosome. The product of the neo gene, neomycin phosphotransferase, inhibits the toxic activity of the G418, while all cells that have not been transfected with the plasmid will die.

HEK293 cells were plated in a 10cm plate at the seeding density of $5x10^6$ cells. After 24 hr, 15 µg of Cre-Neo plasmid was transfected using PEI as described above. The transfected HEK293 cells were plated onto 24-well plates, alongside non-transfected control cells. Serial dilutions of G418 were prepared in DMEM (10% FBS, 1% Pen/Strep, Sodium Pyruvate and 1% L-Glu) and 0.8 ml of each dilution was added to the HEK293 cells in the 24-well plate. The G418 was changed every four days for 3 weeks.

In order to verify the proportion of HEK293 cells that express Cre in the surviving population after G418 selection, cells were transfected with Cre-dependent AAV plasmid, pAAV-flex-DIO-TdTomato, every week whilst they were under G418 selection. As a positive control, non Cre-dependent constitutive GFP plasmid was transfected to check the efficiency of transfection and estimate the number of cells that were potentially transfected.

7.2.2.2 QUANTIFICATION OF AAV TITRE

Establishing titers of the viral products is crucial for expedient use of the products since testing the product in animals is inefficient. It is, however, worth noting that the efficacy of infection of AAV serotypes also vary in terms of the animal species and area of the CNS being targeted (Holehonnur et al., 2014; Wang et al., 2003). The titer of the lab-produced AAV was determined since it is important to ensure that the virus will be efficiently transduced and to maintain consistency between experiments.

The titre of the AAV produced was also calculated using qPCR. Initially, I used a kit from Clontech (Takada), but since this was not cost-effective, I generated a similar protocol by designing primers for the AAV ITR region (F: 5'-GTCTTGTAAATGCGGGCCAA-3', R: 5'- ACTCCATCGCATAAAACCCC-3'). The titre of the AAVs measured using my method yielded similar results compared to the kit that was purchased. In order to calculate the titre, a known control was used to create a standard curve. The standard was made by amplifying the DNA of a pAAV using the same primer set. The amplified DNA was measured using nanodrop. From this, the copy number and titre (vg/ml) can be determined using the following formulae:

Copy number= e^((Ct-b)/a)

where a = the coefficient of x on the standard curve

b = the y-intercept on the standard curve

Ct = the threshold cycle of the AAV being titred.

Vg/ml = Copy number/µl x 1000

The qPCR measures the Ct value for a certain sequence of DNA within the primers to be amplified, relative to the known standard.

The AAVs titres are shown in **Table 7-5**.

Table 7-5 Titres of the AAVs used

AAV	*vg/ml*	*Source*
AAV-EF1a-DIO-membraneGFP	5.9 x10^{13}	Delogu Lab
AAV-EF1a-DIO-tdTomato	1.6 x10^{9}	Delogu Lab
AAV-flex-taCasp3-TEVp	1.2 x10^{10}	Delogu Lab
AAV-EF1a-Flex-TVA-Cherry	6.7 x10^{9}	Delogu Lab
AAV-EF1a-Flex-TVA-Cherry	6.0 x10^{12}	VC North Carolina

7.3 MOUSE SURGICAL TECHNIQUES

7.3.1 STEREOTAXIC INJECTION

A list of injections is shown in **Table 7-6**. P14 $Sox14^{Cre/+}$ mice were injected in the cerebellar nuclei with approximately 500nl of AAV viruses for all experiments. P19 $Sox14^{Gfp/+}$ mice were injected in the inferior olive and in the contralateral oculomotor nuclei with approximately 100nl of Red and Green Retrograde Beads (Lumafluor).

Table 7-6 Injection paradigms and replicates.

CN= cerebellar nuclei, IO = Inferior olive, OMN = oculomotor nucleus

Injection paradigm			Age at injection	Age analysed	*n*
Mouse line	Injectate	Target			
$Sox14^{Cre/+}$	AAV-EF1α-DIO-mGFP	unilateral CN	P14	P28	14
$Sox14^{Cre/+}$	AAV-EF1α-DIO-mGFP	bilateral CN	P14	P28	2
$Sox14^{Cre/+}$	AAV-EF1α-DIO-mGFP AAV-EF1α-DIO-tdTom	left CN right CN	P14	P28	7
$Sox14^{Gfp/+}$	Red RetroBeads Green RetroBeads	ipsilateral OMN Contralateral IO	P19	P21	1
$Sox14^{Gfp/+}$	Green RetroBeads Red RetroBeads	ipsilateral OMN Contralateral IO	P19	P21	4
$Sox14^{Gfp/+}$	Red RetroBeads	Contralateral IO	P19	P21	1
$Sox14^{Gfp/+}$	Green RetroBeads	ipsilateral OMN	P19	P21	1
$Sox14^{Gfp/+}$	Green RetroBeads	Contralateral IO	P19	P21	1
$Sox14^{Cre/+}$	AAV-flex-taCasp3-TEVp + AAV-EF1α-DIO-tdTom	unilateral CN	P14	adult	4
$Sox14^{Cre/+}$	AAV-flex-taCasp3-TEVp + AAV-EF1α-DIO-tdTom	bilateral CN	P14	adult	2
$Sox14^{Cre/+}$	AAV-EF1α-DIO-tdTom	bilateral CN	P14	adult	1
$Sox14^{Cre/+}$	AAV-EF1a-Flex-TVA-Cherry	bilateral CN	P14	P28	5
$Sox14^{+/+}$	AAV-EF1a-Flex-TVA-Cherry	bilateral CN	P14	P28	3
$Sox14^{Cre/+}$	AAV-EF1a-Flex-TVA-Cherry	bilateral CN	P14	adult	16
$Sox14^{+/+}$	AAV-EF1a-Flex-TVA-Cherry	bilateral CN	P14	adult	12
$Sox14^{Cre/+}$	AAV-EF1α-DIO-tdTom	bilateral CN	P14	adult	4
$Sox14^{+/+}$	AAV-EF1α-DIO-tdTom	bilateral CN	P14	adult	8

Stereotaxic coordinates in early postnatal mice were approximated from adult stereotaxic coordinates and then refined through successive trials. The final coordinates are shown in **Table 7-7**. <1µl fast green dye was injected in each experiment. The mouse was immediately sacrificed by decapitation whilst still under anaesthesia. The brains were dissected and the injection site was then compared to a brain atlas. The coordinates were also checked before each experiment with a wildtype littermate to account for any inter-litter changes since each litter may be born at different times of day and at early postnatal stages, the growth of the mouse is rapid.

Table 7-7 Coordinates from lambda, where x is the mediolateral axis, y is the rostrocaudal axis and z is the dorsoventral axis.

	x ***(relative to midline)***	**y** ***(relative to lambda)***	**z** ***(relative to lambda)***
Cerebellar nuclei	±2.00mm	−1.60mm	−4.00mm
Oculomotor nucleus	±0.10mm	+0.10mm	−2.50mm
Inferior olive	±0.10mm	−1.90mm	−5.00mm

The procedure was performed with under anaesthesia with isoflurane gas. Full anaesthesia was maintained throughout the procedure. The depth of anesthesia was assessed before manipulating the animals by pinching the paw without any responses. Animals were placed in a stereotaxic frame (World Precision Instruments), and the fixture of the head position was assessed before starting the surgery. Body temperature was kept at 37-38 ºC using a heating pad.

Incision was made with a scalpel blade on the top of the head and the surface of the skull was cleaned with cotton buds and physiological serum. Sometimes, the neck

muscles are gently detached from the occipital bone to allow better access to the cerebellum during injections. The skull was aligned with respect to the position of bregma and lambda references. The skull was leveled and a glass was used to bore a small hole in the skull over the injection location. A borosilicate glass capillary needle previously loaded with injectate was gently lowered in the brain at the proper coordinates. After waiting few seconds to allow the tissue to relax from the constraints applied during the going down, the injection was performed manually using IM-11-2 Pneumatic Microinjector (Narishige, Japan). The needle was left in position for 8min before slowly raising the needle to prevent the injectate from flowing up the injection tract. The wound was cleans with sterile PBS and the closed up using minimal amounts of Vetbond (3M). The mouse was allowed to recover in a warm recovery chamber until conscious, then returned to its mother, and closely monitored for 5 days.

7.4 MOUSE BEHAVIOURAL STUDIES

7.4.1 ROTAROD

Motor learning and coordination were assessed using a Rota-Rod 47600 testing device (Ugo Basile, Milan, Italy). Mice were tested over 3 days, with 24h between the sessions; on each day, mice underwent 3 trials, with 1h intervals between them. On each trial the rod was set to accelerate from 2rpm to 40rpm over 300s. Latency to fall was measured as the time from the start of the acceleration of the rod to the point the mouse fell onto the sensor below the rod. If the mouse clung to the rod to rotate around with it more than 3 consecutive rotations instead of falling, this was also deemed the end of the trial, since this implies an inability to maintain locomotion at that speed. Very infrequently, a mouse jumped off the ladder during the trail. Since this is independent of locomotive inability, the mouse was

immediately put back on the ladder to continue the trial. Across the trials, increasing latencies are indicative of improving performance and thus of motor learning if there was retention of long latencies.

7.4.2 ERASMUS LADDER

The Erasmus Ladder v1.1 (Noldus, Netherlands) was used to assess both locomotive performance and associative motor learning capabilities of mice. It consists of a horizontal ladder in between two goal boxes, all of which is fully automated. The ladder has 2 x 37 rungs for the left and right side, which are separated 2 mm apart. The rungs are 12 mm long and 3 mm in diameter, and the distance between two rungs on one side is 15 mm, with alternate rungs in a descended position, so as to create an alternating stepping pattern with 30 mm gaps. Every crossing of the ladder from one side to the other is considered one trial. Each rung is equipped with touch sensors, which are activated when subject to a pressure corresponding to more than 4 grams. Using the feedback from the sensors, the the position and the walking pattern of the mouse are continuously recorded. Along with the ladder the computer software operates in a fixed cycle of 2 ms for prediction and also stores data. The goal boxes are equipped with two pressurised air outlets to prevent premature departure and to provide a tail-wind to encourage the mouse not to pause on the ladder.

Each mouse was tested over 10 days, with 4 days training to cross the ladder without obstacles, followed by 2 days of rest, and another 4 days of the associative motor learning paradigm. Each day, 42 trials were performed consecutively for each mouse with intervals for resting in the goal boxes between each trial, which were randomly

assigned between 9 and 11secs. The goal boxes and ladder were thoroughly cleaned between each mouse.

For the associative motor learning paradigm, a third set of rungs (12 at one side, 13 at the other), whose default position is lowered, were employed as obstacles. Based on the prediction of the position of the mouse and the speed of walking, an obstacle rung can be raised by a high-speed pneumatic slide. This perturbation acts as an unconditioned stimulus (US). A 90 dB, 2 kHz tone lasting by default 250 ms, was used as a conditioned stimulus (CS).

7.5 SAMPLE COLLECTION

For adult brain tissue collection, mice were anaesthetised with 0.6 ml/kg of pentobarbital sodium 20% w/v i.p. (Pentoject) administered intraperitoneally and subsequently transcardially perfused with saline and 4% PFA through the left cardiac ventricle. Brains were post-fixed overnight in 4% PFA at 4°C, and subsequently washed three times at RT on a shaker for 15min each.

For brains that were used for *in situ* hybridization, the brains were allowed to be post-fixed for 36 hr in 4% PFA at 4°C. The PBS and sucrose solutions were treated with 0.1% v/v diethylpyrocarbonate (DEPC) overnight, and then autoclaved to remove the DEPC.

For embryonic brain tissue collection, the embryos were collected into ice cold PBS, then checked under a fluorescent stereoscope in order to identify the $Sox14^{Gfp/+}$ heterozygous mice. The $Sox14^{+/+}$ embryos were discarded. The whole brain (for

E13.5-E14.5) or hindbrain (for E15.5- E18.5) was dissected before fixation by immersion in 4% PFA at 4°C. E10.5-E12.5 embryos were fixed with the head intact. Fixation lasted between 1 hr (E12.5) and 1hr 40 min (E18.5), or up to 6 hr for "long-fixed" brains to be used for *in situ* hybridization.

For the BrdU experiments, dams were allowed to deliver naturally and litters from injected mice were were perfused on postnatal day seven with 4% PFA as above. Only $Sox14^{Gfp/+}$ heterozygous mice were used for analysis.

All brains were successively equilibrated with 10% sucrose (Sigma) in PBS for 1 hr, then 20% sucrose in PBS for 1 hr and finally 30% sucrose in PBS overnight at 4°C. They were perfused with OCT compound (VWR) then embedded into moulds in OCT, orientated, and frozen by floating on liquid nitrogen or in a bed of dry ice. The blocks were then stored at -80°C.

7.6 PRIMARY CELL CULTURE TECHNIQUES

7.6.1 COVERSLIP PREPARATION

The 13mm diameter glass coverslips were placed in a glass petri dish containing 1M HCl for two hr. The HCl was then aspirated and the coverslips were rinsed with sterile water twice. The coverslips were washed with 70% EtOH for one hr followed by another one hr wash in 100% EtOH. The EtOH was completely aspirated, then rinsed briefly with 100% EtOH and completely aspirated again. The petri dish was then covered with foil and incubated in an oven, overnight at 180°C.

The following day, the coverslips were placed in the culture plates with washed side facing up and coated with poly-D-Lysine (0.2 mg/ml) by adding 0.8 ml of poly-D-Lysine to each well. The plate was placed in cell culture incubator overnight at 37°C, 5% CO_2. On the day of primary culture preparation, the poly-D-Lysine was completely aspirated, and each well was rinsed three times with 0.8 ml of Milli-Q water. The coverslips were then left in the cell culture hood to air-dry for 2 hr.

7.6.2 PRIMARY CELL CULTURE

Sox14$^{Cre/+}$ or *Sox14*$^{Gfp/+}$ mice pups were sacrificed at P0 by numbing on ice and decapitation. The cerebellum was dissected out immediately in ice cold sterile PBS and transferred into ice-cold HEPES buffer. In the tissue culture hood, HEPES buffer was removed and the tissue was cut into very small chunks using sterile forceps before being disintegrated using 3 ml warmed papain mix (papain, EDTA, DNAse, Neurobasal, L-cysteine). Neurobasal medium (Neurobasal+ B27+ Pen/Strep+ Glutamax). After 15-20 min of incubation at 37°C, the individual cells were separated by gentle trituration (10 times in 45 seconds) using specially prepared fire-polished pipette tips. The suspension was then allowed to settle for a min for the multi-cellular clumps to fall down. The top 2 ml was collected into a fresh tube to obtain the single cell suspension. 2 ml of fresh neurobasal medium was added to the original cell mix and the trituration, settlement and collection process was repeated 3 times. Collected cells were then centrifuged for 2 min at 1100 rpm. The supernatant was discarded and the cell pellet was re-suspended in 5 ml of Neurobasal medium. The centrifugation process was repeated and cell pellet re-suspended in 3 ml of medium.

7.6.3 CELL COUNTING

Cell counts were used to estimate the number of cells per ml of the cell suspension. 10µl of cell suspension was mixed with 10µl of Trypan blue dye. 10µl of this mix was then loaded on haematocytometer and the cell count obtained by following formula:

$$\text{Number of cells/ml} = \frac{\text{number of cells counted in the squares} \times \text{dilution Factor} \times 10^4}{\text{Number of total squares counted}}$$

The cells were then seeded on 13mm coverslips at a density of $2x10^5$ cells per well and incubated at 37°C. After an hr the medium was replaced with fresh neurobasal medium.

7.6.4 PRIMARY CELL FIXATION

4% Sucrose, 4% FA in PBS was warmed to 37˚C and 0.7 ml was added to each empty well. The coverslip was transferred into the prepared wells, cells facing up and left to fix at RT for 10min. The wells were washed three times with 1xPBS for 2 min each using a shaker. A secondary fixation was performed in 100% MeOH for 10 min on ice. The wells were washed three times with 1xPBS for 2 min each using a shaker.

7.7 STAINING TECHNIQUES

7.7.1 IMMUNOCHEMISTRY

The primary and secondary antibodies used are shown in **Table 7-8** and **Table 7-9**. A list of solutions used is found in Appendix A.

7.7.1.1 IHC ON FLOATING SECTIONS

Frozen brains were sectioned using a cryostat (Leica CM1830). Embedded blocks were placed in the cryostat chamber for 30 min to raise their temperature prior to mounting on cryostat chuck using OCT compound. 60 µm sections were cut using with the cryostat and collected into PBS. The sections were washed in PBS for 15 min x3 at RT to remove the OCT and the sections were used immediately or kept at 4°C for up to a week.

The sections were selected and placed onto a 12 well plate with maximum 5 sections/well. The sections were blocked in IHC Block solution in 300µl/well for 2 hr at room temperature (RT). The blocking solution was also used as a diluent for the next steps. The sections were then incubated with 300µl/well primary antibody in diluent overnight at 4°C. The antibody was washed in PBSTr for 20min x4 at RT on a shaker. The sections were then incubated with 300µl/well secondary antibody in diluent for 1-2hr at RT. The antibody was washed in PBSTr for 20min x4 at RT on a shaker.

7.7.1.2 IHC ON CRYOSTAT TISSUE SECTIONS

20µm sections were cut using with the cryostat and collected on SuperFrost® Plus slides (VWR). The slides were left to air-dry for 30min before storage at -80°C. Slides were taken out and thawed for 30min at RT, then washed in PBS for 20min x3 to remove trace OCT. The slides were blocked in 400µl/slide IHC Block Solution for 2hr at RT. The blocking solution was also used as a diluent for the next steps. The sections were then incubated with 300µl/slide primary antibody in diluent overnight at 4°C. The antibody was washed in PBSTr for 20min x4 at RT on a shaker. The sections were then incubated with 300µl/slide secondary antibody in diluent for 1-2hr at RT. The antibody was washed in PBSTr for 20min x4 at RT on a shaker.

7.7.1.3 BRDU STAINING

For neurogenesis studies by BrdU/GFP double labelling, 60-80 µm floating sections were cut into PBS and washed with PBS at RT. This was followed by denaturation with 1M HCl in H_2O at 45˚C for 30 min, neutralization with 3 washes of PBS for 10 min. Sections were then blocked in Primary Cell staining Block for 1 hr at RT, and probed with rat anti-BrdU and chicken anti-GFP primary antibodies at 4°C for 24-48hr, followed by Goat Alexa-568 anti-rat and Alexa-488 anti-chicken secondary antibodies.

7.7.1.4 PRIMARY CELL STAINING

The coverslips were placed into a well to incubate in 0.7 ml Primary Cell staining Block for 1hr at RT. The blocking solution was also used as a diluent for the next steps. The sections were then incubated with 0.7 ml primary antibody in diluent

overnight at 4°C. The antibody was washed in PBS for 5 min x3 at RT on a shaker. The sections were then incubated with 0.7 ml secondary antibody in 0.1% Triton-X in PBS for 2 hr at RT. The antibody was washed in PBSTr for 10 min x3 at RT on a shaker.

Table 7-8 Primary Antibodies

Species	Target protein	Dilution	Company
Chicken	GFP	1:10000	Abcam ab13970
Rabbit	GABA	1:2000	Sigma-Aldrich, A2052
Rabbit	PValb	1:400	Abcam ab11427
Mouse	Calb1	1:400	
Rabbit	Calb2	1:200	Abcam ab702
Mouse	Map2	1:300	
Rabbit	dsRed	1:200	Clontech
Guinea-Pig	Lhx9	1:2000	with thanks to Jane Dodd (Columbia University)
Mouse	Lhx1/5	1:20	Developmental Studies Hybridoma Bank
Chicken	Pax6	1:100	Developmental Studies Hybridoma Bank
Rat	BrdU	1:500	Bio-Rad OBT0030CX

Table 7-9 Secondary Antibodies

Species	Target species	Fluorophore	Dilution	Company
Goat	Chicken	AlexaFluor488	1:500	Invitrogen A11039
Goat	Rabbit	AlexaFluor568	1:500	Invitrogen
Goat	Mouse	AlexaFluor568	1:500	Invitrogen
Goat	Mouse	AlexaFluor633	1:500	Invitrogen A21052
Goat	Guinea-Pig	AlexaFluor633	1:500	Invitrogen
Goat	Chicken	AlexaFluor568	1:500	Invitrogen
Goat	Rat	AlexaFluor568	1:500	Invitrogen

7.7.2 IN SITU HYBRIDISATION

Bacteria and RNase on work surfaces and equipment can cause problems with experiments concerning RNA and DNA. Particularly, RNase can degrade RNA, while contaminating bacteria can amplify non-specific PCR products. To prevent these problems, the bench and routinely used equipment, such as the pipettes, were regularly cleaned with 70% v/v EtOH. Milli-Q water (Millipore) or RNase-free water were used in all reagents for the following molecular biology protocols. Where RNase-free water was not supplied in prepared kits and the protocol was involved RNA, Milli-Q water was autoclaved with 0.1% diethylpyrocarbonate (DEPC) (Sigma). DEPC treatment was also used to prepare RNase-free sucrose solution for cryoprotection of brains that were used in *in situ* hybridisation. All glassware and plastic-ware were autoclaved or sterile (new in manufacturer-certified packaging) prior to use.

DNA *in situ* plasmids (**Table 7-10**) were linearised with the appropriate restriction enzyme (Roche) by incubating 5 µg DNA with 5 µl of enzyme in a 50 µl volume with the appropriate concentration of buffer for 1 hr at 37°C. Linearised DNA was purified using Phenol-Chloroform Extraction. Alternatively, the DNA fragment was amplified using PCR and M13 forward and reverse primers. 1 µg of linearised DNA, or 250 ng of PCR product was then mixed with 1µl of the appropriate RNA polymerase (Roche) in a 20 µl volume with 1x transcription buffer (Roche), 0.5 µl RNase inhibitor (Roche) and either 1x DIG RNA labelling mix (Roche) or 1x fluorescein RNA labelling mix (Roche). Reaction was incubated for 3 hr at 37°C before adding 2 µl of DNaseI RNAse free (Roche) and incubating for a further 20 min at 37°C. The reaction was made up to a volume of 50 µl using Probe Buffer and purified Illusta Microspin G50 Columns (GE Healthcare).

The riboprobe was diluted in 1:10 ddH2O and checked on a 1% agarose electrophoresis gel with 5% of SYBR-safe (Sigma-Aldrich), prepared in 1X TBE buffer, alongside 5 µl of 1kb ladder. RNA concentration was quantified using a Nanodrop.

Slides were taken out and thawed for 30min at RT, then washed in DEPC treated PBS for 20 min x3 to remove trace OCT. The riboprobe was diluted to around 1µg/ml in hybridization buffer and denatured at 70°C of 5 min. 200 µl/slide of the probe mix was added (after slides were dried around the sections with tissue) and a coverslip placed on top. Hybridization with riboprobes was carried out overnight at

65°C in a sealed box containing paper wetted with ISH washing solution. Slides were washed once for 15 min (to remove coverslips) and twice for 30 min at 65°C with prewarmed ISH washing solution followed by three 10min washes at RT with MATB. Slides, dried with tissue, were then covered with 400 µl/slide filtered ISH blocking solution for 1hr at RT. Block was removed and replaced with 250-400 µl filtered blocking solution with 1:2000 Anti-DIG or anti-FITC AP-conjugated antibodies (Roche) overnight at 4°C in a humidified box. Slides were washed in MABT for 20 min x4 and then washed in NTMT pH9.5 (for NBT/BCIP substrate) or in Tris pH8.2 (for Fast Red substrate) for 10 min. Color reaction was performed using 20 µl/ml NBT/BCIP substrate developed in NTMT pH9.5 or 1 Fast Red tablet dissolved in 2 ml Tris pH8.2. The colour reaction was developed in a dark, humidified box and, when complete, slides were washed twice for 10min with 0.25% Triton-X +2 mM EDTA in PBS to terminate the reaction, then washed in PBS.

For double-ISH, the first AP-conjugated antibody was removed from the section by incubating in 5 mM EDTA/PBS at 70°C for 10 min, followed by a wash in PBS at RT for 15 min. Slides were washed in MABT for 20 min and blocked a second time. The process was repeated as above for the second colour reaction. Following ISH, sections were immunoreacted against GFP for 48 hr at 4 °C for all *Sox14*$^{Gfp/+}$ sections.

Table 7-10 Riboprobes

Gene	IMAGE ID	Restriction enzyme for linearisation	Polymerase for transcription
Gad1	5358787	SalI	T7
Gad2	4482097	NotI	T7
Calb1	1972495	EcoRI	T7
Calb2	4527074	SalI	T7
PValb	4925213	SalI	T7
Lhx9	6825043	EcoRI	T3
Tbr1	6825394	Sal1	T7

7.8 IMAGING

7.8.1 MOUNTING

Nuclear counterstain was achieved with 1:5000 4,6-diamino-2- phenylidone (DAPI) in PBS for 15 min at RT. Slides were mounted with Prolong Gold Anti-fade mounting medium (Thermofisher) (Invitrogen). RetroBead experiments were mounted using Fluoromount. The slides were left to cure for at least overnight at RT before imaging and sealed with nail varnish.

7.8.2 MICROSCOPY

Low power digital images of flat-mounted or dissected brains were acquired on a stereomicroscope (Leica MZFLIII) equipped with epifluorescence. General overview images were acquired using an upright microscope (ZEISS Axio Imager

2), taken at 4x, 10x and 20x. It was also equipped with the Zeiss ApoTome for images taken at 100x. High power images and z-stacks of thick sections were acquired with a spinning disk confocal microscope (Nikon Eclipse Ti Inverted) or laser scanning confocal microscopes (Olympus Fluoview AX70, Eclipse Ni-E Upright, Nikon), taken at 20X, 40x and 100x magnification.
Images were acquired using the following software: Zeiss AxioVision, Olympus Fluoview 300, and Nikon NIS Elements, then processed with FIJI (https://fiji.sc/), Photoshop CS5.1 and Illustrator CS6 (Adobe).

7.9 ANALYSIS

7.9.1 CELL COUNTING

For counting the proportion of of co-expression of immunoreactivity, the "cell counter" plugin in ImageJ was used to manually label each cell in an image. The numbers were averaged across different sections and different brains.
To measure the approximate size of cell soma, the selection tools were used to draw around the cell soma. The "Measure" tool was set to measure the area of the selection as well as the "Fit ellipse" measurement, which reports the major and minor axis of the best fitting ellipse as the minimum and maximum diameters of the selected area. The average measurements are underestimates of the true soma size since measurements will often be above or below the maximum girth of the ellipsoid soma.

The number of cells reactive for *Gad1* was counted for the ablation experiment was automated. In order to count the cells within the different sub-regions of the

cerebellar nuclei, regions of interest (ROI) were drawn and saved for each image. I wrote a macro code (Appendix B) in order to make the process more efficient, which opened each image, allowed me to draw the ROIs, rename the ROIs to correspond with the nuclei and saved it in a specified directory.

The count was performed using the “Find Maxima…” function in ImageJ, using a second macro that I wrote to automate the count (Appendix C). The resulting excel file produces a table of the ROIs and number of cells detected in each, while a flattened image with each detected cell is saved to check for errors in the counting. If a particular image had a severe miscount (over or under estimate of the number of cells), the threshold was adjusted.

7.9.2 BEHAVIOURAL STATISTICS

Statistics and charts were created using Prism 7 software (GraphPad). For normally distributed results, the student’s t-test and two-way ANOVA with Bonferroni's multiple comparisons test were conducted and charts present the mean ± standard error of the mean. For non-parametric data, the Mann-Whitney U test was used to test if the independent sham and experimental groups have the same distribution and the charts present the median with 95% confidence limit.

APPENDIX A

Table 7-11 Common Solutions

PBS	(pH = 7.4 from PBS tablets, Sigma-Aldrich)
PFA 4%	paraformaldehyde (Sigma) in PBS.
PBSTr	PBS with 0.3% Triton-X 100 (VWR)
PBTw	PBS with 0.1% Tween-20 (Sigma).
Tris-HCL	Trizma base, minimum (Sigma) in ddH_2O. pH to desired pH with 2M HCl. Autoclave.
5x MAB	pH7.5 500mM maleic acid (Sigma), 750mM NaCl (BDH). pH using 2M NaOH. Autoclave.
MABT	1xMAB with 0.1% Tween-20 (Sigma).
20x SSC	(pH 4.5) 3M NaCl (BDH), 0.3M sodium citrate (Fisher Scientific). pH using 5M citric acid. Autoclave.
Hybridisation buffer	50% formamide (Sigma), 5x SSC (pH4.5), 2% SDS (Sigma), 2% BBR.
ISH block	2% Boehringer Blocking Reagent (BBR) (Roche), 20% heat-inactivated sheep Serum in MABT (filtered with Whatman filter paper for use on cryostat section)
ISH washing solution	1x SSC, 50% formamide, 0.1% tween-20
NTMT pH9.5	100mM NaCl, 100mM Tris pH9.5, 0.1% tween-20
Tris pH8.2	100mM Tris pH8.2, 0.1% Tween-20
IHC Block	7% normal goat serum (NGS) (Sigma-Aldrich), 0.3% Triton-X in PBS
Tail buffer	100 mM Tris-HCl (pH 8.0) – 50ml of 1M 5mM EDTA – 5ml of 0.5M 200mM NaCl – 20ml of 5M SDS 5ml of 10% Deionized water 420 ml
Primary Cell staining Fixative	4% Sucrose, 4% FA in PBS
Primary Cell staining Block	2% New Goat Serum, 0.3% Triton-X, in PBS

APPENDIX B

```
macro "draw ROIs, rename and save"

roiManager("Select", 0);
roiManager("Rename", "Med");
roiManager("Select", 1);
roiManager("Rename", "IntP");
roiManager("Select", 2);
roiManager("Rename", "IntA");
roiManager("Select", 3);
roiManager("Rename", "IntDL");
roiManager("Select", 4);
roiManager("Rename", "Lat");
roiManager("Select", 5);
roiManager("Rename", "LatPC");
roiManager("Deselect");
name = getInfo("image.filename")

roiManager("Save", "/Users/Documents/PhD docs/Gad 1/Counting/"+name+".zip");
roiManager("delete")
 close();
    //closes main image window
                        if (isOpen("Exception")) {
                              selectWindow("Exception");
                              run("Close");          //close error windows to avoid saving
to results.
                              }
```

APPENDIX C

```
macro "Scale image and count within ROIs and save measurements and flattened
image"
{
	run("Set Measurements...", "area mean min integrated limit display
redirect=None decimal=3");
	dir1 = getDirectory("Choose an Image Directory ");
	dir2 = getDirectory("Choose an ROI file Directory");
	dir3 = getDirectory("Choose an Results Directory");
	setBatchMode(false);

	list = getFileList(dir1);
	list2 = getFileList(dir2);
	  for (i=0; i<list.length; i++) {
		path = dir1+list[i];
		showProgress(i, list.length);
		open(path);
		//loading ROIs here
			path2 = dir2+list2[i];
			roiManager("Open", path2);
	run("Scale...", "x=0.25 y=0.25 width=1020 height=768 interpolation=Bilinear
create");
// Iterate all ROIs in ROI Manager
  for (j=0; j<roiManager("count"); ++j) {
	roiManager("Select", j);
	// Scale ROI
	run("Scale... ", "x=0.25 y=0.25");
	// Replace old ROI with scaled one
	roiManager("update")
	run("Find Maxima...", "noise=25 output=Count light");
	}
// select all ROI and image the point selections within
			count=roiManager("count");
			array=newArray(count);
			  for(a=0; a<count;a++) {
			  array[a] = a;
			  }
	roiManager("Select", array);
	roiManager("Combine");
	run("Find Maxima...", "noise=25 output=Count light");
	run("Find Maxima...", "noise=25 output=[Point Selection] light");
	run("Flatten");
```

```
// save image in results file
        = dir3;
        filename = File.getName(dir1+list[i]);
        saveAs("Tiff",path3+filename+"_"+"countimage.xls");
        roiManager("reset")
        run("Close All");
//closes all image windows
                        if (isOpen("Exception")) {
                            selectWindow("Exception");
                            run("Close");
//close error windows to avoid saving to results.
                            }
    }
    dir1name = File.getName(dir1);
saveAs("Results", path3+dir1name+"_"+"Results.xls");
run("Clear Results");
    if (isOpen("Results")) {
        selectWindow("Results");
        run("Close");
    }
}
```

APPENDIX D

INJECTION OF AAV-FLEX-TACASP3-TEVP

The AAV-flex-taCasp3-TEVp encodes a pro-caspase 3 protein and a tobacco etch virus protease (TEVp). The TEVp cleaves the pro-caspase to induce apoptosis in *Cre*-expressing cells (Gray et al., 2010; Yang et al., 2013). As a pilot study, I injected the AAV into the lateral nuclei at P14:

♀ unilateral AAV-Casp3 n=4

♂ bilateral AAV-Casp3: n=2

♂ bilateral Sham: n=1.

PILOT BEHAVIOURAL TESTS

The mice were tested at 6 weeks post-birth. I took advantage of the trial injections to also familiarise myself with the behavioural tests that were available to me to study motor phenotypes and and other gross phenotypic functions:

1) gross phenotype assessment was made using the SHIRPA tests

2) balance was assessed using the balance beam

3) general gait was assessed by paw printing analysis

4) motor coordination and learning the Rotarod.

The SHIRPA is a protocol made up of three stages of screening, designed to comprehensively test a variety of motor, sensory and autonomic functions (Rogers et al., 1997). The mice showed no deficits throughout the whole battery of tests,

including those that test general ambulation, posture, grip strength and wire manoeuvre. No defects were observed on the balance beam tasks.

Gait was tested using the paw printing analysis. Non-toxic paint was used to mark the forepaws in pink and hindpaws in black, as described in Heck et al. (2008). The stride lengths and stride widths were measured between both forepaw and hindpaw steps. **Figure 1** shows that while the overlap in forepaw and hind paw is consistent in the sham, this was not the case for some of the mice injected with AAV-Casp3 unilaterally. There was also variation in the stride lengths, but this may be due to differences in anxiety leading to faster pace and longer strides.

There was variation in the results for the Rotarod (**Figure 2**). As expected, the sham displayed prolonged latency to fall each subsequent trial, exhibiting motor learning skills in order to stay on the accelerating rod. By the third day, it was able to remain for the entire course of the trial (300s). For the mice injected with AAV-Casp3, the latencies displayed by each mouse were highly variable. This suggests that while the mouse had the general motor coordination skills to remain on the apparatus, there does not seem to be acquisition of learned motor skills to score consistent latencies.

Figure 1 Gait analysis using paw printing.

The gait pattern of the sham animal is shown on the left, while the gait patterns of two animals injected with AAV-Casp3 unilaterally are on the right. The forepaw steps are in pink, and the hindpaw steps are in black. The green lines represent the forepaw stride length and the purple lines represent the hindpaw stride length. The orange lines represent the forepaw stride width and the blue lines represent the hindpaw stride width.

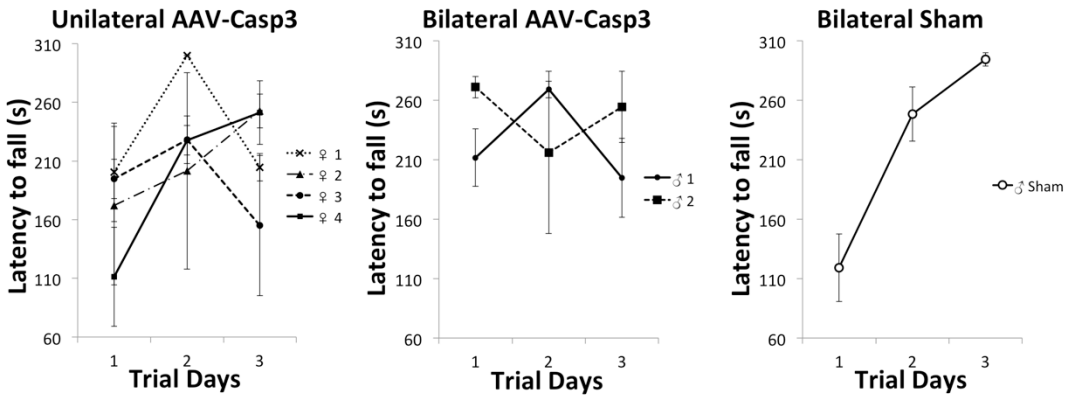

Figure 2 Rotarod latencies

The left chart shows latencies for 4 mice injected with AAV-Casp3 on one side, while the middle chart shows latencies for 2 mice injected with AAV-Casp3 on both sides. The right chart shows latencies for a mouse injected with AAV-mGFP as a sham injection on both sides.

ASSESSMENT OF ABLATION

Following the behavioural tests, the sections were analysed by counting of *Gad1*$^+$ cells in the lateral nuclei, assuming that the numbers correlate with the true number of *Sox14*$^+$ neurons. Representative sections were counted by taking every 6 sections across the cerebellum. From the results, it would appear that only one brain suffered significant cell loss in the lateral cerebellar nucleus (**Figure 3**). **Figure 3** shows *Gad1 in situ* hybridization in the rostral lateral cerebellar nuclei on both sides of two mice injected unilaterally with AAV-Casp3. The number of *Sox14*$^+$ cells, approximated by *Gad1 in situ* hybridization labelling, in ♀2 do not differ between the two sides, suggesting that the injection was not correctly targeted. However, while the right side lateral nucleus of ♀3 has similar numbers of *Gad1*$^+$ cells as ♀2, the left side shows significantly fewer cells. The individual plots of the Rotarod latencies for each mouse is shown on the right and they appear to correlate. The ablation observed in ♀3 correlates with shorter latencies. Thus it is possible to effectively ablate the *Sox14*$^+$ cells using AAVs.

Figure 4 shows the dorsal medulla of ♀4 compared to the sham. The right side medial vestibular nucleus (MVe) has fewer *Gad1*$^{+}$ cells, but no loss of Gad1 labelling was seen in the cerebellar nuclei. This highlights the potential limitations of the ablation method, which requires specific targeting in order for surrounding Sox14^{+} cells not to be affected.

Considering the gait patterns in **Figure 2**, the uneven fore/hindpaw overlap between left and right sides in ♀4 may be the result of the ablation in medial vestibular nucleus. The vestibular nuclei are involved in postural control. The gait pattern for ♀3 shows that the stride width is shorter in the forepaws compared to the hindpaws. It is not known what the basis of this change is.

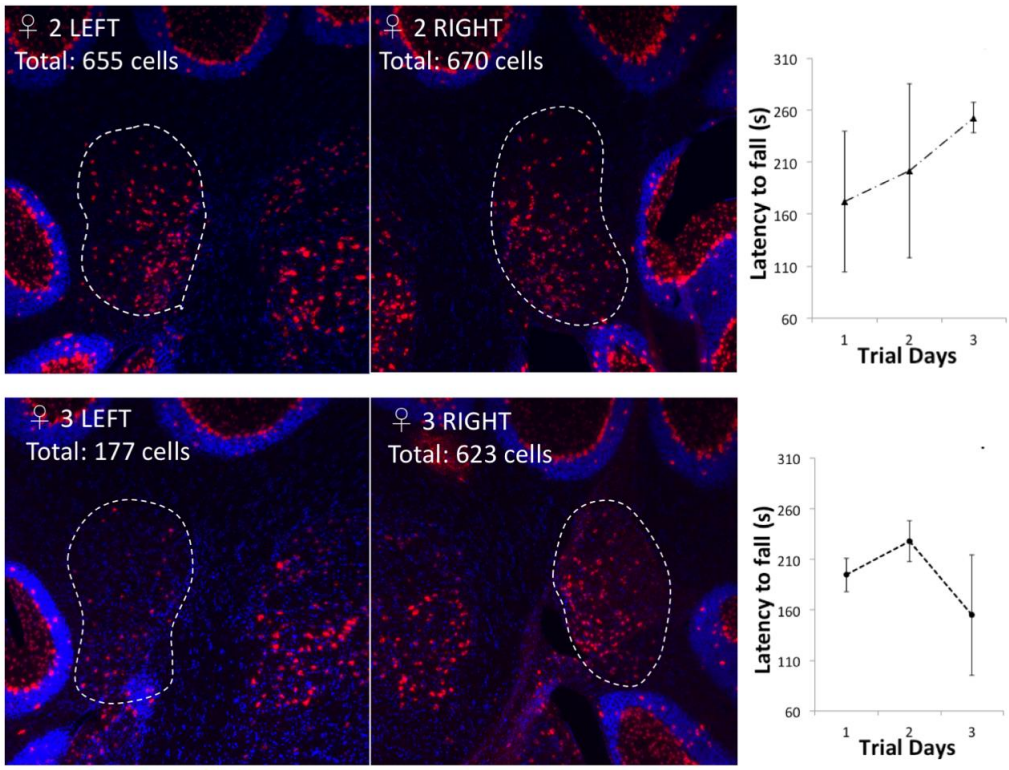

Figure 3 Gad1 in situ hybridization labelling in ♀2 (top row) and ♀3 (bottom row), along with the Rotarod performance of each mouse. *Fewer Gad1 labelled cells are observed in the left lateral nucleus of ♀3 mouse. This is associated with a worse Rotarod performance. Mean ± SEM.*

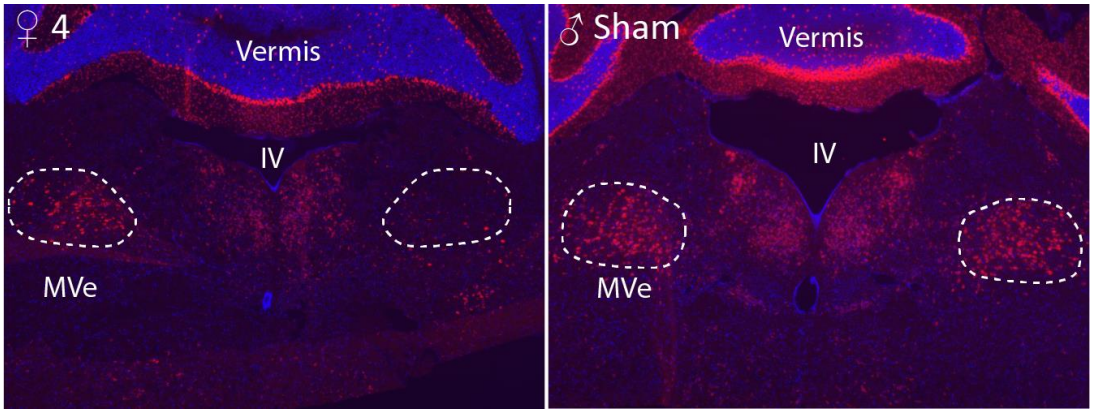

Figure 4 Gad1 in situ hybridization labelling in ♀4 (left) and sham (right). *Fewer Gad1 labelled cells are observed in the right medial vestibular nucleus of ♀4 mouse.*

BIBLIOGRAPHY

Achim, K., Salminen, M., and Partanen, J. (2014). Mechanisms regulating GABAergic neuron development. *Cellular and Molecular Life Sciences* **71**(8), 1395-1415.

Aizenman, C.D., Huang, E.J., and Linden, D.J. (2003). Morphological correlates of intrinsic electrical excitability in neurons of the deep cerebellar nuclei. *Journal of neurophysiology* **89**(4), 1738-1747.

Albus, J.S. (1971). A theory of cerebellar function. *Mathematical Biosciences* **10**(1-2), 25-61.

Alcantara, S., Ruiz, M., De Castro, F., Soriano, E., and Sotelo, C. (2000). Netrin 1 acts as an attractive or as a repulsive cue for distinct migrating neurons during the development of the cerebellar system. *Development* **127**(7), 1359-1372.

Altman, J., and Bayer, S.A. (1978). Prenatal development of the cerebellar system in the rat. I. Cytogenesis and histogenesis of the deep nuclei and the cortex of the cerebellum. *Journal of Comparative Neurology* **179**(1), 23-48.

Altman, J., and Bayer, S.A. (1985). Embryonic development of the rat cerebellum. II. Translocation and regional distribution of the deep neurons. *Journal of Comparative Neurology* **231**(1), 27-41.

Andersson, G., Garwicz, M., and Hesslow, G. (1988). Evidence for a GABA-mediated cerebellar inhibition of the inferior olive in the cat. *Experimental brain research* **72**(3), 450-456.

Angaut, P., and Cicirata, F. (1982). Cerebello-olivary projections in the rat. *Brain, behavior and evolution* **21**(1), 24-33.

Angevine, J., and Sidman, R.L. (1961). Autoradiographic study of cell migration during histogenesis of cerebral cortex in the mouse. *Nature* **192**(4804), 766-768.

Apps, R. (1999). Movement-related gating of climbing fibre input to cerebellar cortical zones. *Progress in neurobiology* **57**(5), 537-562.

Apps, R., and Garwicz, M. (2000). Precise matching of olivo-cortical divergence and cortico-nuclear convergence between somatotopically corresponding areas in the medial C1 and medial C3 zones of the paravermal cerebellum. *European Journal of Neuroscience* **12**(1), 205-214.

Apps, R., and Garwicz, M. (2005). Anatomical and physiological foundations of cerebellar information processing. *Nature reviews. Neuroscience* **6**(4), 297.

Apps, R., and Hawkes, R. (2009). Cerebellar cortical organization: a one-map hypothesis. *Nature Reviews Neuroscience* **10**(9), 670-681.

Apps, R., and Ruigrok, T.J.H. (2007). A fluorescence-based double retrograde tracer strategy for charting central neuronal connections. *Nat Protoc* **2**(8), 1862-1868.

Arends, J.J., and Zeigler, H.P. (1991). Organization of the cerebellum in the pigeon (Columba livia): II. Projections of the cerebellar nuclei. *J Comp Neurol* **306**(2), 245-272.

Armstrong, D., and Edgley, S. (1984a). Discharges of nucleus interpositus neurones during locomotion in the cat. *The Journal of physiology* **351**, 411.

Armstrong, D., and Edgley, S. (1984b). Discharges of Purkinje cells in the paravermal part of the cerebellar anterior lobe during locomotion in the cat. *The Journal of Physiology* **352**, 403.

Aschauer, D.F., Kreuz, S., and Rumpel, S. (2013). Analysis of transduction efficiency, tropism and axonal transport of AAV serotypes 1, 2, 5, 6, 8 and 9 in the mouse brain. *PloS one* **8**(9), e76310.

Awapara, J., Landua, A.J., Fuerst, R., and Seale, B. (1950). Free γ-aminobutyric acid in brain. *Journal of Biological Chemistry* **187**, 35-39.

Bagnall, M.W., Zingg, B., Sakatos, A., Moghadam, S.H., Zeilhofer, H.U., and du Lac, S. (2009). Glycinergic projection neurons of the cerebellum. *The Journal of Neuroscience* **29**(32), 10104-10110.

Ban, M., and Ohno, T. (1977). Projection of cerebellar nuclear neurones to the inferior olive by descending collaterals of ascending fibres. *Brain Res* **133**(1), 156-161.

Bastianelli, E. (2003). Distribution of calcium-binding proteins in the cerebellum. *The Cerebellum* **2**(4), 242-262.

Batini, C., Compoint, C., Buisseret‐Delmas, C., Daniel, H., and Guegan, M. (1992). Cerebellar nuclei and the nucleocortical projections in the rat: retrograde tracing coupled to GABA and glutamate immunohistochemistry. *Journal of Comparative Neurology* **315**(1), 74-84.

Bäurle, J., and Grüsser‐Cornehls, U. (1997). Differential number of glycine‐and GABA‐immunopositive neurons and terminals in the deep cerebellar nuclei of normal and Purkinje cell degeneration mutant mice. *Journal of Comparative Neurology* **382**(4), 443-458.

Bazzigaluppi, P., Ruigrok, T., Saisan, P., De Zeeuw, C.I., and De Jeu, M. (2012). Properties of the nucleo-olivary pathway: an in vivo whole-cell patch clamp study. *PLoS One* **7**(9), e46360.

Belecky-Adams, T., Cook, B., and Adler, R. (1996). Correlations between Terminal Mitosis and Differentiated Fate of Retinal Precursor Cellsin Vivoandin Vitro: Analysis with the "Window-Labeling" Technique. *Developmental biology* **178**(2), 304-315.

Bellamy, T.C. (2006). Interactions between Purkinje neurones and Bergmann glia. *The Cerebellum* **5**(2), 116-126.

Ben-Arie, N., Bellen, H.J., Armstrong, D.L., McCall, A.E., Gordadze, P.R., Guo, Q., Matzuk, M.M., and Zoghbi, H.Y. (1997). Math1 is essential for genesis of cerebellar granule neurons. *Nature* **390**(6656), 169-172.

Bengtsson, F., and Hesslow, G. (2006). Cerebellar control of the inferior olive. *The cerebellum* **5**(1), 7-14.

Bengtsson, F., and Hesslow, G. (2013). *Feedback Control in the Olivo-Cerebellar Loop*.

Bentivoglio, M., Kuypers, H., Catsman-Berrevoets, C., Loewe, H., and Dann, O. (1980). Two new fluorescent retrograde neuronal tracers which are transported over long distances. *Neuroscience letters* **18**(1), 25-30.

Best, A.R., and Regehr, W.G. (2009). Inhibitory regulation of electrically coupled neurons in the inferior olive is mediated by asynchronous release of GABA. *Neuron* **62**(4), 555-565.

Betley, J.N., and Sternson, S.M. (2011). Adeno-associated viral vectors for mapping, monitoring, and manipulating neural circuits. *Human gene therapy* **22**(6), 669-677.

Blenkinsop, T.A., and Lang, E.J. (2006). Block of inferior olive gap junctional coupling decreases Purkinje cell complex spike synchrony and rhythmicity. *Journal of Neuroscience* **26**(6), 1739-1748.

Blenkinsop, T.A., and Lang, E.J. (2011). Synaptic Action of the Olivocerebellar System on Cerebellar Nuclear Spike Activity. *The Journal of Neuroscience* **31**(41), 14708-14720.

Boele, H.-J., Koekkoek, S.K.E., and De Zeeuw, C.I. (2009). Cerebellar and Extracerebellar Involvement in Mouse Eyeblink Conditioning: the ACDC Model. *Frontiers in Cellular Neuroscience* **3**, 19.

Bormann, J. (1988). Electrophysiology of GABA A and GABA B receptor subtypes. *Trends in neurosciences* **11**(3), 112-116.

Bostan, A.C., Dum, R.P., and Strick, P.L. (2010). The basal ganglia communicate with the cerebellum. *Proceedings of the national academy of sciences* **107**(18), 8452-8456.

Bowery, N. (1993). GABAB receptor pharmacology. *Annual review of pharmacology and toxicology* **33**(1), 109-147.

Bradley, D., Ghelarducci, B., and Spyer, K. (1991). The role of the posterior cerebellar vermis in cardiovascular control. *Neuroscience research* **12**(1), 45-56.

Brochu, G., Maler, L., and Hawkes, R. (1990). Zebrin II: a polypeptide antigen expressed selectively by Purkinje cells reveals compartments in rat and fish cerebellum. *Journal of Comparative Neurology* **291**(4), 538-552.

Broussard, D.M., Titley, H.K., Antflick, J., and Hampson, D.R. (2011). Motor learning in the VOR: the cerebellar component. *Experimental brain research* **210**(3-4), 451-463.

Brown, J.T., Chan‐Palay, V., and Palay, S.L. (1977). A study of afferent input to the inferior olivary complex in the rat by retrograde axonal transport of horseradish peroxidase. *Journal of Comparative Neurology* **176**(1), 1-22.

Buckner, R.L. (2013). The cerebellum and cognitive function: 25 years of insight from anatomy and neuroimaging. *Neuron* **80**(3), 807-815.

Buhusi, C.V., and Meck, W.H. (2005). What makes us tick? Functional and neural mechanisms of interval timing. *Nature reviews. Neuroscience* **6**(10), 755.

Buisseret-Delmas, C., and Angaut, P. (1993). The cerebellar olivo-corticonuclear connections in the rat. *Progress in neurobiology* **40**(1), 63-87.

Buisseret-Delmas, C., and Batini, C. (1978). Topology of the pathways to the inferior olive as? study in cat. *Neuroscience letters* **10**(3), 207-214.

Bulfone, A., Martinez, S., Marigo, V., Campanella, M., Basile, A., Quaderi, N., Gattuso, C., Rubenstein, J.L., and Ballabio, A. (1999). Expression pattern of the Tbr2 (Eomesodermin) gene during mouse and chick brain development. *Mechanisms of development* **84**(1), 133-138.

Bulfone, A., Smiga, S.M., Shimamura, K., Peterson, A., Puelles, L., and Rubenstein, J.L. (1995). T-brain-1: a homolog of Brachyury whose expression defines molecularly distinct domains within the cerebral cortex. *Neuron* **15**(1), 63-78.

Burger, C., Gorbatyuk, O.S., Velardo, M.J., Peden, C.S., Williams, P., Zolotukhin, S., Reier, P.J., Mandel, R.J., and Muzyczka, N. (2004). Recombinant AAV viral vectors pseudotyped with viral capsids from serotypes 1, 2, and 5 display differential efficiency and cell tropism after delivery to different regions of the central nervous system. *Mol Ther* **10**.

Butler, A.B., and Hodos, W. (2005). *Comparative vertebrate neuroanatomy: evolution and adaptation* (John Wiley & Sons).

Butts, T., Chaplin, N., and Wingate, R.J. (2011). Can clues from evolution unlock the molecular development of the cerebellum? *Mol Neurobiol* **43**(1), 67-76.

Cajal, S.R. (1911). Histologie du syste me nerveux de I'Homme et des verte be s. *Maloine (Paris)* **2**, 891-942.

Carletti, B., and Rossi, F. (2008). Neurogenesis in the cerebellum. *The Neuroscientist* **14**(1), 91-100.

Cerminara, N.L., and Apps, R. (2011). Behavioural significance of cerebellar modules. *The Cerebellum* **10**(3), 484-494.

Cerminara, N.L., Lang, E.J., Sillitoe, R.V., and Apps, R. (2015). Redefining the cerebellar cortex as an assembly of non-uniform Purkinje cell microcircuits. *Nature Reviews Neuroscience* **16**(2), 79-93.

Chamberlin, N.L., Du, B., de Lacalle, S., and Saper, C.B. (1998). Recombinant adeno-associated virus vector: use for transgene expression and anterograde tract tracing in the CNS. *Brain Res* **793**(1), 169-175.

Chambers, W., and Sprague, J.M. (1955a). Functional localization in the cerebellum. I. Organization in longitudinal cortico - nuclear zones and their contribution to the control of posture, both extrapyramidal and pyramidal. *Journal of Comparative Neurology* **103**(1), 105-129.

Chambers, W.W., and Sprague, J.M. (1955b). Functional localization in the cerebellum: Somatotopic organization in cortex and nuclei. *AMA Archives of Neurology & Psychiatry* **74**(6), 653-680.

Chan-Palay, V. (1973a). Afferent axons and their relations with neurons in the nucleus lateralis of the cerebellum: a light microscopic study. *Zeitschrift fur Anatomie und Entwicklungsgeschichte* **142**(1), 1-21.

Chan-Palay, V. (1973b). Cytology and organization in the nucleus lateralis of the cerebellum: the projections of neurons and their processes into afferent axon bundles. *Zeitschrift fur Anatomie und Entwicklungsgeschichte* **141**(2), 151-159.

Chan-Palay, V. (1973c). A light microscope study of the cytology and organization of neurons in the simple mammalian nucleus lateralis: columns and swirls. *Zeitschrift fur Anatomie und Entwicklungsgeschichte* **141**(2), 125-150.

Chan-Palay, V. (1973d). On the identification of the afferent axon terminals in the nucleus lateralis of the cerebellum. An electron microscope study. *Zeitschrift fur Anatomie und Entwicklungsgeschichte* **142**(2), 149-186.

Chan-Palay, V. (1977). *The cerebellar dentate nucleus* (Springer).

Chen, S., and Hillman, D.E. (1993). Colocalization of neurotransmitters in the deep cerebellar nuclei. *Journal of neurocytology* **22**(2), 81-91.

Chintapalli, V., Wang, J., and Dow, J. (2008). Using Flyatlas to identify better Drosophila models of human disease. *Comparative Biochemistry and Physiology Part A: Molecular & Integrative Physiology* **150**(3), S136-S137.

Chizhikov, V.V., Lindgren, A.G., Currle, D.S., Rose, M.F., Monuki, E.S., and Millen, K.J. (2006). The roof plate regulates cerebellar cell-type specification and proliferation. *Development (Cambridge, England)* **133**(15), 2793-2804.

Chizhikov, V.V., Lindgren, A.G., Mishima, Y., Roberts, R.W., Aldinger, K.A., Miesegaes, G.R., Currle, D.S., Monuki, E.S., and Millen, K.J. (2010). Lmx1a regulates fates and location of cells originating from the cerebellar rhombic lip and telencephalic cortical hem. *Proceedings of the National Academy of Sciences of the United States of America* **107**(23), 10725-10730.

Choi, S.-M. (2016). Movement Disorders Following Cerebrovascular Lesions in Cerebellar Circuits. *Journal of Movement Disorders* **9**(2), 80-88.

Chubb, M.C., and Fuchs, A.F. (1982). Contribution of y group of vestibular nuclei and dentate nucleus of cerebellum to generation of vertical smooth eye movements. *Journal of Neurophysiology* **48**(1), 75-99.

Chung, S., Zhang, Y., Van Der Hoorn, F., and Hawkes, R. (2007). The anatomy of the cerebellar nuclei in the normal and scrambler mouse as revealed by the expression of the microtubule-associated protein kinesin light chain 3. *Brain Res* **1140**, 120-131.

Chung, S.-H., Marzban, H., Aldinger, K., Dixit, R., Millen, K., Schuurmans, C., and Hawkes, R. (2011). Zac1 plays a key role in the development of specific neuronal subsets in the mouse cerebellum. *Neural development* **6**(1), 25.

Chung, S.-H., Marzban, H., and Hawkes, R. (2009). Compartmentation of the cerebellar nuclei of the mouse. *Neuroscience* **161**(1), 123-138.

Clark, G.A., McCormick, D.A., Lavond, D.G., and Thompson, R.F. (1984). Effects of lesions of cerebellar nuclei on conditioned behavioral and hippocampal neuronal responses. *Brain Res* **291**(1), 125-136.

Coffman, K.A., Dum, R.P., and Strick, P.L. (2011). Cerebellar vermis is a target of projections from the motor areas in the cerebral cortex. *Proceedings of the National Academy of Sciences* **108**(38), 16068-16073.

Coulter, C.L., Leech, R.W., Brumback, R.A., and Schaefer, G.B. (1991). Cerebral abnormalities in thanatophoric dysplasia. *Child's Nervous System* **7**(1), 21-26.

Cowan, W.M. (1998). The Emergence of Modern Neuroanatomy and Developmental Neurobiology. *Neuron* **20**(3), 413-426.

Crémazy, F., Berta, P., and Girard, F. (2001). Genome-wide analysis of Sox genes in Drosophila melanogaster. *Mechanisms of development* **109**(2), 371-375.

Cupido, A. (2009). Detecting Cerebellar Phenotypes with the Erasmus Ladder.

Czubayko, U., Sultan, F., Thier, P., and Schwarz, C. (2001). Two Types of Neurons in the Rat Cerebellar Nuclei as Distinguished by Membrane Potentials and Intracellular Fillings. *Journal of Neurophysiology* **85**(5), 2017-2029.

D'Angelo, E., and Casali, S. (2013). Seeking a unified framework for cerebellar function and dysfunction: from circuit operations to cognition. *Frontiers in neural circuits* **6**, 116.

Dastjerdi, F.V., Consalez, G.G., and Hawkes, R. (2012). Pattern formation during development of the embryonic cerebellum. *Frontiers in neuroanatomy* **6**, 10.

De Schutter, E., and Steuber, V. (2009). Patterns and pauses in Purkinje cell simple spike trains: experiments, modeling and theory. *Neuroscience* **162**(3), 816-826.

De Zeeuw, C., Holstege, J., Ruigrok, T., and Voogd, J. (1989). Ultrastructural study of the GABAergic, cerebellar, and mesodiencephalic innervation of the cat medial accessory olive: anterograde tracing combined with immunocytochemistry. *Journal of Comparative Neurology* **284**(1), 12-35.

De Zeeuw, C., Ruigrok, T., Holstege, J., Jansen, H., and Voogd, J. (1990). Intracellular labeling of neurons in the medial accessory olive of the cat: II Ultrastructure of dendritic spines and their GABAergic innervation. *Journal of Comparative Neurology* **300**(4), 478-494.

De Zeeuw, C., Van Alphen, A., Hawkins, R., and Ruigrok, T. (1997). Climbing fibre collaterals contact neurons in the cerebellar nuclei that provide a GABAergic feedback to the inferior olive. *Neuroscience* **80**(4), 981-986.

De Zeeuw, C., Wylie, D., DiGiorgi, P., and Simpson, J. (1994). Projections of individual Purkinje cells of identified zones in the flocculus to the vestibular and cerebellar nuclei in the rabbit. *Journal of Comparative Neurology* **349**(3), 428-447.

De Zeeuw, C.I., and Berrebi, A.S. (1995). Postsynaptic Targets of Purkinje Cell Terminals in the Cerebellar and Vestibular Nuclei of the Rat. *European Journal of Neuroscience* **7**(11), 2322-2333.

De Zeeuw, C.I., Chorev, E., Devor, A., Manor, Y., Van Der Giessen, R.S., De Jeu, M.T., Hoogenraad, C.C., Bijman, J., Ruigrok, T.J.H., French, P., *et al.* (2003). Deformation of Network Connectivity in the Inferior Olive of Connexin 36-Deficient Mice Is Compensated by Morphological and Electrophysiological Changes at the Single Neuron Level. *The Journal of Neuroscience* **23**(11), 4700-4711.

De Zeeuw, C.I., and Ten Brinke, M.M. (2015). Motor learning and the cerebellum. *Cold Spring Harbor perspectives in biology* **7**(9), a021683.

Del Cerro, M., and Swarz, J.R. (1976). Prenatal development of Bergmann glial fibres in rodent cerebellum. *Journal of neurocytology* **5**(6), 669-676.

Delogu, A., Sellers, K., Zagoraiou, L., Bocianowska-Zbrog, A., Mandal, S., Guimera, J., Rubenstein, J.L.R., Sugden, D., Jessell, T., and Lumsden, A. (2012). Subcortical visual shell nuclei targeted by ipRGCs develop from a Sox14 -GABAergic progenitor and require Sox14 to regulate daily activity rhythms. *Neuron* **75**(4), 648-662.

Diño, M.R., and Mugnaini, E. (2008). Distribution and phenotypes of unipolar brush cells in relation to the granule cell system of the rat cochlear nuclear nucleus. *Neuroscience* **154**(1), 29-50.

Dixon, K.J., Hilber, W., Speare, S., Willson, M.L., Bower, A.J., and Sherrard, R.M. (2005). Post-lesion transcommissural olivocerebellar reinnervation improves motor function following unilateral pedunculotomy in the neonatal rat. *Experimental neurology* **196**(2), 254-265.

Dom, R., King, J.S., and Martin, G.F. (1973). Evidence for two direct cerebello-olivary connections. *Brain Res* **57**(2), 498-501.

Dum, R.P., Li, C., and Strick, P.L. (2002). Motor and nonmotor domains in the monkey dentate. *Annals of the New York Academy of Sciences* **978**(1), 289-301.

Dum, R.P., and Strick, P.L. (2003). An unfolded map of the cerebellar dentate nucleus and its projections to the cerebral cortex. *Journal of neurophysiology* **89**(1), 634-639.

Ebbesson, S.O., and Campbell, C. (1973). On the organization of cerebellar efferent pathways in the nurse shark (Ginglymostoma cirratum). *Journal of Comparative Neurology* **152**(3), 233-254.

Elsen, G., Juric-Sekhar, G., Daza, R., and Hevner, R.F. (2013). Development of cerebellar nuclei. In *Handbook of Cerebellum and Cerebellum Disorders*, Manto, M., Gruol, D., Schmahmann, J., Koibuchi, N., and Rossi, F., (eds.) (Heidelberg: Springer), pp. 179-205.

Engelkamp, D., Rashbass, P., Seawright, A., and van Heyningen, V. (1999). Role of Pax6 in development of the cerebellar system. *Development (Cambridge, England)* **126**(16), 3585-3596.

Englund, C., Kowalczyk, T., Daza, R.A., Dagan, A., Lau, C., Rose, M.F., and Hevner, R.F. (2006). Unipolar brush cells of the cerebellum are produced in the rhombic lip and migrate through developing white matter. *The Journal of neuroscience : the official journal of the Society for Neuroscience* **26**(36), 9184-9195.

Erlander, M.G., and Tobin, A.J. (1991). The structural and functional heterogeneity of glutamic acid decarboxylase: a review. *Neurochemical research* **16**(3), 215-226.

Esclapez, M., Tillakaratne, N., Kaufman, D.L., Tobin, A., and Houser, C. (1994). Comparative localization of two forms of glutamic acid decarboxylase and their mRNAs in rat brain supports the concept of functional differences between the forms. *Journal of Neuroscience* **14**(3), 1834-1855.

Ezure, K., and Graf, W. (1984). A quantitative analysis of the spatial organization of the vestibulo-ocular reflexes in lateral-and frontal-eyed animals—II. Neuronal networks underlying vestibulo-oculomotor coordination. *Neuroscience* **12**(1), 95-109.

Fenno, L., Yizhar, O., and Deisseroth, K. (2011). The development and application of optogenetics. *Annual review of neuroscience* **34**.

Fink, A.J., Englund, C., Daza, R.A., Pham, D., Lau, C., Nivison, M., Kowalczyk, T., and Hevner, R.F. (2006). Development of the deep cerebellar nuclei: transcription factors and cell migration from the rhombic lip. *The Journal of neuroscience : the official journal of the Society for Neuroscience* **26**(11), 3066-3076.

Florio, M., Leto, K., Muzio, L., Tinterri, A., Badaloni, A., Croci, L., Zordan, P., Barili, V., Albieri, I., and Guillemot, F. (2012). Neurogenin 2 regulates progenitor cell-cycle progression and Purkinje cell dendritogenesis in cerebellar development. *Development* **139**(13), 2308-2320.

Frederickson, C.J., and Trune, D.R. (1986). Cytoarchitecture and saccular innervation of nucleus Y in the mouse. *The Journal of Comparative Neurology* **252**(3), 302-322.

Fredette, B.J., Adams, J.C., and Mugnaini, E. (1992). GABAergic neurons in the mammalian inferior olive and ventral medulla detected by glutamate decarboxylase immunocytochemistry. *Journal of Comparative Neurology* **321**(4), 501-514.

Fredette, B.J., and Mugnaini, E. (1991). The GABAergic cerebello-olivary projection in the rat. *Anatomy and Embryology* **184**(3), 225-243.

Ganguly, K., Schinder, A.F., Wong, S.T., and Poo, M.-m. (2001). GABA itself promotes the developmental switch of neuronal GABAergic responses from excitation to inhibition. *Cell* **105**(4), 521-532.

Geborek, P., Jörntell, H., and Bengtsson, F. (2012). Stimulation within the cuneate nucleus suppresses synaptic activation of climbing fibers. *Frontiers in Neural Circuits* **6**, 120.

Gellman, R., Gibson, A.R., and Houk, J.C. (1985). Inferior olivary neurons in the awake cat: detection of contact and passive body displacement. *Journal of Neurophysiology* **54**(1), 40-60.

Giaquinta, G., Casabona, A., Smecca, G., Bosco, G., and Perciavalle, V. (1999). Cortical control of cerebellar dentato‐rubral and dentato‐olivary neurons. *Neuroreport* **10**(14), 3009-3013.

Gilthorpe, J.D., Papantoniou, E.K., Chedotal, A., Lumsden, A., and Wingate, R.J. (2002). The migration of cerebellar rhombic lip derivatives. *Development* **129**(20), 4719-4728.

Glasgow, S.M., Henke, R.M., Macdonald, R.J., Wright, C.V., and Johnson, J.E. (2005). Ptf1a determines GABAergic over glutamatergic neuronal cell fate in the spinal cord dorsal horn. *Development (Cambridge, England)* **132**(24), 5461-5469.

Golden, J.A., and Harding, B.N. (2004). *Developmental neuropathology* (ISN Neuropath Press).

Golding, B., Pouchelon, G., Bellone, C., Murthy, S., Di Nardo, A.A., Govindan, S., Ogawa, M., Shimogori, T., Lüscher, C., and Dayer, A. (2014). Retinal input directs the recruitment of inhibitory interneurons into thalamic visual circuits. *Neuron* **81**(5), 1057-1069.

Goodman, D.C., Hallett, R.E., and Welch, R.B. (1963). Patterns of localization in the cerebellar cortico‐nuclear projections of the albino rat. *Journal of Comparative Neurology* **121**(1), 51-67.

Gratzner, H.G. (1982). Monoclonal antibody to 5-bromo-and 5-iododeoxyuridine: a new reagent for detection of DNA replication. *Science* **218**(4571), 474-475.

Gray, D.C., Mahrus, S., and Wells, J.A. (2010). Activation of specific apoptotic caspases with an engineered small-molecule-activated protease. *Cell* **142**(4), 637-646.

Graybiel, A.M., and Hartwieg, E.A. (1974). Some afferent connections of the oculomotor complex in the cat: an experimental study with tracer techniques. *Brain Res* **81**(3), 543-551.

Graybiel, A.M., Nauta, H., Lasek, R., and Nauta, W. (1973). A cerebello-olivary pathway in the cat: an experimental study using autoradiographic tracing techniques. *Brain Res* **58**(1), 205-211.

Green, M.J., Myat, A.M., Emmenegger, B.A., Wechsler-Reya, R.J., Wilson, L.J., and Wingate, R.J. (2014). Independently specified Atoh1 domains define novel developmental compartments in rhombomere 1. *Development (Cambridge, England)* **141**(2), 389-398.

Green, M.J., and Wingate, R.J. (2014). Developmental origins of diversity in cerebellar output nuclei. *Neural development* **9**, 1-8104-8109-8101.

Greif, K.F., Erlander, M.G., Tillakaratne, N.J., and Tobin, A.J. (1991). Postnatal expression of glutamate decarboxylases in developing rat cerebellum. *Neurochemical research* **16**(3), 235-242.

Grieger, J.C., Choi, V.W., and Samulski, R.J. (2006). Production and characterization of adeno-associated viral vectors. *Nat. Protocols* **1**(3), 1412-1428.

Grimaldi, P., Parras, C., Guillemot, F., Rossi, F., and Wassef, M. (2009). Origins and control of the differentiation of inhibitory interneurons and glia in the cerebellum. *Developmental biology* **328**(2), 422-433.

Guo, P., El-Gohary, Y., Prasadan, K., Shiota, C., Xiao, X., Wiersch, J., Paredes, J., Tulachan, S., and Gittes, G.K. (2012). Rapid and simplified purification of recombinant adeno-associated virus. *Journal of Virological Methods* **183**(2), 139-146.

Gutierrez, D.V., Mark, M.D., Masseck, O., Maejima, T., Kuckelsberg, D., Hyde, R.A., Krause, M., Kruse, W., and Herlitze, S. (2011). Optogenetic control of motor coordination by Gi/o protein-coupled vertebrate rhodopsin in cerebellar Purkinje cells. *Journal of Biological Chemistry* **286**(29), 25848-25858.

Hamburger, V., and Hamilton, H.L. (1951). A series of normal stages in the development of the chick embryo. *Journal of Morphology* **88**(1), 49-92.

Harding, B., and Boyd, S. (1991). Intractable seizures from infancy can be associated with dentato-olivary dysplasia. *Journal of the neurological sciences* **104**(2), 157-165.

Hargrave, M., James, K., Nield, K., Toomes, C., Georgas, K., Sullivan, T., Verzijl, H.T.F.M., Oley, C.A., Little, M., and De Jonghe, P. (2000a). Fine mapping of the neurally expressed gene SOX14 to human 3q23, relative to three congenital diseases. *Human genetics* **106**(4), 432-439.

Hargrave, M., James, K., Yamada, T., and Koopman, P. (2000b). Sox14 maps to mouse Chromosome 9 and shows no mutations in the neurological mouse mutants ducky and tippy. *Mammalian Genome* **11**(3), 231-233.

Hargrave, M., Karunaratne, A., Cox, L., Wood, S., Koopman, P., and Yamada, T. (2000c). The HMG Box Transcription Factor Gene< i> Sox14</i> Marks a Novel Subset of Ventral Interneurons and Is Regulated by Sonic Hedgehog. *Developmental biology* **219**(1), 142-153.

Harvey, R., and Napper, R. (1991). Quantitatives studies on the mammalian cerebellum. *Progress in neurobiology* **36**(6), 437-463.

Hashimoto, K., and Kano, M. (2003). Functional differentiation of multiple climbing fiber inputs during synapse elimination in the developing cerebellum. *Neuron* **38**(5), 785-796.

Hashimoto, M., and Hibi, M. (2012). Development and evolution of cerebellar neural circuits. *Development, growth & differentiation* **54**(3), 373-389.

Hashimoto, M., and Mikoshiba, K. (2003). Mediolateral compartmentalization of the cerebellum is determined on the "birth date" of Purkinje cells. *The Journal of neuroscience* **23**(36), 11342-11351.

Hashimoto-Torii, K., Motoyama, J., Hui, C.-C., Kuroiwa, A., Nakafuku, M., and Shimamura, K. (2003). Differential activities of Sonic hedgehog mediated by Gli transcription factors define distinct neuronal subtypes in the dorsal thalamus. *Mechanisms of development* **120**(10), 1097-1111.

Hatten, M.E., and Heintz, N. (1995). Mechanisms of neural patterning and specification in the development cerebellum. *Annual review of neuroscience* **18**(1), 385-408.

Heck, D., Zhao, Y., Roy, S., S LeDoux, M., and Reiter, L. (2008). *Analysis of cerebellar function in Ube3a-deficient mice reveals novel genotype-specific behaviors*, Vol **17**.

Heck, D.H., De Zeeuw, C.I., Jaeger, D., Khodakhah, K., and Person, A.L. (2013). The neuronal code(s) of the cerebellum. *J Neurosci* **33**(45), 17603-17609.

Herreros, I., and Verschure, P.F. (2013). Nucleo-olivary inhibition balances the interaction between the reactive and adaptive layers in motor control. *Neural Networks* **47**, 64-71.

Hesslow, G. (1986). Inhibition of inferior olivary transmission by mesencephalic stimulation in the cat. *Neuroscience letters* **63**(1), 76-80.

Hesslow, G., and Ivarsson, M. (1996). Inhibition of the inferior olive during conditioned responses in the decerebrate ferret. *Experimental brain research* **110**(1), 36-46.

Hevner, R.F. (2005). The cerebral cortex malformation in thanatophoric dysplasia: neuropathology and pathogenesis. *Acta neuropathologica* **110**(3), 208-221.

Highstein, S.M., Partsalis, A., and Arikan, R. (1997). Role of the Y-group of the vestibular nuclei and flocculus of the cerebellum in motor learning of the vertical vestibulo-ocular reflex. *Progress in brain research* **114**, 383-397.

His, W. (1890). Die entwickelung des menschlichen rautenhirns vom ende des ersten bis zum beginn des dritten monats. I. Verlängertes Mark. *Abh. Kön. Sächs. Ges. d. Wiss., Mat. Phys. Kl.* **29**, 1-74.

Hoebeek, F.E., Witter, L., Ruigrok, T.J., and De Zeeuw, C.I. (2010). Differential olivo-cerebellar cortical control of rebound activity in the cerebellar nuclei. *Proceedings of the National Academy of Sciences* **107**(18), 8410-8415.

Holehonnur, R., Luong, J.A., Chaturvedi, D., Ho, A., Lella, S.K., Hosek, M.P., and Ploski, J.E. (2014). Adeno-associated viral serotypes produce differing titers and differentially transduce neurons within the rat basal and lateral amygdala. *BMC Neuroscience* **15**(1), 28.

Honig, M.G., and Hume, R.I. (1989). Dil and diO: versatile fluorescent dyes for neuronal labelling and pathway tracing. *Trends in neurosciences* **12**(9), 333-341.

Hori, K., Cholewa-Waclaw, J., Nakada, Y., Glasgow, S.M., Masui, T., Henke, R.M., Wildner, H., Martarelli, B., Beres, T.M., Epstein, J.A., *et al.* (2008). A nonclassical bHLH–Rbpj transcription factor complex is required for specification of GABAergic neurons independent of Notch signaling. *Genes & Development* **22**(2), 166-178.

Horn, K.M., Pong, M., and Gibson, A.R. (2004). Discharge of inferior olive cells during reaching errors and perturbations. *Brain Res* **996**(2), 148-158.

Horn, K.M., Pong, M., and Gibson, A.R. (2010). Functional relations of cerebellar modules of the cat. *Journal of Neuroscience* **30**(28), 9411-9423.

Hoshino, M. (2012). Neuronal subtype specification in the cerebellum and dorsal hindbrain. *Development, growth & differentiation* **54**(3), 317-326.

Hoshino, M., Nakamura, S., Mori, K., Kawauchi, T., Terao, M., Nishimura, Y.V., Fukuda, A., Fuse, T., Matsuo, N., Sone, M., *et al.* (2005). Ptf1a, a bHLH transcriptional gene, defines GABAergic neuronal fates in cerebellum. *Neuron* **47**(2), 201-213.

Houck, B.D., and Person, A.L. (2014). Cerebellar Loops: A Review of the Nucleocortical Pathway. *The Cerebellum* **13**(3), 378-385.

Huang, X., Hartley, A.-V., Yin, Y., Herskowitz, J.H., Lah, J.J., and Ressler, K.J. (2013). AAV2 production with optimized N/P ratio and PEI-mediated transfection results in low toxicity and high titer for in vitro and in vivo applications. *Journal of virological methods* **193**(2), 270-277.

Husson, Z. (2015). *Glycinergic neurons and inhibitory transmission in the cerebellar nuclei*, (THESIS.DOCTORAL). [Accessed 2016/06/15/].

Husson, Z., Rousseau, C.V., Broll, I., Zeilhofer, H.U., and Dieudonné, S. (2014). Differential GABAergic and glycinergic inputs of inhibitory interneurons and purkinje cells to principal cells of the cerebellar nuclei. *Journal of Neuroscience* **34**(28), 9418-9431.

Ito, M. (2001). Cerebellar long-term depression: characterization, signal transduction, and functional roles. *Physiological reviews* **81**(3), 1143-1195.

Ito, M. (2008). Control of mental activities by internal models in the cerebellum. *Nature Reviews Neuroscience* **9**(4), 304-313.

Ito, M. (2013). Error detection and representation in the olivo-cerebellar system. *Frontiers in neural circuits* **7**.

Ivry, R.B., and Spencer, R.M. (2004). The neural representation of time. *Current opinion in neurobiology* **14**(2), 225-232.

Jager, P., Ye, Z., Yu, X., Zagoraiou, L., Prekop, H.-T., Partanen, J., Jessell, T.M., Wisden, W., Brickley, S.G., and Delogu, A. (2016). Tectal-derived interneurons contribute to phasic and tonic inhibition in the visual thalamus. *Nature communications* **7**, 13579.

Jeong, J.-W., Chugani, D.C., Behen, M.E., Tiwari, V.N., and Chugani, H.T. (2012). Altered white matter structure of the dentatorubrothalamic pathway in children with autistic spectrum disorders. *The Cerebellum* **11**(4), 957-971.

Ji, F., and Obata, K. (1999). Development of the GABA system in organotypic culture of hippocampal and cerebellar slices from a 67-kDa isoform of glutamic acid decarboxylase (GAD67)-deficient mice. *Neuroscience Research* **33**(3), 233-237.

Jinno, S., and Kosaka, T. (2004). Parvalbumin is expressed in glutamatergic and GABAergic corticostriatal pathway in mice. *The Journal of Comparative Neurology* **477**(2), 188-201.

Jones, E.G. (2001). The thalamic matrix and thalamocortical synchrony. *Trends in Neurosciences* **24**(10), 595-601.

Jörntell, H., Bengtsson, F., Schonewille, M., and De Zeeuw, C.I. (2010). Cerebellar molecular layer interneurons–computational properties and roles in learning. *Trends in neurosciences* **33**(11), 524-532.

Joubert, M., Eisenring, J.-J., Robb, J.P., and Andermann, F. (1968). Familial agenesis of the cerebellar vermis: A syndrome of episodic hyperpnea, abnormal eye movements, ataxia and retardation. Paper presented at: *American Academy of Neurology meeting, 1968, Chicago, US; Read in part at the aforementioned conference.* (BC Decker).

Kahn, I., Knoblich, U., Desai, M., Bernstein, J., Graybiel, A., Boyden, E., Buckner, R., and Moore, C. (2013). Optogenetic drive of neocortical pyramidal neurons generates fMRI signals that are correlated with spiking activity. *Brain Res* **1511**, 33-45.

Karlsen, A.E., Hagopian, W.A., Grubin, C.E., Dube, S., Disteche, C.M., Adler, D.A., Bärmeier, H., Mathewes, S., Grant, F.J., and Foster, D. (1991). Cloning and primary

structure of a human islet isoform of glutamic acid decarboxylase from chromosome 10. *Proceedings of the National Academy of Sciences* **88**(19), 8337-8341.

Katz, L., Burkhalter, A., and Dreyer, W. (1984). Fluorescent latex microspheres as a retrograde neuronal marker for in vivo and in vitro studies of visual cortex. *Nature* **310**(5977), 498-500.

Katz, L., and Iarovici, D. (1990). Green fluorescent latex microspheres: a new retrograde tracer. *Neuroscience* **34**(2), 511-520.

Kaufman, D.L., Houser, C.R., and Tobin, A.J. (1991). Two forms of the γ - aminobutyric acid synthetic enzyme glutamate decarboxylase have distinct intraneuronal distributions and cofactor interactions. *Journal of neurochemistry* **56**(2), 720-723.

Kawamura, S., Hattori, S., Higo, S., and Matsuyama, T. (1982). The cerebellar projections to the superior colliculus and pretectum in the cat: An autoradiographic and horseradish peroxidase study. *Neuroscience* **7**(7), 1673-1689.

Kazantsev, V., Nekorkin, V., Makarenko, V., and Llinas, R. (2004). Self-referential phase reset based on inferior olive oscillator dynamics. *Proceedings of the National Academy of Sciences* **101**(52), 18183-18188.

Kebschull, J.M., da Silva, P.G., Reid, A.P., Peikon, I.D., Albeanu, D.F., and Zador, A.M. (2016). High-throughput mapping of single-neuron projections by sequencing of barcoded RNA. *Neuron* **91**(5), 975-987.

Kelly, R.M., and Strick, P.L. (2003). Cerebellar loops with motor cortex and prefrontal cortex of a nonhuman primate. *The Journal of neuroscience : the official journal of the Society for Neuroscience* **23**(23), 8432-8444.

Kim, E.J., Battiste, J., Nakagawa, Y., and Johnson, J.E. (2008). Ascl1 (Mash1) lineage cells contribute to discrete cell populations in CNS architecture. *Molecular and cellular neuroscience* **38**(4), 595-606.

Kim, E.J., Hori, K., Wyckoff, A., Dickel, L.K., Koundakjian, E.J., Goodrich, L.V., and Johnson, J.E. (2011). Spatiotemporal fate map of neurogenin1 (Neurog1) lineages in the mouse central nervous system. *Journal of Comparative Neurology* **519**(7), 1355-1370.

Kim, J.J., Krupa, D.J., and Thompson, R.F. (1998). Inhibitory cerebello-olivary projections and blocking effect in classical conditioning. *Science* **279**(5350), 570-573.

Kipping, J.A., Grodd, W., Kumar, V., Taubert, M., Villringer, A., and Margulies, D.S. (2013). Overlapping and parallel cerebello-cerebral networks contributing to sensorimotor control: an intrinsic functional connectivity study. *NeuroImage* **83**, 837-848.

Kirilly, D., Gu, Y., Huang, Y., Wu, Z., Bashirullah, A., Low, B.C., Kolodkin, A.L., Wang, H., and Yu, F. (2009). A genetic pathway composed of Sox14 and Mical governs severing of dendrites during pruning. *Nat Neurosci* **12**(12), 1497-1505.

Kistler, W., Jeu, M., Elgersma, Y., Giessen, R., Hensbroek, R., Luo, C., Koekkoek, S., Hoogenraad, C., Hamers, F., and Gueldenagel, M. (2002). Analysis of Cx36 knockout does not support tenet that olivary gap junctions are required for complex spike

synchronization and normal motor performance. *Annals of the New York Academy of Sciences* **978**(1), 391-404.

Koekkoek, S.K., Den Ouden, W.L., Perry, G., Highstein, S.M., and De Zeeuw, C.I. (2002). Monitoring kinetic and frequency-domain properties of eyelid responses in mice with magnetic distance measurement technique. *J Neurophysiol* **88**(4), 2124-2133.

Korneliussen, H. (1968). On the morphology and subdivision of the cerebellar nuclei of the rat. *Journal fur Hirnforschung* **10**(2), 109-122.

Krupa, D.J., Thompson, J.K., and Thompson, R.F. (1993). Localization of a memory trace in the mammalian brain. *SCIENCE-NEW YORK THEN WASHINGTON-* **260**, 989-989.

Lampl, I., and Yarom, Y. (1997). Subthreshold oscillations and resonant behavior: two manifestations of the same mechanism. *Neuroscience* **78**(2), 325-341.

Lang, E., Sugihara, I., and Llinás, R. (1996). GABAergic modulation of complex spike activity by the cerebellar nucleoolivary pathway in rat. *Journal of Neurophysiology* **76**(1), 255-275.

Lang, E., Sugihara, I., and Llins, R. (1992). The ability of motor cortex stimulation to evoke vibrissal movements is modulated by a 10 Hz signal arising in the inferior olive. Paper presented at: *Society of Neuroscience Abstracts*.

Lang, E.J. (2001). Organization of olivocerebellar activity in the absence of excitatory glutamatergic input. *Journal of Neuroscience* **21**(5), 1663-1675.

Lang, E.J. (2002). GABAergic and glutamatergic modulation of spontaneous and motor-cortex-evoked complex spike activity. *Journal of Neurophysiology* **87**(4), 1993-2008.

Lang, E.J., Llinás, R., and Sugihara, I. (2006). Isochrony in the olivocerebellar system underlies complex spike synchrony. *The Journal of physiology* **573**(1), 277-279.

Lang, E.J., Sugihara, I., Welsh, J.P., and Llinás, R. (1999). Patterns of spontaneous Purkinje cell complex spike activity in the awake rat. *Journal of Neuroscience* **19**(7), 2728-2739.

Langer, T.P. (1985). Basal interstitial nucleus of the cerebellum: cerebellar nucleus related to the flocculus. *Journal of Comparative Neurology* **235**(1), 38-47.

Lefler, Y., Torben-Nielsen, B., and Yarom, Y. (2013). Oscillatory activity, phase differences, and phase resetting in the inferior olivary nucleus. *Frontiers in systems neuroscience* **7**.

Lefler, Y., Yarom, Y., and Uusisaari, M.Y. (2014). Cerebellar inhibitory input to the inferior olive decreases electrical coupling and blocks subthreshold oscillations. *Neuron* **81**(6), 1389-1400.

Legendre, A., and Courville, J. (1987). Origin and trajectory of the cerebello-olivary projection: an experimental study with radioactive and fluorescent tracers in the cat. *Neuroscience* **21**(3), 877-891.

Leto, K., Carletti, B., Williams, I.M., Magrassi, L., and Rossi, F. (2006). Different types of cerebellar GABAergic interneurons originate from a common pool of multipotent

progenitor cells. *The Journal of neuroscience : the official journal of the Society for Neuroscience* **26**(45), 11682-11694.

Leto, K., Rolando, C., and Rossi, F. (2012). The genesis of cerebellar GABAergic neurons: fate potential and specification mechanisms.

Leznik, E., and Llinás, R. (2005). Role of gap junctions in synchronized neuronal oscillations in the inferior olive. *Journal of neurophysiology* **94**(4), 2447-2456.

Leznik, E., Makarenko, V., and Llinas, R. (2002). Electrotonically mediated oscillatory patterns in neuronal ensembles: an in vitro voltage-dependent dye-imaging study in the inferior olive. *Journal of Neuroscience* **22**(7), 2804-2815.

Lidierth, M., and Apps, R. (1990). Gating in the spino‐olivocerebellar pathways to the c1 zone of the cerebellar cortex during locomotion in the cat. *The Journal of physiology* **430**(1), 453-469.

Liu, Z.R., Shi, M., Hu, Z.L., Zheng, M.H., Du, F., Zhao, G., and Ding, Y.Q. (2010). A refined map of early gene expression in the dorsal rhombomere 1 of mouse embryos. *Brain Res Bull*.

Llinas, R. (2014). The olivo-cerebellar system: a key to understanding the functional significance of intrinsic oscillatory brain properties. *Frontiers in Neural Circuits* **7**(96).

Llinás, R. (1974). Motor aspects of cerebellar control. *Physiologist* **17**, 19-46.

Llinás, R. (1991). The noncontinuous nature of movement execution. *Motor control: Concepts and issues*, 223-242.

Llinas, R., Baker, R., and Sotelo, C. (1974). Electrotonic coupling between neurons in cat inferior olive. *Journal of Neurophysiology* **37**(3), 560-571.

Llinás, R., Leznik, E., and Makarenko, V. (2002). On the amazing olivocerebellar system. *Annals of the New York Academy of Sciences* **978**(1), 258-272.

Llinás, R., Walton, K., Hillman, D.E., and Sotelo, C. (1975). Inferior olive: its role in motor learing. *Science* **190**(4220), 1230-1231.

Llinás, R.R. (2011). Cerebellar motor learning versus cerebellar motor timing: the climbing fibre story. *The Journal of physiology* **589**(14), 3423-3432.

Long, C., Grueter, C., Song, K., Qin, S., Qi, X., Kong, Y., Shelton, J., Richardson, J., Zhang, C., and Bassel-Duby, R. (2014). Ataxia and Purkinje cell degeneration in mice lacking the CAMTA1 transcription factor. *Proceedings of the National Academy of Sciences of the United States of America* **111**(31), 11521-11526.

Long, M.A., Deans, M.R., Paul, D.L., and Connors, B.W. (2002). Rhythmicity without Synchrony in the Electrically Uncoupled Inferior Olive. *The Journal of Neuroscience* **22**(24), 10898-10905.

Lu, H., Yang, B., and Jaeger, D. (2016). Cerebellar nuclei neurons show only small excitatory responses to optogenetic olivary stimulation in transgenic mice: in vivo and in vitro studies. *Frontiers in neural circuits* **10**.

Lugaro, E. (1895). Sulla struttura del nucleo dentato del cervelletto nell'uomo. *Monit Zool Ital* **6**, 5-12.

Lundell, T., Zhou, Q., and Doughty, M. (2009). Neurogenin1 expression in cell lineages of the cerebellar cortex in embryonic and postnatal mice. *Developmental Dynamics* **238**(12), 3310-3325.

Macdonald, R.L., and Twyman, R.E. (1991). Biophysical properties and regulation of GABA A receptor channels. Paper presented at: *Seminars in Neuroscience* (Elsevier).

Machold, R., and Fishell, G. (2005). Math1 is expressed in temporally discrete pools of cerebellar rhombic-lip neural progenitors. *Neuron* **48**(1), 17-24.

Maricich, S.M., and Herrup, K. (1999). Pax‐2 expression defines a subset of GABAergic interneurons and their precursors in the developing murine cerebellum. *Journal of neurobiology* **41**(2), 281-294.

Marr, D., and Thach, W.T. (1991). A theory of cerebellar cortex. In *From the Retina to the Neocortex* (Springer), pp. 11-50.

Martin, D.L., and Rimvall, K. (1993). Regulation of γ‐aminobutyric acid synthesis in the brain. *Journal of neurochemistry* **60**(2), 395-407.

Martin, G.F., Henkel, C.K., and King, J.S. (1976). Cerebello-olivary fibers: Their origin, course and distribution in the North American opossum. *Experimental Brain Research* **24**(3), 219-236.

Martinez, S., and Alvarado‐Mallart, R.M. (1989). Rostral Cerebellum Originates from the Caudal Portion of the So‐Called ′Mesencephalic′Vesicle: A Study Using Chick/Quail Chimeras. *European Journal of Neuroscience* **1**(6), 549-560.

Martinez, S., Andreu, A., Mecklenburg, N., and Echevarria, D. (2013). Cellular and molecular basis of cerebellar development. *Frontiers in neuroanatomy* **7**.

Martland, T., Harding, B.N., Morton, R.E., and Young, I. (1997). Dentato-olivary dysplasia in sibs: an autosomal recessive disorder? *Journal of medical genetics* **34**(12), 1021-1023.

Marzban, H., Del Bigio, M.R., Alizadeh, J., Ghavami, S., Zachariah, R.M., and Rastegar, M. (2015). Cellular commitment in the developing cerebellum. *Frontiers in cellular neuroscience* **8**, 450.

Mathis, L., Bonnerot, C., Puelles, L., and Nicolas, J.F. (1997). Retrospective clonal analysis of the cerebellum using genetic laacZ/lacZ mouse mosaics. *Development* **124**(20), 4089-4104.

Mathis, L., and Nicolas, J.-F. (2003). Progressive restriction of cell fates in relation to neuroepithelial cell mingling in the mouse cerebellum. *Developmental Biology* **258**(1), 20-31.

Matsui, A., Yoshida, A.C., Kubota, M., Ogawa, M., and Shimogori, T. (2011). Mouse in utero electroporation: controlled spatiotemporal gene transfection. *Journal of visualized experiments: JoVE*(54).

Matsuno, H., Kudoh, M., Watakabe, A., Yamamori, T., Shigemoto, R., and Nagao, S. (2016). Distribution and Structure of Synapses on Medial Vestibular Nuclear Neurons Targeted by Cerebellar Flocculus Purkinje Cells and Vestibular Nerve in Mice: Light and Electron Microscopy Studies. *PloS one* **11**(10), e0164037.

McCarty, D.M., Young Jr, S.M., and Samulski, R.J. (2004). Integration of adeno-associated virus (AAV) and recombinant AAV vectors. *Annu. Rev. Genet.* **38**, 819-845.

McClellan, K.M., Parker, K.L., and Tobet, S. (2006). Development of the ventromedial nucleus of the hypothalamus. *Frontiers in neuroendocrinology* **27**(2), 193-209.

Mccormick, D.A., Lavond, D.G., Clark, G.A., Kettner, R.E., Rising, C.E., and Thompson, R.F. (1981). The engram found? Role of the cerebellum in classical conditioning of nictitating membrane and eyelid responses. *Bulletin of the Psychonomic Society* **18**(3), 103-105.

McCormick, D.A., Steinmetz, J.E., and Thompson, R.F. (1985). Lesions of the inferior olivary complex cause extinction of the classically conditioned eyeblink response. *Brain Res* **359**(1-2), 120-130.

McCormick, D.A., and Thompson, R.F. (1984). Neuronal responses of the rabbit cerebellum during acquisition and performance of a classically conditioned nictitating membrane-eyelid response. *Journal of Neuroscience* **4**(11), 2811-2822.

McDevitt, C.J., Ebner, T.J., and Bloedel, J.R. (1987a). Changes in the responses of cerebellar nuclear neurons associated with the climbing fiber response of Purkinje cells. *Brain Res* **425**(1), 14-24.

McDevitt, C.J., Ebner, T.J., and Bloedel, J.R. (1987b). Relationships between simultaneously recorded Purkinje cells and nuclear neurons. *Brain Res* **425**(1), 1-13.

Medina, J.F., Nores, W.L., and Mauk, M.D. (2002). Inhibition of climbing fibres is a signal for the extinction of conditioned eyelid responses. *Nature* **416**(6878), 330-333.

Meredith, D.M., Masui, T., Swift, G.H., MacDonald, R.J., and Johnson, J.E. (2009). Multiple Transcriptional Mechanisms Control Ptf1a Levels during Neural Development Including Autoregulation by the PTF1-J Complex. *The Journal of Neuroscience* **29**(36), 11139-11148.

Miale, I.L., and Sidman, R.L. (1961). An autoradiographic analysis of histogenesis in the mouse cerebellum. *Experimental Neurology* **4**(4), 277-296.

Middleton, F.A., and Strick, P.L. (1994). Anatomical evidence for cerebellar and basal ganglia involvement in higher cognitive function. *Science (New York, N.Y.)* **266**(5184), 458-461.

Middleton, F.A., and Strick, P.L. (2001). Cerebellar projections to the prefrontal cortex of the primate. *The Journal of neuroscience : the official journal of the Society for Neuroscience* **21**(2), 700-712.

Millen, K.J., and Gleeson, J.G. (2008). Cerebellar development and disease. *Curr Opin Neurobiol* **18**(1), 12-19.

Millen, K.J., Steshina, E.Y., Iskusnykh, I.Y., and Chizhikov, V.V. (2014). Transformation of the cerebellum into more ventral brainstem fates causes cerebellar agenesis in the absence of Ptf1a function. *Proc Natl Acad Sci U S A.*

Miller, E., Blaser, S., Shannon, P., and Widjaja, E. (2009). Brain and bone abnormalities of thanatophoric dwarfism. *American Journal of Roentgenology* **192**(1), 48-51.

Miller, M.W., and Nowakowski, R. (1988). Use of bromodeoxyuridine-immunohistochemistry to examine the proliferation, migration and time of origin of cells in the central nervous system. *Brain Res* **457**(1), 44-52.

Millet, S., Bloch-Gallego, E., Simeone, A., and Alvarado-Mallart, R.M. (1996). The caudal limit of Otx2 gene expression as a marker of the midbrain/hindbrain boundary: a study using in situ hybridisation and chick/quail homotopic grafts. *Development* **122**(12), 3785-3797.

Minaki, Y., Nakatani, T., Mizuhara, E., Inoue, T., and Ono, Y. (2008). Identification of a novel transcriptional corepressor, Corl2, as a cerebellar Purkinje cell-selective marker. *Gene Expr Patterns* **8**(6), 418-423.

Miyata, T., Nakajima, K., Aruga, J., Takahashi, S., Ikenaka, K., Mikoshiba, K., and Ogawa, M. (1996). Distribution of a reeler gene‐related antigen in the developing cerebellum: An immunohistochemical study with an allogeneic antibody CR‐50 on normal and reeler mice. *Journal of Comparative Neurology* **372**(2), 215-228.

Miyata, T., Ono, Y., Okamoto, M., Masaoka, M., Sakakibara, A., Kawaguchi, A., Hashimoto, M., and Ogawa, M. (2010). Migration, early axonogenesis, and Reelin-dependent layer-forming behavior of early/posterior-born Purkinje cells in the developing mouse lateral cerebellum. *Neural development* **5**(1), 23.

Miyoshi, G., Bessho, Y., Yamada, S., and Kageyama, R. (2004). Identification of a novel basic helix-loop-helix gene, Heslike, and its role in GABAergic neurogenesis. *The Journal of neuroscience : the official journal of the Society for Neuroscience* **24**(14), 3672-3682.

Mizuhara, E., Minaki, Y., Nakatani, T., Kumai, M., Inoue, T., Muguruma, K., Sasai, Y., and Ono, Y. (2010). Purkinje cells originate from cerebellar ventricular zone progenitors positive for Neph3 and E-cadherin. *Developmental biology* **338**(2), 202-214.

Morales, D., and Hatten, M.E. (2006). Molecular markers of neuronal progenitors in the embryonic cerebellar anlage. *J Neurosci* **26**(47), 12226-12236.

Morishita, W., and Sastry, B.R. (1996). Postsynaptic mechanisms underlying long-term depression of GABAergic transmission in neurons of the deep cerebellar nuclei. *Journal of Neurophysiology* **76**(1), 59-68.

Morton, S.M., and Bastian, A.J. (2004). Cerebellar control of balance and locomotion. *The Neuroscientist* **10**(3), 247-259.

Moy, S.S., Nadler, J.J., Young, N.B., Perez, A., Holloway, L.P., Barbaro, R.P., Barbaro, J.R., Wilson, L.M., Threadgill, D.W., and Lauder, J.M. (2007). Mouse behavioral tasks relevant to autism: phenotypes of 10 inbred strains. *Behavioural brain research* **176**(1), 4-20.

Mugnaini, E., and Oertel, W.H. (1985). An atlas of the distribution of GABAergic neurons and terminals in the rat CNS as revealed by GAD immunohistochemistry. *Handbook of chemical neuroanatomy* **4**(Part I), 436-622.

Mugnaini, E., Sekerkova, G., and Martina, M. (2011). THE UNIPOLAR BRUSH CELL: A REMARKABLE NEURON FINALLY RECEIVING THE DESERVED ATTENTION. *Brain research reviews* **66**(1-2), 220-245.

Mugnaini, E., Warr, W.B., and Osen, K.K. (1980). Distribution and light microscopic features of granule cells in the cochlear nuclei of cat, rat, and mouse. *Journal of Comparative Neurology* **191**(4), 581-606.

Müller, C.C., Nguyen, T.H., Ahlemeyer, B., Meshram, M., Santrampurwala, N., Cao, S., Sharp, P., Fietz, P.B., Baumgart-Vogt, E., and Crane, D.I. (2011). PEX13 deficiency in mouse brain as a model of Zellweger syndrome: abnormal cerebellum formation, reactive gliosis and oxidative stress. *Disease Models and Mechanisms* **4**(1), 104-119.

Murakami, T., and Morita, Y. (1987). Morphology and distribution of the projection neurons in the cerebellum in a teleost, Sebastiscus marmoratus. *Journal of Comparative Neurology* **256**(4), 607-623.

Najac, M., and Raman, I.M. (2015). Integration of Purkinje cell inhibition by cerebellar nucleo-olivary neurons. *Journal of Neuroscience* **35**(2), 544-549.

Najac, M., and Raman, I.M. (2017). Synaptic excitation by climbing fibre collaterals in the cerebellar nuclei of juvenile and adult mice. *The Journal of Physiology*.

Nakamura, H., Wu, R., Watanabe, K., Onozuka, M., and Itoh, K. (2006). Projections of glutamate decarboxylase positive and negative cerebellar neurons to the pretectum in the cat. *Neuroscience Letters* **403**(1–2), 30-34.

Nakatani, T., Minaki, Y., Kumai, M., and Ono, Y. (2007). Helt determines GABAergic over glutamatergic neuronal fate by repressing Ngn genes in the developing mesencephalon. *Development (Cambridge, England)* **134**(15), 2783-2793.

Namavar, Y., Barth, P.G., and Baas, F. (2011). Classification, diagnosis and potential mechanisms in pontocerebellar hypoplasia. *Orphanet journal of rare diseases* **6**(1), 1.

Nassi, J.J., Cepko, C.L., Born, R.T., and Beier, K.T. (2015). Neuroanatomy goes viral! *Frontiers in Neuroanatomy* **9**(80).

Ngô-Muller, V., and Muneoka, K. (2010). In utero and exo utero surgery on rodent embryos. *Methods in enzymology* **476**, 205-226.

Nilaweera, W.U., Zenitsky, G.D., and Bracha, V. (2006). Inactivation of cerebellar output axons impairs acquisition of conditioned eyeblinks. *Brain Res* **1122**(1), 143-153.

O'hearn, E., and Molliver, M. (1993). Degeneration of Purkinje cells in parasagittal zones of the cerebellar vermis after treatment with ibogaine or harmaline. *Neuroscience* **55**(2), 303-310.

Obana, E.A., Lundell, T.G., Kevin, J.Y., Radomski, K.L., Zhou, Q., and Doughty, M.L. (2015). Neurog1 genetic inducible fate mapping (GIFM) reveals the existence of complex spatiotemporal cyto-architectures in the developing cerebellum. *The Cerebellum* **14**(3), 247-263.

Ohyama, T., Nores, W.L., Medina, J.F., Riusech, F.A., and Mauk, M.D. (2006). Learning-Induced Plasticity in Deep Cerebellar Nucleus. *The Journal of Neuroscience* **26**(49), 12656-12663.

Ohyama, T., Nores, W.L., Murphy, M., and Mauk, M.D. (2003). What the cerebellum computes. *Trends in neurosciences* **26**(4), 222-227.

Olivito, G., Clausi, S., Laghi, F., Tedesco, A.M., Baiocco, R., Mastropasqua, C., Molinari, M., Cercignani, M., Bozzali, M., and Leggio, M. (2016). Resting-State Functional Connectivity Changes Between Dentate Nucleus and Cortical Social Brain Regions in Autism Spectrum Disorders. *The Cerebellum*, 1-10.

Otero, R.A., Sotelo, C., and Alvarado‐Mallart, R.M. (1993). Chick/quail chimeras with partial cerebellar grafts: an analysis of the origin and migration of cerebellar cells. *Journal of Comparative Neurology* **333**(4), 597-615.

Pascual, M., Abasolo, I., Mingorance-Le Meur, A., Martinez, A., Del Rio, J.A., Wright, C.V., Real, F.X., and Soriano, E. (2007). Cerebellar GABAergic progenitors adopt an external granule cell-like phenotype in the absence of Ptf1a transcription factor expression. *Proceedings of the National Academy of Sciences of the United States of America* **104**(12), 5193-5198.

Pasquier, L., Marcorelles, P., Loget, P., Pelluard, F., Carles, D., Perez, M.-J., Bendavid, C., de La Rochebrochard, C., Ferry, M., and David, V. (2009). Rhombencephalosynapsis and related anomalies: a neuropathological study of 40 fetal cases. *Acta neuropathologica* **117**(2), 185-200.

Paxinos, G. (1985). *The Rat Nervous System. Volume 2: Hindbrain and Spinal cord* (Academic Press).

Paxinos, G., and Franklin, K.B. (2004). *The mouse brain in stereotaxic coordinates* (Gulf Professional Publishing).

Person, A.L., and Raman, I.M. (2011). Purkinje neuron synchrony elicits time-locked spiking in the cerebellar nuclei. *Nature* **481**(7382), 502-505.

Person, A.L., and Raman, I.M. (2012a). Purkinje neuron synchrony elicits time-locked spiking in the cerebellar nuclei. *Nature* **481**(7382), 502-505.

Person, A.L., and Raman, I.M. (2012b). Synchrony and neural coding in cerebellar circuits. *Frontiers in neural circuits* **6**, 97.

Phochanukul, N., and Russell, S. (2010). No backbone but lots of Sox: Invertebrate Sox genes. *The international journal of biochemistry & cell biology* **42**(3), 453-464.

Pierce, E.T. (1973). Time of origin of neurons in the brain stem of the mouse. *Progress in brain research* **40**, 53-65.

Pierce, E.T. (1975). Histogenesis of the deep cerebellar nuclei in the mouse: an autoradiographic study. *Brain Res* **95**(2), 503-518.

Pijpers, A., Voogd, J., and Ruigrok, T.J. (2005). Topography of olivo‐cortico‐nuclear modules in the intermediate cerebellum of the rat. *Journal of Comparative Neurology* **492**(2), 193-213.

Pijpers, A., Winkelman, B.H., Bronsing, R., and Ruigrok, T.J. (2008). Selective impairment of the cerebellar C1 module involved in rat hind limb control reduces step-dependent modulation of cutaneous reflexes. *Journal of Neuroscience* **28**(9), 2179-2189.

Powers, J.M., Moser, H.W., Moser, A.B., Upshur, J.K., Bradford, B.F., Pai, S.G., Kohn, P.H., Frias, J., and Tiffany, C. (1985). Fetal cerebrohepatorenal (Zellweger) syndrome: dysmorphic, radiologic, biochemical, and pathologic findings in four affected fetuses. *Human pathology* **16**(6), 610-620.

Prekop, H.-T., Delogu, A., and Wingate, R.J. (2017). Cerebellar Developmental Disorders and Cerebellar Nuclei. In *Development of the Cerebellum from Molecular Aspects to Diseases* (Springer, Cham), pp. 87-104.

Pugh, J.R., and Raman, I.M. (2008). Mechanisms of potentiation of mossy fiber EPSCs in the cerebellar nuclei by coincident synaptic excitation and inhibition. *The Journal of Neuroscience* **28**(42), 10549-10560.

Rasmussen, A., and Hesslow, G. (2014). Feedback control of learning by the cerebello-olivary pathway. *Progress in brain research* **210**, 103-119.

Rasmussen, A., Jirenhed, D.-A., and Hesslow, G. (2008). Simple and complex spike firing patterns in Purkinje cells during classical conditioning. *The Cerebellum* **7**(4), 563.

Reeber, S.L., Loeschel, C.A., Franklin, A., and Sillitoe, R.V. (2013). Establishment of topographic circuit zones in the cerebellum of scrambler mutant mice. *Frontiers in neural circuits* **7**.

Reeber, S.L., and Sillitoe, R.V. (2011). Patterned expression of a cocaine‐and amphetamine‐regulated transcript peptide reveals complex circuit topography in the rodent cerebellar cortex. *Journal of Comparative Neurology* **519**(9), 1781-1796.

Reeber, S.L., White, J.J., George-Jones, N.A., and Sillitoe, R.V. (2012). Architecture and development of olivocerebellar circuit topography. *Frontiers in neural circuits* **6**.

Repka, A.M., and Adler, R. (1992). Accurate determination of the time of cell birth using a sequential labeling technique with [3H]-thymidine and bromodeoxyuridine ("window labeling"). *Journal of Histochemistry & Cytochemistry* **40**(7), 947-953.

Rice, D.S., and Curran, T. (2001). Role of the reelin signaling pathway in central nervous system development. *Annual review of neuroscience* **24**(1), 1005-1039.

Roberts, E., and Frankel, S. (1950). Gamma-aminobutyric acid in brain. Paper presented at: *Federation Proceedings* (FEDERATION AMER SOC EXP BIOL 9650 ROCKVILLE PIKE, BETHESDA, MD 20814-3998).

Rogan, S.C., and Roth, B.L. (2011). Remote control of neuronal signaling. *Pharmacological reviews* **63**(2), 291-315.

Rogers, D.C., Fisher, E., Brown, S., Peters, J., Hunter, A., and Martin, J. (1997). Behavioral and functional analysis of mouse phenotype: SHIRPA, a proposed protocol for comprehensive phenotype assessment. *Mammalian Genome* **8**(10), 711-713.

Rose, M.F., Ahmad, K.A., Thaller, C., and Zoghbi, H.Y. (2009). Excitatory neurons of the proprioceptive, interoceptive, and arousal hindbrain networks share a developmental

requirement for Math1. *Proceedings of the National Academy of Sciences* **106**(52), 22462-22467.

Roth, B.L. (2016). DREADDs for neuroscientists. *Neuron* **89**(4), 683-694.

Rowell, J.J., and Ragsdale, C.W. (2012). BrdU birth dating can produce errors in cell fate specification in chick brain development. *Journal of Histochemistry & Cytochemistry* **60**(11), 801-810.

Rudnik‐Schöneborn, S., Barth, P.G., and Zerres, K. (2014). Pontocerebellar hypoplasia. Paper presented at: *American Journal of Medical Genetics Part C: Seminars in Medical Genetics* (Wiley Online Library).

Ruigrok, T., and Voogd, J. (1990). Cerebellar nucleo‐olivary projections in the rat: An anterograde tracing study with Phaseolus vulgaris‐leucoagglutinin (PHA‐L). *Journal of Comparative Neurology* **298**(3), 315-333.

Ruigrok, T.J. (1997). Cerebellar nuclei: the olivary connection. *Progress in brain research* **114**, 167-192.

Ruigrok, T.J., and De Zeeuw, C.I. (1993). Electron microscopy of in vivo recorded and intracellularly injected inferior olivary neurons and their GABAergic innervation in the cat. *Microscopy research and technique* **24**(1), 85-102.

Ruigrok, T.J.H. (2011). Ins and outs of cerebellar modules. *The Cerebellum* **10**(3), 464-474.

Saccozzi, A. (1887). Sul nucleo dentato del cervelletto. *Riv. Sper. Fren. Med. Legale* **13**, 93-99.

Sanverdi, S.E., Oguz, K.K., and Haliloglu, G. (2012). Hypertrophic olivary degeneration in children: four new cases and a review of the literature with an emphasis on the MRI findings. *The British Journal of Radiology* **85**(1013), 511-516.

Sauer, B., and Henderson, N. (1988). Site-specific DNA recombination in mammalian cells by the Cre recombinase of bacteriophage P1. *Proceedings of the National Academy of Sciences* **85**(14), 5166-5170.

Sawada, K., Fukui, Y., and Hawkes, R. (2008). Spatial distribution of corticotropin-releasing factor immunopositive climbing fibers in the mouse cerebellum: analysis by whole mount immunohistochemistry. *Brain Res* **1222**, 106-117.

Schaal, S., Sternad, D., Osu, R., and Kawato, M. (2004). Rhythmic arm movement is not discrete. *Nat Neurosci* **7**(10), 1136.

Schepers, G.E., Teasdale, R.D., and Koopman, P. (2002). Twenty Pairs of Sox. *Developmental Cell* **3**(2), 167-170.

Schmahmann, J.D. (2010). The role of the cerebellum in cognition and emotion: personal reflections since 1982 on the dysmetria of thought hypothesis, and its historical evolution from theory to therapy. *Neuropsychology review* **20**(3), 236-260.

Schmahmann, J.D., and Sherman, J.C. (1998). The cerebellar cognitive affective syndrome. *Brain : a journal of neurology* **121 (Pt 4)**(Pt 4), 561-579.

Schmued, L.C., and Fallon, J.H. (1986). Fluoro-Gold: a new fluorescent retrograde axonal tracer with numerous unique properties. *Brain Res* **377**(1), 147-154.

Schofield, B.R., Schofield, R.M., Sorensen, K.A., and Motts, S.D. (2007). On the use of retrograde tracers for identification of axon collaterals with multiple fluorescent retrograde tracers. *Neuroscience* **146**(2), 773-783.

Schonewille, M., Gao, Z., Boele, H.-J., Veloz, M.F.V., Amerika, W.E., Šimek, A.A., De Jeu, M.T., Steinberg, J.P., Takamiya, K., and Hoebeek, F.E. (2011). Reevaluating the role of LTD in cerebellar motor learning. *Neuron* **70**(1), 43-50.

Schwartz, A.B., Ebner, T.J., and Bloedel, J.R. (1987). Responses of interposed and dentate neurons to perturbations of the locomotor cycle. *Experimental Brain Research* **67**(2), 323-338.

Schweighofer, N., Lang, E.J., and Kawato, M. (2013). Role of the olivo-cerebellar complex in motor learning and control. *Frontiers in neural circuits* **7**.

Sears, L.L., and Steinmetz, J.E. (1991). Dorsal accessory inferior olive activity diminishes during acquisition of the rabbit classically conditioned eyelid response. *Brain Res* **545**(1), 114-122.

Sekirnjak, C., Vissel, B., Bollinger, J., Faulstich, M., and du Lac, S. (2003). Purkinje cell synapses target physiologically unique brainstem neurons. *Journal of Neuroscience* **23**(15), 6392-6398.

Sellers, K., Zyka, V., Lumsden, A.G., and Delogu, A. (2014). Transcriptional control of GABAergic neuronal subtype identity in the thalamus. *Neural development* **9**, 14-8104-8109-8114.

Seoane, A., Apps, R., Balbuena, E., Herrero, L., and Llorens, J. (2005). Differential effects of trans‐crotononitrile and 3‐acetylpyridine on inferior olive integrity and behavioural performance in the rat. *European Journal of Neuroscience* **22**(4), 880-894.

Seto, Y., Nakatani, T., Masuyama, N., Taya, S., Kumai, M., Minaki, Y., Hamaguchi, A., Inoue, Y.U., Inoue, T., and Miyashita, S. (2014). Temporal identity transition from Purkinje cell progenitors to GABAergic interneuron progenitors in the cerebellum. *Nature communications* **5**.

Sgaier, S.K., Millet, S., Villanueva, M.P., Berenshteyn, F., Song, C., and Joyner, A.L. (2005). Morphogenetic and cellular movements that shape the mouse cerebellum; insights from genetic fate mapping. *Neuron* **45**(1), 27-40.

Shin, S.-L., and De Schutter, E. (2006). Dynamic synchronization of Purkinje cell simple spikes. *Journal of neurophysiology* **96**(6), 3485-3491.

Shinoda, Y., Sugihara, I., Wu, H., and Sugiuchi, Y. (1999). The entire trajectory of single climbing and mossy fibers in the cerebellar nuclei and cortex. *Progress in brain research* **124**, 173-186.

Sillitoe, R.V., and Joyner, A.L. (2007). Morphology, molecular codes, and circuitry produce the three-dimensional complexity of the cerebellum. *Annu. Rev. Cell Dev. Biol.* **23**, 549-577.

Song, H., Lee, B., Pyun, D., Guimera, J., Son, Y., Yoon, J., Baek, K., Wurst, W., and Jeong, Y. (2015). Ascl1 and Helt act combinatorially to specify thalamic neuronal identity by repressing Dlxs activation. *Developmental Biology* **398**(2), 280-291.

Sotelo, C. (2004). Cellular and genetic regulation of the development of the cerebellar system. *Progress in neurobiology* **72**(5), 295-339.

Sotelo, C., Bourrat, F., and Triller, A. (1984). Postnatal development of the inferior olivary complex in the rat. II. Topographic organization of the immature olivocerebellar projection. *Journal of Comparative Neurology* **222**(2), 177-199.

Sotelo, C., Gotow, T., and Wassef, M. (1986). Localization of glutamic‐acid‐decarboxylase‐immunoreactive axon terminals in the inferior olive of the rat, with special emphasis on anatomical relations between GABAergic synapses and dendrodendritic gap junctions. *Journal of Comparative Neurology* **252**(1), 32-50.

Sotelo, C., Llinas, R., and Baker, R. (1974). Structural study of inferior olivary nucleus of the cat: morphological correlates of electrotonic coupling. *Journal of Neurophysiology* **37**(3), 541-559.

Spencer, R.M., Zelaznik, H.N., Diedrichsen, J., and Ivry, R.B. (2003). Disrupted timing of discontinuous but not continuous movements by cerebellar lesions. *science* **300**(5624), 1437-1439.

Sprague, J.M., and Chambers, W.W. (1953). Regulation of posture in intact and decerebrate cat: I. Cerebellum, reticular formation, vestibular nuclei. *Journal of neurophysiology* **16**(5), 451-463.

Stanton, G.B. (1980). Afferents to oculomotor nuclei from area "Y" in Macaca mulatta: An anterograde degeneration study. *Journal of Comparative Neurology* **192**(2), 377-385.

Steiger, H.J., and Büttner-Ennever, J.A. (1979). Oculomotor nucleus afferents in the monkey demonstrated with horseradish peroxidase. *Brain Res* **160**(1), 1-15.

Stoodley, C.J. (2014). Distinct regions of the cerebellum show gray matter decreases in autism, ADHD, and developmental dyslexia. *Frontiers in Systems Neuroscience* **8**.

Stoodley, C.J., Valera, E.M., and Schmahmann, J.D. (2012). Functional topography of the cerebellum for motor and cognitive tasks: an fMRI study. *NeuroImage* **59**(2), 1560-1570.

Strick, P.L., Dum, R.P., and Fiez, J.A. (2009). Cerebellum and nonmotor function. *Annual Review of Neuroscience* **32**, 413-434.

Sudarov, A., Turnbull, R.K., Kim, E.J., Lebel-Potter, M., Guillemot, F., and Joyner, A.L. (2011). Ascl1 genetics reveals insights into cerebellum local circuit assembly. *The Journal of neuroscience : the official journal of the Society for Neuroscience* **31**(30), 11055-11069.

Sugihara, I., Fujita, H., Na, J., Quy, P.N., Li, B.Y., and Ikeda, D. (2009). Projection of reconstructed single Purkinje cell axons in relation to the cortical and nuclear aldolase C compartments of the rat cerebellum. *Journal of Comparative Neurology* **512**(2), 282-304.

Sugihara, I., Lohof, A.M., Letellier, M., Mariani, J., and Sherrard, R.M. (2003). Post‐lesion transcommissural growth of olivary climbing fibres creates functional synaptic microzones. *European Journal of Neuroscience* **18**(11), 3027-3036.

Sugihara, I., and Quy, P.N. (2007). Identification of aldolase C compartments in the mouse cerebellar cortex by olivocerebellar labeling. *Journal of Comparative Neurology* **500**(6), 1076-1092.

Sugihara, I., and Shinoda, Y. (2007). Molecular, topographic, and functional organization of the cerebellar nuclei: analysis by three-dimensional mapping of the olivonuclear projection and aldolase C labeling. *The Journal of Neuroscience* **27**(36), 9696-9710.

Sugihara, I., Wu, H., and Shinoda, Y. (1999). Morphology of single olivocerebellar axons labeled with biotinylated dextran amine in the rat. *The Journal of comparative neurology* **414**(2), 131-148.

Sugitani, Y., Nakai, S., Minowa, O., Nishi, M., Jishage, K.-i., Kawano, H., Mori, K., Ogawa, M., and Noda, T. (2002). Brn-1 and Brn-2 share crucial roles in the production and positioning of mouse neocortical neurons. *Genes & development* **16**(14), 1760-1765.

Sullivan, M.R., Nimmerjahn, A., Sarkisov, D.V., Helmchen, F., and Wang, S.S.-H. (2005). In vivo calcium imaging of circuit activity in cerebellar cortex. *Journal of neurophysiology* **94**(2), 1636-1644.

Sultan, F., König, T., Möck, M., and Thier, P. (2002). Quantitative organization of neurotransmitters in the deep cerebellar nuclei of the Lurcher mutant. *Journal of Comparative Neurology* **452**(4), 311-323.

Suzuki, L., Coulon, P., Sabel-Goedknegt, E.H., and Ruigrok, T.J. (2012). Organization of cerebral projections to identified cerebellar zones in the posterior cerebellum of the rat. *Journal of Neuroscience* **32**(32), 10854-10869.

Svensson, P., Bengtsson, F., and Hesslow, G. (2006). Cerebellar inhibition of inferior olivary transmission in the decerebrate ferret. *Experimental brain research* **168**(1-2), 241-253.

Tanahira, C., Higo, S., Watanabe, K., Tomioka, R., Ebihara, S., Kaneko, T., and Tamamaki, N. (2009). Parvalbumin neurons in the forebrain as revealed by parvalbumin-Cre transgenic mice. *Neuroscience Research* **63**(3), 213-223.

Tanaka, I., and Ezure, K. (2004). Overall distribution of GLYT2 mRNA-containing versus GAD67 mRNA-containing neurons and colocalization of both mRNAs in midbrain, pons, and cerebellum in rats. *Neuroscience research* **49**(2), 165-178.

Taupin, P. (2007). BrdU immunohistochemistry for studying adult neurogenesis: paradigms, pitfalls, limitations, and validation. *Brain research reviews* **53**(1), 198-214.

Teune, T.M., van der Burg, J., de Zeeuw, C.I., Voogd, J., and Ruigrok, T.J.H. (1998). Single Purkinje cell can innervate multiple classes of projection neurons in the cerebellar nuclei of the rat: A light microscopic and ultrastructural triple-tracer study in the rat. *The Journal of Comparative Neurology* **392**(2), 164-178.

Teune, T.M., van der Burg, J., van der Moer, J., Voogd, J., and Ruigrok, T.J. (2000). Topography of cerebellar nuclear projections to the brain stem in the rat. *Progress in brain research* **124**, 141-172.

Thach, W.T., Goodkin, H., and Keating, J. (1992). The cerebellum and the adaptive coordination of movement. *Annual review of neuroscience* **15**(1), 403-442.

Tolbert, D., Massopust, L., Murphy, M., and Young, P. (1976). The anatomical organization of the cerebello‐olivary projection in the cat. *Journal of Comparative Neurology* **170**(4), 525-544.

Torriero, S., Oliveri, M., Koch, G., Gerfo, E.L., Salerno, S., Petrosini, L., and Caltagirone, C. (2007). Cortical networks of procedural learning: evidence from cerebellar damage. *Neuropsychologia* **45**(6), 1208-1214.

Tsai, P.T., Chu, Y., Greene-Colozzi, E., Sadowski, A.R., Leech, J.M., Steinberg, J., Crawley, J.N., Regehr, W.G., and Sahin, M. (2012). Autistic-like behaviour and cerebellar dysfunction in Purkinje cell Tsc1 mutant mice. *Nature* **488**(7413), 647-651.

Tsubota, T., Ohashi, Y., and Tamura, K. (2013). Optogenetics in the cerebellum: Purkinje cell-specific approaches for understanding local cerebellar functions. *Behavioural brain research* **255**, 26-34.

Uchikawa, M., Kamachi, Y., and Kondoh, H. (1999). Two distinct subgroups of Group B Sox genes for transcriptional activators and repressors: their expression during embryonic organogenesis of the chicken. *Mechanisms of development* **84**(1), 103-120.

Ugolini, G. (2010). Advances in viral transneuronal tracing. *Journal of neuroscience methods* **194**(1), 2-20.

Utsunomiya, H., Takano, K., Ogasawara, T., Hashimoto, T., Fukushima, T., and Okazaki, M. (1998). Rhombencephalosynapsis: cerebellar embryogenesis. *American Journal of Neuroradiology* **19**(3), 547-549.

Uusisaari, M., and De Schutter, E. (2011). The mysterious microcircuitry of the cerebellar nuclei. *The Journal of physiology* **589**(Pt 14), 3441-3457.

Uusisaari, M., and Knöpfel, T. (2008). GABAergic synaptic communication in the GABAergic and non-GABAergic cells in the deep cerebellar nuclei. *Neuroscience* **156**(3), 537-549.

Uusisaari, M., and Knöpfel, T. (2010). GlyT2 neurons in the lateral cerebellar nucleus. *The Cerebellum* **9**(1), 42-55.

Uusisaari, M., and Knöpfel, T. (2011). Functional classification of neurons in the mouse lateral cerebellar nuclei. *The Cerebellum* **10**(4), 637-646.

Uusisaari, M., Obata, K., and Knöpfel, T. (2007). Morphological and electrophysiological properties of GABAergic and non-GABAergic cells in the deep cerebellar nuclei. *Journal of neurophysiology* **97**(1), 901-911.

Uusisaari, M.Y., and Knöpfel, T. (2012). Diversity of Neuronal Elements and Circuitry in the Cerebellar Nuclei. *The Cerebellum* **11**(2), 420-421.

Van Der Giessen, R.S., Koekkoek, S.K., van Dorp, S., De Gruijl, J.R., Cupido, A., Khosrovani, S., Dortland, B., Wellershaus, K., Degen, J., and Deuchars, J. (2008). Role of olivary electrical coupling in cerebellar motor learning. *Neuron* **58**(4), 599-612.

van der Vaart, T., Van Woerden, G., Elgersma, Y., De Zeeuw, C., and Schonewille, M. (2011). Motor deficits in neurofibromatosis type 1 mice: the role of the cerebellum. *Genes, Brain and Behavior* **10**(4), 404-409.

Van Essen, T.A., Van Der Giessen, R.S., Koekkoek, S.K., VanderWerf, F., De Zeeuw, C.I., Van Genderen, P.J., Overbosch, D., and De Jeu, M.T. (2010). Anti-malaria drug mefloquine induces motor learning deficits in humans. *Frontiers in neuroscience* **4**.

Vinueza Veloz, M.F., Zhou, K., Bosman, L.W., Potters, J.-W., Negrello, M., Seepers, R.M., Strydis, C., Koekkoek, S.K., and De Zeeuw, C.I. (2015). Cerebellar control of gait and interlimb coordination. *Brain Structure and Function* **220**(6), 3513-3536.

Virolainen, S.-M., Achim, K., Peltopuro, P., Salminen, M., and Partanen, J. (2012). Transcriptional regulatory mechanisms underlying the GABAergic neuron fate in different diencephalic prosomeres. *Development* **139**(20), 3795-3805.

Volpe, J.J., and Adams, R.D. (1972). Cerebro-hepato-renal syndrome of Zellweger: an inherited disorder of neuronal migration. *Acta neuropathologica* **20**(3), 175-198.

Voogd, J. (2014). What we do not know about cerebellar systems neuroscience. *Frontiers in Systems Neuroscience* **8**(227).

Voogd, J., and Glickstein, M. (1998). The anatomy of the cerebellum. *Trends in cognitive sciences* **2**(9), 307-313.

Voogd, J., and Ruigrok, T.J.H. (2004). The organization of the corticonuclear and olivocerebellar climbing fiber projections to the rat cerebellar vermis: the congruence of projection zones and the zebrin pattern. *Journal of neurocytology* **33**(1), 5-21.

Voogd, J., and van Baarsen, K. (2014). The horseshoe-shaped commissure of Wernekinck or the decussation of the brachium conjunctivum methodological changes in the 1840s. *The Cerebellum* **13**(1), 113-120.

Wang, C., Wang, C., Clark, K., and Sferra, T. (2003). Recombinant AAV serotype 1 transduction efficiency and tropism in the murine brain. *Gene therapy* **10**(17), 1528.

Wang, V.Y., Rose, M.F., and Zoghbi, H.Y. (2005). Math1 expression redefines the rhombic lip derivatives and reveals novel lineages within the brainstem and cerebellum. *Neuron* **48**(1), 31-43.

Watakabe, A., Ohtsuka, M., Kinoshita, M., Takaji, M., Isa, K., Mizukami, H., Ozawa, K., Isa, T., and Yamamori, T. (2015). Comparative analyses of adeno-associated viral vector serotypes 1, 2, 5, 8 and 9 in marmoset, mouse and macaque cerebral cortex. *Neuroscience Research* **93**, 144-157.

Watanabe, M., and Kano, M. (2011). Climbing fiber synapse elimination in cerebellar Purkinje cells. *European Journal of Neuroscience* **34**(10), 1697-1710.

Wegner, M. (2011). SOX after SOX: SOXession regulates neurogenesis. *Genes & Development* **25**(23), 2423-2428.

Weisheit, G., Gliem, M., Endl, E., Pfeffer, P.L., Busslinger, M., and Schilling, K. (2006). Postnatal development of the murine cerebellar cortex: formation and early dispersal of basket, stellate and Golgi neurons. *European Journal of Neuroscience* **24**(2), 466-478.

Welsh, J.P., Lang, E.J., Sugihara, I., and Llinás, R. (1995). Dynamic organization of motor control within the olivocerebellar system. *Nature* **374**(6521), 453.

Wickersham, I.R., Sullivan, H.A., and Seung, H.S. (2010). Production of glycoprotein-deleted rabies viruses for monosynaptic tracing and high-level gene expression in neurons. *Nat Protoc* **5**(3), 595.

Willson, M.L., Bower, A.J., and Sherrard, R.M. (2007). Developmental neural plasticity and its cognitive benefits: olivocerebellar reinnervation compensates for spatial function in the cerebellum. *European Journal of Neuroscience* **25**(5), 1475-1483.

Wilson, M.J., and Dearden, P.K. (2008). Evolution of the insect Sox genes. *BMC evolutionary biology* **8**(1), 120.

Wingate, R. (2005). Math-Map(ic)s. *Neuron* **48**(1), 1-4.

Wingate, R., and Kwint, M. (2006). Imagining the brain cell: the neuron in visual culture. *Nat Rev Neurosci* **7**(9), 745-752.

Wingate, R.J., and Hatten, M.E. (1999). The role of the rhombic lip in avian cerebellum development. *Development (Cambridge, England)* **126**(20), 4395-4404.

Wingate, R.J.T. (2001). The rhombic lip and early cerebellar development. *Current opinion in neurobiology* **11**(1), 82-88.

Witter, L., Canto, C.B., Hoogland, T.M., De Gruijl, J.R., and De Zeeuw, C.I. (2013). Strength and timing of motor responses mediated by rebound firing in the cerebellar nuclei after Purkinje cell activation. *Frontiers in neural circuits* **7**.

Wu, H., Sugihara, I., and Shinoda, Y. (1999). Projection patterns of single mossy fibers originating from the lateral reticular nucleus in the rat cerebellar cortex and nuclei. *The Journal of comparative neurology* **411**(1), 97-118.

Wullimann, M.F., Mueller, T., Distel, M., Babaryka, A., Grothe, B., and Köster, R.W. (2011). The long adventurous journey of rhombic lip cells in jawed vertebrates: a comparative developmental analysis. *Frontiers in neuroanatomy* **5**.

Yachnis, A.T. (2002). Rhombencephalosynapsis with massive hydrocephalus: case report and pathogenetic considerations. *Acta neuropathologica* **103**(3), 301-304.

Yachnis, A.T., and Rorke, L.B. (1999). Cerebellar and brainstem development: an overview in relation to Joubert syndrome. *J Child Neurol* **14**(9), 570-573.

Yamada, K., and Watanabe, M. (2002). Cytodifferentiation of Bergmann glia and its relationship with Purkinje cells. *Anatomical science international* **77**(2), 94-108.

Yamada, M., Seto, Y., Taya, S., Owa, T., Inoue, Y.U., Inoue, T., Kawaguchi, Y., Nabeshima, Y.-i., and Hoshino, M. (2014). Specification of Spatial Identities of Cerebellar Neuron Progenitors by Ptf1a and Atoh1 for Proper Production of GABAergic and Glutamatergic Neurons. *The Journal of Neuroscience* **34**(14), 4786-4800.

Yamada, M., Terao, M., Terashima, T., Fujiyama, T., Kawaguchi, Y., Nabeshima, Y.-i., and Hoshino, M. (2007). Origin of climbing fiber neurons and their developmental dependence on Ptf1a. *Journal of Neuroscience* **27**(41), 10924-10934.

Yamamoto, F., Sato, Y., and Kawasaki, T. (1986). The neuronal pathway from the flocculus to the oculomotor nucleus: an electrophysiological study of group y nucleus in cats. *Brain Res* **371**(2), 350-354.

Yang, C.F., Chiang, M.C., Gray, D.C., Prabhakaran, M., Alvarado, M., Juntti, S.A., Unger, E.K., Wells, J.A., and Shah, N.M. (2013). Sexually dimorphic neurons in the ventromedial hypothalamus govern mating in both sexes and aggression in males. *Cell* **153**(4), 896-909.

Yeo, C., Hardiman, M., and Glickstein, M. (1985). Classical conditioning of the nictitating membrane response of the rabbit. *Experimental brain research* **60**(1), 99-113.

Yeung, J., Ha, T.J., Swanson, D.J., and Goldowitz, D. (2016). A Novel and Multivalent Role of Pax6 in Cerebellar Development. *J Neurosci* **36**(35), 9057-9069.

Yip, J., Soghomonian, J.J., and Blatt, G.J. (2009). Decreased GAD65 mRNA levels in select subpopulations of neurons in the cerebellar dentate nuclei in autism: an in situ hybridization study. *Autism Research* **2**(1), 50-59.

Yu, J., and Eidelberg, E. (1983). Recovery of locomotor function in cats after localized cerebellar lesions. *Brain Res* **273**(1), 121-131.

Yu, T., Meiners, L.C., Danielsen, K., Wong, M.T., Bowler, T., Reinberg, D., Scambler, P.J., van Ravenswaaij-Arts, C.M., and Basson, M.A. (2013). Deregulated FGF and homeotic gene expression underlies cerebellar vermis hypoplasia in CHARGE syndrome. *elife* **2**, e01305.

Yuasa, S. (1996). Bergmann glial development in the mouse cerebellum as revealed by tenascin expression. *Anatomy and embryology* **194**(3), 223-234.

Zervas, M., Millet, S., Ahn, S., and Joyner, A.L. (2004). Cell behaviors and genetic lineages of the mesencephalon and rhombomere 1. *Neuron* **43**(3), 345-357.

Zhao, Y., Kwan, K.M., Mailloux, C.M., Lee, W.K., Grinberg, A., Wurst, W., Behringer, R.R., and Westphal, H. (2007). LIM-homeodomain proteins Lhx1 and Lhx5, and their cofactor Ldb1, control Purkinje cell differentiation in the developing cerebellum. *Proc Natl Acad Sci U S A* **104**(32), 13182-13186.

Zheng, N., and Raman, I.M. (2009). Ca currents activated by spontaneous firing and synaptic disinhibition in neurons of the cerebellar nuclei. *Journal of Neuroscience* **29**(31), 9826-9838.

Zheng, N., and Raman, I.M. (2010). Synaptic inhibition, excitation, and plasticity in neurons of the cerebellar nuclei. *The Cerebellum* **9**(1), 56-66.

Zordan, P., Croci, L., Hawkes, R., and Consalez, G.G. (2008). Comparative analysis of proneural gene expression in the embryonic cerebellum. *Developmental Dynamics* **237**(6), 1726-1735.